ADVANCES IN SEISMIC PERFORMANCE AND RISK ESTIMATION OF PRECAST CONCRETE BUILDINGS

EDITED BY: Andrea Belleri, Bruno Dal Lago and Hugo Rodrigues

PUBLISHED IN: Frontiers in Built Environment

frontiers Research Topics

frontiers

ISSN 1664-8714
ISBN 978-2-88974-307-0
DOI 10.3389/978-2-88974-307-0

About Frontiers

Frontiers is more than just an open-access publisher of scholarly articles: it is a pioneering approach to the world of academia, radically improving the way scholarly research is managed. The grand vision of Frontiers is a world where all people have an equal opportunity to seek, share and generate knowledge. Frontiers provides immediate and permanent online open access to all its publications, but this alone is not enough to realize our grand goals.

Frontiers Journal Series

The Frontiers Journal Series is a multi-tier and interdisciplinary set of open-access, online journals, promising a paradigm shift from the current review, selection and dissemination processes in academic publishing. All Frontiers journals are driven by researchers for researchers; therefore, they constitute a service to the scholarly community. At the same time, the Frontiers Journal Series operates on a revolutionary invention, the tiered publishing system, initially addressing specific communities of scholars, and gradually climbing up to broader public understanding, thus serving the interests of the lay society, too.

Dedication to Quality

Each Frontiers article is a landmark of the highest quality, thanks to genuinely collaborative interactions between authors and review editors, who include some of the world's best academicians. Research must be certified by peers before entering a stream of knowledge that may eventually reach the public - and shape society; therefore, Frontiers only applies the most rigorous and unbiased reviews.
Frontiers revolutionizes research publishing by freely delivering the most outstanding research, evaluated with no bias from both the academic and social point of view. By applying the most advanced information technologies, Frontiers is catapulting scholarly publishing into a new generation.

What are Frontiers Research Topics?

Frontiers Research Topics are very popular trademarks of the Frontiers Journals Series: they are collections of at least ten articles, all centered on a particular subject. With their unique mix of varied contributions from Original Research to Review Articles, Frontiers Research Topics unify the most influential researchers, the latest key findings and historical advances in a hot research area! Find out more on how to host your own Frontiers Research Topic or contribute to one as an author by contacting the Frontiers Editorial Office: frontiersin.org/about/contact

ADVANCES IN SEISMIC PERFORMANCE AND RISK ESTIMATION OF PRECAST CONCRETE BUILDINGS

Topic Editors:
Andrea Belleri, University of Bergamo, Italy
Bruno Dal Lago, University of Insubria, Italy
Hugo Rodrigues, University of Aveiro, Portugal

Citation: Belleri, A., Lago, B. D., Rodrigues, H., eds. (2022). Advances in Seismic Performance and Risk Estimation of Precast Concrete Buildings. Lausanne: Frontiers Media SA. doi: 10.3389/978-2-88974-307-0

Table of Contents

04 ***Editorial: Advances in Seismic Performance and Risk Estimation of Precast Concrete Buildings***
Andrea Belleri, Bruno Dal Lago and Hugo Rodrigues

06 ***Seismic Retrofitting Solutions for Precast RC Industrial Buildings Struck by the 2012 Earthquakes in Northern Italy***
Fabio Minghini and Nerio Tullini

25 ***Cyclic Behavior of Beam-Column Connections in Precast Structures***
Hilal Meydanli Atalay and Sevket Ozden

38 ***Modeling of the Beam-To-Column Dowel Connection for a Single-Story RC Precast Building***
Gennaro Magliulo, Chiara Di Salvatore and Marianna Ercolino

48 ***Crescent-Moon Beam-To-Column Connection for Precast Industrial Buildings***
Michele Egidio Bressanelli, Marco Bosio, Andrea Belleri, Paolo Riva and Piergiovanni Biagiotti

63 ***Recent Advances in the Research of the Seismic Response of RC Precast Buildings at the University of Ljubljana***
Blaž Zoubek, Anže Babič, Matjaž Dolšek, Matej Fischinger and Tatjana Isaković

80 ***Unbonded Post-Tensioned Precast Concrete Walls With Rocking Connections: Modeling Approaches and Impact Damping***
Dimitrios Kalliontzis and Maryam Nazari

99 ***Influence of Modelling Assumptions on the Seismic Risk of Industrial Precast Concrete Structures***
Michele Egidio Bressanelli, Davide Bellotti, Andrea Belleri, Francesco Cavalieri, Paolo Riva and Roberto Nascimbene

115 ***Design Approach for Lateral Capacity of Dowel-Type Steel Connections in Precast Reinforced Concrete Elements***
Giovanni Muciaccia

122 ***Multi-Stripe Seismic Assessment of Precast Industrial Buildings With Cladding Panels***
Krunal Gajera, Bruno Dal Lago, Luca Capacci and Fabio Biondini

137 ***Seismic Behavior of Precast Buildings With Dissipative Connections***
Lorenzo De Stefani and Roberto Scotta

frontiers in Built Environment

EDITORIAL
published: 21 December 2021
doi: 10.3389/fbuil.2021.822262

Editorial: Advances in Seismic Performance and Risk Estimation of Precast Concrete Buildings

Andrea Belleri[1]*, *Bruno Dal Lago*[2] *and Hugo Rodrigues*[3]

[1]Department of Engineering and Applied Sciences, University of Bergamo, Dalmine, Italy, [2]Department of Theoretical and Applied Sciences, Università degli Studi dell'Insubria, Varese, Italy, [3]Civil Engineering Department, University of Aveiro, Aveiro, Portugal

Keywords: precast concrete, seismic risk, connections, joints, structural retrofit

Editorial on the Research Topic

Advances in Seismic Performance and Risk Estimation of Precast Concrete Buildings

INTRODUCTION

The design of precast buildings during past years was typically carried out without considering the complex seismic interaction between elements, both structural and non-structural, due to the peculiar nature of precast connections and overall building behaviour. This fact was recently and dramatically shown by several earthquakes. The seismic safety of the building stock is a requirement of modern societies and remains a concern in seismic prone areas. Recently, a growing research interest has been observed on the seismic behaviour of reinforced concrete (RC) precast elements and connection systems, mainly considering current code-conforming solutions. However, the knowledge gap is far from being filled. The Engineering community is currently facing the following challenges to reduce the seismic vulnerability and risk associated with precast structures: 1) refinement and harmonization of design criteria for new buildings and new precast technologies, 2) seismic assessment and risk analysis of the existing building stock, and 3) setting and employing robust retrofit solutions.

The present research topic contributes to these goals by gathering a diverse set of recent studies, which provide original papers and review articles addressing the current challenges related to the seismic performance of precast structures. A total of 10 papers authored by 29 experts of the field have been finally selected to integrate the present issue, encompassing the objectives described above.

The topics addressed in the papers are from several fields across civil engineering, including: an overview of the recent advances carried out by one among the most active research groups in the field; four papers related with the different challenges in the design and in the experimental and numerical assessment of different beam-column connections, including dissipative, moment resisting, and dowel; two contributions regarding the vulnerability assessment of precast industrial buildings with cladding panels employing novel connection devices; a paper considering unbonded post-tensioned precast walls and their modelling challenges; a paper discussing the modelling assumptions and its influence in the seismic risk assessment of industrial precast structures; a paper dealing with the effectiveness of retrofitting solutions for post-earthquake interventions in industrial precast buildings.

PAPERS IN THE COLLECTION

The first paper of the collection (Zoubek et al.) reviews and comments the outcome of a long-lasting research activity carried out at the University of Ljubljana concerning the seismic behaviour of

Edited and reviewed by:
Izuru Takewaki,
Kyoto University, Japan

***Correspondence:**
Andrea Belleri
andrea.belleri@unibg.it

Specialty section:
This article was submitted to Earthquake Engineering, a section of the journal Frontiers in Built Environment

Received: *25 November 2021*
Accepted: *03 December 2021*
Published: *21 December 2021*

Citation:
Belleri A, Dal Lago B and Rodrigues H (2021) Editorial: Advances in Seismic Performance and Risk Estimation of Precast Concrete Buildings. Front. Built Environ. 7:822262. doi: 10.3389/fbuil.2021.822262

precast structures, focusing on a new capacity model of beam-column dowel connections, new insights into the cyclic behaviour and design procedures of fastening systems of concrete cladding panels, a methodology for seismic fragility analysis of RC precast buildings, and back-up (strengthening) system to prevent the falling of cladding panels in case of a strong earthquake.

The second paper of the collection (Muciaccia) contributes to filling the gap between the lack of agreement regarding the applicability of Eurocode 2 rules for fastening in concrete to the design cases related to dowel connections, specifically concerning the role of the edge reinforcement and the effectiveness of multiple reinforcement layers in the proximity of the steel bar.

The third paper of the collection (Bressanelli et al.) presents a novel dissipative beam-to-column crescent moon connection device to be employed for the retrofit of existing precast industrial buildings, encompassing the descriptions of experimental tests, numerical modelling, and design criteria related to the single device and the retrofitted precast building.

The fourth paper of the collection (Magliulo et al.) presents a study aimed at assessing the seismic behaviour of a single-story RC precast building in terms of global collapse implementing two different models of the beam-to-column connection, a simplified and a refined one, through non-linear static and dynamic analyses of a single-story RC precast building.

The fifth paper of the collection (Atalay and Ozden) presents and discuss a new moment resisting precast concrete beam-column connection detail with post-tensioning bolts, made out of high yield strength steel, comparing its moment capacity, stiffness, energy dissipation and the residual displacement performance with traditional solutions.

The sixth paper of the collection (De Stefani and Scotta) aims to evaluate the efficiency of dissipative panel-to-structure and roof connections in precast buildings. The results of the analysis highlight a better performance of buildings including such connections, particularly when a rigid roof diaphragm is provided.

The seventh paper of the collection (Gajera et al.) presents the seismic assessment of precast frame structures employing pendulum, cantilever, and rocking cladding connection systems with a probabilistic approach based on the results of static and multi-stripe dynamic non-linear analyses. The results indicate a low vulnerability of well-detailed modern precast industrial frame structures provided with decoupling cladding connections.

The eighth paper of the collection (Kalliontzis and Nazari) discusses and compares numerical and analytical modelling techniques for rocking walls precast panels, where dry wall-to-foundation connections employing unbonded post-tensioning tendons provide a re-centring capability even for strong earthquakes.

The ninth paper of the collection (Bressanelli et al.) aims at evaluating the influence of modelling assumptions in the seismic risk assessment of industrial precast buildings, in particular assessing the modelling influence of mass, overhead crane, beam-to-column and roof-to-beam connections, and cladding systems.

The 10th paper of the collection (Minghini and Tullini) aims at evaluating the effectiveness of real retrofit interventions on industrial buildings struck by the Emilia earthquakes, addressing in particular the force transfer mechanisms between the existing structure and the new strengthening system.

The editorial team is sure that the papers reflect significant contributions to the research and development in the various topics addressed. We hope that readers will find all articles of the research topic useful and exciting and that the articles will stimulate further research activities in the area of seismic performance of precast concrete structures.

AUTHOR CONTRIBUTIONS

AB, BL, and HR conceived and edited the Research Topic. All authors have made a substantial, direct and intellectual contribution to the work, and approved it for publication.

ACKNOWLEDGMENTS

AB and BDL handled manuscripts with the collaboration of Prof. Massimo Latour and Prof. Arturo Tena-Colunga, who are kindly acknowledged. The interest of all the authors and the contribution of all the reviewers is greatly acknowledged.

Conflict of Interest: The authors declare that the research was conducted in the absence of any commercial or financial relationships that could be construed as a potential conflict of interest.

Publisher's Note: All claims expressed in this article are solely those of the authors and do not necessarily represent those of their affiliated organizations, or those of the publisher, the editors and the reviewers. Any product that may be evaluated in this article, or claim that may be made by its manufacturer, is not guaranteed or endorsed by the publisher.

frontiers in Built Environment

ORIGINAL RESEARCH
published: 05 February 2021
doi: 10.3389/fbuil.2021.631315

Seismic Retrofitting Solutions for Precast RC Industrial Buildings Struck by the 2012 Earthquakes in Northern Italy

Fabio Minghini[1]* *and Nerio Tullini*[1]

Engineering Department, University of Ferrara, Ferrara, Italy

In 2012, the North of Italy was hit by a seismic sequence characterized by two main events occurred on May 20 and 29 with M_W = 6.1 and 6.0, respectively. Those earthquakes were particularly severe toward precast Reinforced Concrete (RC) structures not designed for seismic resistance. In the past years, the authors implemented a database collecting damage data and typological information on the industrial buildings struck by the Emilia earthquakes. That database was used to develop empirical fragility curves, which highlighted the considerable vulnerability of precast buildings conceived in accordance with pre-seismic code provisions. More recently, the interventions of seismic retrofitting on the same buildings, funded by the Emilia-Romagna region and designed by engineers which were directly hired by the companies, were examined in detail and critically revisited. A selection of these interventions is presented in this paper, which analyzes the effectiveness of the various retrofitting solutions, with a specific attention to the force transfer mechanisms between existing structures and strengthening systems. The interventions are divided between column strengthening (based, for example, on RC or steel jacketing) and interventions aimed at providing the building with a suitable earthquake resistant system (based, for example, on either the use of the existing cladding panels or the implementation of new bracing systems). Graphical representations of the analyzed solutions with the relevant construction details are provided.

Keywords: seismic retrofitting, precast building, industrial building, jacketing, steel bracing, Emilia earthquake

OPEN ACCESS

Edited by:
Andrea Belleri,
University of Bergamo, Italy

Reviewed by:
Francesco Clementi,
Marche Polytechnic University, Italy
Daniele Perrone,
University Institute of Higher Studies in Pavia, Italy

***Correspondence:**
Fabio Minghini
fabio.minghini@unife.it

Specialty section:
This article was submitted to Earthquake Engineering, a section of the journal Frontiers in Built Environment

Received: *19 November 2020*
Accepted: *05 January 2021*
Published: *05 February 2021*

Citation:
Minghini F and Tullini N (2021) Seismic Retrofitting Solutions for Precast RC Industrial Buildings Struck by the 2012 Earthquakes in Northern Italy. Front. Built Environ. 7:631315. doi: 10.3389/fbuil.2021.631315

INTRODUCTION

The region hit by the 2012 Emilia earthquakes is one of the most productive areas in Italy. It is enough to think of the number of industrial buildings located in the Emilia-Romagna region, which is almost 80,000, corresponding to about 12% of the industrial buildings in the whole Italy.

The majority of these buildings are single-storey precast Reinforced Concrete (RC) structures, with columns clamped at the base, main girders simply supported at the column tops and secondary beams or slab elements spanning in the direction orthogonal to the main girders and simply supported on them (Colombo et al., 2012). Some buildings might have an intermediate floor portion hosting offices, usually located in eccentric position along one of the two short edges. In some case, a precast vaulted roof may be present (Poiani et al., 2020).

The struck region was not covered by seismic design provisions until October 2005. As a consequence, most of the industrial buildings in the region featured friction-based connections

between the various precast members and were lacking of any structural redundancy. This led to a huge number of brittle failure mechanisms associated with the loss-of-support of beams and slabs, and with the out-of-plane collapse of cladding panels. In addition, heavy damages to columns were observed in several cases, such as the formation of a plastic hinge at the base.

Several researches have analyzed the causes of damages and collapses that affected the industrial buildings in Emilia (Liberatore et al., 2013; Bournas et al., 2014; Magliulo et al., 2014; Belleri et al., 2015a; Ercolino et al., 2016; Minghini et al., 2016; Savoia et al., 2017). All studies agrees that deficiencies of connections represent the main cause of collapses, followed by inadequacy of column reinforcement and foundations. Recent studies show that also the vertical component of the ground motion (Bovo and Savoia, 2019), particularly in the free field, and masses of overhead cranes and hoist loads (Belleri et al., 2017), which may be often present in industrial buildings, could have played a role in the landscape of damages.

Due to the above rembered critical issues, a growing interest for fragility assessments of pre-seismic industrial buildings from a regional perspective is observed in Italy (Casotto et al., 2015). With specific regard to the Emilia earthquakes, a damage database was implemented by Minghini et al. (2016) and used by Buratti et al. (2017) for the evaluation of empirical fragility functions. The information collected in that database includes geolocalization, structural typology, dimensions, construction details and damage state for more than 1,400 precast RC buildings. The damage data were derived from reports prepared by professional engineers appointed by building owners to survey the buildings, design retrofitting interventions and apply for regional funds. These reports were validated by a public in-house company in charge of assessing the coherence of public funding with the planned interventions. Depending of the damage state, the funding was available for either reconstruction or retrofitting (Emilia-Romagna Regional Decree No. 57, 2012), but also the interventions on undamaged buildings characterized by structural deficiencies were funded. From the fragility assessment performed by Buratti et al. (2017), pre-seismic precast buildings result to be much more vulnerable than cast-in-place framed buildings, so requiring the introduction of specific fragility models.

These results are confirmed by recent analyses based on the official database of the Emilia-Romagna region (Rossi et al., 2019; Rossi et al., 2020). The latter includes information concerning not only industrial buildings, but also precast structures used for business activities in trade or agriculture, and allowed for comprehensive loss analyses.

The predominance of damages related with connections deficiencies justifies the two-step intervention strategy which was planned for the struck territory since June 2012 (Legislative Decree No. 74, 2012).

In the first step, in order to ensure the temporary usability of the buildings, it was mandatory to provide connections with mechanical devices able to prevent the unseating of precast elements and collapse of cladding panels. Sometimes, friction-based connections were strengthened using post-inserted dowels. These connections may exhibit a pseudo-ductile behavior, provided that they are designed to develop dowel yielding and avoid concrete splitting failure. For a detailed analysis of the seismic response of precast buildings with dowel-type connections the reader is referred to recent studies by Clementi et al. (2016) and Mezzapelle et al. (2017).

In the second step, structural safety verifications of the buildings were to be carried out, followed, if necessary, by seismic retrofitting.

For some recent study on how to reproduce numerically the seismic response of precast buildings for safety verifications, the reader is, for example, referred to Fischinger et al. (2014). Some solutions for first- and second-step interventions were discussed by Belleri et al. (2015b). Proposals for soil and foundation strengthening were presented by Maugeri et al. (2013). The graphical data sheets for the retrofitting interventions proposed by Colombo et al. (2012) inspired several engineers in developing design solutions for precast buildings damaged by the Emilia earthquakes. However, those proposals, have not always been tailored to specific design situations and existing precast members' dimensions. As a result, they may have been misinterpreted, sometimes resulting in a not full effectiveness of the retrofitting.

AIMS AND OBJECTIVES

The database implemented by Minghini et al. (2016) was recently enriched to include information on retrofitting solutions adopted for precast buildings in Emilia. This paper presents a graphical representation of some of these interventions, and presents for them a critical analysis. The main objective of this study is to investigate the stress transfer mechanisms which potentially arise between existing structures and strengthening systems. A further objective is to propose, for some case, an improved solution characterized by more effective stress transfers.

In order to cover a spectrum of design solutions as large as possible, the described retrofitting interventions make use of quite common materials, methods and technologies. Hence, advanced devices, such as, for example, those investigated by Pollini et al. (2018), although of great significance, are out of the scope of this study.

Finally, some consideration on the influence of roof stiffening is presented. For the building typologies covered by this study, the roof slabs do not possess, in general, an in-plane stiffness sufficient to behave as a rigid diaphragm. However, some retrofitting solution may involve roof stiffening for various reasons. For example, to make effective the introduction of bracing systems, the deformable roofs must be stiffened. This will imply a change in the force distributions which should be accounted for.

CRITICAL ANALYSIS OF RETROFITTING INTERVENTIONS

For reading convenience the intervention proposals described are divided in column strengthening, interventions on cladding panels and implementation of new bracing systems.

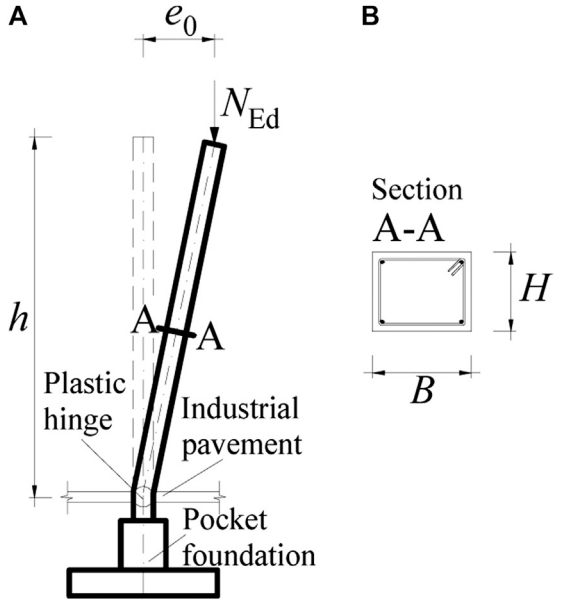

FIGURE 1 | Precast column with flexural plastic hinge at the base: **(A)** elevation and **(B)** cross-sectional view. Longitudinal reinforcement comprised of four 18 mm-diameter corner bars (A_s = 1,018 mm^2).

Column Strengthening

In modern precast buildings, columns and their connections with the foundations are designed to exhibit stable cyclic behavior with good dissipating properties and capacity comparable with that of cast-in-place columns (Dal Lago et al., 2016; Tullini and Minghini, 2020). In existing buidings, these characteristics are not present.

The retrofitting solutions presented in this section derive from the need for column strenghtening due to either the presence of an insufficient longitudinal reinforcement inside the column or a flexural capacity degraded as a consequence of seismic damage. For example, the interventions described in *Steel Jacketing* section may serve to increase the column capacity up to acceptable values, whereas the intervention presented in *RC Jacketing* section could be applied even to an heavily damaged column with plastic hinge fully developed at its base. In this case, the contribution due to existing concrete and reinforcing steel is nullified, and the strengthening material should be designed to completely balance the bending moment and shear acting at the column base in the relevant design situations.

However, in the presence, at the end of a seismic event, of residual deformations, the columns may often result to be unrepairable. This is the case, for example, for columns experiencing either rigid base rotations due to foundation settlements or so significant flexural damage to remain inclined after the earthquake.

Despite the fact that Regional Decree No. 57 (2012) discriminates between unsalvageable and heavily damaged, but still repairable industrial buildings on the basis of, in addition to other damage parameters, the number of columns suffering a residual drift larger than 2% (see Table 1 reported by Minghini et al., 2016), it is worth observing that a smaller drift limit should be used to identify the damage level at the end of the seismic event. In fact, a 2% drift is more likely to represent the maximum deformation attained during the seismic event (FEMA 356, 2000) rather than the permanent deformation at the end of shaking. A proof of this feature is reported in the following with regard to the precast column shown in **Figure 1**, presenting a permanent drift e_0/h due to the formation of a plastic hinge at the base. The column belongs to an industrial building damaged by the first mainshock of the Emilia seismic sequence. The limiting residual drift for the column is estimated in **Table 1**, using the method based on the nominal curvature (CEN, 2004a) to take account of second order effects. According with these calculations, a permanent drift larger than 0.7% is sufficient to cause buckling collapse of the column under the roof self weight.

Therefore, the following retrofitting solutions are strictly tailored to columns not affected by significant permanent drift.

Steel Jacketing

Steel jackets for rectangular RC columns are usually comprised of four angles placed at the corners and a certain amount of horizontal steel strips. These strips, welded to the angles with a certain spacing between one another, are often pre-heated just prior to welding in order to trigger a confinement action on the column.

It is widely recognized (CEN, 2005) that steel jackets may profitably be used in seismic retrofitting of existing RC columns to 1) enhance the shear capacity; 2) prevent failure of lap splices through increased confinement and 3) improve the available curvature ductility in critical regions, once again due to confinement (**Figure 2A**). In this case, the angles must not necessarily be anchored to the foundation. Several post-earthquake survey reports indicate that the RC pavement, although not mechanically connected with the columns, may play a role in cooperation with the pocket foundation in restraining rotations at the column base. This is testified by evidence showing that at the base of inner columns, where the pavement is present at all sides, the plastic hinge tends to form immediately above the pavement (Liberatore et al., 2013; Minghini et al., 2016; Savoia et al., 2017). Therefore, to enhance curvature ductility at the column base it is sufficient to insert the jacket into the pavement up to midplane.

As a possible alternative to the use of steel jackets, Fiber Reinforced Polymer (FRP) plating and wrapping of columns may be used with analogous benefits.

In Northern Italy, particularly after the 2012 Emilia earthquakes, in addition to the three main uses remembered above, steel (and also FRP) jackets are being used to increase the flexural capacity of precast RC columns (Colombo et al., 2012). In this section, we are referred to steel jackets in which the corner angles are attributed the role of longitudinal reinforcement for the column.

The effectiveness of such interventions strictly depends on stiffness and strength of the connection between angles and column. In fact, the angles may be considered as an additional column reinforcement only if they are connected to the column in a manner that the slip at the interface between angles and column

TABLE 1 | Estimate of the residual drift corresponding to instability under permanent loads for a typical precast RC column (**Figure 1**) not designed for earthquake resistance.

Symbol/description [Unit]		Equation	Value
Column geometry and loads			
h	Column height [m]		7
B	Cross section width [mm]		500
H	Cross section depth [mm]		400
d	Effective cross section depth [mm]		350
l_0	Effective column length [m]	$l_0 = 2h$	14
i_{min}	Minimum radius of gyration [mm]	$i_{min} = H/\sqrt{12}$	115
λ_{min}	Column slenderness [-]	$\lambda_{min} = l_0/i_{min}$	121
g_g	Self-weight of girder per unit length [kN/m]		7.1
g_s	Self-weight of roof elements per unit area [kN/m^2]		3.5
L_1	Span length of the girder [m]		15
L_2	Span length of roof elements [m]		7.5
N_{Ed}	Column axial load [kN]	$N_{Ed} = g_g L_1 + g_s L_1 L_2$	500
Material properties and base section bending resistance			
f_{ck}	Characteristic concrete compressive strength [MPa]		28
γ_c	Concrete partial factor [-]		1.5
α_{cc}	Factor for long term effects [-]		0.85
f_{cd}	Design concrete compressive strength [MPa]	$f_{cd} = \alpha_{cc} f_{ck}/\gamma_c$	15.9
f_{yk}	Characteristic yield stress for steel [MPa]		430
γ_s	Steel partial factor [-]		1.15
f_{yd}	Design yield stress for steel [MPa]	$f_{yd} = f_{yk}/\gamma_s$	374
E_s	Modulus of elasticity for steel [GPa]		200
ε_{yd}	Design yield strain [‰]	$\varepsilon_{yd} = f_{yk}/(\gamma_s E_s)$	1.87
A_s	Total area of longitudinal reinforcement [mm^2]		1,018
M_{Rd}	Ultimate moment resistance of column base section [kNm]		140
Second order effects [see Sect. 5.8.8 of CEN (2004a)]			
$1/r$	Curvature at the column base section [‰/m]	$1/r = K_r K_\varphi \varepsilon_{yd}/(0.45d)$	11.9
K_r	Correction factor for the axial load [-]		1
K_φ	Correction factor for creep [-]		1
M_2	Nominal second order moment [kNm]	$M_2 = N_{Ed} e_2$	117
e_2	Second order horizontal displacement [mm]	$e_2 = (1/r) l_0^2/c$	233
c	Factor depending on curvature distribution [-]		$\pi^2 \approx 10$
$(e_0/h)_{max}$	Drift causing column buckling [%]	$(e_0/h)_{max} = (M_{Rd} - M_2)/(N_{Ed} h)$	0.7

is prevented. Moreover, when undergoing compressive stresses, the angles should not suffer early buckling. Therefore, the angle-to-column connections play an even more important role, as well as the spacing of the steel strips. Another essential requirement is that the angles are effectively connected with the foundation. In fact, the angles may serve as an additional column reinforcement at the base, i.e., at the point where the earthquake-induced bending moment in the column takes its maximum, only in the presence of an effective connection with the foundation.

An example showing some of the critical issues raised from steel jacket-to-RC foundation connections is briefly discussed hereinafter. The column shown in **Figure 2B**, having cross-section dimensions of 400 mm × 500 mm, is considered. The mean values of concrete compressive strength and reinforcing steel yield strength are f_{cm} = 40 MPa and f_{ym} = 380 MPa, respectively. A knowledge level KL2 is adopted according to CEN (2005), resulting in a confidence factor CF = 1.2. The column axial compression corresponding to the relevant seismic load combination is N_{Ed} = 233 kN. In the absence of any seismic retrofitting, the stress transfer between column and pocket foundation is analogous to that reported by Eurocode 2 (see CEN, 2004a, Fig. 10.7b). Provided that the pocket walls do not experience premature failure due to bending moment and shear load at the column base, the bending resistance of the column due to the existing reinforcement would result to be equal to $M_{Rd,c}$ = 236 kN m. The seismic demand in terms of bending moment at the column base is given by M_{Ed} = 449 kN m, leading to column safety level $\zeta_E = M_{Rd,c}/M_{Ed}$ = 0.53. Therefore, it is decided to retrofit the column. To this purpose, a steel jacket comprised of four angles with cross-section dimensions 150 mm × 150 mm × 10 mm and 400 mm-spaced strips was used. Both angles and strips are made of steel of class S 275, with characteristic yield and ultimate strengths of f_{yk} = 275 MPa and f_{tk} = 430 MPa, respectively. At the column base, the angles are welded to steel plates, which are connected to the foundation by means of 16 threaded rods with the diameter of 16 mm (**Figure 2C**). These rodes are adhesively bonded to the 150 mm-thick pocket walls with an embedment depth of h_{ef} = 450 mm.

Such a jacket-to-column connection modifies the stress transfer mechanism between column and pocket foundation. The bending moment and shear force at the column base, particularly in the case of a reduced hole clearance between anchors and steel plate, are now transferred directly to the top of the pocket walls. On the tension side, if the anchors were able to develop the whole yield strength of the angles, the bending resistance at the column base would become $M_{Rd,c}$ = 809 kN m, resulting in $\zeta_E > 1$. However, with regard to the

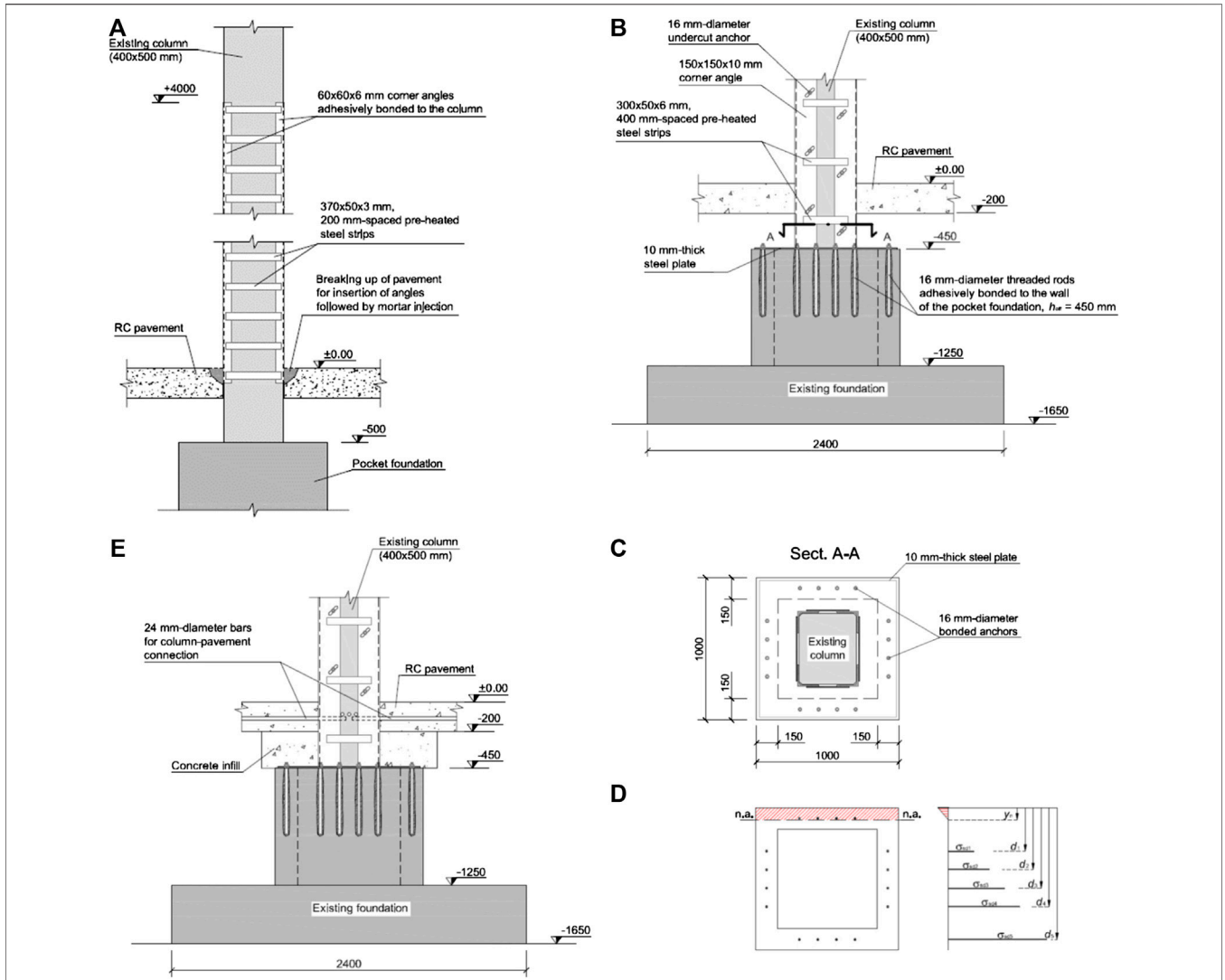

FIGURE 2 | Steel jackets applied to precast RC columns: **(A)** corner angles inserted into the pavement but not anchored to the foundation; **(B)** jacket connected to the pocket walls by means of bonded anchors, **(C)** corresponding in-plan anchors arrangement and **(D)** calculation model for bending resistance of the pocket; **(E)** the same as **(B)** plus column-to-pavement connection. Dimensions in mm.

concrete-related failure mechanisms that can develop for the four anchors in tension, the maximum anchored force cannot balance the angle yield force. The design anchored force may be estimated based on the following relation (CEN, 2018):

$$N_{\mathrm{Rd,p}} = \frac{\tau_{\mathrm{Rk}}}{\gamma_{\mathrm{Mp}}} \pi d h_{\mathrm{ef}} \frac{A_{\mathrm{p},N}}{A^0_{\mathrm{p},N}} \psi_{\mathrm{g},Np} \psi_{s,Np} \tag{1}$$

corresponding to combined pull-out and concrete failure. In **Eq. 1**, τ_{Rk} represents the characteristic bond strength, d is the anchor diameter, ratio $A_{\mathrm{p},N}/A^0_{\mathrm{p},N}$ depends on anchors spacing and edge distances, whereas coefficients $\psi_{\mathrm{g},Np}$ and $\psi_{s,Np}$ take account of group effects for closely spaced anchors and disturbance of the stress distribution due to edge proximity, respectively. Moreover, partial safety factor takes the form

$$\gamma_{\mathrm{Mp}} = \gamma_{\mathrm{c}} \gamma_{\mathrm{inst}} \tag{2}$$

with γ_{c} = 1.5 and γ_{inst} being the usual partial safety factor for concrete and a safety factor related to the installation conditions, respectively. Assuming normal installation safety, γ_{inst} = 1.2 in **Eq. 2**, leading to γ_{Mp} = 1.8.

For a foundation made of concrete of class C25/30, in the case of cracked concrete and a characteristic bond strength τ_{Rk} = 7 MPa (a typical value for adhesives available on the market), $\psi_{\mathrm{g},Np}$ = 1.29, $\psi_{s,Np}$ = 0.82 and $A_{\mathrm{p},N}/A^0_{\mathrm{p},N}$ = 0.83 due to the very narrow walls. Substituting these coefficients into **Eq. 1** yields $N_{\mathrm{Rd,p}}$ = 78 kN. Therefore, indicating with A_{res} = 157 mm^2 the effective cross-section area of each threaded rod, the anchors can develop a tensile stress of $\sigma_{\mathrm{sd}} = N_{\mathrm{Rd,p}}/(4A_{\mathrm{res}})$ = 124 MPa, corresponding to only 19% of their nominal yield strength (=640 MPa). The horizontal section of the pocket walls may

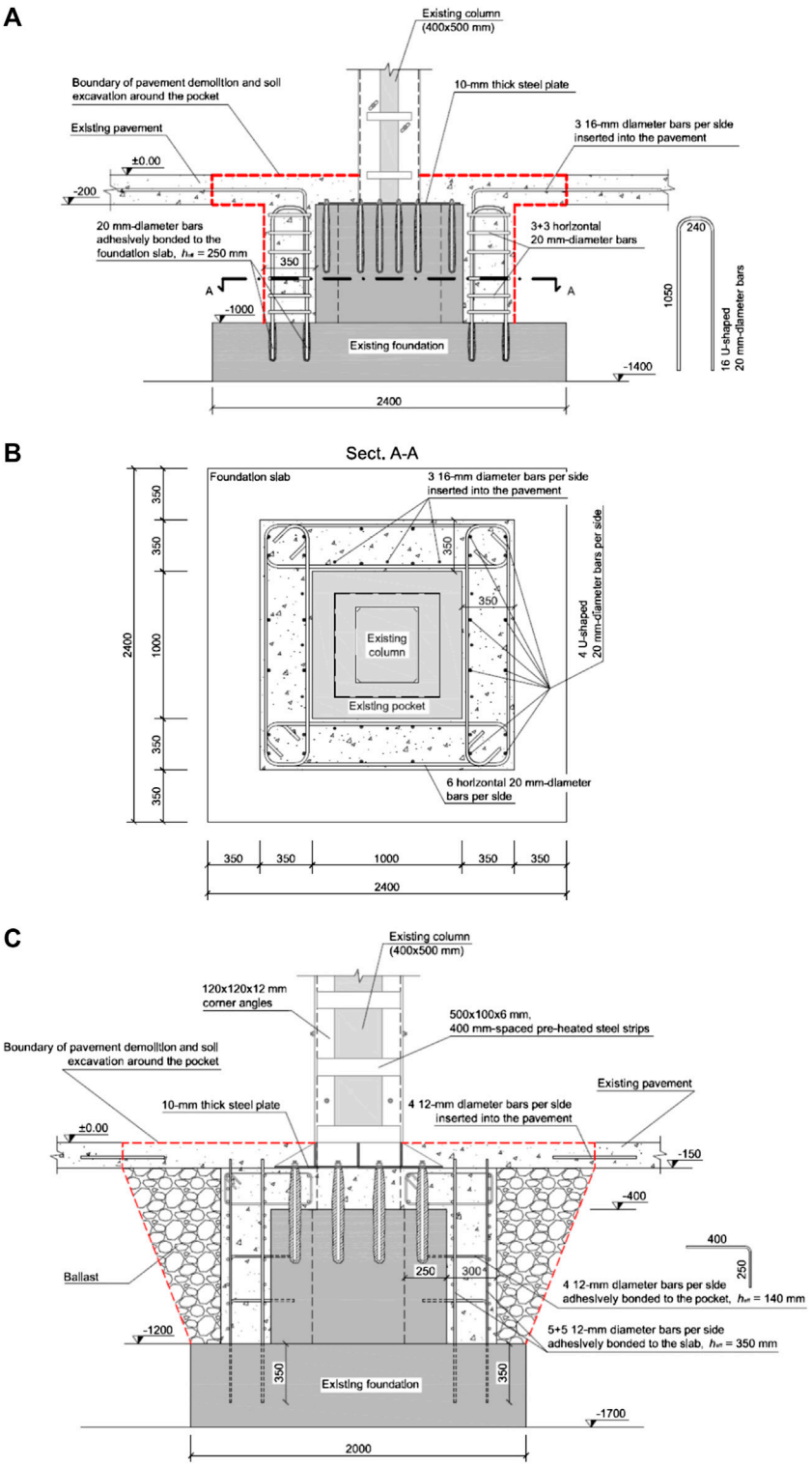

FIGURE 3 | Steel jacketing of precast columns in association with foundation strengthening: **(A)** vertical and **(B)** horizontal sectional views of pocket strengthened by a cast-in-contact RC jacket; **(C)** RC jacket applied to the sides and top of the existing pocket walls and connected to them by means of bonded ancors. Dimensions in mm.

be regarded as a RC section, with the reinforcement being represented by the anchors (**Figure 2D**). The bending resistance of this section, for the tensile stress in the anchors limited to σ_{sd}, turns out to be $M_{Rd,f}$ = 108 kN m, corresponding to a largely insufficient safety level of $\zeta_E = M_{Rd,f}/M_{Ed}$ = 0.24. However, this prediction neglects the contribution of the reinforcement which is present in the foundation. Each pocket wall is reinforced with six 10 mm-diameter bars, corresponding to a reinforcement area A_{sb} = 471 mm^2. It is thus evident that the yield strength of the anchors cannot be achieved. The maximum tensile stress which can be developed by the anchorage may be computed from the following relation:

$$N_{yd,b} = \frac{A_{sb} f_{ym}}{CF} = 4A_{res}\sigma_{sd} \quad (3)$$

where for the reinforcing bars in the foundation the mean yield strength f_{ym} = 380 MPa is assumed in analogy with the column reinforcement. Solving **Eq. 3** for the tensile stress in the anchors leads to $\sigma_{sd} = N_{yd,b}/(4A_{res})$ = 238 MPa, corresponding to 37% of their nominal yield strength. Recalculating the bending resistance of the foundation for this updated value of σ_{sd} yields M_{Rd} = 206 kN m and ζ_E = 0.46. Therefore, the anchorage of the steel jacket to the foundation still represents the weak link in the chain. Being $\zeta_E \leq 0.6$, the safety level is insufficient and precludes usability of the building. This feature may become even more critical for all cases in which reinforcement ratio or thickness of the pocket walls are smaller than for the example presented. The strength of the jacket-to-foundation connection should then be improved.

As a first improvement, the intervention shown in **Figure 2E** is considered. Compared with the previous case, a soil volume between top of the pocket walls and bottom pavement surface is replaced with a concrete infill, and column-to-pavement connections are performed. In particular, three 24 mm-diameter bars per column side are positioned in grooves specially created within the pavement and inserted into the column, to which they are connected through adhesive bonding. On the column tension side, the out-of-plane bending of the base steel plate induced by vertical tension forces in the angles may activate a compression field in the concrete infill, and then in the pavement. This concrete strut will have an approximately vertical direction and will exert a shear force on the bars used for column-to-pavement connection. The associated shear resistance potentially represents an additional contribution to the bending resistance of the foundation.

A further improvement may be obtained by strengthening the pocket walls as shown in **Figures 3A,B**. To this purpose, the pavement should be demolished around the column to allow for RC jacketing the existing pocket walls. The vertical reinforcement in the new four RC walls provides additional bending strength to the foundation, especially if a sufficient friction between the existing pocket and its jacket is ensured. In this case, inclined compression struts originating from the anchors in tension make activate the vertical reinforcing bars contained in the jacket, providing the foundation with the necessary bending strength. Depending on the vertical reinforcement ratio of the pocket jacket, a capacity design of type "strong foundation-weak column" may be achieved, in which the foundation is given a suitable bending overstrength. This intervention also improves the shear strength of the foundation.

In order to enhance the stress transfer within the foundation, a number of mechanical connections between the existing pocket and its RC jacket may be prescribed. Compared with the previous solution, the shear strength of the interface between new and existing concretes now relies not only on the roughness of the interface itself, but also on the area of reinforcement crossing it (see Eq. 6.25 reported by CEN, 2004a). Therefore, the contribution of the vertical reinforcement contained in the pocket jacket is even more likely to be activated. In the proposal shown in **Figure 3C**, 12 mm-diameter bonded bars are used to connect the new RC jacket to both slab and pocket walls of the existing foundation. Moreover, in addition to the side strengthening, a slab is cast at the same time on the top of the pocket walls, resulting in a column-to-foundation connection emulating a monolithic connection. Before the described interventions of steel jacketing of columns and foundation strengthening, the safety level of the building in terms of capacity-to-demand ratio was of 0.37. The ultimate limit state conditions were governed by columns bending failure. Due to the retrofitting, an increase of 62% in the global safety level is obtained, leading to a capacity-to-demand ratio of 0.6.

RC Jacketing

RC jackets are particularly suited to columns requiring a significant increase of both bending resistance and stiffness. For example, slender columns with $b/H < 0.1$, with b and H being maximum column cross-section dimension and column height, respectively, may profitably be retrofitted by RC jacketing, becoming less vulnerable to second-order effects. Moreover, also shear strength, ductility of critical regions and strength of deficient lap-splices are usually improved by the presence of a RC jacket. The calculation of enhanced column properties is usually based on the following simplifying assumptions (CEN, 2005):

1) full composite action between new and existing concretes;
2) axial load acting on the entire jacketed column section;
3) concrete properties of the jacket extended to the existing concrete too.

In the case of precast RC columns with pocket foundations, the jacket-to-foundation connection should be designed with particular care to obtain an efficient stress transfer mechanism and full development of the jacket bending resistance.

An intervention proposal is described hereinafter with regard to the precast column shown in **Figure 4A**, for which the safety verifications indicate insufficient bending resistance, excessive lateral deformability and inadequate confinement at the base due to the presence of stirrups without hooked ends. A concrete jacket reinforced with sixteen 20 mm-diameter bars is then used to retrofit the column. The intervention is carried out in the following steps:

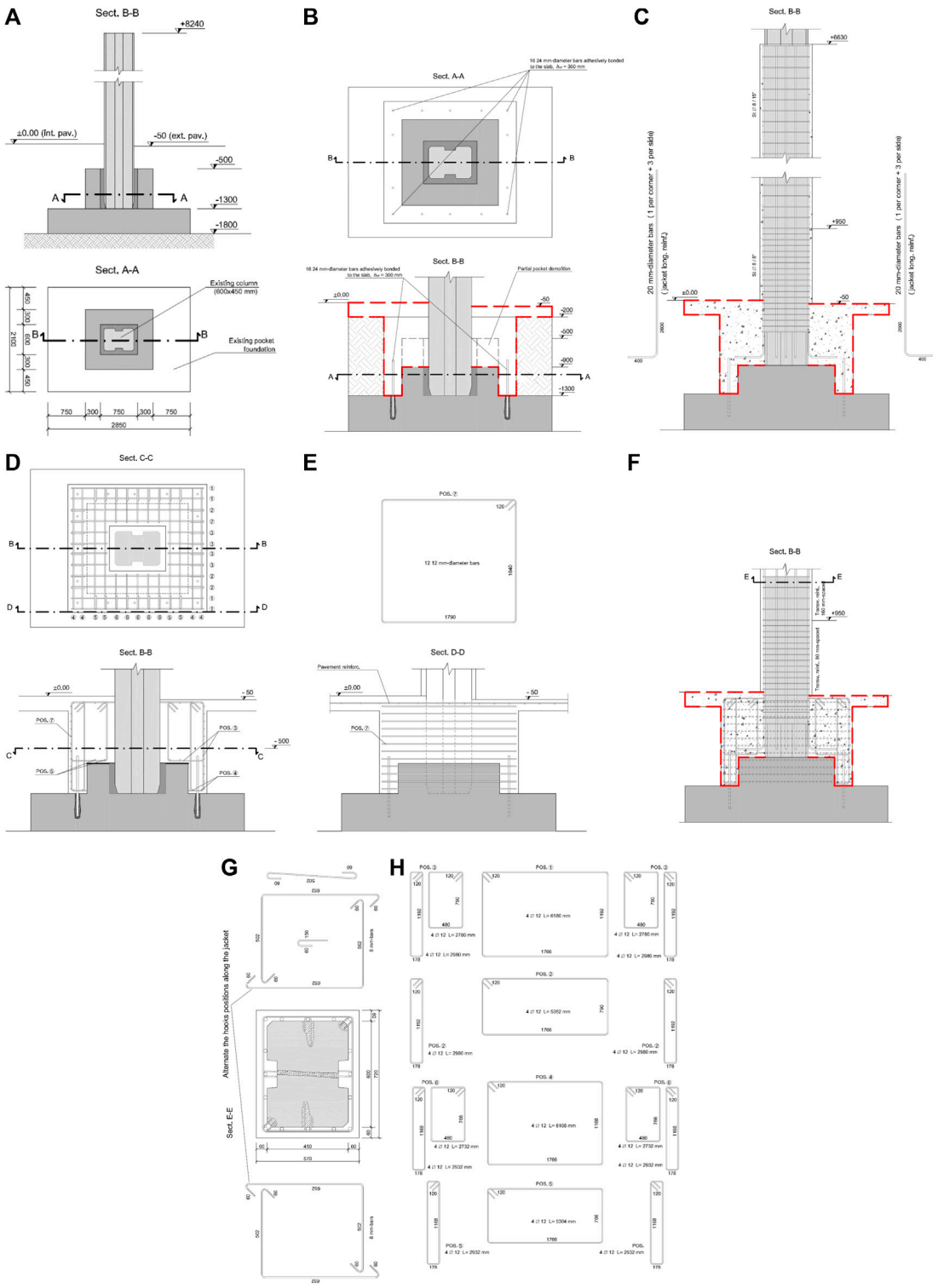

FIGURE 4 | (A) Precast RC column needing both flexural strengthening and stiffening; RC jacketing for the column of **(A)**: **(B)** partial pocket demolition and installation of bonded anchors into the existing slab; **(C)** positioning of jacket reinforcement; positioning of **(D)** vertical and **(E)** horizontal reinforcement for foundation strengthening; details of **(F)** final column-to-foundation connection, **(G)** jacketed column cross-section, and **(H)** foundation vertical reinforcement shown in **(D)**. Dimensions in mm.

1) pavement demolition around the column;
2) partial soil excavation up to the top surface of the foundation slab;
3) partial demolition of pocket walls,
4) insertion of bonded anchors into the slab (for steps 1 to 4 see **Figure 4B**);
5) positioning of jacket (longitudinal and transverse) reinforcement (**Figure 4C**);
6) positioning of vertical reinforcement (**Figure 4D**) and of
7) horizontal reinforcement (**Figure 4E**) for foundation strengthening;
8) casting of concrete for both jacket and foundation.

The strengthened foundation is a sort of new, better performing pocket foundation and the resulting column-to-foundation connection emulates typical cast-in-place connections (**Figure 4F**). The confinement action along the critical region at the column base is achieved by means of 80 mm-spaced suitably designed links. In particular, peripheral transverse reinforcement and links crossing the whole column section, or adhesively bonded to it, are used so as to engage one every two longitudinal bars of the jacket (**Figure 4G**). Construction details for the vertical reinforcement used for foundation strengthening are given in **Figure 4H**.

The described intervention was proposed for a building located at about 10 km from the epicentre of the first mainshock of the Emilia earthquake. The building reported flexural and shear cracks in some of the columns and severe damages to nonstructural elements. The building capacity-to-demand ratio before the retrofitting was of 0.12. In addition to the application of a RC jacket to all of the columns, the retrofitting included a mass reduction, obtained by replacing the concrete cladding panels with lightweight sandwich panels (see *Substitution of Cladding Panels With Lightweight Sandwich Panels* section). Disassembling the existing cladding allowed to easily jacket also peripheral columns before the installation of the new cladding system. Due to these interventions, the building safety level increased up to 0.62.

For another precast building, substantially undamaged but characterized by insufficient column reinforcement, analogous interventions were designed. The building is located in the Scientific-Technological campus of the University of Ferrara, at about 40 km from the epicentre. The mass reduction was judged not necessary in this case, being the cladding already comprised of lightweight sandwich panels. However, due to proximity to another structure, there was the need to stiffen, and not only to strengthen, the columns, so as to avoid pounding. Design calculations showed that jacketing only eight of the 21 columns results to be sufficient to ensure an increase of 54% in the safety level, leading to a global safety factor of 0.63.

Column Doubling

For slightly damaged or undamaged buildings, an additional requirement for the seismic retrofitting may sometimes be that the productive activity should not be interrupted during the works. In order to maintain the building fully operational and avoid any interference in production, retrofitting solutions involving building strengthening on the outside only should be preferred.

The solutions shown in **Figure 5** are concerned with strengthening each of the existing precast columns of a single-storey industrial building with a new Cast-In-Place (CIP) column joined on the outside. All CIP columns are connected with one another at the base by a new foundation beam. In the proposal reported in **Figure 5A**, the CIP column has the same cross-section dimensions as the existing column and is connected with it by means of adhesively bonded bars with the diameter of d_b = 25 mm, entirely crossing the RC cladding panels. These connections should be designed to transfer part of the earthquake induced shear force to the CIP column, which is assumed non-dissipative and results to be heavily reinforced. As an indirect, but not less important benefit, the CIP columns help maintaining the RC cladding panels attached to the building, so that no specific device is required to overcome the panel-to-column connection deficiencies and avoid the out-of-plane collapse of panels. However, due to the presence of a drain pipe in centroidal position in the precast column, the bonded anchors are staggered along the column height and present a minimum edge distance of $c = 4d_b = 100$ mm only (**Figure 5B**). Therefore, especially for the horizontal ground motion component parallel to the cladding panels shown in **Figure 5B**, a significant connection strength degradation must be expected due to cyclic loading, and the most probable failure mechanism for the anchors will be a splitting failure (Vintzeleou and Tassios, 1987; CEN, 2018). In fact, for $c/d_b \leq 6$ more ductile failure mechanisms involving bar yielding and limited strength degradation are not activated. The strength associated to these mechanisms (Fischinger et al., 2014) would be proportional to the square root of the product of the concrete compressive strength (f_c) times the anchor yield strength (f_y). However, the concrete cover is too weak to allow for the development of f_y. Moreover, the transverse reinforcement of the existing columns, comprised of 6 mm-diameter stirrups with 200 mm spacing, is largely insufficient to balance the shear forces arising in the 25 mm-diameter bonded bars.

An improved solution is shown in **Figure 5C**, which proposes the use of a protective steel sheet connected to the existing column on the inside. The steel sheet is designed to act as a dense transverse reinforcement in avoiding premature splitting failure of the existing column. In this case, the dowel action mechanism of the bonded anchors will tend to develop a higher strength. The upper bound of the anchor shear strength associated to such a mechanism can be estimated from the following equation:

$$F_{Rd} = \frac{A_s f_{yd}}{\sqrt{3}}, \tag{4}$$

with A_s and f_{yd} representing anchor cross-section area and design yield strength, respectively. It is worth noting that when the concrete in proximity of the dowel is effectively protected against brittle failure, this upper bound may really be achieved and strength degradation due to cyclic loading will be negligible (Tullini and Minghini, 2016). However, the application of steel

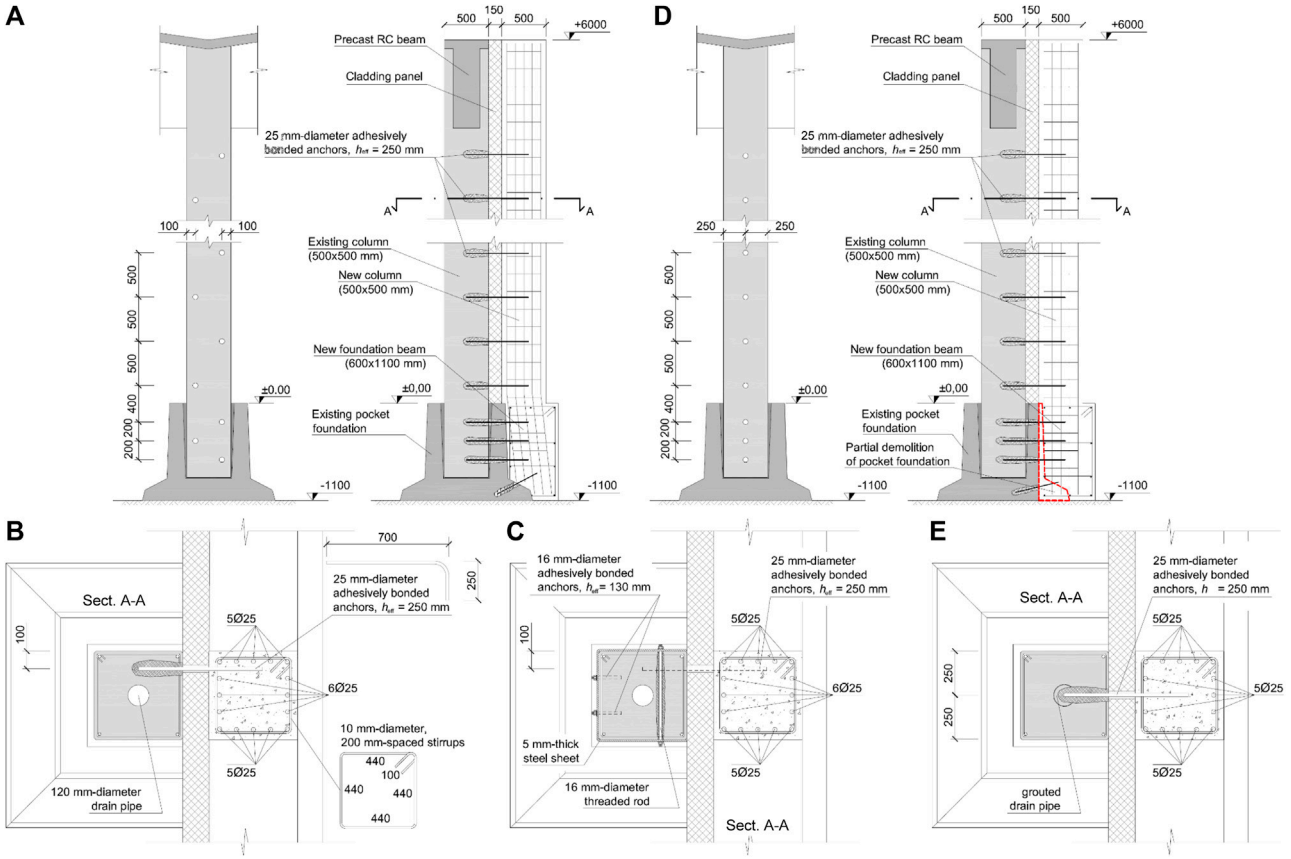

FIGURE 5 | Column doubling on the outside: **(A)** solution preserving the existing foundation with connectors near the column edges and **(B)** without or **(C)** with protective metal sheet; **(D)** solution involving partial demolition of existing foundation and **(E)** connectors far from edges. Dimensions in mm.

sheets to the columns may involve interference with the productive activity carried out in the building.

An alternative solution may thus be based on grouting the drain pipe so as to allow for the insertion of adhesively bonded bars into the column in correspondence of the external edge midside (**Figures 5D,E**). In this case, the edge distance to anchor diameter ratio is c/d_b = 10, and the maximum dowel action strength may develop without any further intervention.

Bending of starter bars of the strengthening columns may be avoided by partially demolishing the existing pocket foundations (**Figure 5D**).

The described intervention was proposed for a building located at about 15 km from the epicentre of the second mainshock of the Emilia earthquake. The building reported heavy damages to nonstructural elements and cracks at the base of some of the columns. The column doubling ensures an increase in the safety factor from 0.12 up to 0.6.

Interventions on RC Cladding Panels

It is well known that RC cladding panels may represent a source of significant seismic vulnerability for pre-seismic precast buildings. This is essentially due to the following two reasons:

1) they generally possess a significant mass;
2) their connections to precast columns or beams are not conceived to resist the shear forces due to in-plane seismic action.

Many available researches deal with vulnerability of RC cladding panels (Belleri et al., 2016; Belleri et al., 2018) and possible strategies to mitigate it (Biondini et al., 2013). In this section, two alternative approaches are presented.

Substitution of Cladding Panels With Lightweight Sandwich Panels

The substitution of RC cladding panels with lightweight sandwich panels obviously leads to a reduction of nonstructural masses, which may be significant especially for single-storey buildings. This mass reduction, at equal column stiffnesses, gives rise to a decrease in the fundamental period of the building and then to a demand increase in terms of spectral acceleration. It can be finally shown that, taking account of both mass reduction and acceleration increase, the cladding substitution may yield a decrease in the elastic base shear demand of about 8–15%. This intervention can thus be considered as a full-fledged seismic retrofitting.

For a single-storey building located in the Scientific-Technological campus of the University of Ferrara, Minghini

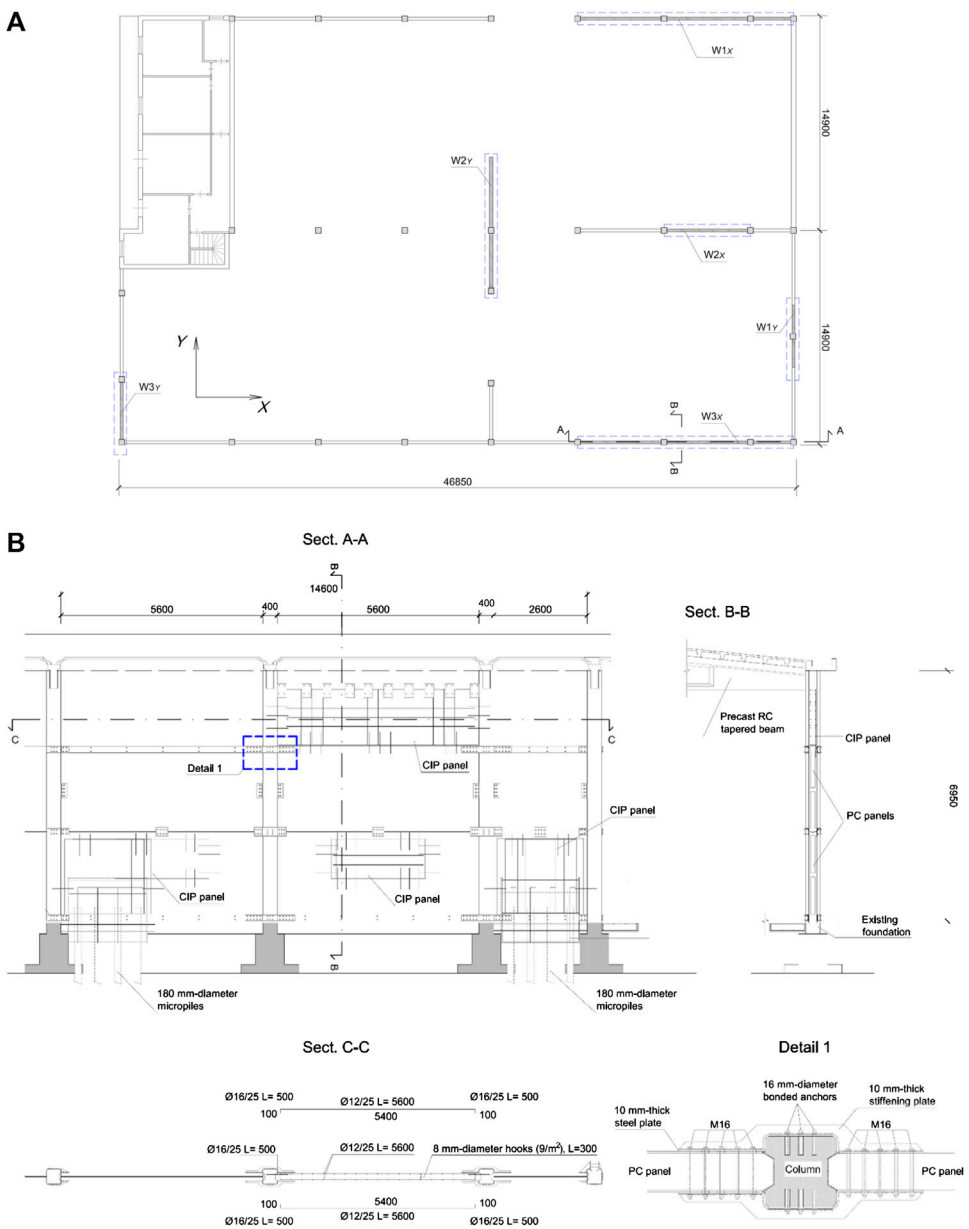

FIGURE 6 | RC cladding panels readapted as shear walls: **(A)** plan view of a building where three shear walls were obtained in both *X* and *Y* direction; **(B)** details for shear wall W_{3X}. Dimensions in mm.

et al. (2015) showed the benefit arising from cladding substitution through a set of nonlinear time-history analyses. Due to increase of confinement by means of steel jackets applied to critical regions of columns (similarly to what is shown in **Figure 2A**) and global mass reduction obtained from cladding substitution, the 9.5 m-high columns, although designed in origin with no particular seismic provisions, resulted characterized by a very stable cyclic behavior with limited post-peak degradation.

Use of Existing RC Cladding Panels as Shear Walls

This intervention proposal results to be effective in the presence of a roof slab behaving as a rigid diaphragm. For example purposes, the plan view of a precast industrial building is reported in **Figure 6A**. The 200 mm-thick cladding panels are spanning horizontally between 6 m-spaced columns, and are inserted vertically into specifically suited grooves in the column section.

The intervention consists in connecting the panels with one another along their horizontal common edges, and the panel vertical edges with the columns, so as to form a shear wall. For the building shown in **Figure 6A**, three shear walls are obtained for both *X* and *Y* direction. The construction details for one of these walls are reported in **Figure 6B**. To maximize the stiffening effects of this solution, the openings which were originally present

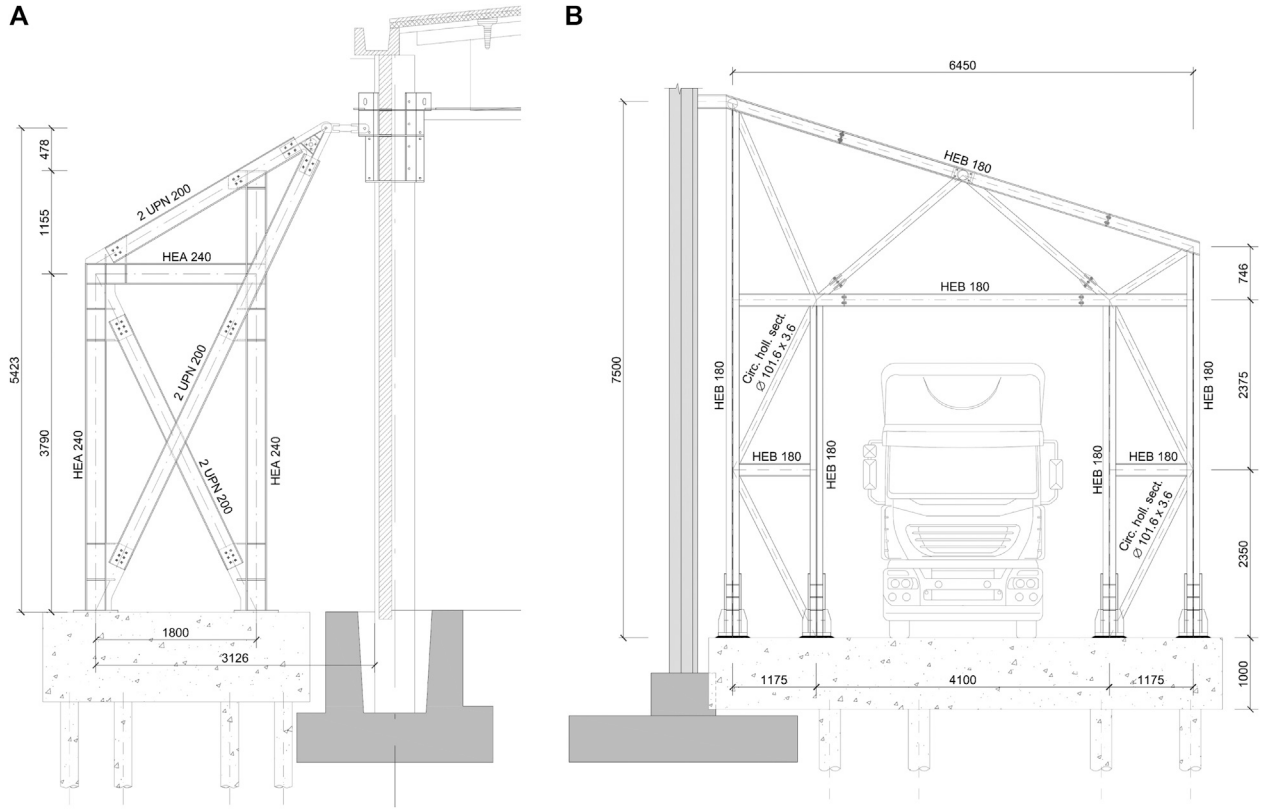

FIGURE 7 | Steel bracing systems applied to the outside of single-storey precast RC buildings: **(A)** single braced frame; **(B)** frame on laced built-up columns allowing for trucks circulation around the building. Dimensions in mm.

in the cladding panels are filled with CIP concrete, and a dense reinforcement is used to anchor CIP with existing precast concrete. Analogously, new RC panels are cast in the place of missing precast panels. Finally, in order to allow a more rigid and effective connection with micropiles used to strengthen the foundations, a portion of the existing panels at the bottom ends of the walls is cut out and replaced with a CIP panel.

The obtained shear walls can be designed to resist the entire seismic force on the building, so as to leave the columns not belonging to the strengthening system subjected to gravity loads only. Due to the very high ratio of horizontal to vertical loads acting on these walls, the deep foundations at the wall ends may result to be unavoidable to withstand global in-plane rocking.

A key role is played by panel-to-panel and panel-to-column connections, which may determine success or failure of the retrofitting solution. Therefore, a capacity design strategy assigning some overstrength to these connections can be useful. Alternatively, the connections may be attributed the role of dissipating energy by means of properly designed devices (see, for example, Biondini et al., 2013).

The evaluation of design forces may follow equilibrium-based simplified approaches analogous to those reported in Sect. 9 of Eurocode 5 for multi-panel timber structures (CEN, 2004b).

For the building shown in **Figure 6**, the intervention described leads to an increase of 80% in the safety factor.

New Steel Bracing Systems

Steel bracings may be effective in increasing the seismic resistance of precast buildings, especially for their reduced self weight and relative ease of connection with RC members. These systems are usually designed to resist the whole seismic force acting on the building or a significant portion of it. Two different design strategies should be followed depending of the in-plane stiffness of floor slabs and roof. In the case of rigid slabs and roof, steel bracing systems may be implemented in some "key points" of the building and their stiffening effect is transferred to all precast columns due to the in-plane floor stiffness. In the case of deformable slabs and roof, steel bracings in two orthogonal directions are required for each line of columns. In single-storey precast buildings struck by the Emilia earthquakes, typically featuring deformable roofs, the most used strategy is the latter.

The retrofitting solution shown in **Figure 7A** features steel frames comprised of I-section columns and beams, braced by diagonal built-up members using two back-to-back channels. These bracings converge into a node which is linked to the precast building in proximity of the beam-column node. The intervention is mainly carried out from the outside, so limiting the disturbance to the productive activity. However, the upper part of the precast column should generally be strengthened to resist the point forces transferred from the bracing system. Due to

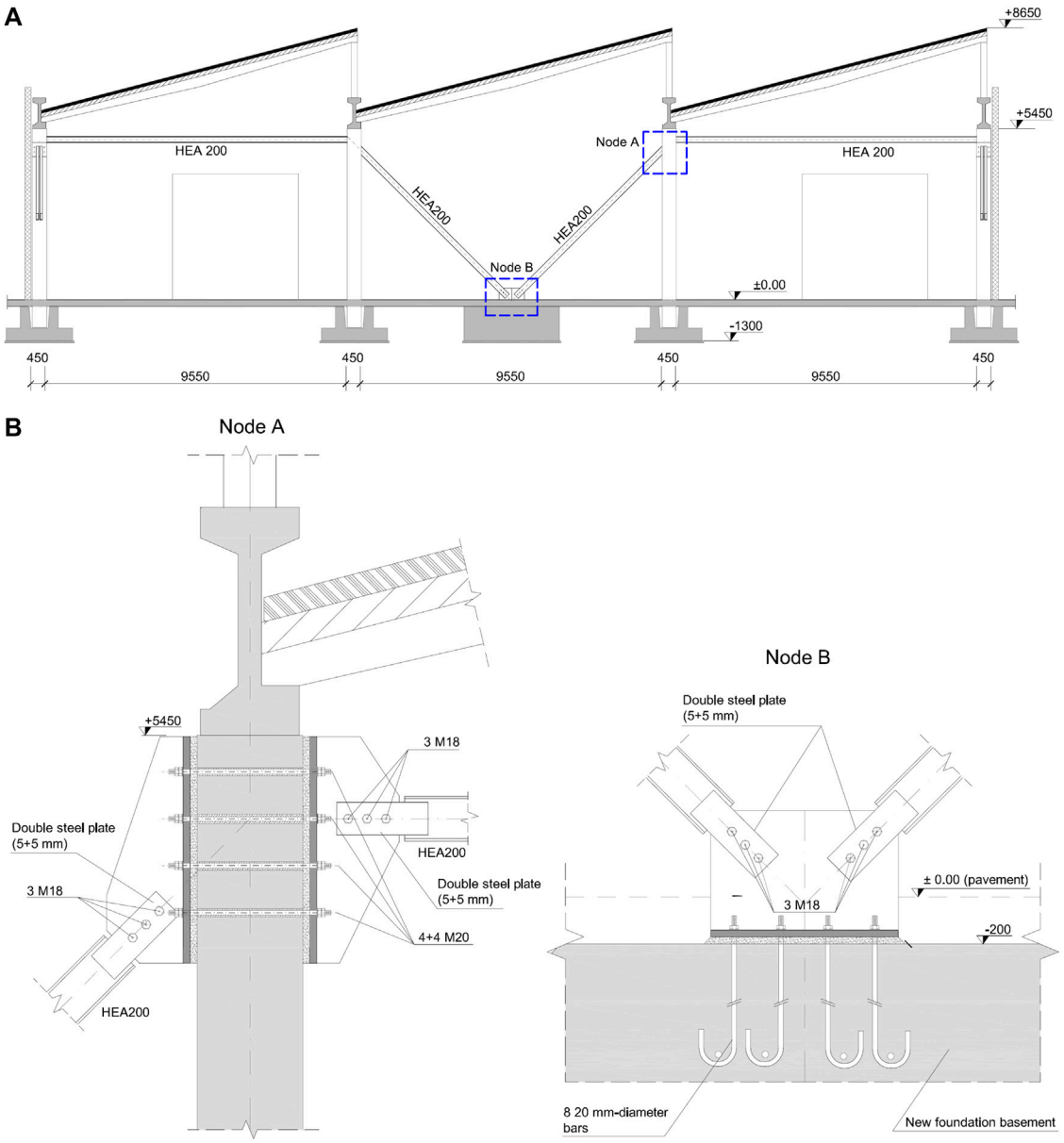

FIGURE 8 | V-shaped steel bracing used to stiffen four columns in a precast building with shed-type roof: **(A)** front view; detail view of **(B)** bracing-to-column and **(C)** bracing-to-foundation nodes. Dimensions in mm.

this intervention, the safety level of the building is increased from 0.09 up to 0.61.

With regard to the analogous solution shown in **Figure 7B**, the steel frames have two laced columns designed to leave a 4 m wide passage for trucks circulation. An increase in the capacity-to-demand ratio from 0.21 up to 0.63 is obtained in this case.

The steel bracing shown in **Figure 8A** was proposed for a single-storey precast building with shed-type roof and is comprised by HEA 200 profiles. The bracing effect is ensured by the V-shape. When the building is subjected to lateral forces, the two diagonal profiles experience tensile and compressive axial loads. Provided that the bracing remains within the elastic range, and the compressed profile does not buckle, the sum of the vertical components of these loads tends to vanish. Therefore, the new foundation into which the diagonal profiles are converging must essentially be checked against sliding. Detail views of the bracing-to-column and bracing-to-foundation connections are shown in **Figures 8B,C**, respectively. Due to the described intervention, the building safety level increases from 0.20 to 0.68.

The retrofitting solution presented in **Figure 9** was applied to a two-storey office building. The cladding panels of the building are made of precast concrete, whereas beams, columns and floor slabs are cast-in-place. However, the slabs do not behave as rigid diaphragms. Thus, the overall building response to seismic

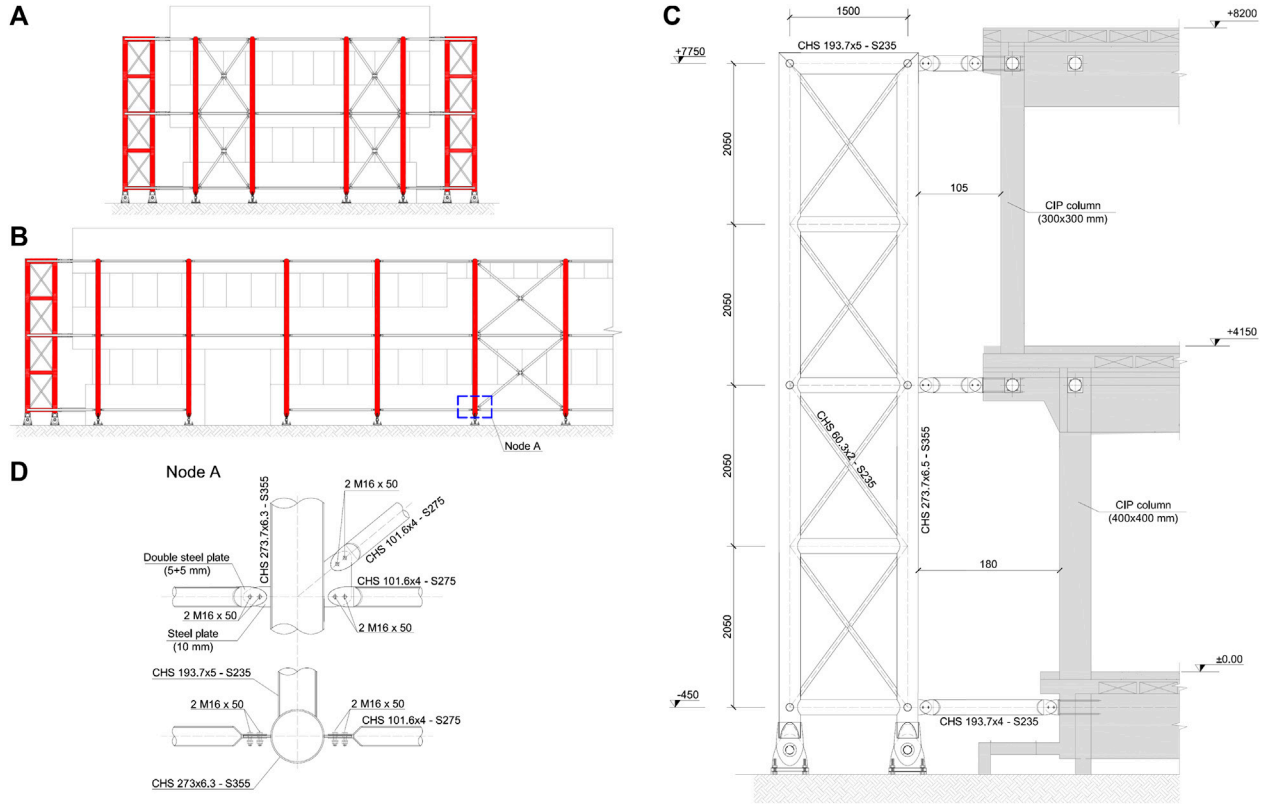

FIGURE 9 | Spatial steel bracing system applied to a two-storey building: **(A),(B)** building front views; **(C)** lateral view of one of the truss frames of the bracing system comprised of circular hollow section profiles and **(D)** detail view of a node. Dimensions in mm.

actions is analogous to that of the most of the precast buildings in the struck territory. For this reason, one plane braced frame is used for each line of columns in two orthogonal directions (**Figures 9A,B**). These plane frames, made of circular hollow section profiles, are restrained in the transverse direction against buckling. The connections with the building are positioned in correspondence of the floor and roof slabs (**Figure 9C**). Reported in **Figure 9D** are the construction details of node A highlighted in **Figure 9B**. The safety level of the building before the interventions was of 0.2. Due to an explicit request of the building owner, the target capacity adopted in retrofitting design was comparable to that prescribed for new buildings.

Finally, the proposal shown in **Figure 10** relies upon the use of steel portal frames at the outside of the building to be retrofitted. The laced built-up columns of these frames are positioned adjacent to the existing RC columns (**Figure 10A**) and connected to them in proximity of their top end section. The cross-section depth of the steel columns increases with the elevation above the soil level in order to save space for vehicular traffic around the building. Pinned connections are adopted at the base of the steel columns because of practical difficulties in obtaining moment-resisting joints. Then, the in-plane bracing effect exerted by steel frames on the building is ensured by bending stiffness and strength of the nodes between laced columns and 1.6 m-deep truss beams. The portal frames are connected to one another, so forming a unique three-dimensional truss structure (**Figure 10B**). In particular, the steel columns are stiffened in the transverse direction by peripheral truss beams, whereas the top chords of the main beams are braced by the stabilizing effect due to inclined ties and purlins. Also in this case a unity safety factor is obtained due to retrofitting, whereas the pre-interventions capacity-to-demand ratio was of 0.1.

EFFECT OF ROOF STIFFENING: SOME CONSIDERATION

The distribution of seismic forces among columns depends of the in-plane stiffness of floor slabs and roof. For example, in typical single-storey buildings featuring in-plane deformable roof comprised of precast elements independent of one another and simply-supported on precast frames, the seismic forces on columns are mass proportional. If F_h indicates the overall seismic force orthogonal to the roof elements and k the number of roof spans, the forces acting on perimeter ($F_{def,p}$) and internal precast frames ($F_{def,i}$) can be evaluated from:

$$F_{def,p} = \frac{F_h}{2k}, \quad F_{def,i} = \frac{F_h}{k} \tag{5}$$

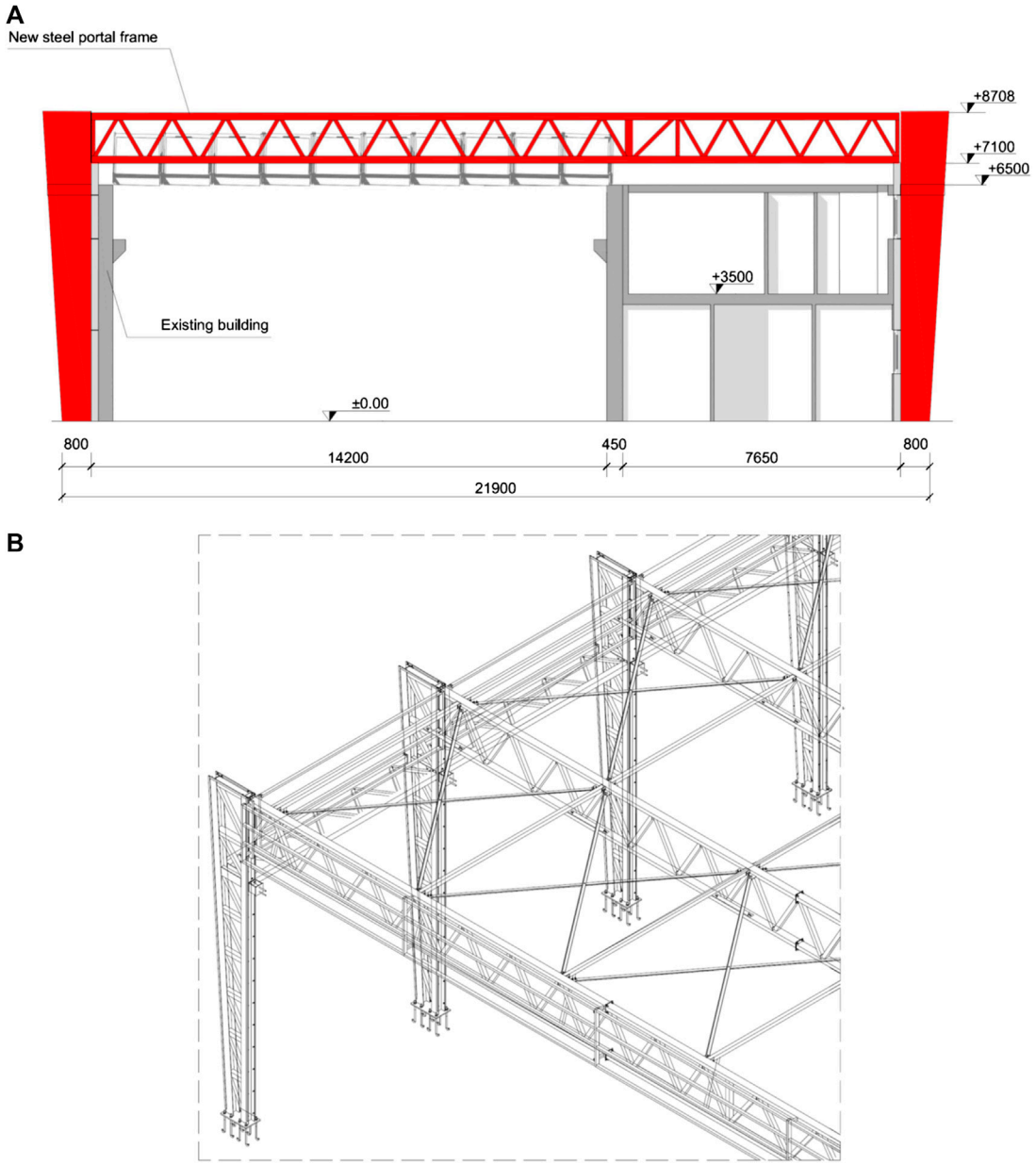

FIGURE 10 | Steel portal frames with laced built-up columns and truss beams used as earthquake resistant system at the outside of an existing precast building: **(A)** cross-sectional view of the building after the intervention; **(B)** three-dimensional view of the new steel structure. Dimensions in mm.

Conversely, in the case of in-plane rigid roof the overall seismic force is distributed among columns in proportion to their translational stiffness. Then, if the roof is stiffened so as to behave as a rigid diaphragm, the columns are identical to one another, and F_h is assumed to be unchanged (although stiffening has in general the effect of reducing the periods of vibration and then increasing the shear demand), the expressions for forces acting on perimeter ($F_{rig,p}$) and internal frames ($F_{rig,i}$) take the form:

$$F_{rig,p} = F_{rig,i} = \frac{F_h}{k+1} \tag{6}$$

Therefore, roof stiffening leads to a reduction of shear demand on internal frames and to an increase of shear demand on perimeter frames. These shear force variations are given by:

$$F_{rig,i} - F_{def,i} = -\frac{F_h}{k(k+1)}, \tag{7}$$

$$F_{rig,p} - F_{def,p} = \frac{(k-1)F_h}{2k(k+1)} \tag{8}$$

for internal and perimeter frames, respectively, and are reported divided by the corresponding forces for deformable roof ($F_{def,i}$, $F_{def,p}$)

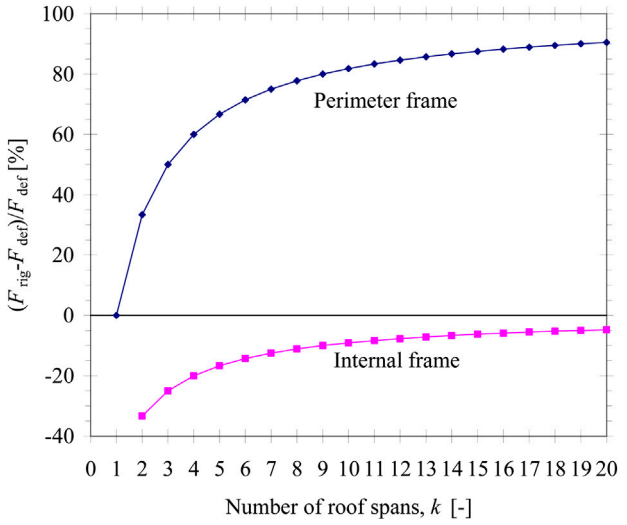

FIGURE 11 | Influence of roof stiffening on seismic forces acting on perimeter and internal frames.

in **Figure 11** vs. k. It can be noted that the effect of roof stiffening on perimeter frames is much more pronounced and increases with k. For example, for a building with $k = 4$ roof spans, the roof stiffening would yield an increase in shear demand on perimeter frames of 60% and a corresponding decrease in shear demand on internal frames of 20%. Retrofitting solutions involving an increase of roof stiffness could then require a strengthening of perimeter columns and should be assessed with care.

Another issue related with roof in-plane stiffness is concerned with roofs comprised of Pi-shaped precast elements. This type of roof is quite common among industrial buildings struck by the 2012 earthquakes in Northern Italy. In Italian pre-seismic buildings the roof elements were often simply supported on the main beams without any mechanical connection device. In Emilia, the 2012 earthquake sequence caused the roof unseating in many buildings near the epicentres of the two mainshocks, highlighting the inadequacy of these friction-based connections. Immediately after the second mainshock, to avoid loss-of-support collapses at a larger scale in the struck territory and ensure the temporary usability of the buildings, Legislative Decree No. 74 (2012) imposed to remove all connection deficiencies by introducing suitable devices. For roofs comprised of Pi-shaped precast elements, the roof-to-beam connections were frequently strengthened by anchoring to the beam, at each support, both webs of each roof element. This intervention implies an increase of the roof stiffness, because the Pi-shaped elements become able to transfer, in the plane of the roof, bending moments to the beams through tensile and compressive forces arising in the webs.

For example purposes, the precast building shown in **Figure 12A,B** is analyzed through the Response Spectrum Method (RSM). The building has in-plan dimensions of about 60 m × 24 m. The columns are mainly placed on the perimeter. In particular, the column along the longest sides have cross-section dimensions of 600 mm × 700 mm, height of 9.5 m and spacing of 10 m. The main beams are spanning parallel to the longest building sides and support a roof with the span of 24 m comprised of 1 m-deep prestressed Pi-shaped elements. Beam Finite Elements (FE) are used for column, beams and cladding panels. In order to reproduce accurately the roof vibration, the Pi-shaped elements are modeled using shell FE (**Figure 12C,D**). Three different models are obtained by changing the way the roof elements are connected to the beams (**Table 2**). In Model #1, only one of the webs of the roof elements (say, web A in **Figure 12C**) is connected at each of the supporting beams. These connections are assumed to be pinned in both vertical and horizontal plane. In Model #2, each roof element is connected to the beams through web A at one end and web B at the other end. Finally, in Model #3 both webs are connected to the supporting beam at each end (**Figure 12D**). The resulting fundamental periods and maximum tensile forces in the webs of the roof elements are reported in **Table 3**. These forces should be used to design the roof-to-beam connections, but are not the sole forces to be considered. In fact, due to the usual combination rules for horizontal ground motion components, the roof-to-beam connections are subjected to combined tensile and shear loads.

TABLE 2 | FE models of the bulding in Figures 12A,B obtained for different methods of connection of the precast Pi-shaped roof elements with the main beams.

Model #	Constrained webs of Pi-shaped roof elements	
	Node *i*	Node *j*
1	A	A
2	A	B
3	A, B	A, B

TABLE 3 | Effect of the roof element-to-main beam connections on fundamental period of the building and design tensile load acting on the anchorage.

Model #	Fundamental period of the building	Maximum tensile axial load in the webs
	T_1 [s]	$N_{Pi,Ed}$ [kN]
1	1.27	104
2	1.24	264
3	0.76	880

While the fundamental period remains substantially unchanged in the passage from Model #1 to Model #2, a significant stiffening effect is observed for Model #3. The type of connection dramatically affects the web forces, which for Models #2 and #3 result to be 2.6 and 8.8 times larger, respectively, than those obtained for Model #1. The reason for the force increase observed for Model #2 should be searched in the fact that when different webs are connected to the supporting beams the Pi-shaped elements may be viewed as inclined trusses subjected to tension and compression. The huge tensile forces obtained for connections in Model #3 make them impractical in that case. In other words, it is not economically sustainable to stiffen the roof by acting on the roof-to-beam connections only. It is concluded that to avoid excessive design load demands the

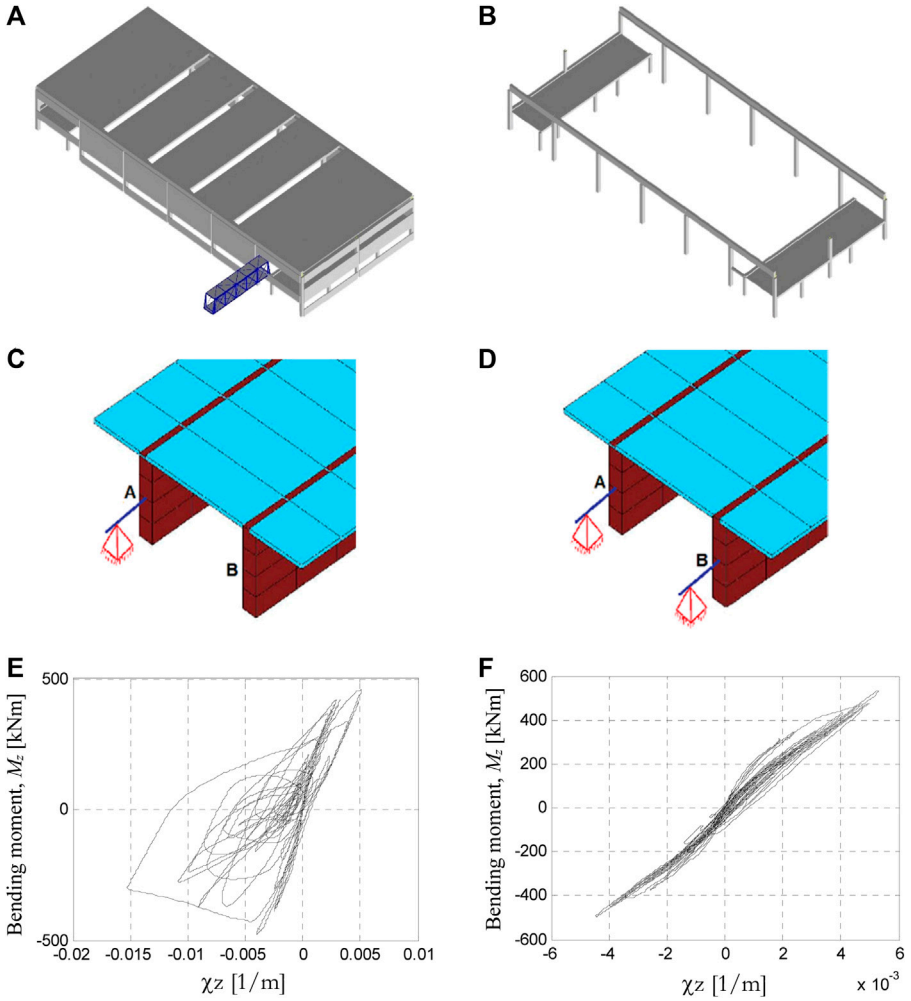

FIGURE 12 | FE model of a precast building located in the Scientific-Technological campus of the University of Ferrara: global model **(A)** showing and **(B)** hiding roof elements and cladding panels; end support of a Pi-shaped roof element with connections to the main beams applied to **(C)** one single web or **(D)** both webs. Moment-curvature cyclic diagram at the base of one of the columns obtained from NRH analysis **(E)** before and **(F)** after retrofitting.

connections should ensure an isostatic behavior of the roof in both vertical and horizontal plane.

DISCUSSION

The safety factors reported in *Critical Analysis of Retrofitting Interventions* were extracted from the database implemented by Minghini et al. (2016). The information collected derives from reports prepared by engineers hired by the companies to design retrofitting interventions. Linear elastic seismic analyses based on the RSM were generally adopted in these reports. This may result in a too conservative design approach, sometimes involving overdesigned interventions and corresponding unnecessary costs. A better approximation of the building earthquake response, both pre- and post-interventions, can be obtained using Nonlinear Response History (NRH) analyses. This kind of analysis is very demanding from a computational point of view and still remains restricted to research.

For the building shown in Figures 12A,B, in addition to strengthening connections between roof elements and main beams, the retrofitting interventions are comprised of 1) substitution of existing RC cladding with lightweight panels (see *Substitution of Cladding Panels With Lightweight Sandwich Panels* section) and 2) increase in the confinement of columns critical regions with the use of steel jackets (**Figure 2A**). Based on RSM analysis, the acceleration based capacity-to-demand ratio for the building increases from 0.57 (before interventions) to 0.85 (after interventions). These safety factors are calculated adopting mean values of concrete and steel strengths and a coefficient of 0.5 reducing the columns stiffness to account for cracking. Yet, NRH analysis results show that the post-interventions safety level of the building is greater than required for new buildings. The seismic input is applied in the form of seven sets of natural accelerograms, selected and scaled to achieve compatibility with the elastic response spectrum provided by the Italian Building Code (IMIT, 2018). Reported in Figures

12E,F are moment-curvature cyclic diagrams for one of these sets obtained for a column from NRH analysis of the building before and after interventions, respectively. The beneficial effect due to mass reduction is evident from the plots. In particular, the damage highlighted by the hysteresis cycles in Figure 12E is not present in the column after interventions (Figure 12F), which substantially remains undamaged.

CONCLUSION

Retrofitting solutions for precast buildings struck by the 2012 Emilia, Italy, earthquakes are examined in this paper. The described interventions are divided into three categories: 1) column strengthening; 2) interventions on cladding panels, and 3) use of steel bracing systems.

With regard to the first category, it is shown that column strengthening either by steel or RC jacketing generally needs to be combined with strengthening of the pocket foundation. This is essentially due to the poor reinforcement ratio of existing pocket walls, which are unable to anchor adequately the reinforcement added to the column. Moreover, when new columns are joined to the existing ones to increase the overall building capacity, an effective connection should be obtained by avoiding stress concentrations in the concrete cover.

With regard to the second category, two completely different approaches are analyzed. The first approach proposes the substitution of RC cladding with sandwich panels. In this case, the increase in building safety is related with the mass reduction. The second approach makes use of the existing cladding panels to create very stiff shear walls. Obviously this solution requires a preliminary intervention to make the roof a rigid diaphragm.

With regard to the third intervention category, various solutions are examined. Most of them are based on steel bracing systems positioned on the outside of the buildings, so allowing for the continuation of the productive activities during the installation works. The bracing systems are usually designed to withstand the entire (or a significant portion of the) base shear demand on the building. Therefore, the zones where the bracing are connected to the existing structure must be protected against stress concentrations. A solution suitable for two-storey buildings is also presented.

Finally, some consideration on the effects due to roof stiffening is reported. In particular, it is shown that roof stiffening may lead to a significant increase in the base shear demand on perimeter columns. In addition, for roofs comprised of Pi-shaped precast elements, connecting both webs of each element to the supporting beams may yield excessive design forces, resulting in impractical connections.

For several retrofitting solution, the increase obtained in the building safety level is reported. These safety measures, obtained from linear analyses, underestimate the actual safety of the building. A proof of this statement is provided for a case study, for which nonlinear response history analyses are also carried out. These analyses indicate that, due to retrofitting, the building may reach a seismic resistance greater than prescribed for new buildings, although preliminary linear analyses led to a significantly smaller safety level.

DATA AVAILABILITY STATEMENT

The original contributions presented in the study are included in the article, further inquiries can be directed to the corresponding author.

AUTHOR CONTRIBUTIONS

All authors listed have made a substantial, direct, and intellectual contribution to the work and approved it for publication.

FUNDING

The present investigation was developed in the framework of the Research Program FAR 2020 of the University of Ferrara. Moreover, the analyses were carried out within the activities of the (Italian) University Network of Seismic Engineering Laboratories–ReLUIS in the research program funded by the (Italian) National Civil Protection—Progetto Esecutivo 2019/21—WP2, Unique Project Code (CUP) F54I19000040005.

ACKNOWLEDGMENTS

The contributions of Alice Vincenzi and Mirko Gallerani to the preparation of drawings of the construction details analyzed in the present study are gratefully acknowledged.

REFERENCES

Belleri, A., Brunesi, E., Nascimbene, R., Pagani, M., and Riva, P. (2015a). Seismic performance of precast industrial facilities following major earthquakes in the Italian Territory. *J. Perform. Constr. Facil.* 29, 04014135. doi:10.1061/(asce)cf.1943-5509.0000617

Belleri, A., Cornali, F., Passoni, C., Marini, A., and Riva, P. (2018). Evaluation of out-of-plane seismic performance of column-to-column precast concrete cladding panels in one-storey industrial buildings. *Earthq. Eng. Struct. Dyn.* 47 (2), 397–417. doi:10.1002/eqe.2956

Belleri, A., Labò, S., Marini, A., and Riva, P. (2017). The influence of overhead cranes in the seismic performance of industrial buildings. *Front. Built Environ.* 3, 64. doi:10.3389/fbuil.2017.00064

Belleri, A., Torquati, M., Marini, A., and Riva, P. (2016). Horizontal cladding panels: in-plane seismic performance in precast concrete buildings. *Bull. Earthq. Eng.* 14, 1103–1129. doi:10.1007/s10518-015-9861-8

Belleri, A., Torquati, M., Riva, P., and Nascimbene, R. (2015b). Vulnerability assessment and retrofit solutions of precast industrial structures. *Earthq. Struct.* 8 (3), 801–820. doi:10.12989/eas.2015.8.3.801

Biondini, F., Dal Lago, B., and Toniolo, G. (2013). Role of wall panel connections on the seismic performance of precast structures. *Bull. Earthq. Eng.* 11, 1061–1081. doi:10.1007/s10518-012-9418-z

Bournas, D. A., Negro, P., and Taucer, F. F. (2014). Performance of industrial buildings during the Emilia earthquakes in Northern Italy and recommendations for their strengthening. *Bull. Earthq. Eng.* 12, 2283–2404. doi:10.1007/s10518-013-9466-z

Bovo, M., and Savoia, M. (2019). Evaluation of force fluctuations induced by vertical seismic component on reinforced concrete precast structures. *Eng. Struct.* 178, 70–87. doi:10.1016/j.engstruct.2018.10.018

Buratti, N., Minghini, F., Ongaretto, E., Savoia, M., and Tullini, N. (2017). Empirical seismic fragility for the precast RC industrial buildings damaged by the 2012 Emilia (Italy) earthquakes. *Earthq. Eng. Struct. Dyn.* 46, 2317–2335. doi:10.1002/eqe.2906

Casotto, C., Silva, V., Crowley, H., Nascimbene, R., and Pinho, R. (2015). Seismic fragility of Italian RC precast industrial structures. *Eng. Struct.* 94, 122–136. doi:10.1016/j.engstruct.2015.02.034

CEN (2004a). EN 1992-1-1:2004. Eurocode 2: design of concrete structures–part 1-1: general rules and rules for buildings. Brussels, Belgium: European Committee for Standardization.

CEN (2004b). EN 1995-1-1:2004. Eurocode 5: design of timber structures–Part 1-1: general-common rules and rules for buildings. Brussels, Belgium: European Committee for Standardization.

CEN (2005). EN 1998-3:2005. Eurocode 8: design of structures for earthquake resistance–part 3: assessment and retrofitting of buildings. Brussels, Belgium: European Committee for Standardization.

CEN (2018). EN 1992-4:2018. Eurocode 2: design of concrete structures–part 4: design of fastenings for use in concrete. Brussels, Belgium: European Committee for Standardization.

Clementi, F., Scalbi, A., and Lenci, S. (2016). Seismic performance of precast reinforced concrete buildings with dowel pin connections. *J. Build. Eng.* 7, 224–238. doi:10.1016/j.jobe.2016.06.013

Colombo, A., Ronchetti, A., Cardinale, G., Mariani, M., Gambuzzi, A., Dolce, M., et al. (2012). Guidelines for local and global interventions on single-story industrial buildings not designed with anti-seismic criteria working Group for seismic usability assessment of industrial buildings. Available at: www.reluis.it (Accessed September 1, 2020) [in Italian].

Dal Lago, B., Toniolo, G., and Lamperti Tornaghi, M. (2016). Influence of different mechanical column-foundation connection devices on the seismic behaviour of precast structures. *Bull. Earthq. Eng.* 14, 3485–3508. doi:10.1007/s10518-016-0010-9

Emilia-Romagna Regional Decree No. 57 (2012). Emilia-Romagna regional decree No. 57/2012. Available at: https://www.regione.emilia-romagna.it/terremoto/gli-atti-per-la-ricostruzione/2012/ (Accessed October 30, 2020) [in Italian].

Ercolino, M., Magliulo, G., and Manfredi, G. (2016). Failure of a precast RC building due to Emilia-Romagna earthquakes. *Eng. Struct.* 118, 262–273. doi:10.1016/j.engstruct.2016.03.054

FEMA 356 (2000). *Prestandard and commentary for the seismic rehabilitation of buildings*. Washington, DC: Federal Emergency Management Agency.

Fischinger, M., Zoubek, B., and Isaković, T. (2014). "Seismic response of precast industrial buildings," in *Perspectives on European earthquake engineering and seismology, geotechnical, geological and earthquake engineering*. Editor A. Ansal (London, United Kingdom: Springer), Vol. 34, 131–177. doi:10.1007/978-3-319-07118-3_4

IMIT (Italian Ministry of Infrastructure and Transport) (2018). *Italian building code-D.M. 17/01/2018*. Rome, Italy: IMIT [in Italian].

Legislative Decree No.74 (2012). Italian parliament. Available at: https://www.gazzettaufficiale.it/eli/id/2014/06/28/14A04940/sg (Accessed November 3, 2020) [in Italian].

Liberatore, L., Sorrentino, L., Liberatore, D., and Decanini, L. D. (2013). Failure of industrial structures induced by the Emilia (Italy) 2012 earthquakes. *Eng. Fail. Anal.* 34, 629–647. doi:10.1016/j.engfailanal.2013.02.009

Magliulo, G., Ercolino, M., Petrone, C., Coppola, O., and Manfredi, G. (2014). The Emilia earthquake: seismic performance of precast reinforced concrete buildings. *Earthq. Spectra* 30, 891–912. doi:10.1193/091012eqs285m

Maugeri, M., Abate, G., Aversa, S., Boldini, D., Dezi, F., Fioravante, V., et al. (2013). Guidelines for interventions on single-story industrial buildings struck by the May 2012 Po River Plain earthquake and not designed with anti-seismic criteria: geotechnical aspects. working group of the Italian geotechnical association (AGI) for the industrial buildings. Available at: www.ateservizi.it (Accessed September 1, 2020). [in Italian].

Mezzapelle, P. A., Scalbi, A., Clementi, F., and Lenci, S. (2017). The influence of dowel-pin connections on the seismic fragility assessment of RC precast industrial buildings. *Open Civ. Eng. J.* 11 (Suppl. 5, M8), 1138–1157. doi:10.2174/1874149501711011138

Minghini, F., Ongaretto, E., Ligabue, V., Savoia, M., and Tullini, N. (2016). Observational failure analysis of precast buildings after the 2012 Emilia earthquakes. *Earthq. Struct.* 11, 327–346. doi:10.12989/eas.2016.11.2.327

Minghini, F., Piccoli, F., Rizzato, N., and Tullini, N. (2015). "Assessment of the seismic retrofitting for two precast RC buildings using nonlinear time-history analyses," in Opensees days Italy, Ferrara, Italy, June 10–11, 2015 (Fisciano, Italy: University of Salerno).

Poiani, M., Gazzani, V., Clementi, F., and Lenci, S. (2020). Aftershock fragility assessment of Italian cast-in-place RC industrial structures with precast vaults. *J. Build. Eng.* 29, 101206. doi:10.1016/j.jobe.2020.101206

Pollini, A. V., Buratti, N., and Mazzotti, C. (2018). Experimental and numerical behaviour of dissipative devices based on carbon-wrapped steel tubes for the retrofitting of existing precast RC structures. *Earthq. Eng. Struct. Dyn.* 47 (5), 1270–1290. doi:10.1002/eqe.3017

Rossi, L., Holtschoppen, B., and Butenweg, C. (2019). Official data on the economic consequences of the 2012 Emilia-Romagna earthquake: a first analysis of database SFINGE. *Bull. Earthq. Eng.* 17, 4855–4884. doi:10.1007/s10518-019-00655-8

Rossi, L., Stupazzini, M., Parisi, D., Holtschoppen, B., Ruggieri, G., and Butenweg, C. (2020). Empirical fragility functions and loss curves for Italian business facilities based on the 2012 Emilia-Romagna earthquake official database. *Bull. Earthq. Eng.* 18, 1693–1721. doi:10.1007/s10518-019-00759-1

Savoia, M., Buratti, N., and Vincenzi, L. (2017). Damage and collapses in industrial precast buildings after the 2012 Emilia earthquake. *Eng. Struct.* 137, 162–180. doi:10.1016/j.engstruct.2017.01.059

Tullini, N., and Minghini, F. (2016). Grouted sleeve connections used in precast reinforced concrete construction-experimental investigation of a column-to-column joint. *Eng. Struct.* 127, 784–803. doi:10.1016/j.engstruct.2016.09.021

Tullini, N., and Minghini, F. (2020). Cyclic test on a precast reinforced concrete column-to-foundation grouted duct connection. *Bull. Earthq. Eng.* 18, 1657–1691. doi:10.1007/s10518-019-00766-2

Vintzeleou, E. N., and Tassios, T. P. (1987). Behavior of dowels under cyclic deformations. *ACI Struct. J.* 84 (1), 18–30. doi:10.14359/2749

Conflict of Interest: The authors declare that the research was conducted in the absence of any commercial or financial relationships that could be construed as a potential conflict of interest.

frontiers in Built Environment

ORIGINAL RESEARCH
published: 11 February 2021
doi: 10.3389/fbuil.2021.639778

Cyclic Behavior of Beam-Column Connections in Precast Structures

Hilal Meydanli Atalay[1]* *and Sevket Ozden*[2]

[1]*Department of Civil Engineering, Faculty of Engineering, Kocaeli University, Kocaeli, Turkey,* [2]*Department of Civil Engineering, Faculty of Engineering, Okan University, Istanbul, Turkey*

The performance of precast concrete structures is greatly influenced by the response of beam–to-column connections. In this study, a new moment resisting precast concrete beam-column connection detail with post-tensioning bolts, made out of high yield strength spring steel, has been experimentally investigated as an alternative to the conventional precast moment resisting connections. Precast specimens and an aseismic monolithic reference specimen have been tested under reverse cycling loads. The contribution of the mild steel in the connection region to the flexural moment capacity, and to the initial pre-stressing force on post-tensioning bolt have been the main test variables. The moment capacity, stiffness, energy dissipation capacity and the residual displacement performance of the precast connections have been compared with those of the aseismically detailed monolithic connection. The conducted tests reveal that the connection detail with steel corbel along with the post-tensioning bolt and mild steel has superior performance properties as compared to the companion precast specimens.

Keywords: precast structures, moment-resisting connection, post-tensioning bolt, spring steel, strength, ductility

OPEN ACCESS

Edited by:
Andrea Belleri,
University of Bergamo, Italy

Reviewed by:
Vasile-Mircea Venghiac,
Gheorghe Asachi Technical University of Iași, Romania
Davor Skejic,
University of Zagreb, Croatia

***Correspondence:**
Hilal Meydanli Atalay
hilal.meydanli@kocaeli.edu.tr

Specialty section:
This article was submitted to Earthquake Engineering, a section of the journal Frontiers in Built Environment

Received: *09 December 2020*
Accepted: *07 January 2021*
Published: *11 February 2021*

Citation:
Meydanli Atalay H and Ozden S (2021) Cyclic Behavior of Beam-Column Connections in Precast Structures. Front. Built Environ. 7:639778. doi: 10.3389/fbuil.2021.639778

INTRODUCTION

Precast concrete construction is considerably advantageous in terms of quality and notably the duration of the construction. Almost all building types inclusive of car parks, commercial buildings, cultural buildings, hotels, dormitories, apartment buildings, bridges and especially industrial buildings can easily be constructed by using precast concrete systems. Structural performance of precast concrete systems, which consist of strength, stiffness, ductility, and ease of field applicability, is generally managed by the behavior of beam-to-column connections. In earthquakes of the past, it was observed that precast concrete structures were mainly inflicted damaged due to improper design, detailing and production of the connections. Many researchers claimed that the main problem leading to earthquake damage is insufficient strength and low energy dissipation capacity of the connections (Hawkins and Iverson, 1994; Ghosh, 1995; Mitchell et al., 1995; Adalier and Aydingun, 2001; Bruneau, 2002; Toniolo and Colombo, 2012; Ozden et al., 2014). As joints are considered to be the most important component of the precast structures, reported studies generally aimed to improve the connection performance. In this contextthere are many studies showing that the behavior of moment-resisting beam-column connections, which are frequently applied in multi-story precast concrete structure, should behave similar to those of the aseismically detailed cast in place connections, in terms of strength, rigidity, ductility and energy dissipation capacity under reversed cyclic loads (Englekirk, 1990; Stanton et al., 1991). In these studies, different types of moment-resisting connection details have been examined. These connection types can be categorized in the three groups which are; wet connections, dry connections, and post-tensioned connections. The most common connection type among the precast concrete moment resisting

connections is the wet connection, either between precast members or between precast and cast-in-place members. The reinforcement is usually connected with laps or spiral stirrups and it sometimes contains quite few welds or bolts. However, the wet connections necessitate more field work. It is reported that the use of fiber reinforced concrete in a connection increases ductility, and energy dissipation capacity of the connection. At the assembly stage, wet connections require some formwork that affects the construction phases and scheduling (Soubra et al., 1993; Park, 1995; Restrepo et al., 1995; Vasconez et al., 1998; Ertas et al., 2006; Parastesha et al., 2014).

Dry connections, preferred due to their ease of field applicability and low construction cost, are usually formed by welding steel plates and bars located on the bottom and top surfaces of the beam to similar plates on the columns when assembling the precast members. Although sometimes bolts are used in order to connect precast members, dry connections are usually formed by welding (Pillai and Kirk, 1981; Bhatt and Kirk, 1985; Dolan et al., 1987; Dolan and Pessiki, 1989; Seckin and Fu, 1990; Crisafulli and Restrepo, 2003). The capacity design of the plastic hinge location for such connections is significantly important (Ersoy and Tankut, 1993; Ochs and Ehsani, 1993; Nakaki et al., 1994; Korkmaz and Tankut, 2005). Shearing force transfer mechanism as well as anchorage length and type of bolts should be taken into consideration in bolted connection design (French et al., 1989a; French et al., 1989b; Nakaki et al., 1994).

The third type of connection detail is the post-tensioned connection, which is formed by connecting precast beam and column with a post-tensioning steel. Post-tensioned connections have been widely investigated in the NIST (National Institute of Standards and Technology) research projects. The objective of this comprehensive research program is to develop economical and easily applicable moment-resisting beam-column connections to be used in multi-story precast concrete structures, especially in high seismic areas. In the beginning, the basic conceptual target for precast connections was to put precast beams and columns together by using post-tensioning steel and to ensure that the required interface shear transfer to be without corbels and shear keys. The test variables were the post-tensioning steel reinforcement ratio, strength, location and bonding type of the post tensioning steel (full bonding, partial bonding or without bonding), the use of mild steel reinforcement together with the post-tensioning steel and the mild steel reinforcement ratio and its type in the connection. NIST research program has been conducted in four stages. At the final stage of the research, a connection detail has been formed and tested by using post-tensioning reinforcement at the center of the beam x-section and mild steel reinforcement at top and bottom of the beam section. This connection type, called hybrid connection was the most significant output of the NIST project. Locating post-tensioning steel in the beam center significantly decreases the strain that may occur in the post-tensioning steel. Thus, it is proved that the post-tensioning reinforcement remains in the elastic range. Because of clamping force created on the beam-column connection interface with post-tensioning force, shearing force transfer mechanism is formed in hybrid connections (Cheok and Lew, 1993; Cheok et al., 1994; Stone et al., 1995; Stanton et al., 1997). Four different moment-resisting precast concrete connection details have been developed and tested in PRESSS (Precast Structural Systems) research project (Hawkins and Ghosh, 2004). Additionally, a five-storey prototype structure has been produced with developed connection details and tested in order to examine the connection's performance in the structure system under the scope of NIST and PRESSS programs (Palmieri et al., 1997; Nakaki et al., 1999; Priestly et al., 1999). The effect of mild steel reinforcement ratio on the hybrid connection flexural moment capacity has been investigated extensively by Ozden and Ertas, 2007. The energy dissipation of monolithic frames is mainly provided by the inelastic rotation occurred in the plastic hinge zones of the frame. However, the post-tensioned connection has been dissipating energy by the beam rotation at the column surface (opening and closing of the connection interface). Since the energy dissipation through rocking of beam on the column surface, where the shear transfer is secured by the post-tensioning steel, is too low; additional energy dissipation is required to reduce the earthquake effect in the frame and the joints. Using mild steel reinforcement at the bottom and the top beam sections of the connection increases energy dissipation capacity of the connection. Similar achievements may be accomplished by using energy dissipation apparatus placed inside or outside the connection. Moreover, it is also important to ensure the transfer of the shear force and torsional moment which in the connection due to the combined effect gravity loads and transverse lateral loads before and during the in plane rotation of the frame considered (Pampanin, 2005; Amaris et al., 2006; Ozden and Ertas, 2007).

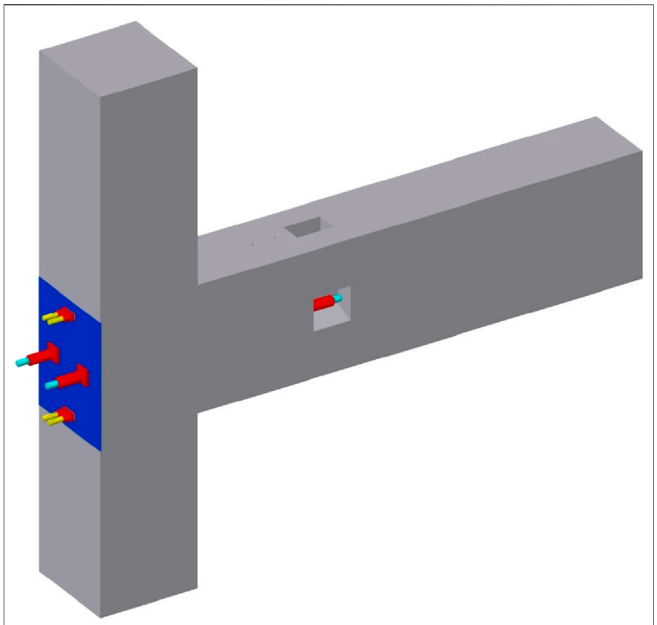

FIGURE 1 | Connection detail of post-tensioned precast specimen.

Due to the lateral loads affecting the structure during the earthquake, inelastic rotations occur with the opening and closing

TABLE 1 | Test specimens.

Specimen name	Initial post-tensioning force (kN)	M_{ms}/M_r	Diameter of PT (mm)	Un-bonded length of PT (mm)	Diameter of MS, ϕ (mm)	Un-bonded length of MS (mm)
MONO_0	—	—	—	—	—	—
HBD_10_0	—	0.22	19	1,150	10	100
HBD_16_0	—	0.40	19	1,150	16	128
HBD_16_20	135 (2 @ 67.5)	0.40	19	1,150	16	128
HBD_16_20_C	135 (2 @ 67.5)	0.40	19	1,150	16	128

PT, post-tensioning bolt; MS, mild steel.

of the prefabricated post-tensioned connections and this behavior improves the seismic performance of the precast structures. Thus, damage to precast elements can be avoided and significant economic advantages can be achieved as compared to monolithic frame structures. Hence, the damage to the building caused by the earthquake does not prevent the building from being used after the earthquake. Because of this advantage, in order to develop an easy-to-manufacture, practical and economical moment-resistance beam-column connection detail to improve the seismic performance of precast buildings in high seismicity region is the aim of in this research. Mild steel reinforcement is placed at both the bottom and top of the beam x-section while high-strength post-tensioning bolts are placed along the center-line of the beam section in the proposed precast connection depicted in **Figure 1**. Such connection detail, different from the conventional post-tensioned connections may well be used in precast concrete structures. The force transfer mechanism between precast elements is provided by using high-strength steel "post-tensioning bolts" applied only to the beam ends. It is usually not possible to use post-tensioning tendons in such connection detail since stress loss in tendons stemming from the chuck set-back results in high losses for the short post-tensioning tendons. In the proposed connection, high-strength steel post-tensioning bolts with 60SiCr7 quality, known as spring steel, was used to develop the clamping force between the beam and column faces. Not only the shearing force transfer mechanism and the self-centering mechanism are assured by using the post tensioned bolts but also the flexural moment capacity is developed by them. However, energy dissipation capacity of the connection is affected mainly by the existence and the percentage of the mild steel in the connection. In design of such precast connections, the precast columns and beams should be designed with a higher capacity than the joint moment capacity in order to create the plastic hinge mechanisms in the connection, by overcoming the clamping stress.

EXPERIMENTAL PROGRAM

Test Specimens

A testing program has been designed to evaluate the earthquake performance of the proposed moment resisting precast concrete beam-to-column connection detail under reversed cyclic loading in order to investigate its seismic performance in terms of moment capacity, stiffness, energy dissipation and residual displacements. The test specimens have been designed as exterior joints of a multistory building assuming that the point of contraflexure in the columns and beams take place at the mid-height and mid-span under the earthquake loads, resulting an isostatic test specimen.

In this study five specimens; one monolithic and four precast, have been tested. The variables of the test specimens are summarized in **Table 1**. The contribution of mild steel reinforcement to the flexural moment capacity have been 22 and 40%, respectively, for the precast specimens HBD_10_0 and HBD_16_0. No initial post tensioning force has been applied to post tensioning bolts in those specimens. Although HBD_16_20 specimen has been same as HBD_16_0 for the contribution of mild steel reinforcement ratio, the initial post tensioning force has been applied on post tensioning bolts at an approximate level of 20% of the post tensioning bolt yield strength. Differentiating from the HBD_16_20 specimen, steel corbel has been placed above and below the beam to prevent beam sliding on column surface in HBD_16_20_C specimen.

Test specimen geometry is selected approximately as half of the prototype structure, considering the capacity and space limitations of the laboratory and loading criteria stated in ACI T1.1-01 (ACI T1.1-01, 2001). The designed precast connection detail is shown in **Figure 1**. Beam dimension was 300 × 500 mm with an 1850 mm unbonded length for the post-tensioning bolts, while the 2030 mm high column's dimension was 400 × 400 mm. Concrete cover in precast columns and beams was 20 mm.

Column longitudinal reinforcement ratio was 2.40% for the monolithic specimen. Three 10 mm diameter reinforcing bars were placed as the longitudinal reinforcement for both sides of the beam. Reinforcement configuration of the monolithic specimen is given in **Figure 2**. Column flexural moment capacity is designed higher than the beam flexural moment capacity in order to initiate the plastic hinging in the beam and thus strong column-weak beam design philosophy is ensured for the monolithic specimen.

The design of precast specimens was based on both the ACI-T1.2-03 guidelines and on the recommendations along with the conclusions from previously published research (ACI-T1.2-03, 2003). The flexural moment capacity of the precast connection was aimed to be close to that of the monolithic connection, provided that the beam and column capacities to be higher than the connection ultimate moment capacity. The columns and the

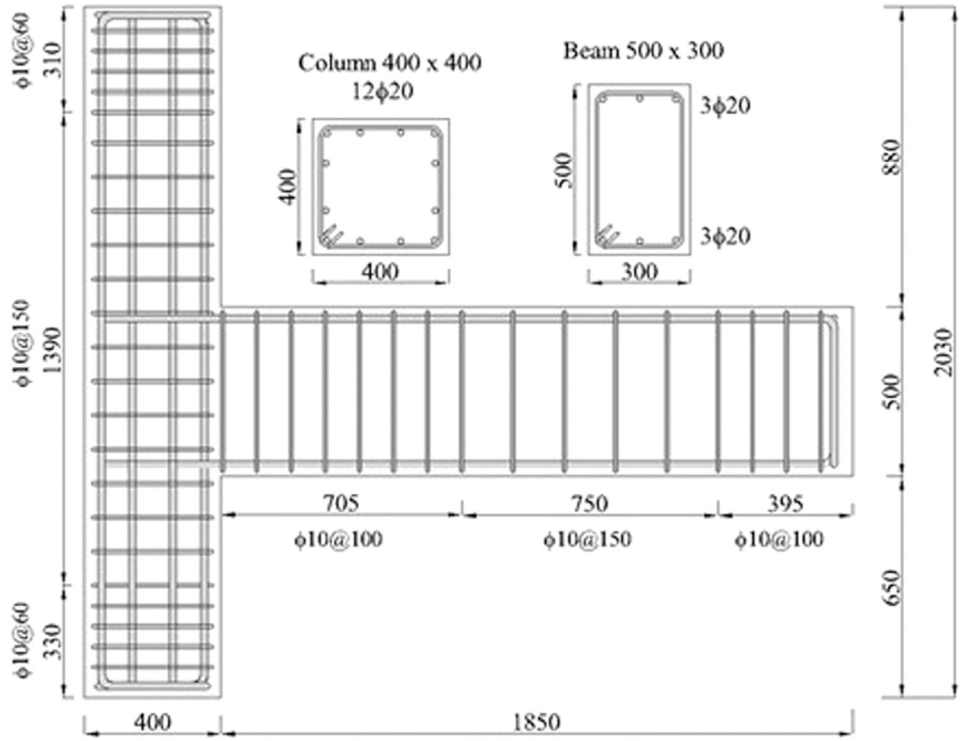

FIGURE 2 | Reinforcement detail of monolithic test specimen (dimensions in mm).

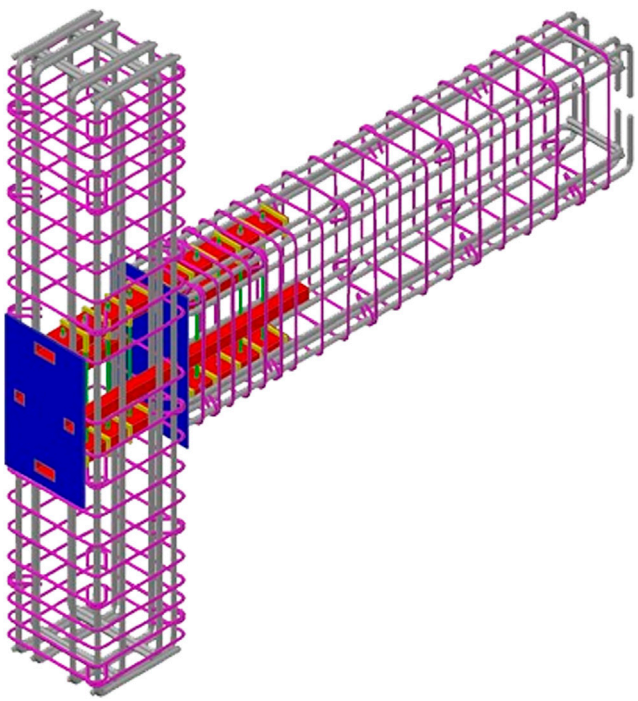

FIGURE 3 | Reinforcement and connection detail of precast test specimens.

beams of the specimens were manufactured the same in all precast connections. The main test variables in the connection are the mild steel reinforcement ratio and the initial post tensioning force applied on high-strength post tensioning bolts.

Precast column longitudinal reinforcement ratio was 2.40% similar to the monolithic specimen. The cross-section dimension of the prefabricated beam on the connection region is the same as the monolithic connection. Six 20 mm diameter mild steel reinforcing bars were placed at the top and bottom of the precast concrete beams as main flexural reinforcement. In order to mount the mild steel reinforcement and post-tensioning bolts easily, steel box sections were placed along the same axis inside the prefabricated columns and beams shown in **Figure 3**. The steel box, in which the mild steel reinforcement is placed, had a cross section of 80 × 40 mm; while 40 × 40 mm steel box was used on both side faces of the beam in order to place the post-tensioning bolts. The box sections of the beam were fixed to a 20 mm-thick steel plate before casting concrete. This steel plate was used also as a cushion to delay the crushing of beam concrete along the column surface throughout the loading. A similar plate with a thickness of 10 mm was placed on the column free surface to reduce the effect of point load induced by the post tensioning bolts. Steel ribs were welded around the steel boxes for better bonding between the box and the surrounding concrete, while cross-bolts were used to ensure the integrity of concrete infill and the 40 × 80 mm steel boxes used for the mild steel.

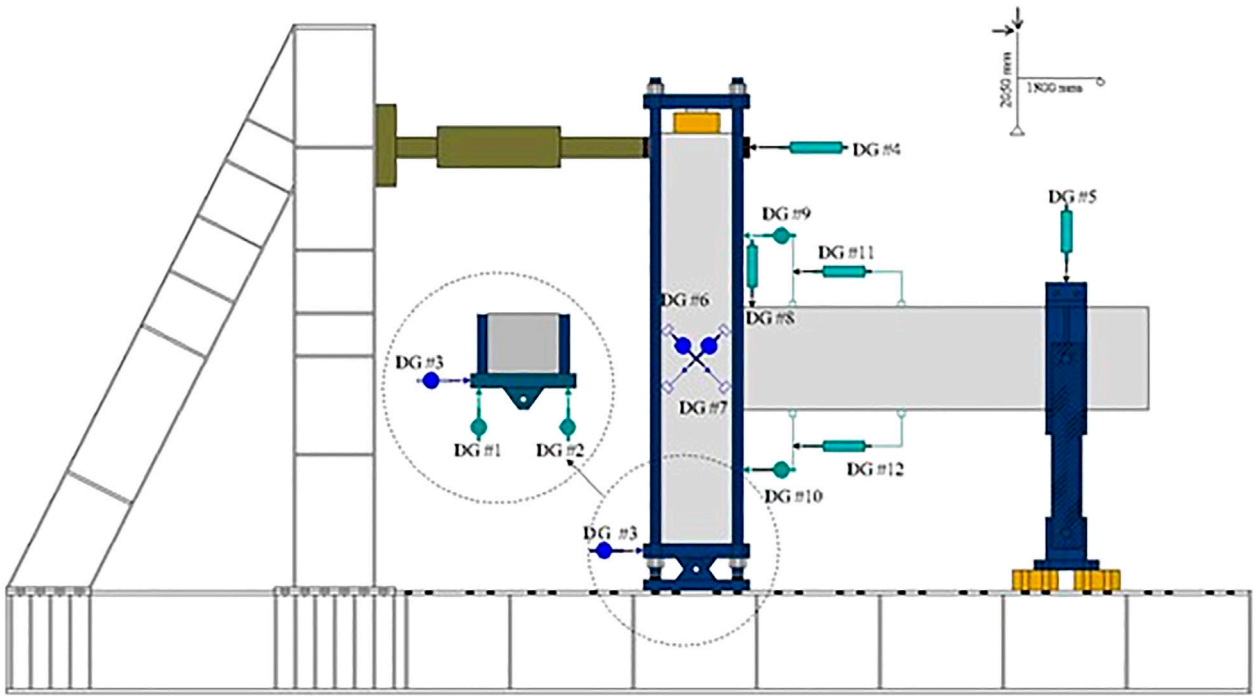

FIGURE 4 | Test setup and instrumentation.

Fabrication and Materials Properties

In the assembly phase of the precast elements, the beam was seated on a scaffolding leaving a 20 mm gap to the column, later was filled with a non-shrink steel fiber reinforced concrete with an ultimate compressive strength of 90 MPa. After 24 h, mild steel reinforcements were placed inside the 40 × 80 mm steel boxes and fastened without pre-stressing. The steel box with the mild reinforcement was filled with high strength mortar for full bond. On the other hand, a short unbounded length was created on the mild steel through the application of a smooth surface plastic cover on the rebar, and was centered to the beam-column interface given in **Table 1**. The aim of the un-bonded length was to avoid the reinforcement rupture at small drift levels. Finally, post tensioning bolts were placed inside the 40 × 40 mm. No mortar was used for the post-tensioning bolts.

The compressive strength of concrete was 42 MPa. The diameter of reinforcing steel for the flexural and shearing reinforcement in the monolithic and precast members were 20 and 10 mm, respectively. In addition, 10 and 16 mm diameter reinforcement were used as mild steel reinforcement for post tensioning precast connection specimens. For all test specimens, the yield and ultimate strength of the flexural reinforcement were 530 and 630 MPa, while these values for the shear reinforcement were 470 and 700 MPa, respectively. However, yield and ultimate strength of the 16 mm reinforcing bar were 540 and 637 MPa, respectively. The reinforcing steel elongation at ultimate strength was 16% for the 10 and 20 mm diameter bar, and 13% for the 16 mm diameter bar. The high strength post tensioning bolt has a tensile strength of 1,400 MPa, and a yield strength of 1,200 MPa. Elongation at ultimate strength is 15% for steel bolts. The post tensioning bolts were specially manufactured in length and property suitable for the connection geometry. Material strengths were determined by tests carried out in the accredited testing laboratory.

Loading and Instrumentation

Quasi-static, reversed cyclic loading was applied to the specimens. In the first step of the loading, an axial load of 10% of the column capacity was applied to the column and this axial force was kept constant through the lateral loading scheme. Test setup and the measurement system shown in **Figure 4** were designed accordingly in order to use the criteria described in ACI-T1.1-01. The lateral load was applied to the top of the column, while the bottom of the specimen was free to rotate and the beam end was designed as roller support. The lateral load protocol was applied to the top end of the column by a displacement controlled hydraulic actuator, according to the loading history proposed in ACI T1.01. Three full cycles were realized at each displacement level. The first cycle was in the linear region (0.15 and 0.20% story drift) and loading steps were gradually increased.

Linear variable displacement transducers (LVDTs) are mounted on the test specimens to measure the story displacement of the column, sliding deformation that may occur at the bottom joint and beam end, curvature at the beam end, sliding of the beam end relative to the precast column surface and the openings on the column-to-beam

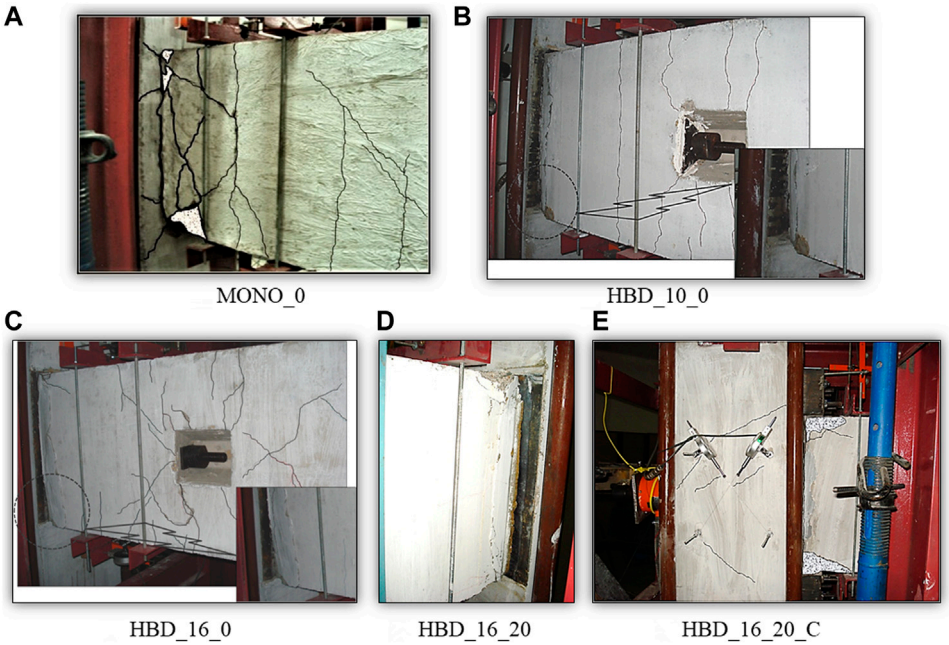

FIGURE 5 | Damage in test specimens at the 4% story drift ratio. **(A)** MONO_0. **(B)** HBD_10_0. **(C)** HBD_16_0. **(D)** HBD_16_20. **(E)** HBD_16_20_C.

interface. All experimental data have been collected and stored electronically and cracking, yielding, failure loads and displacements of specimens were monitored and crack patterns were recorded simultaneously. The drift level is computed as the ratio of story displacement to column height. The net displacement at the column top is called the story displacement and calculated according to **Eq. 1**.

$$\Delta_{net} = \Delta_{ct} - \Delta_{cb} - \left(\frac{2050}{1800} \times \Delta_{bv}\right) \quad (1)$$

In this equation, the net column displacement (Δ_{net}) is obtained by subtracting the column base lateral displacement (Δ_{cb}) and the vertical beam end displacement (Δ_{bv}) from the measured lateral displacement on the column top (Δ_{ct}). Actually, the rigid body movement was deducted from the top displacement of the column, in order to obtain the net displacement causing internal forces. Load cells were installed at the external surface of column in order to measure the initial effective post-tensioning force in the post-tensioning bolts and to measure the changes in the post-tensioning force during the experiment. Strain gauges were placed on the steel bars to determine the yield displacement of the mild steel reinforcements.

EXPERIMENTAL RESULTS

Experimental results and the observed connection behavior during the experiment are presented in this section. The damage mode of failure for the specimens are presented in **Figure 5**.

Monolithic Specimen (MONO_0)

The monolithic specimen performed nearly elastic in the first two cycles of the 0.25% drift level. At the 0.75% story drift level, flexural cracks observed on the column close to the connection region. Diagonal microcracks on beam appeared at 1.00% story drift level. Yielding of beam flexural reinforcement was observed at 1.40% story drift cycle. Concrete spalling on lower compression block of the beam took place 2.20% story driftratio. At the second cycle of the drift ratio 4.0%, bottom reinforcement was buckled as shown in **Figure 5A**. Lateral load-story drift response of the specimen is shown in **Figure 6**. The measured ultimate lateral load for the push and pull cycles is 120 and −117 kN, respectively. No significant strength degradation has been observed in the monolithic connection until 4.00% story drift level, and the behavior was ductile.

Precast Specimens

The damage in precast connections is usually gathered at the connection region due to opening and closing of the crack that occurs on the connection interface. As the moment capacity of prefabricated members has been designed higher than the moment capacity of the connection, no significant damage has been observed in prefabricated members during the tests.

Hybrid Specimen (HBD_10_0)

No initial post-tensioning was applied to the post-tensioning bolts. The first hairline crack took place at 0.20% story drift level on the connection interface, while the mild steel reinforcement of the connection yielded during the 0.75% drift cycle. Residual displacements in the form of vertical sliding at the interface became visible at 1.40% drift ratio. Due to the early yielding, the

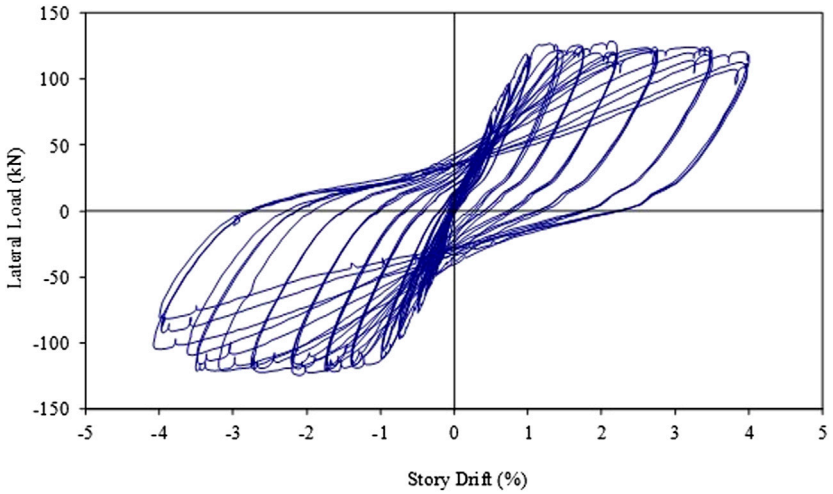

FIGURE 6 | Load—story drift response of specimen MONO_0.

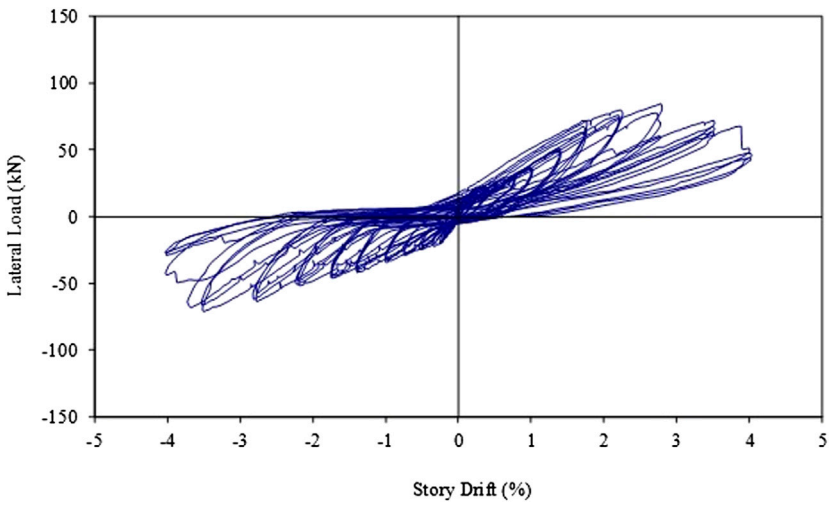

FIGURE 7 | Load—story drift response of specimen HBD_10_0.

bottom mild steel reinforcement in the connection was buckled in the first cycle at 2.75% story drift level. At 4.00% story drift level, the concrete on the compression face was crushed at the connection region as shown in **Figure 5B**. The lateral load versus-story drift behavior is presented in **Figure 7**. Maximum lateral load was measured as 84 kN during compression and -71 kN during tension. Maximum tension in the post tensioning bolts was measured as 790 MPa (Force is 224 kN). The gap opening at the beam-column interface reached a maximum level of 30.0 mm at the 4.00% drift cycle, and the vertical sliding of the beam on column surface was 15.5 mm.

Hybrid Specimen (HBD_16_0)

No initial post-tensioning was applied to the post-tensioning bolts. Yielding of the top mild steel reinforcement at the interface took place at the first cycle of 0.75% drift level. The gap opening at the interface reached to 6 mm at 1.40% story drift level. In the first cycle of the 4% story drift ratio, the mild steel reinforcement at the bottom of the connection. Residual displacement in the specimen was about 51.8 mm at the end of the test and **Figure 5C** illustrated the last damage mode of the precast specimen. Lateral load-story drift graph is presented in **Figure 8**. Maximum lateral load was 114 kN at push and −104 kN at pull cycles. The maximum measured tensile stress in the post tensioning bolts was 889 MPa (Force is 252 kN). The gap opening at the column-beam connection interface reached a maximum level of 26.8 mm at the 4.00% story drift level. The amount of vertical sliding of the beam on the column surface was measured as 13.1 mm.

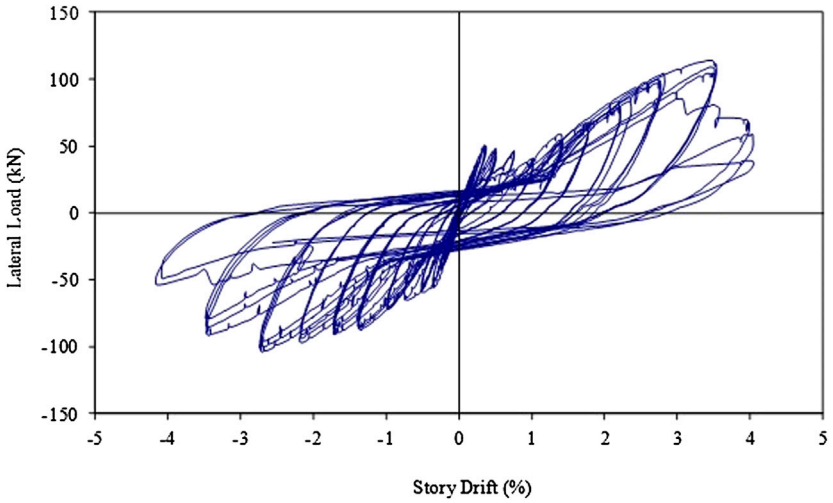

FIGURE 8 | Load—story drift response of specimen HBD_16_0.

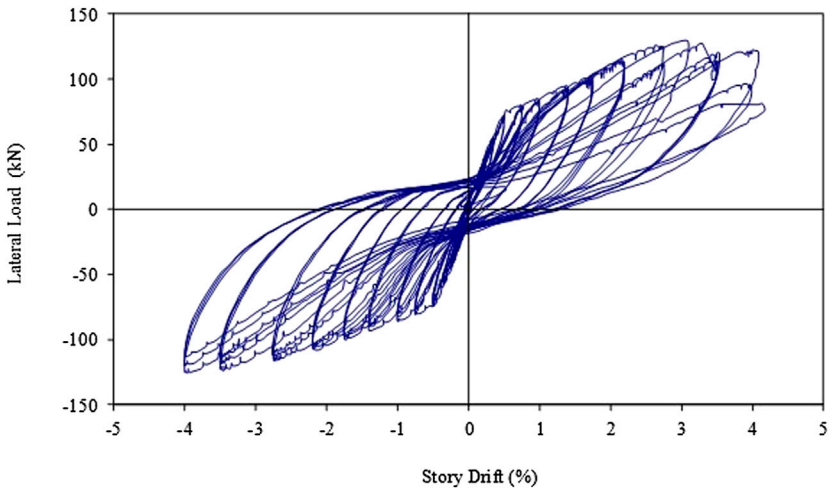

FIGURE 9 | Load—story drift response of specimen HBD_16_20.

Hybrid Specimen (HBD_16_20)

Since sudden increase in the force transferred to the post tensioning bolts took place right after the yielding of mild steel, significant relative deformations observed at the beam-column interface resulting stiffness degradations and residual sliding deformations in the previous precast specimens. For this reason, an initial post tensioning force at a level equal to the 20% of the bolt yield capacity (240 MPa) was applied in order to increase the clamping force at the interface. Similar to the previous specimens, the mild steel reinforcement yielded at 0.75% storey drift ratio. Post-tensioning force applied on bolts was effective on the overall behavior. Mild steel reinforcement at the bottom of the interface ruptured at the second push cycle of 4.00% drift ratio as shown in **Figure 5D**. Lateral load-storey drift behavior is presented in **Figure 9**. Maximum measured lateral load is 130 kN during push and −126 kN pull cycles. The maximum measured tensile stress in the post tensioning bolts was 995 MPa (Force is 282 kN) at the 3.50% storey drift level. The gap opening at the beam-column interface reached 27.3 mm at 4.00% storey drift level.

Hybrid Specimen (HBD_16_20_C)

Specimen HBD_16_20_C was with small steel brackets at the top and bottom of the beam at interface in order to limit the sliding type of deformations. The first hairline cracks indicating the opening of the beam-column interface were observed at the 0.25% storey drift level, and the mild steel reinforcement yielding took place at 0.75% drift level. Hairline diagonal cracks observed in the beam at 1.40% cycle while crushing of concrete was observed on the beam-column interface at the 4.00% drift ratio as **Figure 5E**. No loss in the load bearing capacity was observed during the loading scheme. Lateral load-storey drift graph is given in

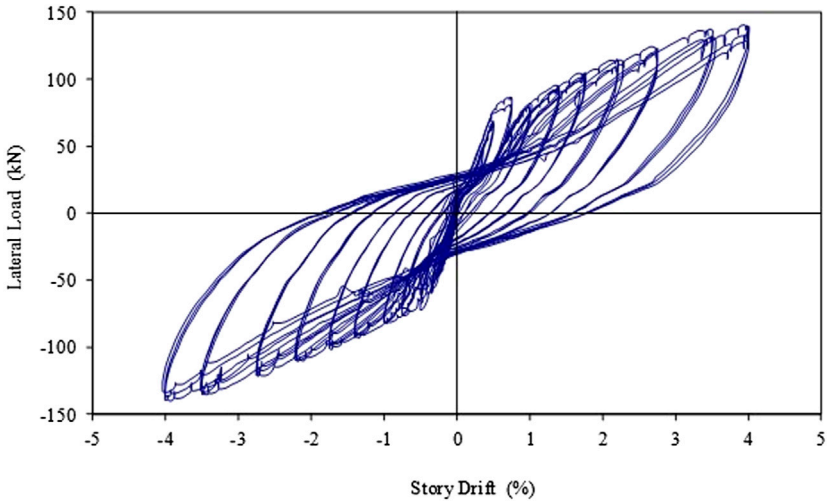

FIGURE 10 | Load—story drift response of specimen HBD_16_20_C.

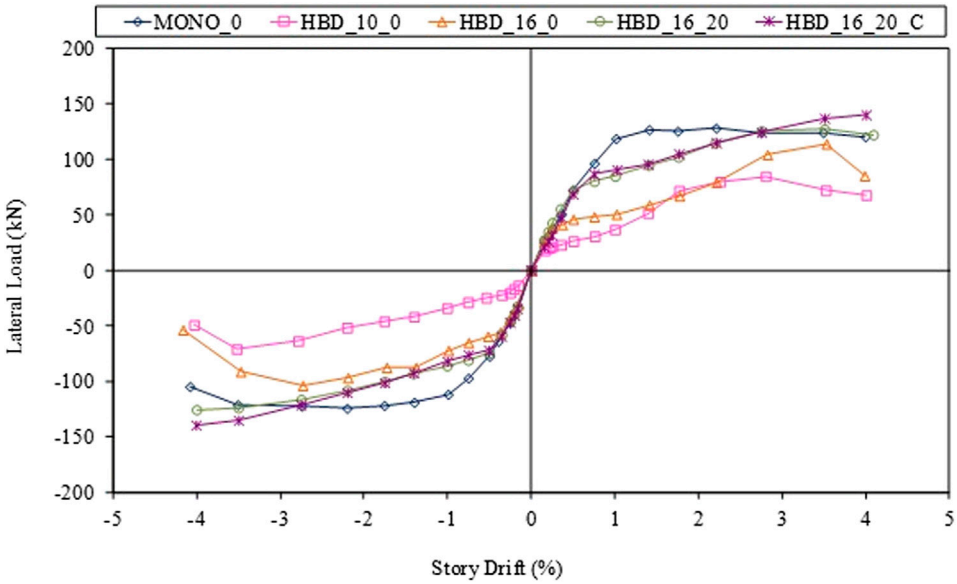

FIGURE 11 | Envelop curves of specimens.

Figure 10. Maximum measured push load was 140 kN while the pull capacity was −140 kN. Maximum tension force measured in the post tensioning bolts was 1,055 MPa (Force is 299 kN) at the 4.00% cycle. The opening at the beam-column interface reached a maximum level of 17.3 mm. Vertical relative sliding at the beam-column interface minimized with the help of steel brackets.

EVALUATION OF TEST RESULTS

The comparison of the strength, failure modes, stiffness degradation, energy dissipation characteristics and residual displacement values of the monolithic and hybrid precast specimens are presented in the following section.

Strength and Failure Modes

In most of the design codes, it is required to demonstrate that the precast connection behavior is similar or at best, equivalent to that of the monolithic connection. In this study, the strength and behavior of precast connections are compared to the monolithic specimen by using the lateral load—story drift envelope curves presented in **Figure 11**. In addition, the moment capacity of each connection is determined by processing the load displacement curves obtained from experiments. According to the results, while

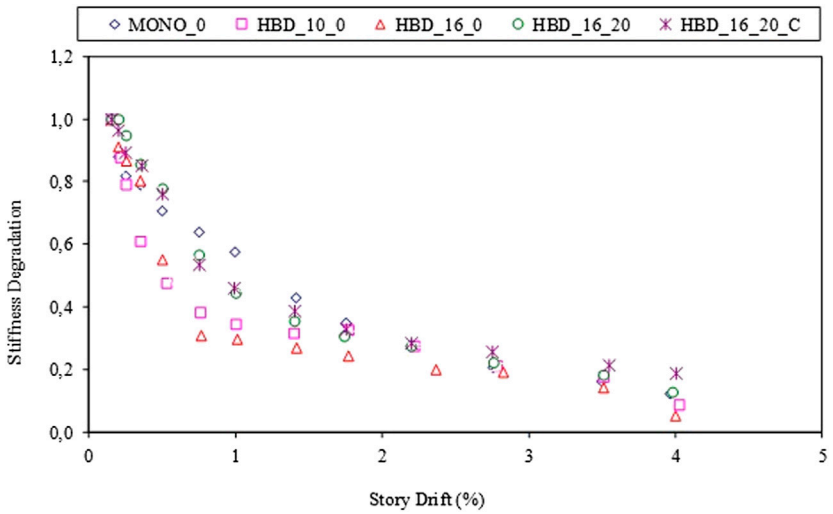

FIGURE 12 | Stiffness degradation of specimens.

the moment capacity of the monolithic connection is 218 kN m, the HBD_10_0 connection moment capacity decrease to 133 kN m. The moment capacity of the HBD_16_0 connection reached 85% of the capacity of the monolithic connection and 95% of the HBD_16_20 connection. HBD_16_20_ C connection moment capacity is determined as 231 kN m and the moment capacities of the HBD_16_20_ C connection exceeded that of the monolithic connection by 7%. The behavior of the precast specimens with prestressing force applied to the high strength tendons are very similar to the monolithic connection. The load carrying capacity of the HBD_16_20_C continued has increased without loss until the end of the 4.00% drift cycle. In this case, when the vertical sliding of the precast connection is prevented with a corbel, it behaves similar to a monolithic connection.

Stiffness Degradation

The high-strength steel post-tensioning bolts in the precast connections provided higher initial stiffness values as compared to the monolithic connection. This higher initial stiffness values may be considered beneficial in reducing the damage in non-structural (architectural) elements at low level seismic excitations.

The stiffness degradation is calculated by considering the secant stiffness (K_{sec}) changes in the specimens. The secant stiffness values, K_{sec} are calculated according to the ACI T1.1-01 approach, by taking the push and pull peak points into account in the third cycle of each story drift level (Priestly et al., 2007). Test results are normalized by dividing the measured K_{sec} of each drift level to that of the 0.15% story drift cycle and the stiffness degradation curves are shown accordingly as shown in **Figure 12**. Secant Stiffness values, K_{sec} in precast and cast-in-place monolithic connections are similar at the beginning of the loading history. However, a pronounced stiffness degradation took place in the specimens without post-tensioning due to the yielding of the mild steel. On the other hand, initial post-tensioning force and placing steel corbels at the bottom and the top side of the beam reduces the stiffness degradation as presented in **Figure 12**.

Energy Dissipation

The energy dissipation capacities of test specimens are calculated according to the method given in ACI T1.1-01. In order to emphasize the energy dissipation characteristics of the precast connections, the relative energy dissipation ratio vs. the story drift graphs are presented in **Figure 13**. The concept of energy dissipation is defined in ACI T11-01 as an acceptance criterion for such connections. The dissipated energy can be measured as the loop area in the third cycle of a given story drift level. Normalization of this value is evaluated according to the elasto-plastic behavior of the specimen at this specified drift cycle. As an acceptance criterion according to ACI T1.1-01, the maximum relative energy loss rate of a subassembly must be equal to 1/8 of the third cycle value at the 3.5% drift ratio.

Precast connections without steel corbel display almost the same behavior and dissipated more energy than the monolithic connection until the 1.70% storey drift ratio. Beyond this drift level, the trend changes and the energy dissipation values of precast connections decrease as compared to the monolithic specimen. The energy dissipation graphs yield that the specimen with post tensioning and with steel corbel (HBD_16_20_C) revealed the best performance, similar to the monolithic specimen.

Residual Displacements

Residual displacements are observed in many structures instead of inelastic deformations take place. This residual displacement is closely related to the maximum ductility level for the yielding beam-to-column connection. It should be noted that, although the energy dissipation of the connection is positively affected by the increasing residual displacements, it also causes an increase in the repair and strengthening costs of the buildings after the earthquake (Christopoulos and Pampanin, 2004). The

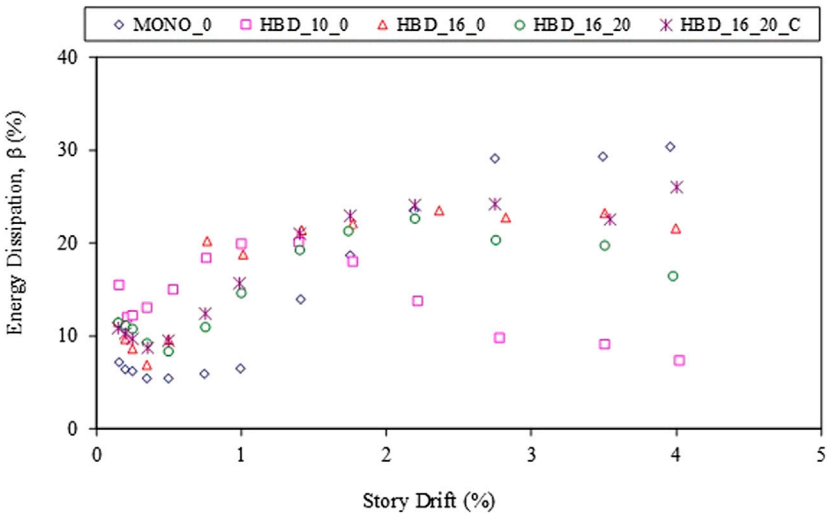

FIGURE 13 | The relative energy dissipation ratios vs. story drift response.

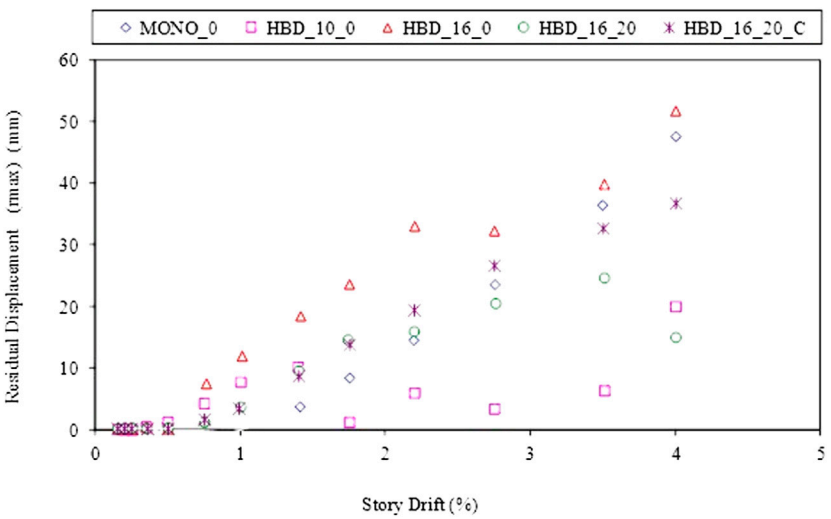

FIGURE 14 | Residual displacements at the specimens depending on the story drift.

maximum possible residual displacement is mainly a function of the unloading curve stiffness and the last residual displacement value (Christopoulos et al., 2003a; Christopoulos et al., 2003b).

The design philosophy of post tensioned connections is based on preventing residual damage in structural members after an earthquake. In case of residual story displacement in the structure, residual rotation will occur at beam ends according to the strong column-weak beam design philosophy. **Figure 14** illustrates the residual displacement-story drift behavior for test specimens. Residual displacements, observed until the mild steel reinforcement yielding load level in precast connections, are at their minimum. On the other hand, the behavior of precast connection with mild steel ratio of %10 depending on the residual displacement is not consistent. At the 4% story drift level, a 20 mm residual displacement was recorded for specimen HBD_10_0. Prior to yielding of the mild steel reinforcement in specimens HBD_16_20, the residual displacements were minor. After the reinforcement yielding point, permanent displacements reached 15 mm at the end of the test. The residual deformation characteristics of monolithic specimen and the specimen with post tensioning and with steel corbel (HBD_16_20_C) are remarkably similar.

CONCLUSION

The following conclusions are from the results of the current experimental investigation.

- The damage in post tensioned precast connections is mainly observed in the beam-column interface due to the opening and closing of the first crack. The damage in all precast members is at a negligible level. However, vertical relative sliding of the beam on the column surface after the yielding of mild steel reinforcement becomes more dominant in specimens without post-tensioning. The sliding at the interface leads to mild steel reinforcement rupture less than the expected story drift levels.
- The post tensioned precast connection with steel corbel system as in the HBD_16_20_C specimen prevents the rupture of mild steel reinforcement and maintains the connections load bearing capacity even at higher story drift levels, even during the 4.00% story drift ratio. Also, this specimen may well be an alternative to the monolithic connection with reduced onsite construction time.
- In precast connections the stiffness was similar to the monolithic specimen at the beginning of the drift ratios. However, a pronounced degradation is started due to the opening and closing of the crack at the beam-column interface. Application of initial post-tensioning instead of the high strength bolts and placing a corbel to reduce the relative sliding of beam, as with the HBD_16_20_C connection, not only increases the initial stiffness but also reduces stiffness degradation.
- The HBD_16_20_C, one of the precast connections, displayed the closest energy dissipation behavior similar to the monolithic connection.
- The results of this experimental study show that the performance of the HBD_16_20_C precast connection was satisfactory based on the seismic performance evaluation recommended by ACI T1.1R-0. This indicates that the precast structure utilizing the beam-column connection has a proper lateral force resistance against seismic loads.

DATA AVAILABILITY STATEMENT

All datasets presented in this study are included in the article.

AUTHOR CONTRIBUTIONS

HA designed the connection specimens, conducted the experiments, analyzed the results, and wrote the manuscript. SO supervised the studies and support her. Both authors contributed to the article and approved the submitted version.

FUNDING

Part of the present study was supported by the Republic of Turkey Kocaeli Governorship.

ACKNOWLEDGMENTS

The authors extend their appreciation to Kocaeli University Structures Laboratory staff for their invaluable contributions in the preparation and testing of the specimens.

REFERENCES

ACI Innovation Task Group 1 (2003). ACI T1. 2-03-Special hybrid moment frames composed of discretely jointed precast and post-tensioned concrete members. *American Concrete Institute*, Farmington Hills, MI.

Adalier, K., and Aydingun, O. (2001). Structural engineering aspects of the june, 1998 adana–ceyhan (Turkey) earthquake. *Eng. Struct.* 23, 343–355. doi:10.1016/s0141-0296(00)00046-8

Amaris, A., Pampanin, S., and Palermo, A. (2006). "Uni and bi-directional quasi static tests on alternative hybrid precast beam column joint subassemblies," The New Zealand society for earthquake engineering conference, New Zealand, June 2006.

Bhatt, P., and Kirk, D. W. (1985). Test on an improved beam column connection for precast concrete. *ACI Struct. J.* 82, 834–843.

Bruneau, M. (2002). Building damage from the marmara, Turkey earthquake of august, 1999. *J. Seismol.* 6, 257–377. doi:10.1023/a:1020035425531

Cheok, G. S., and Lew, H. S. (1993). Model precast concrete beam to column connections subject to cyclic loading. *PCI J.* 38, 80–92. doi:10.15554/pcij.07011993.80.92

Cheok, G., Stone, W., Stanton, J., and Seagen, D. (1994). Beam-to column connection for precast concrete moment-resisting frames, Proc.4th joint technical coordinating committee on precast seismic structural systems. Tsukuba, Japan, May 1994.

Christopoulos, C., Pampanin, S., and Priestley, M. J. N. (2003a). Performanced-based design seismic response of frame structures including residual deformations. part-I: single-degree of freedom systems. *J. Earthq. Eng.* 7, 97–118. doi:10.1080/13632460309350443

Christopoulos, C., Pampanin, S., and Priestley, M. J. N. (2003b). Performanced-based design seismic response of frame structures including residual deformations. part-II: multi-degree of freedom systems. *J. Earthq. Eng.* 7, 119–147. doi:10.1080/13632460309350443

Christopoulos, C., and Pampanin, S. (2004). Towards performance-based seismic design of MDOF structures with explicit consideration of residual deformations. *ISET J. Earthq. Technol.* 41, 53–73.

Crisafulli, F. J., and Restrepo, J. I. (2003). Ductile steel connections for seismic resistant precast buildings. *J. Earthq. Eng.* 7, 541–553. doi:10.1080/13632460309350463

Dolan, C. W., and Pessiki, S. P. (1989). Model testing of precast concrete connections. *PCI J.* 34, 84–103. doi:10.15554/pcij.03011989.84.103

Dolan, C. W., Stanton, J. F., and Anderson, R. G. (1987). Moment resistant connection and simple connection. *PCI J.* 32, 62–74. doi:10.15554/pcij.03011987.62.74

Englekirk, R. E. (1990). Seismic design consideration for precast concrete multistory buildings. *PCI J.* 35, 40–51. doi:10.15554/pcij.05011990.40.51

Ersoy, U., and Tankut, T. (1993). Precast concrete members with welded plate connections under reversed cyclic loading. *PCI J.* 38, 94–100. doi:10.15554/pcij.07011993.94.100

Ertas, O., Ozden, S., and Ozturan, T. (2006). Ductile connections in precast concrete moment resisting frames. *PCI J.* 51, 2–12. doi:10.15554/pcij.05012006.66.76

French, C. W., Amu, O., and Tarzikhan, C. (1989a). Connection between precast elements-failure outside connection region. *J. Struct. Eng.* 115, 316–340. doi:10.1061/(asce)0733-9445(1989)115:2(316)

French, C. W., Amu, O., and Tarzikhan, C. (1989b). Connection between precast elements-failure within connection region. *J. Struct. Eng.* 115, 3171–3192. doi:10.1061/(asce)0733-9445(1989)115:12(3171)

Ghosh, S. K. (1995). Observations on the performance of structures in the kobe earthquake of january 17, 1995. *Pcij* 40, 14–22. doi:10.15554/pcij.03011995.14.22

Hawkins, H. M., and Iverson, J. K. (1994). Performance of precast prestressed building structure during Northridge earthquake. *PCI J.* 39, 38–55.

Hawkins, N. M., and Ghosh, S. K. (2004). Requirements for the use of PRESSS moment-resisting frame systems. *PCI J.* 49, 98–103. doi:10.15554/pcij.03012004.98.103

Korkmaz, H. H., and Tankut, T. (2005). Performance of a precast concrete beam-to-beam connection subject to reversed cyclic loading. *Eng. Struct.* 27, 1392–1407. doi:10.1016/j.engstruct.2005.04.004

Mitchell, D., DeVall, R. H., Saatçioğlu, M., Simpson, R., Tinavi, R., and Tremblay, R. (1995). Damage to concrete structures due to the 1994 Northridge Earthquake. *Can. J. Civ. Eng.* 22, 361–377. doi:10.1139/l95-047

Nakaki, S. D., Englekirk, R. E., and Plaehn, J. L. (1994). Ductile connectors for a precast concrete frame. *PCI J.* 39, 46–59. doi:10.15554/pcij.09011994.46.59

Nakaki, S. D., Stanton, J. F., and Sritharan, S. (1999). An overview of the PRESSS five-story precast test building. *PCI J.* 44, 26–39. doi:10.15554/pcij.03011999.26.39

Ochs, J. E., and Ehsani, M. R. (1993). Moment resistant connections in precast concrete frames for seismic regions. *PCI J.* 38, 64–75. doi:10.15554/pcij.09011993.64.75

Ozden, S., Akpinar, E., Erdogan, H., and Atalay, H. M. (2014). Performance of precast concrete structures in october 2011 Van earthquake, Turkey. *Mag. Concr. Res.* 66, 543–552. doi:10.1680/macr.13.00097

Ozden, S., and Ertas, O. (2007). Behavior of unbonded post-tensioned precast concrete connections with different percentages of mild steel reinforcement. *PCI J.* 52, 32–44. doi:10.15554/pcij.03012007.32.44

Palmieri, L., Saqan, E., French, C. W., and Kreger, M. (1997). "Ductile connections for precast concrete frame system," in Mete A. Sozen symposium—a tribute from his students SP 162-13, Farmington Hills, MI, January 1997, 313–355.

Pampanin, S. (2005). Emerging solution for high seismic performance of precast/prestressed concrete buildings. *J. Advanced Conc. Tech.* 3, 207–223. doi:10.3151/jact.3.207

Parastesha, H., Hajirasoulihab, I., and Ramezanic, R. (2014). A new ductile moment-resisting connection for precast concrete frames in seismic regions: an experimental investigation. *Eng. Struct.* 70, 144–157. doi:10.1016/j.engstruct.2014.04.001

Park, R. (1995). A perspective on the seismic design of precast concrete structures in New Zealand. *PCI J.* 40, 40–60. doi:10.15554/pcij.05011995.40.60

Pillai, S. U., and Kirk, D. W. (1981). Ductile beam-column connection in precast concrete. *ACI Struct. J.* 8, 480–487.

Priestly, M. J. N., Calvi, G. M., and Kowalsky, M., J. (2007). *Displacement-based seismic design of structures*. Pavia, Italy: IUSS Press.

Priestly, M. J. N., Sritharan, S., Conley, J. R., and Pampanin, S. (1999). Preliminary results and conclusions from the PRESSS five-story precast test building. *PCI J.* 44, 42–67.

Restrepo, J. I., Park, R., and Buchanan, A. H. (1995). Design of connections of earthquake resisting precast reinforced concrete perimeter frames. *PCI J.* 40, 68–80. doi:10.15554/pcij.09011995.68.80

Seckin, M., and Fu, H. C. (1990). Beam-column connections in precast reinforced concrete construction. *ACI Struct. J.* 87, 252–261.

Soubra, K., S., Wight, J. K., and Naaman, A. E. (1993). Cyclic response of fibrous cast-in-place connections in precast beam-column subassemblages. *ACI Struct. J.* 90, 316–323.

Stanton, J. F., Hawkins, N. M., and Hicks, T. R. (1991). PRESSS Project 1.3: connections classifications and evaluations. *PCI J.* 36, 62–71. doi:10.15554/pcij.09011991.62.71

Stanton, J., Stone, W. C., and Cheok, G. S. (1997). A Hybrid reinforced precast frame for seismic regions. *PCI J.* 42, 20–23. doi:10.15554/pcij.03011997.20.23

Stone, W. C., Cheok, G. S., and Stanton, J. F. (1995). Performance of hybrid moment resisting precast beam–column concrete connections subjected to cyclic loading. *ACI Struct. J.* 91, 229–249. doi:10.14359/1145

Toniolo, G., and Colombo, A. (2012). Precast concrete structures: the lessons learned from the L'Aquila earthquake. *Struct Concr*, 13 pp. 78–83. doi:10.1002/suco.201100052

Vasconez, R. M., Naaman, A. E., and Wight, J. K. (1998). Behavior of HPFRC connections for precast concrete frames under reversed cyclic loading. *PCI J.* 43, 58–71. doi:10.15554/pcij.11011998.58.71

Conflict of Interest: The authors declare that the research was conducted in the absence of any commercial or financial relationships that could be construed as a potential conflict of interest.

frontiers in Built Environment

ORIGINAL RESEARCH
published: 12 February 2021
doi: 10.3389/fbuil.2021.627546

Modeling of the Beam-To-Column Dowel Connection for a Single-Story RC Precast Building

Gennaro Magliulo[1,2]*, *Chiara Di Salvatore*[3] *and Marianna Ercolino*[4]

[1]*Department of Structures for Engineering and Architecture, University of Naples Federico II, Naples, Italy,* [2]*Construction Technology Institute ITC-CNR, Naples, Italy,* [3]*Department of Science and Technology, University of Naples Parthenope, Centro Direzionale di Napoli - Isola C4, Naples, Italy,* [4]*Department of Engineering Science, University of Greenwich, Central Avenue, Chatham, United Kingdom*

As widely known, connections performance under seismic loads can significantly affect the structural response of RC precast buildings. Within the scientific community, an increasing number of studies has been carried out on this topic, in the light of the recent earthquake aftermaths all over Europe. Indeed, connections turned out to be the weakest part of the precast structures and their failure often provoked the global collapse of the whole building. The present study aims at assessing the seismic behavior of a single-story RC precast building in terms of global collapse implementing two different models of the beam-to-column connection, a simplified and a refined one. A lumped plasticity approach is used to simulate the structural nonlinear behavior at the column base. In order to assess the refined connection model, a preliminary scheme with an isolated single dowel is validated by comparing the pushover outcomes with experimental results from literature. Nonlinear static and dynamic analyses are performed on two models of a 3D single-story RC precast building, one implementing the simple beam-to-column connection model and the other one implementing the refined mode. The comparison clearly shows that the differences are negligible if the global collapse limit state is considered.

Keywords: precast structures, dowel connection, nonlinear model, pushover analysis, multistripe analysis

OPEN ACCESS

Edited by:
Andrea Belleri,
University of Bergamo, Italy

Reviewed by:
Emanuele Brunesi,
Fondazione Eucentre, Italy
Roberto Nascimbene,
Fondazione Eucentre, Italy

***Correspondence:**
Gennaro Magliulo
gmagliul@unina.it

Specialty section:
This article was submitted to Earthquake Engineering, a section of the journal Frontiers in Built Environment

Received: *09 November 2020*
Accepted: *08 January 2021*
Published: *12 February 2021*

Citation:
Magliulo G, Di Salvatore C and Ercolino M (2021) Modeling of the Beam-To-Column Dowel Connection for a Single-Story RC Precast Building. Front. Built Environ. 7:627546. doi: 10.3389/fbuil.2021.627546

INTRODUCTION

Recent earthquakes in Europe stressed the importance of adequate seismic design as well as vulnerability assessment approaches for precast industrial structures (Sezen et al., 2000; Toniolo and Colombo, 2012; Magliulo et al., 2014b; Ozden et al., 2014; Belleri et al., 2015). The experience of such seismic events pointed out the weakness of connection systems for both structural elements and nonstructural components. The most catastrophic failures were caused by the presence of frictional connections (i.e., without any mechanical devices), which had a very low strength under horizontal loads. Moreover, some damaged structures showed also the deficiencies of some mechanical connections because of inadequate design details, such as in the case of dowel beam-to-column connections. Such connections consist of one or more steel threaded bars (dowels) cast at the column top and inserted in the beam by means of holes filled with mortar. In some applications the dowels can be fastened at the top of the beam to enhance the connection stability during the construction phase (**Figure 1**).

In the last decades, several research studies have been performed to investigate the vulnerability of modern (new) structures with mechanical connections under seismic actions (Vintzeleou and

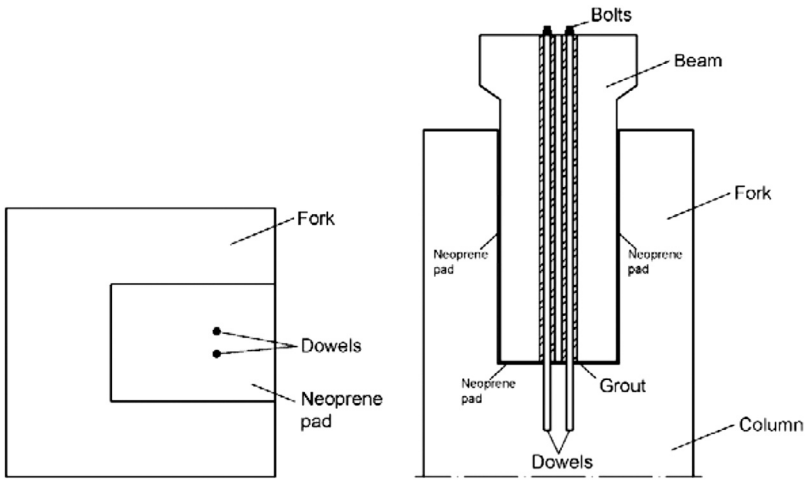

FIGURE 1 | Typical beam-to-column dowel connection.

Tassios, 1987; Safecast, 2012; Zoubek et al., 2013; Magliulo et al., 2014a; Kremmyda et al., 2014; Brunesi et al., 2015; Zoubek et al., 2015; Dal Lago et al., 2018; Bressanelli et al., 2019; Cimmino et al., 2020; Sousa et al., 2020). Vintzeleou and Tassios (1987) conducted an experimental investigation in order to detect the main failure mechanisms of dry connections provided with dowels under cyclic loads. Tests pointed out two different failure modes: failure mode I and failure mode II, depending on the size of the concrete cover. If the concrete cover is greater than 6–7 times the diameter of the dowel, the yielding of the dowels and the consequent crashing of the concrete around them are observed (failure mode I). Otherwise, if the concrete cover is smaller than this value, the connection fails due to the splitting of the concrete cover in one of the two horizontal principal directions (failure mode II). The former mechanism is defined as a ductile collapse, whereas the latter provides a fragile failure. The same authors proposed relationships to calculate the dowel connection strength for both the failure modes under monotonic as well as cyclic loads. More recent studies confirmed these results (Psycharis and Mouzakis, 2012a; Psycharis and Mouzakis, 2012b). The research project "SAFECAST—Performance of innovative mechanical connections in precast building structures under seismic conditions"—(Safecast, 2012) developed a vast experimental campaign to analyze the behavior of different connections typologies as well as to define new design approaches and/or provisions. Several experimental tests were performed on the dowel beam-to-column connection and design formulas were also proposed. However, such investigated dowel systems had peculiar features, typically adopted in Slovenian buildings, such as the use of a steel tube around the dowel in the beam. Therefore, those results have some limitations of applicability and they need further investigation. Zoubek et al. (2013) assessed the dowel connection by means of a numerical model in ABAQUS FEA software (DSS Corp., 2010), which was validated on both the monotonic and cyclic tests of the SAFECAST framework. A key aspect of the model was the contact surface between the dowel and the concrete/grout in the direction of the dowel axis as well as in the orthogonal axis, as already highlighted in Maitra et al. (2009) and Guezouli and Lachal (2012). The failure mode in both the experimental test and the numerical model was a ductile mechanism, i.e., with the yielding of the dowel and simultaneous crashing of the surrounding concrete (Vintzeleou and Tassios, 1987). It was found that the resistance of the dowel increases with the plastic hinge depth. Furthermore, large rotations at the base of the columns can reduce the dowel strength since the steel bars undergo also tensile stresses along with the shear strains. In the framework of the SAFECAST project, Kremmyda et al. (2014) developed a numerical model in ABAQUS (DSS Corp., 2010) to detect the ductile failure mechanism as well as to identify the plastic hinges in the dowel and to measure the dissipated energy. The model was validated with experimental results under both cyclic and monotonic loads. Some research studies dealt with the fragile failure mechanism. Magliulo et al. (2014a) performed monotonic tests on a dowel connection, designed according to Italian codes and construction methodologies. The failure of this connection involved the splitting of the lateral concrete cover in the column because of its inadequate dimension. A numerical model in ABAQUS was also developed by the same authors (Magliulo et al., 2014a) which was capable to reproduce the experimental evidence. A parametric study was then performed to assess the influence of some main geometrical features on the connection response (dowel diameter, frontal cover, and lateral cover). Zoubek et al. (2015) studied the design formulas of the connection strength, for both the ductile and fragile failure mechanism. In particular, the strength of the ductile mechanisms can be calculated by using the already available formulas in the literature, which were extensively validated by both numerical model and evidence. However, if a fragile mechanism occurs, the available formulas were found

inadequate in evaluating the connection capacity because of the neglected contribution of the stirrups in the connection. The authors proposed a new equation for this mechanism and showed a good agreement with past experimental results. Brunesi et al. (2015) carried out an experimental campaign on two planar three-story frames, in order to assess the effectiveness of beam-to-column dowel connections and panel-to-structure links. A ¾ scaled bare frame, designed for a medium to high seismicity, was considered to study the dowel connection response. The frame underwent quasi-static cyclic roof displacements, applied by actuators located at each slab level. The structural collapse was dictated by connection failure; indeed, dowels failed in shear, after yielding, when the structure was still in the elastic field. The observed poor seismic performance has led the authors to discourage the use of this structural type of building in high seismic areas. Bressanelli et al. (2019) performed a wide investigation on the modeling assumption reliability in reproducing the real seismic response of RC precast buildings. The assessed issues mainly concern the mass distribution, the influence of the higher vibrational modes, and the dowel connection implementation. A detailed numerical model for the connections is introduced in the structural scheme, instead of the usual perfect hinge constraint; however, given the variation of several parameters, it is not easy to understand how the change of the connection model affects the results of the dynamic analyses. Cimmino et al. (2020) dealt with the seismic assessment of a precast industrial building designed according to the modern codes. Since the last seismic events showed the inadequacy of some pinned connections, whose failure prevented the development of plastic hinges at the columns base, structural capacity was evaluated with both a global and a local approach; the global failure mode was related to the attainment of the ultimate rotation of the plastic hinges, whereas the local collapse considered the connections breakdown. Furthermore, for both the connections failure modes (ductile and fragile), a comparison between all the available formulations was made. As concerns the ductile failure, expressions by CNR 10025/1984 (CNR 10025/84, 1984), Vintzeleou and Tassios (1987) monotonic and cyclic, EOTA (TR045, 2013) monotonic and cyclic, and Safecast (2012) were applied for the calculation of connections shear strength and it is found that, neglecting the case of Vintzeleou and Tassios—cyclic, which is proved to be too conservative (Magliulo et al., 2015), SAFECAST formula provided the lowest strength. Sousa et al. (2020) developed a very accurate dowel connection model, accounting for the deformability of the neoprene pad, the friction at the concrete-neoprene interface, and the dowels response under horizontal loads. The model is experimentally validated, confirming its goodness in catching connection failure mode and maximum strength. A parametric analysis of the components geometrical and mechanical properties shows the possibility to generalize the application of the proposed model.

The results of nonlinear dynamic and static analyses of a new RC precast building under seismic actions are reported in the manuscript. For the same structure, two models of the dowel connections are compared at the global collapse limit state: 1) a perfect hinge constraint between the beam and the column and 2) a degrading hysteretic model that can simulate a more actual behavior of the connection under horizontal loads. The model of the beam-to-column connection is the only modified parameter of the performed analyses, allowing for a clear identification of the effects of such a modification. Other studies implemented refined beam-to-column dowel connection models, but, to the authors' knowledge, none of them showed the equivalence in terms of building global collapse between a refined model and a very simple approach based on the connection strength monitoring.

BENCHMARK STRUCTURE

Description

The analyzed structure is a single-story RC precast industrial building, located in Central Italy (L'Aquila) on soil type C ($180\ \text{m/s} \leq V_{s,30} \leq 360\ \text{m/s}$), according to EC8 (CEN, 2005). The structure consists of four 6 m long spans in the longitudinal direction (*Z* direction in **Figure 2**) and one 15 m long span in the transversal direction (*X* direction in **Figure 2**). The total height of the columns is equal to 9 m with a crane bracket at 7.5 m from the base. The structure is designed according to the recent Italian seismic code (NTC 2008). The roof has prestressed RC elements connected by means of both mechanical devices and a cast *in situ* concrete slab. The connection between the roof and the principal beams is obtained by means of dowel connections. The main beams are located along the transversal direction; their peculiar shape is illustrated in **Figure 3**. Dowel connections, made by 2ϕ24 mm threaded bars, are used between the main beams and the columns. They are designed with horizontal forces provided by the capacity design, i.e., as the minimum between the column base resisting moment/column height ratio by the factor $\gamma_{\text{Rd}} = 1.20$ and the value given by the seismic analysis assuming the behavior factor q = 1. The diameter and the number of the dowels are designed according to Italian guidelines (CNR 10025/84, 1984), which provide the following formula for the connection horizontal strength:

$$V_{Rd} = n\,\alpha\,d_b^2\,\sqrt{f_{yd}f_{cd}}, \tag{1}$$

where $n = 2$ is the number of dowels, $\alpha = 1.6$ is a coefficient taking into account the confinement provided by the beam-column mutual pressure, d_b is the dowel resistant diameter, $f_{yd} = f_y/\gamma_S = 564\ \text{N/mm}^2$ is the steel design yielding strength, and $f_{cd} = \alpha_{cc} f_{ck}/\gamma_c = 25.87\ \text{N/mm}^2$ is the concrete design strength. The secondary beams have a U-shaped section and they are connected to the columns by dowel connections. The columns are precast elements with a square shaped cross-section (**Figure 4**), connected to a socket foundation at the base. As concerns the structural materials, concrete with characteristic compressive strength equal to $45\ \text{N/mm}^2$ and steel with characteristic yielding strength equal to $450\ \text{N/mm}^2$ are considered in the design stage. Further details about the design steps and results can be found in Ercolino et al. (2018).

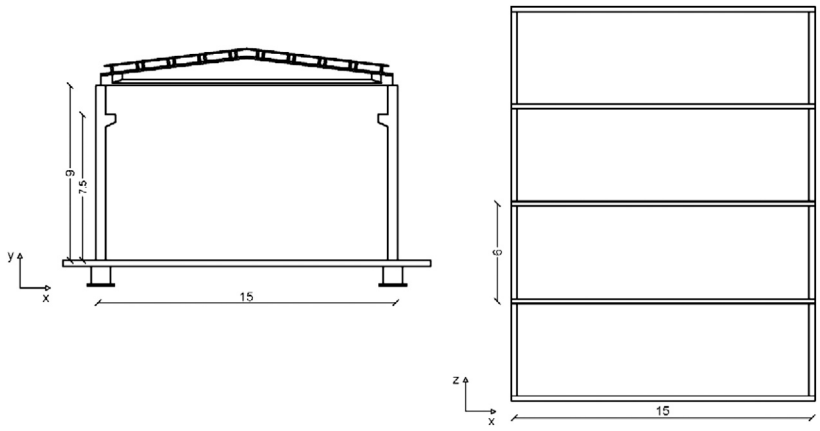

FIGURE 2 | Structural layout.

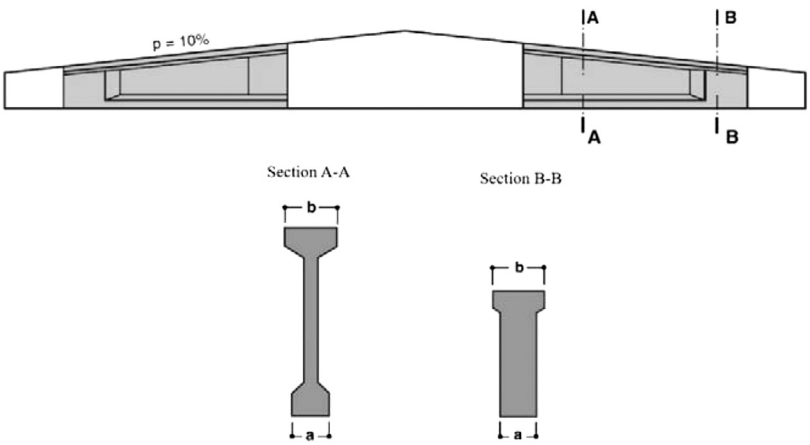

FIGURE 3 | Main beam configuration.

Model of the Structural Elements

A 3D nonlinear model of the structure is developed in OpenSees (PEER, 2007). Columns are fixed at the base, while secondary beams are hinged to the columns. Columns and beams are modeled as elastic elements and a lumped plasticity approach is used to model the nonlinear behavior of the structure with plastic hinges at the columns base. Geometrical nonlinearities are taken into account for columns according to a PDelta coordinate transformation, which adds the second-order bending moments at the element ends. The eccentricities between the longitudinal axes of the structural elements are considered as rigid links at the beam-to-column connection in both the transversal and the longitudinal direction of the building (**Figure 5**). The roof elements are not modeled in the structure and a rigid diaphragm can be assumed at the top of the beams because of the stiffness of the cast *in situ* concrete slab. Thus, all the seismic mass, equal to 543 t, is lumped in the barycenter of the deck. The cladding panels are not modeled and their contribution to the global stiffness of the structure is neglected.

The monotonic moment-rotation envelope curve assigned at the column base consists of three branches: the first branch defines the postcracking response of the column by means of a secant stiffness up to the yielding point; the second branch is characterized by a hardening response until the maximum strength (capping point); and the third branch shows a softening behavior up to the ultimate rotation (postcapping point). It is provided according to Fischinger et al. (2008), where an ideal backbone curve is proposed for precast cantilever columns (i.e., with large shear span ratio) designed according to modern codes, by comparing experimental results with literature formulas. In particular, the suggested envelope consists of 1) the yielding rotation by Fardis and Biskinis (2003); 2) the capping rotation, the capping moment, and the ultimate rotation by Haselton (2006); 3) the yielding moment as the value corresponding to the yielding of the steel reinforcement or the crushing of the concrete in the cover. In **Figure 6** the monotonic backbones for both corner and lateral columns are plotted; the difference is due to the different values of axial loads acting on them (333 kN for the corner columns and

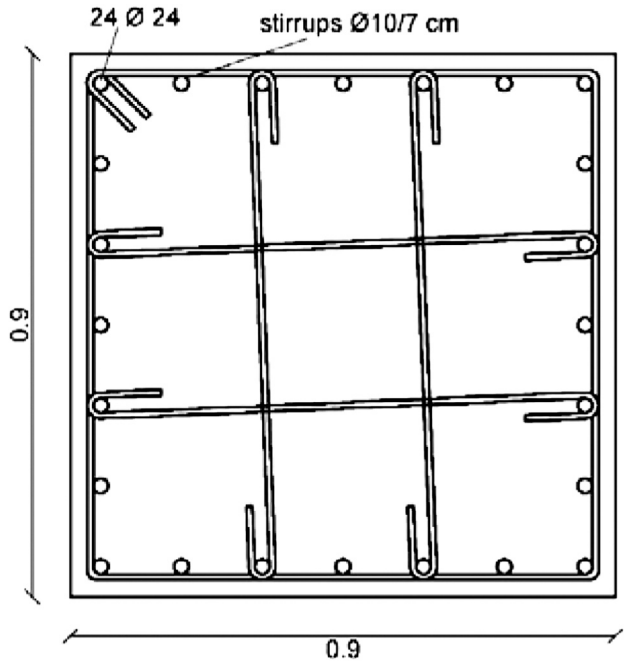

FIGURE 4 | Column cross-section.

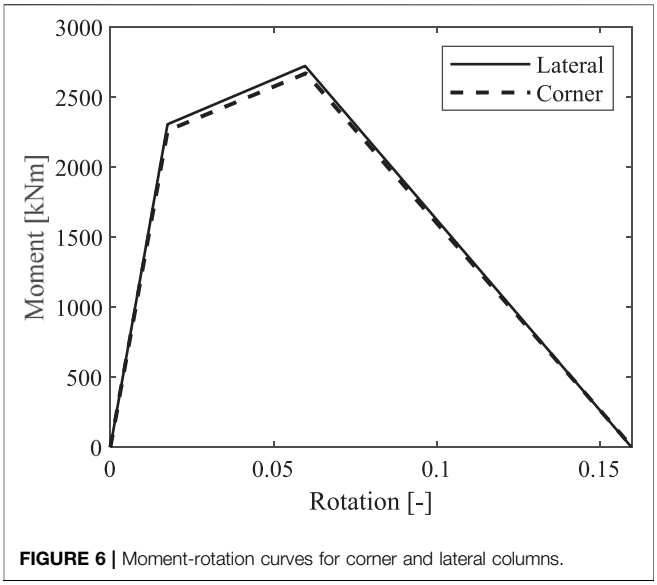

FIGURE 6 | Moment-rotation curves for corner and lateral columns.

456 kN for the lateral columns). The hysteretic model is assigned according to Ibarra et al. (2005), taking into account the cyclic degradation based on energy dissipation criteria.

In the modeling phase, mean mechanical characteristics of the structural materials are considered: mean compressive strength equal to 59.7 N/mm2 for the concrete and mean yielding strength equal to 490 N/mm^2 for the steel reinforcement.

MODELS OF THE MAIN BEAM-TO-COLUMN CONNECTION

The connection between the main beams and the columns is modeled with two different approaches: 1) as a hinge constraint and 2) with a more accurate model providing the actual hysteretic force-displacement behavior, as presented in this section. The latter model is analyzed with a preliminary study as a single connection. Then, it is added to the 3D nonlinear model of the structure to assess how it affects the overall response under earthquake actions.

The refined model is calibrated on the experimental results of the Safecast (2012) project. In particular, the model is based on the outcomes of eleven monotonic tests performed at the Laboratory of the National Technical University of Athens by Kremmyda et al. (2014) and provides the backbone curve shown in **Figure 7**.

The maximum strength of the connection is assumed according to the Safecast (2012) formula:

$$V_{Rd} = n\,0.9\,d_b^2\,\sqrt{f_y f_c\,(1-\alpha^2)}, \tag{2}$$

where f_y and f_c are the mean steel yielding strength and the mean concrete compressive strength, respectively, and α is a coefficient taking into account the possible presence of axial stress in the

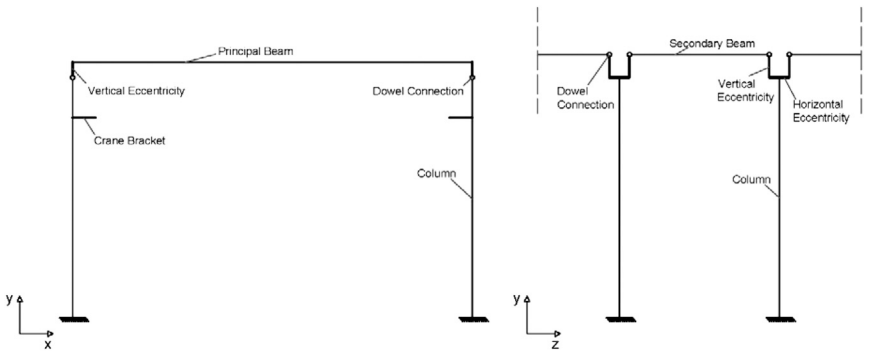

FIGURE 5 | Structural scheme.

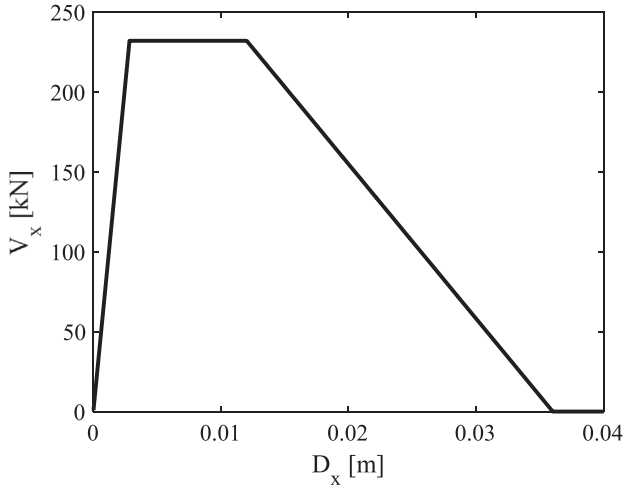

FIGURE 7 | Force-displacement trilinear backbone of the dowel connection.

dowel, which is assumed equal to zero. The Safecast (2012) formula was chosen for the sake of safety, since it gives the minimum value of strength with respect to the other formulas available in the literature (Cimmino et al., 2020). In particular, it provides a value of the connection strength lower than the value provided by the design **Eq. 1**, if in the two formulas the same values of the concrete and steel strength, respectively, are used.

The yielding displacement is evaluated as

$$D_y = \lambda F_y, \tag{3}$$

where F_y is the connection strength (V_{Rd}) and λ is determined according to Ferreira and El Debs (2000). The capping point is defined by the displacement equal to 0.5ϕ (where ϕ is the diameter of the dowels) and the shear force equal to the connection strength (V_{Rd}). Finally, the residual strength of the connection is assumed equal to zero at a displacement equal to 1.5ϕ. **Table 1** shows the values of the forces and displacements of the connection model, assuming the same behavior along the positive and the negative horizontal direction. In order to implement the connection cycling response, the OpenSees model "uniaxial Material ModIMKPeakOriented" (PEER, 2007) was applied to the zero-length element representing the dowel connection along the *x* direction, which provides a degrading hysteretic behavior in terms of force-displacement.

A single dowel connection is modeled (**Figure 6A**) and a nonlinear static analysis is performed in order to verify the efficiency of the proposed modeling approach. The model consists of two nodes, connected by a stiff elastic one-dimensional element. The connection model is assigned between the two nodes in the horizontal direction (X in **Figure 8A**). A pushover analysis is performed in *X* direction and the results are presented in **Figure 8B** with a green solid line. The results of the analysis demonstrate the capability of the numerical model to simulate the expected behavior of the connection.

TABLE 1 | Force-displacement backbone coordinates.

	Displacement [m]	Force [kN]
Yielding	0.0028	232
Capping	0.0120	232
Ultimate	0.0360	0

GLOBAL COLLAPSE OF THE BENCHMARK 3D STRUCTURE: COMPARISON BETWEEN THE TWO BEAM-TO-COLUMN CONNECTION MODELS

Pushover Analysis Outcomes

Nonlinear static (pushover) analyses are performed on two different structural models in order to evaluate how the dowel connection modeling affects the structural capacity in terms of global collapse. In the first model the main beam-to-column dowel connection is assumed as perfect hinge and the collapse is reached when the horizontal force in the hinge equals the connection horizontal strength, i.e., 232 kN. Assuming that all connections contemporaneously reach their maximum strength due to the in-plane rigidity of the roof including the main beams, the total horizontal force at the beam-to-column connection is equal to 2320 kN (**Figure 9A**). The second model takes into account the actual mechanical properties of the dowel connection by means of the above presented refined model. This latter model is assigned to all main beam-to-column connections along the *X* direction.

The analysis outcomes are presented in **Figure 9**. In particular, in **Figure 9A** the pushover results are reported in terms of base shear-top displacement for both models. The thick line shows the results of the refined model, where, at the reaching of the connection maximum strength, a quick drop is observed, denoting the failure of all connections and the global collapse of the building. For the assessed building, the kinematics under seismic actions (Brunesi et al., 2015) does not determine any additional constraint at the connection level, since the beams never come in contact with the columns and the corbels. In the first model the global collapse reaching is pointed out by the dotted horizontal line at 2320 kN. The pushover first branches of the two models are coincident until the attainment of the base shear value equal to 2320 kN, denoting the conventional collapse of the first model and the observed collapse of the second model. It can be concluded that nonlinear static analyses of the two models provide the same results in terms of global collapse of the building.

Figure 9 shows some insights too. The dashed line in **Figure 9A** plots the pushover curve in the case of main beam-to-column connections without strength limitation (Kramar et al., 2010; Magliulo et al., 2018). In this case, the global pushover curve follows the behavior of the plastic hinge at the column base, covering a postcracking, a postyielding, and, finally, a postcapping branch. It is worth noting that the failure

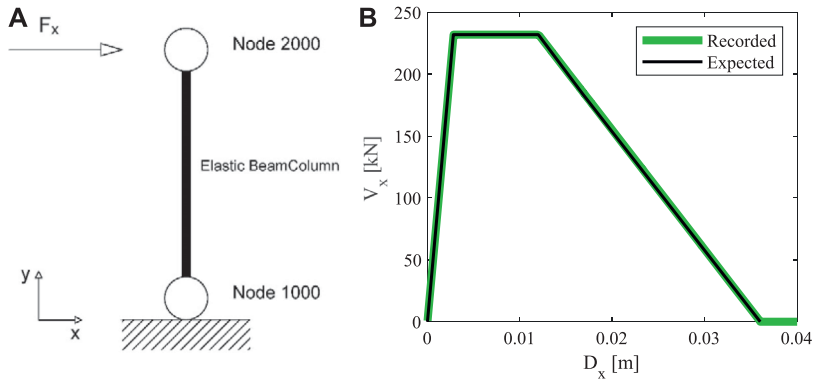

FIGURE 8 | (A) Single dowel connection modeling scheme. **(B)** Comparison between the expected and the recorded pushover curves.

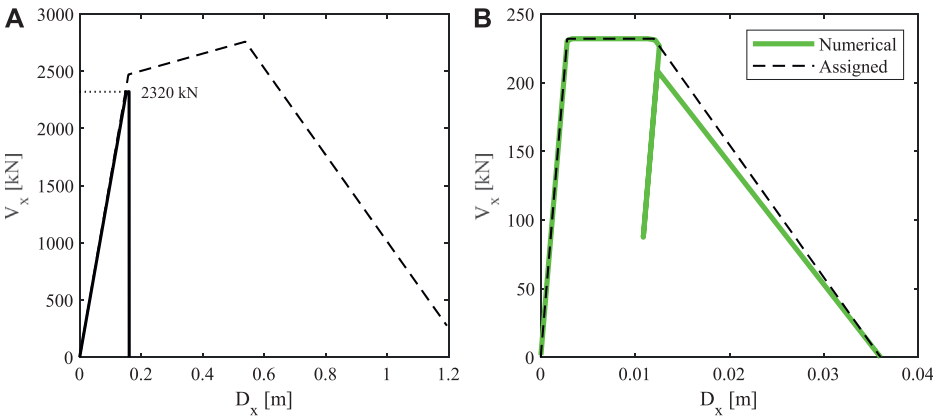

FIGURE 9 | (A) Pushover curves along *X* direction for both the models and **(B)** force-displacement curve in a single dowel connection. Results of the multistripe analyses.

of the connections and the consequent global collapse of the building precede the yielding at the column base, which should never happen if the capacity design is implemented for the connection design. Indeed, the observed behavior is due to the different formulas referenced for the design of the connections (**Eq. 1**) and for their assessment (**Eq. 2**). The latter one, which is an outcome of the recent research, provides a strength significantly lower than the former one, which is extensively used in Italy being provided by technical guidelines (Cimmino et al., 2020). **Figure 9B** shows the force-displacement curve recorded in the refined model of the connection during the nonlinear static analysis. It is evident that the refined model is well functioning, because the force-displacement relationship well follows the assigned model, except for a local numerical instability in the softening branch, which did not affect the analyses.

Results of the Multistripe Analyses

Multistripe nonlinear dynamic analyses are performed in order to compare the performance of the two models described in the previous sections in terms of global collapse. Ten increasing intensity levels (IM) are defined through an accurate hazard analysis (Iervolino et al., 2017) and, for each IM, twenty accelerograms are selected by means of the Conditional Spectrum Method (Lin et al., 2013a; Lin et al., 2013b). The Conditional Spectrum Method was applied by defining the target spectrum with an assigned value of pseudo-acceleration at the fundamental period of the structure (T_1 equal to 2.0 s). The selected acceleration records belong to both the Italian accelerometric archive (Itaca) and the NGwest database. Both the horizontal components are used in the analyses along the *X* and *Z* directions of the structure (**Figure 2**). The spectrum-compatibility procedure was carried out on the component with the maximum value of PGA, which is then applied in the transversal direction (X). **Table 2** shows the considered intensity levels and the conditioned spectral pseudo-acceleration at each return period.

The structural collapse is achieved when the seismic demand (D) exceeds the corresponding capacity value (C) in the *X* direction of the building. The failure criteria already defined for nonlinear static analyses are implemented in order to assess the structural vulnerability of the case study under nonlinear

TABLE 2 | Spectral acceleration values for each selected seismic intensity level.

IM [-]	1	2	3	4	5	6	7	8	9	10
T_R [years]	10	50	100	250	500	1,000	2,500	5,000	10,000	100,000
S_a (2s) [g]	0.011	0.026	0.049	0.080	0.124	0.184	0.270	0.379	0.572	1.077

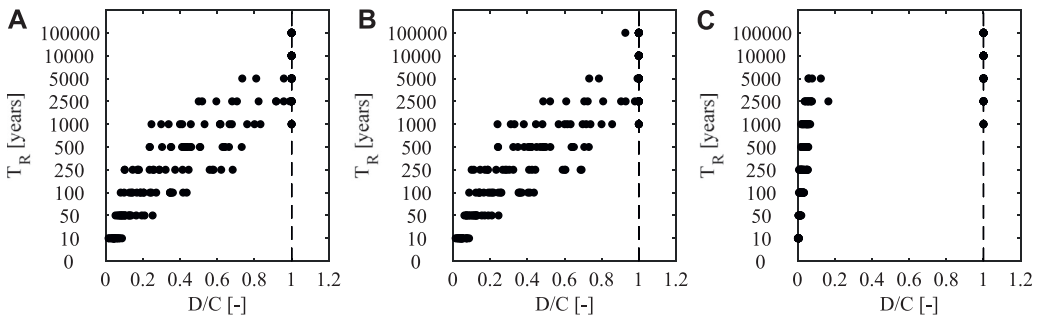

FIGURE 10 | Demand/capacity ratios for each ground motion at each return period: **(A)** internal hinge case, **(B)** refined force parameter, **(C)** refined displacement parameter.

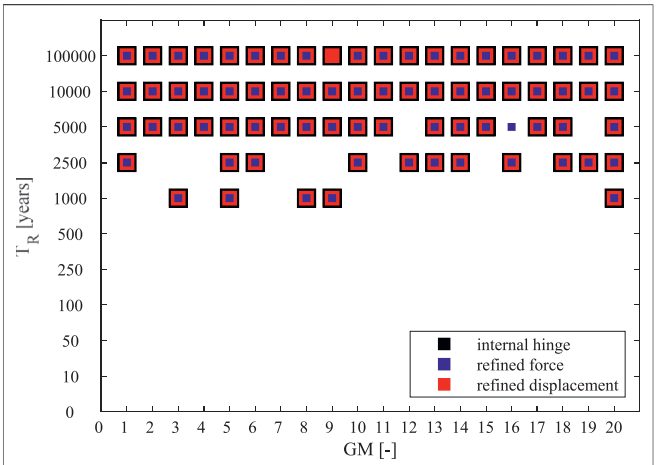

FIGURE 11 | Collapse cases recorded by the multistripe analyses.

dynamic analyses: i. the reaching of the horizontal strength of the main beam-to-column connection when it is modeled as an internal hinge (internal hinge case); ii. the reaching of the maximum strength (flat branch of the backbone curve) of the main beam-to-column connection refined model (refined force parameter); iii. the ultimate displacement of the main beam-to-column connection refined model, i.e., the displacement corresponding to the connection strength equal to zero (refined displacement parameter). The corresponding demand parameters are as follows: i. the global horizontal force at the main beam-to-column connection level; ii. the force recorded in the main beam-to-column connection refined model; iii. the displacement recorded in the main beam-to-column connection refined model.

The results of the multistripe analyses are presented in **Figure 10** as demand/capacity ratios for the internal hinge case (A), the refined force parameter (B), and the refined displacement parameter (C). Obviously, all the attainments of the collapse are identified as D/C = 1. **Figure 11** provides the recorded collapses in all cases for each ground motion. The plots show that the refined model of the connection does not modify the results in terms of global collapse of the building, when it is reported in terms of forces and displacements. The differences evidenced by the three plots shown in **Figure 10** are only related to the different parameters representing the demand/capacity ratio. The obtained result is due to the large stiffness of the connection and to its limited ductility (**Figure 7**), which are not able to modify the global building deformability and ductility.

CONCLUSIONS

In the presented study a refined trilinear model of the main beam-to-column dowel connection of single-story RC precast buildings is proposed, based on literature experimental results. Nonlinear static analyses are performed on both the single connection model and the 3D case study provided with the proposed dowel connection model. Nonlinear dynamic analyses, namely, multistripe analyses, are also performed. Ten stripes, corresponding to ten increasing intensity levels, are considered, and, for each of them, twenty ground motions are selected, resulting in two-hundred time history analyses. The numerical study gave the outcomes and conclusions presented below.

(1) The refined model is able to well simulate the behavior of the dowel beam-to-column connection, as detected in past experimental studies.
(2) Pushover analyses show that the global collapse occurs when the maximum strength of the connections is attained. Such failure occurs before the yielding at the column base. The

recorded collapse is due to the simultaneous failure of all connections, because of both the rigid floor at the roof level and symmetry of the building.

(3) The failure criterion of the beam-to-column connection refined model can be defined equivalently as the attainment of either the maximum resistance or the ultimate displacement.

(4) The refined model of the connection does not affect the global response of the building in terms of collapse and, consequently, does not offer an improved accuracy of the results. Indeed, nonlinear dynamic analyses outcomes show that the global collapses, detected monitoring the proposed connection model capacity, are 73 out of 200, as the ones detected considering the connections as internal hinges and monitoring the reaching of their horizontal strength. Therefore, nonlinear time history analyses of single-story RC precast buildings can be carried out using a simple model of the beam-to-column connection (internal hinge), requesting a lower numerical analysis effort.

DATA AVAILABILITY STATEMENT

The original contributions presented in the study are included in the article/Supplementary Material; further inquiries can be directed to the corresponding author.

AUTHOR CONTRIBUTIONS

GM contributed to conception or design of the work, critical revision of the article, and final approval of the version to be published. CDS contributed to data collection, data analysis and interpretation, and drafting the article. ME contributed to conception or design of the work, critical revision of the article, and the final approval of the version to be published.

FUNDING

This research study has been funded by the Italian Department of Civil Protection, in the framework of the national project DPC-ReLUIS-EUCENTRE RINTC 2019–2021. During the article writing phase the author CDS has been funded by the Ph.D. scholarship of the University of Parthenope "Fenomeni e rischi ambientali––FERIA", tutor prof. Nicola Caterino.

ACKNOWLEDGMENTS

The contribution of Michele Cirillo for some numerical analyses is gratefully acknowledged.

REFERENCES

Belleri, A., Brunesi, E., Nascimbene, R., Pagani, M., and Riva, P. (2015). Seismic performance of precast industrial facilities following major earthquakes in the Italian territory. *J. Perform. Constr. Facil.* 29, 04014135. doi:10.1061/(asce)cf.1943-5509.0000617

Bressanelli, M., Belleri, A., Riva, P., Magliulo, G., Bellotti, D., and Dal Lago, B. (2019). Effects of modeling assumption on the evaluation of the local seismic response for RC precast industrial buildings. COMPDYN 2019-7th ECCOMAS Thematic Conference on Computational Methods in Structural Dynamics and Earthquake Engineering, 1–14. Crete, Greece. 24-26 June 2019.

Brunesi, E., Nascimbene, R., Bolognini, D., and Bellotti, D. (2015). Experimental investigation of the cyclic response of reinforced precast concrete framed structures. *Pcij* 60, 57–79. doi:10.15554/pcij.03012015.57.79

CEN (2005). *Eurocode 8: design of structures for earthquake resistance - Part 3: assessment and retrofitting of buildings*. Brussels, Belgium:CEN.

Cimmino, M., Magliulo, G., and Manfredi, G. (2020). Seismic collapse assessment of new European single-story RC precast buildings with weak connections. *Bull. Earthq. Eng. 18*, 1–26. doi:10.1007/s10518-020-00952-7

CNR 10025/84 (1984). "Istruzioni per il progetto, l'esecuzione ed il controllo delle strutture prefabbricate in conglomerato cementizio e per le strutture construite con sistemi industrializzati (in Italian)". Bollettino Ufficiale del CNR. Rome, Italy:CNR.

DSS Corp. (2010). "Abaqus/CAE 6.10-1". (Providence).

Dal Lago, B., Negro, P., and Dal Lago, A. (2018). Seismic design and performance of dry-assembled precast structures with adaptable joints. *Soil Dynam. Earthq. Eng.* 106, 182–195. doi:10.1016/j.soildyn.2017.12.016

Ercolino, M., Bellotti, D., Magliulo, G., and Nascimbene, R. (2018). Vulnerability analysis of industrial RC precast buildings designed according to modern seismic codes. *Eng. Struct.* 158, 67–78. doi:10.1016/j.engstruct.2017.12.005

Fardis, M. N., and Biskinis, D. (2003). Deformation capacity of RC members, as controlled by flexure or shear. Editor S.H.E.P.-B.E.F.E.R.R.C.S.a.V.H.S.O. Kabeyasawa T (Tokyo, Japan: University of Tokyo).

Ferreira, A., and El Debs, M. (2000). Deformability of beam-column connection with elastomeric cushion and dowel bar to beam axial force. 2nd international symposium on prefabrication.

Fischinger, M., Kramar, M., and Isaković, T. (2008). Cyclic response of slender RC columns typical of precast industrial buildings. *Bull. Earthq. Eng.* 6, 519–534. doi:10.1007/s10518-008-9064-7

Guezouli, S., and Lachal, A. (2012). Numerical analysis of frictional contact effects in push-out tests. *Eng. Struct.* 40, 39–50. doi:10.1016/j.engstruct.2012.02.025

Haselton, C. (2006). Assessing seismic collapse safety of modern reinforced concrete moment-frame Buildings. Editor *P. Report* (Chico: Department of Civil Engineering California State University).

Ibarra, L. F., Medina, R. A., and Krawinkler, H. (2005). Hysteretic models that incorporate strength and stiffness deterioration. *Earthq. Eng. Struct. Dynam.* 34, 1489–1511. doi:10.1002/eqe.495

Iervolino, I., Spillatura, A., and Bazzurro, P. (2017). "RINTC Project - assessing the (implicit) seismic risk of code-conforming structures in Italy COMPDYN 2017,". Editors M. Papadrakakis and M. Fragiadakis6th ECCOMAS Thematic Conference on Computational Methods in Structural Dynamics and Earthquake Engineering, 15–17 June. Rhodes Island, Greece. 15-17 June 2017.

Kramar, M., Isaković, T., and Fischinger, M. (2010). Seismic collapse risk of precast industrial buildings with strong connections. *Earthq. Eng. Struct. Dynam.* 39, 847–868. doi:10.1002/eqe.970

Kremmyda, G. D., Fahjan, Y. M., and Tsoukantas, S. G. (2014). Nonlinear FE analysis of precast RC pinned beam-to-column connections under monotonic and cyclic shear loading. *Bull. Earthq. Eng.* 12, 1615–1638. doi:10.1007/s10518-013-9560-2

Lin, T., Haselton, C. B., and Baker, J. W. (2013a). Conditional spectrum-based ground motion selection. Part I: hazard consistency for risk-based assessments. *Earthq. Eng. Struct. Dynam.* 42, 1847–1865. doi:10.1002/eqe.2301

Lin, T., Haselton, C. B., and Baker, J. W. (2013b). Conditional spectrum-based ground motion selection. Part II: intensity-based assessments and evaluation of alternative target spectra. *Earthq. Eng. Struct. Dynam.* 42, 1867–1884. doi:10.1002/eqe.2303

Magliulo, G., Bellotti, D., Cimmino, M., and Nascimbene, R. (2018). Modeling and seismic response analysis of RC precast Italian code-conforming buildings. *J. Earthq. Eng.* 22, 140–167. doi:10.1080/13632469.2018.1531093

Magliulo, G., Ercolino, M., Cimmino, M., Capozzi, V., and Manfredi, G. (2015). Cyclic shear test on a dowel beam-to-column connection of precast buildings. *Earthq. Struct.* 9, 541–562. doi:10.12989/eas.2015.9.3.541

Magliulo, G., Ercolino, M., Cimmino, M., Capozzi, V., and Manfredi, G. (2014a). FEM analysis of the strength of RC beam-to-column dowel connections under monotonic actions. *Construct. Build. Mater.* 69, 271–284. doi:10.1016/j.conbuildmat.2014.07.036

Magliulo, G., Ercolino, M., Petrone, C., Coppola, O., and Manfredi, G. (2014b). The Emilia earthquake: seismic performance of precast reinforced concrete buildings. *Earthq. Spectra.* 30, 891–912. doi:10.1193/091012eqs285m

Maitra, S. R., Reddy, K. S., and Ramachandra, L. S. (2009). Load transfer characteristics of dowel bar system in jointed concrete pavement. *J. Transport. Eng.* 135, 813–821. doi:10.1061/(asce)te.1943-5436.0000065

Ozden, S., Akpinar, E., Erdogan, H., and Atalay, H. M. (2014). Performance of precast concrete structures in October 2011 Van earthquake, Turkey. *Mag. Concr. Res.* 66, 543–552. doi:10.1680/macr.13.00097

PEER (2007). *OpenSees*. Berkeley, CA: University of California.

Psycharis, I. N., and Mouzakis, H. P. (2012a). Assessment of the seismic design of precast frames with pinned connections from shaking table tests. *Bull. Earthq. Eng.* 10, 1795–1817. doi:10.1007/s10518-012-9372-9

Psycharis, I. N., and Mouzakis, H. P. (2012b). Shear resistance of pinned connections of precast members to monotonic and cyclic loading. *Eng. Struct.* 41, 413–427. doi:10.1016/j.engstruct.2012.03.051

Safecast (2012). *Design guidelines for connections of precast structures under seismic actions*. Editor J.R.C.O.E. Commission (Luxembourg).

Sezen, H., Elwood, K., Whittaker, A., Mosalam, K., Wallace, J., and Stanton, J. (2000). "Structural engineering reconnaissance of the August 17, 1999, Kocaeli (Izmit), Turkey earthquake".

Sousa, R., Batalha, N., and Rodrigues, H. (2020). Numerical simulation of beam-to-column connections in precast reinforced concrete buildings using fibre-based frame models. *Eng. Struct.* 203, 109845. doi:10.1016/j.engstruct.2019.109845

Toniolo, G., and Colombo, A. (2012). Precast concrete structures: the lessons learned from the L'Aquila earthquake. *Struct. Concr.* 13, 73–83. doi:10.1002/suco.201100052

TR045 (2013). *Design of metal anchors for use in concrete under seismic actions*. Brussels, Belgium: EOTA.

Vintzeleou, E. N., and Tassios, T. P. (1987). Behavior of dowels under cyclic deformations. *ACI Struct. J.* 84, 18–30. doi:10.14359/2749

Zoubek, B., Fischinger, M., and Isakovic, T. (2015). Estimation of the cyclic capacity of beam-to-column dowel connections in precast industrial buildings. *Bull. Earthq. Eng.* 13, 2145–2168. doi:10.1007/s10518-014-9711-0

Zoubek, B., Isakovic, T., Fahjan, Y., and Fischinger, M. (2013). Cyclic failure analysis of the beam-to-column dowel connections in precast industrial buildings. *Eng. Struct.* 52, 179–191. doi:10.1016/j.engstruct.2013.02.028

Conflict of Interest: The authors declare that the research was conducted in the absence of any commercial or financial relationships that could be construed as a potential conflict of interest.

frontiers in Built Environment

ORIGINAL RESEARCH
published: 18 March 2021
doi: 10.3389/fbuil.2021.645497

Crescent-Moon Beam-To-Column Connection for Precast Industrial Buildings

Michele Egidio Bressanelli[1], *Marco Bosio*[1], *Andrea Belleri*[1]*, *Paolo Riva*[1] and *Piergiovanni Biagiotti*[2]

[1]Department of Engineering and Applied Sciences, University of Bergamo, Dalmine, Italy, [2]Biemme S.r.l., Lucrezia di Cartoceto, Italy

The 2012 Emilia earthquakes caused significant damage to existing precast reinforced concrete (RC) industrial buildings not specifically designed to resist seismic actions. The main failure mechanisms were related to the loss of support of beams and roof elements caused by high relative displacements, to the failure of the mechanical connections and consequent fall of cladding panels, to the damage at the base of the columns and to the collapse of RC forks at the top of the columns. In all cases, the behavior of the connections, and specifically of beam-to-column connections, demonstrated to be crucial, given that they may inhibit the exploitation of strength and ductility reserves in precast elements. This paper presents a beam-to-column connection restraint-device for precast industrial buildings. The device can be applied to existing structures to transfer horizontal seismic forces between beams and columns and to increase the energy dissipation of the system. Design criteria were defined with the aim to limit the relative maximum displacement at the beam-to-column interface and to mitigate the out-of-plane overturning of the beam. Numerical analyses were carried out to define a suitable shape of the device and to investigate its effectiveness in terms of both local and global behavior. To validate the computational results, experimental tests have been also carried out. The tests allowed to classify the device as "dissipative" according to UNI EN 15129. Finally, the design procedure has been validated considering a one-story industrial building case study designed in accordance with the Italian building code.

Keywords: precast industrial buildings, crescent moon-shaped device, beam-to-column connection, seismic retrofit, energy dissipation

OPEN ACCESS

Edited by:
Arturo Tena-Colunga, Autonomous Metropolitan University, Mexico

Reviewed by:
Massimo Latour, University of Salerno, Italy
Roberto Aguiar, University of the Armed Forces (ESPE), Ecuador

***Correspondence:**
Andrea Belleri
andrea.belleri@unibg.it

Specialty section:
This article was submitted to Earthquake Engineering, a section of the journal Frontiers in Built Environment

Received: *23 December 2020*
Accepted: *05 February 2021*
Published: *18 March 2021*

Citation:
Bressanelli ME, Bosio M, Belleri A, Riva P and Biagiotti P (2021) Crescent-Moon Beam-To-Column Connection for Precast Industrial Buildings. Front. Built Environ. 7:645497. doi: 10.3389/fbuil.2021.645497

INTRODUCTION

Precast concrete structures are widely used for industrial buildings in Italy, as they can cover large surfaces, ensure high quality controls of materials and elements and allow for shorter construction times when compared to conventional reinforced concrete (RC) buildings. For example, there is a significant reduction in construction time associated with concrete curing and a consistent reduction in costs due to the use of precast elements, which are easily transportable and erected on site at low expenses and great speed; these characteristics are essential when dealing with industrial facilities, where buildings develop on large surfaces and construction time is directly related to the time to business for the facility. The typical structural layout develops mainly on a single level and it is characterized by simple and regular layouts, with cantilever columns pin-connected to pre-stressed

beams which support the roof elements. Generally, the columns are either placed inside pocket footings or connected to the foundation by means of mechanical devices or grouted sleeves (Belleri and Riva, 2012; Dal Lago et al., 2016).

Before the enforcement of modern anti-seismic regulations in Italy, the buildings not specifically designed for seismic actions were characterized by beams simply supported on the columns; the contact surface was typically equipped with a neoprene pad to spread the load over the support, and the horizontal load transfer between the beam and column was provided solely by friction. Such beam-to-column friction connections, basically designed to support only gravitational loads, do not contribute to the seismic resistance of the building. Indeed, as stated by current regulations, beam-to-column connections cannot rely on friction in seismic regions; for such reason dowel connections are usually adopted.

The seismic sequence that affected the territory of Emilia-Romagna, Veneto and Lombardia regions in May 2012 had a strong impact on areas characterized by a medium-low seismic hazard, i.e., acceleration on rigid soil in the order of 0.10 ÷ 0.15 g considering a return period T_r equal to 475 years. An updated classification of the seismic hazard was only stated in 2003 (OPCM 3274, 2003). Before that, numerous buildings were designed and built without modern anti-seismic criteria. Such buildings have highlighted considerable vulnerability to recent seismic events (Bournas et al., 2014; Magliulo et al., 2014; Belleri et al., 2015a; Belleri et al., 2015b; Ercolino et al., 2016; Minghini et al., 2016; Belleri, 2017; Nastri et al., 2017; Palanci et al., 2017). These vulnerabilities are related to multiple local collapse mechanisms and vulnerabilities such as the loss of support of the roof elements and/or beams, the overturning of the RC cladding panels and the collapse of RC columns or forks at the top of the columns (Brunesi et al., 2015; Belleri et al., 2016; Belleri et al., 2017a; Dal Lago et al., 2018; Ercolino et al., 2018; Torquati et al., 2018; Iervolino et al., 2019; Bosio et al., 2020).

The vulnerability related to the loss of support in the beam-to-column connection (Casotto et al., 2015; Demartino et al., 2018) is due to the lack, or inefficiency, of an adequate mechanical connection able to transfer the seismic actions from the beams to the top of the columns. To counteract this vulnerability and improve the seismic response of precast structures designed for gravity loads, a possible dissipative beam-to-column connection device has been investigated herein. The optimal device shall be able to improve the seismic performance of precast structures by increasing the degree of fixity of the connection and the energy dissipation while, at the same time, limiting the interference with the existing non-structural elements and systems (Belleri et al., 2017b; Magliulo et al., 2017). The device has been defined on the basis of the following criteria: kinematic compatibility with the existing structure, energy dissipation, ease of mounting and replacement after a seismic event and limited interference with the existing industrial systems (as for instance electrical and plumbing). For the last reason, a crescent-moon-shaped device has been selected (Palermo et al., 2015; Hsu and Halim, 2017). It is interesting to note that other types of devices have been recently applied at the beam-to-column joints, such as the friction devices reported in the FREEDAM project (Santos et al., 2019; Francavilla et al., 2020) and the carbon-wrapped steel tubes reported in Pollini et al. (2020).

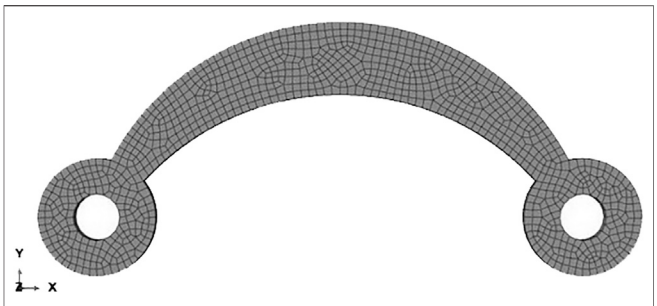

FIGURE 1 | Finite element scheme of the dissipative device.

The design, modeling and analysis procedures used for the definition of the selected device are described considering its application to single-storey precast RC frames. Two configurations have been defined: the first one considers the dissipative device applied directly to the structure while the second one is characterized by placing the dissipative device into an elastic frame to improve the energy dissipation by acting as a lever mechanism. Both solutions allow to increase the frame lateral stiffness and the energy dissipation capacity. The structural performance and the stability of the device have been preliminary evaluated by means of buckling and non-linear cyclic analyses. Then an experimental campaign was carried out. On the basis of the experimental results, it has been possible to classify the device as "dissipative," according to EN 15129 (2018). Finally, a design procedure was defined and validated through non-linear response history analyses on a case study.

DEFINITION OF THE DISSIPATIVE DEVICE

The dissipative device provides an additional source of energy dissipation for the structure and promotes a stiffness increase at the beam-to-column connection. The selected device consists of a steel element with a "crescent-moon" shape that allows to dissipate energy by deforming and plasticizing homogeneously along its surface. The device has been selected and defined for applications in beam-to-column connections with fork or corbels at the top of the columns, which are the main types of existing old beam-to-column connections present in typical precast industrial buildings.

Analytical and Experimental Study of the Device's Geometry

The design of the dissipative device was performed by analyzing the output of various geometry configurations under monotonic and cyclic loading. The geometry of the element was initially calibrated to develop a uniform plasticization (**Figure 1**).

The finite element analyses were carried out considering both geometric and material nonlinearities. Three different device curvatures of the crescent-moon element have been analyzed to define the optimal shape to avoid instability, to maximize the

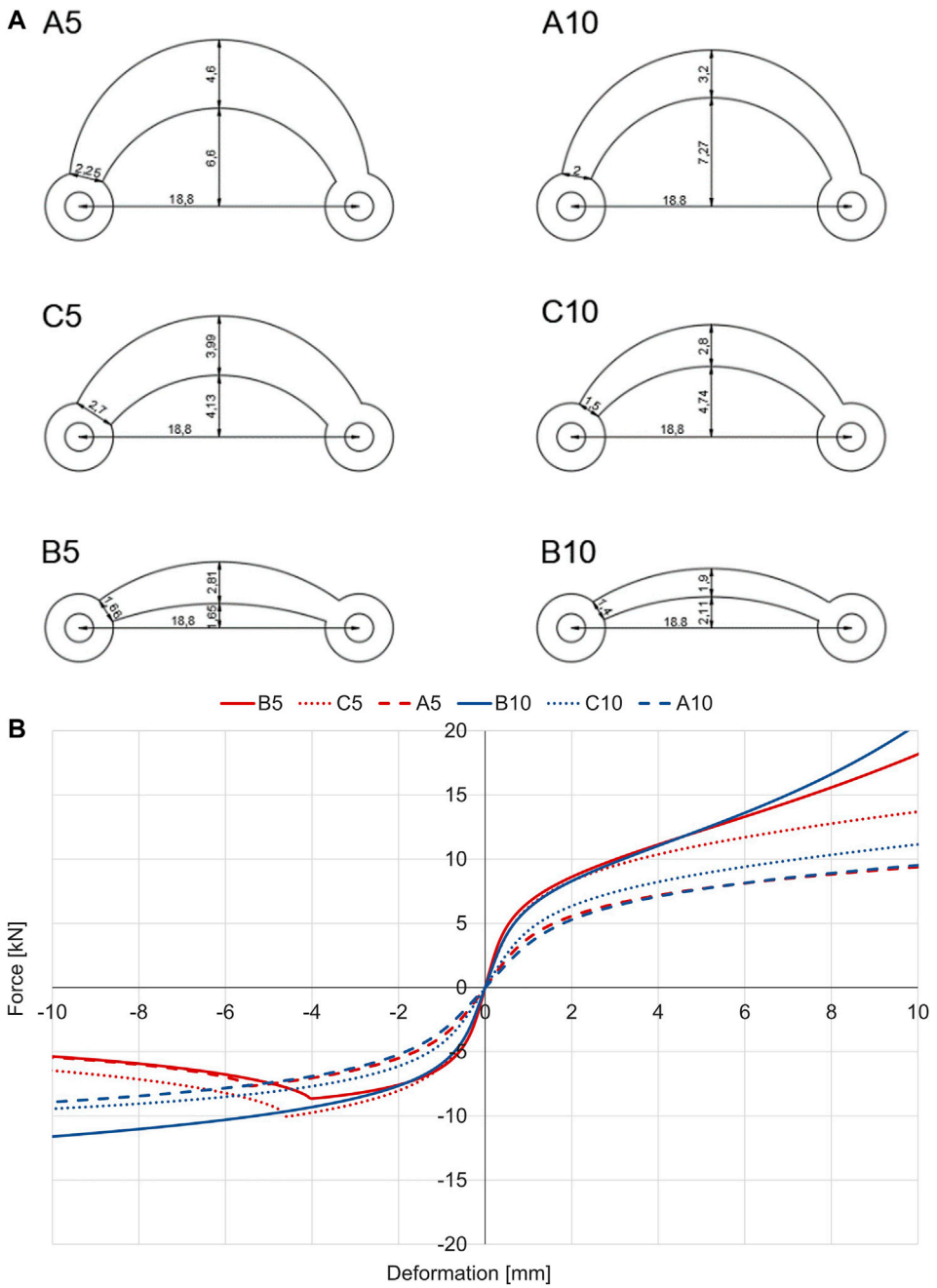

FIGURE 2 | Selected geometries of the device as a function of the curvature and the thickness (measures expressed in centimetres) **(A)** and results of the associated non-linear static analyses **(B)**. Note: considering the device id, the letter A, B or C indicates the curvature of the device while the following number indicates the thickness expressed in millimetres.

energy dissipation and to ensure a symmetrical cyclic behavior in tension and compression. Starting from the device in its basic configuration (**Figure 1**), the rise has been increased (prefix 'A') or reduced (prefix 'B') by 50%. Each solution was analyzed considering a thickness of 5 and 10 mm to investigate its influence on the deformative behavior of the element. **Figure 2A** shows the six configurations analyzed.

Monotonic analyses in compression and tension were conducted. Initially, each of the six configurations was modeled in order to carry out a stability check; subsequently, a non-linear analysis with displacement control was carried out (**Figure 2B**). The selected material non-linearity was in accordance with the Ramberg-Osgood's constitutive law **Eq. 1**.

TABLE 1 | Calculation of buckling with **Eq. 2** for each configuration of devices.

	A5	A10	B5	B10	C5	C10
M_{cr} [kNm]	0.69	4.96	0.28	1.89	0.72	3.17
P_{cr} [kN]	7.75	55.93	9.21	61.75	10.42	51.69

$$E_\varepsilon = \sigma + \alpha \cdot \sigma \left(\frac{|\sigma|}{\sigma_0} \right)^{n-1} \quad (1)$$

Where ε and σ represent the logarithmic deformation and Cauchy stress tensor, respectively, E represents the Young's modulus, σ_0 represents the stress at the yield point, α is a coefficient indicating the increase in yield strength and n is the exponent indicating the level of plasticization. In these analyses, a Young's modulus equal to 210 GPa, a Poisson's ratio equal to 0.3, a yield strength equal to 240°MPa, an exponent n equal to 5 and α equal to 1 were used. The geometric non-linearity was considered by introducing an out-of-plane imperfection according to the first buckling mode. The influence of the temperature was not considered.

The devices with thickness equal to 5 mm showed buckling for displacements close to 5 mm, i.e., deformations of the order of 3%. The devices with a thickness greater than 10 mm were not affected by this issue. When subjected to tension load, the B5 and B10 devices showed a significant increase in capacity due to the rope effect as the devices straightened. In fact, once the maximum deformation for which the device becomes almost rectilinear has been reached, there is a sharp increase in stiffness and load until the rupture of the element, which develops by necking at the smaller cross-section. This effect is less noticeable for devices C10 and A10, which are characterized by a higher rise.

The buckling of the devices has been also assessed through the closed form formulation for curved rods **Eq. 2**, where M_{cr} represents the elastic critical moment for buckling (Timoshenko and Gere, 2009):

$$M_{cr} = \frac{EI_x + C}{2R} \pm \sqrt{\left(\frac{EI_x - C}{2R} \right)^2 + \frac{EI_x C}{R^2} \cdot \frac{\pi^2}{\alpha_1^2}} \quad (2)$$

I_X represents the moment of inertia in the orthogonal plane defined as $1/12 H_{mean} b^3$, E represents the elastic modulus, R represents the mean radius of curvature of the device, b is the thickness of the device, α_1 is the opening angle, H_{mean} is the mean cross-section height and C is defined by the product between the shear module G and the torsional stiffness J_T. Considering that the elastic critical bending moment M_{cr} is equal to the product between the critical load P_{cr} and the lever arm h, we obtain that:

$$P_{cr} = M_{cr}/h \quad (3)$$

Table 1 reports the critical moment and load associated with each configuration. The results confirm what obtained from the finite element analyses (**Figure 2B**).

After analyzing the influence of the rise and the thickness of the device, additional cyclic analyses were carried out to evaluate the symmetry of the device in tension and compression loading. In this case the cyclic analyses were carried out considering an elasto-plastic behavior of the material based on the values obtained from tensile tests conducted on dog-bone specimens. Experimental tests were carried out to validate the results. Full-scale specimens were produced for the six main configurations analyzed: A5, B5, C5, A10, B10 and C10. The tests were conducted in displacement control. **Figure 3** and **Figure 4** compare the results of the FEM analyses with the results obtained from the experimental tests for each of the aforementioned configurations during monotonic and cyclic loading, respectively.

The monotonic results in **Figure 3** show a fair resemblance between the values expected from finite element simulations and those obtained from experimental tests. The main differences were found for the tension phase, where the maximum force is reached for displacements lower than those observed in the experimental tests. The small differences in the origin are due to sliding caused by bolt-hole gap. The devices with higher rise and with thickness equal to 1 cm are characterized by almost symmetrical hysterical cycles (specifically C10 and A10). Except for the device C5, the devices showed higher maximum force values during the experimental test than those obtained from numerical simulations.

The cyclic results in **Figure 4** show a good agreement between the experimental tests and the finite element simulations, especially for the device A10. Significant differences are evident in devices with lower rise, namely B5 and B10, where the finite element analyses are not able to correctly predict the experimental cyclical results. The cyclic tests on devices with a thickness equal to 5 mm confirmed the buckling issues previously encountered with monotonic analyses.

On the basis of the analyses carried out, an optimal geometry for the dissipative device was defined.The rise was increased to obtain a symmetrical hysteresis and avoid the presence of softening during compression. The thickness was increased to 20 mm to inhibit buckling and to dissipate energy in a stable manner. The height of the mid cross-section was increased to reduce the dissipation in this region and to increase the global stability of the device. The final device, referred to as M1 device, (**Figure 5A**) has a span equal to 720 mm and it is made by a steel element pin-connected to end steel plates connected to the column and beam through post installed anchors (as in **Figures 5C,D**). The connecting plates have been designed to remain elastic after the yielding of the device (**Figures 5E,F**). The slots in the plates allow for tolerance of anchor bolts due to the possible interference with longitudinal rebars and stirrups in the connected elements. The anchor bolts could be pretensioned to limit or avoid the plate detachment. The crescent-moon element allows to dissipate energy and to limit the sliding between the beam and the column in the case of friction connections.

As it can be seen from **Figure 5B**, the device is able to offer a symmetrical behavior in tension and compression, a good energy dissipation and it is not subjected to relevant capacity decay following repeated cyclic tests.

Implementation of a device displacement amplification system

In order to increase the stiffness and dissipation capacity offered by the investigated device, the crescent-moon element can be

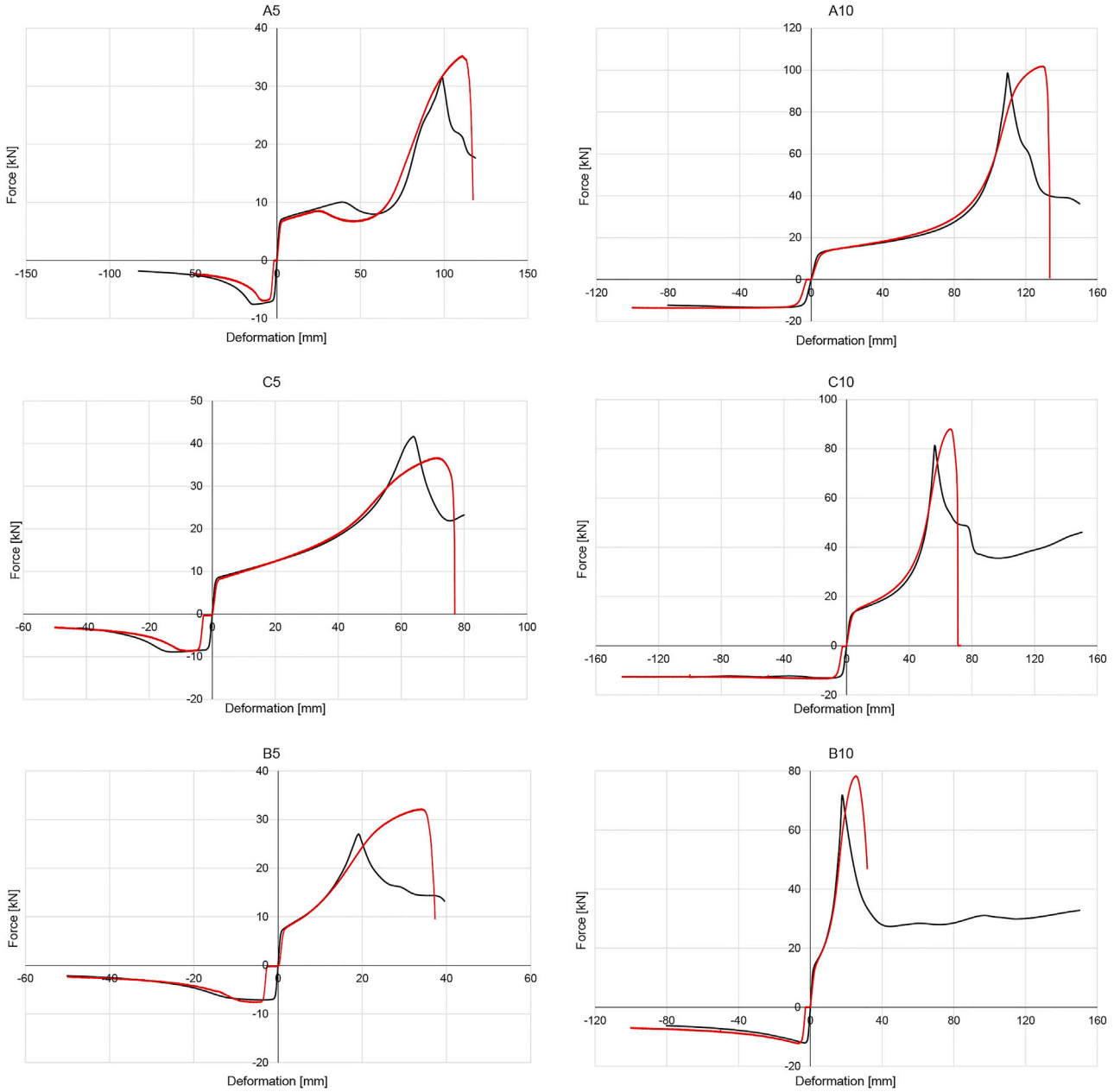

FIGURE 3 | Comparison between monotonic numerical results (black line) and experimental tests (red line).

assembled in an amplification frame able to increase the effects of the relative displacements between the beam and the column. An example of such an assembly is shown in **Figure 6A**. This configuration consists of two steel elements characterized by equal length and three devices: two long span devices (530 mm) and one additional device with a lower span (212 mm). The shape and size of the devices was selected to achieve stable global behavior in tension and compression. This system ensures a stable energy dissipation, an almost symmetrical behavior and a low interference with fixtures. A cyclic nonlinear static analysis was carried out and the results are shown in **Figure 6B** (black line) along with the comparison of a single M1 device (green line).

Experimental Tests in Accordance with EN 15129

Various tests on the investigated device were conducted in accordance with the European Standard EN 15129 "anti-seismic devices" under displacement control. EN 15129 (2018) .covers the design of devices that are provided in structures, with the aim of modifying their response to the seismic action. It

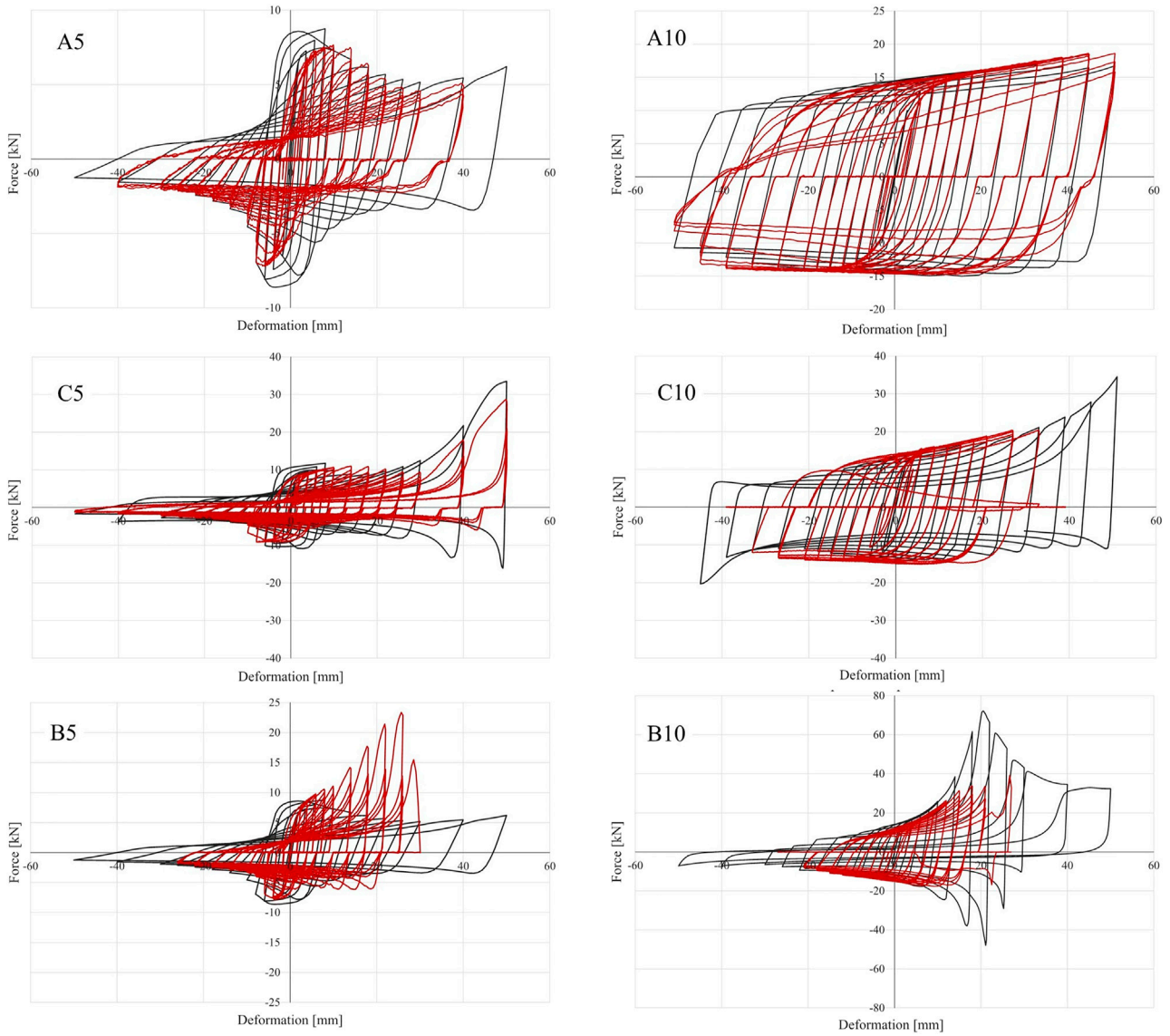

FIGURE 4 | Comparison between cyclic numerical results (black line) and experimental tests (red line).

specifies functional requirements and general design rules of the devices for the seismic design situations, material characteristics, manufacturing and testing requirements, as well as assessment and verification of constancy of performance, installation and maintenance requirements. The procedure used in the cyclic tests was defined according to paragraph six of EN 15129 (2018). The device could be classified as a non-linear displacement dependent device characterized by a non-linear force-displacement response, with a stable behavior for the required number of cycles and substantially independent of speed. For these devices, the standard requires the following tests:

1. Monotonic failure tests at low speed to determine the failure displacement. The collapse shall not occur before reaching a displacement value equal to the design displacement (dbd) multiplied by two coefficients γb and γx and for a load equal to the design load (VEbd) multiplied by the same coefficients;
2. Cyclic tests with repeated cycles of increasing amplitude: 5 cycles at 0.25˚dbd, 5 cycles at 0.5˚dbd and 10 cycles at dbd. The number of cycles was taken as the minimum indicated in EN15129.

For each cyclically tested sample, an overload test was also carried out to assess the stability of the device and the absence of decreasing trends in the load-displacement curve. The parameters necessary to define the behavior of the device are: the maximum load reached F_{max}, the displacement at the maximum load d_{lim}, the design displacement d_{bd}, the design load V_{Ebd} (i.e., the load associated with the design displacement), the stiffness of the first elastic branch k_1, the stiffness of the second plastic branch k_2, the effective stiffness k_{effb} (defined as the ratio of V_{Ebd} design load to

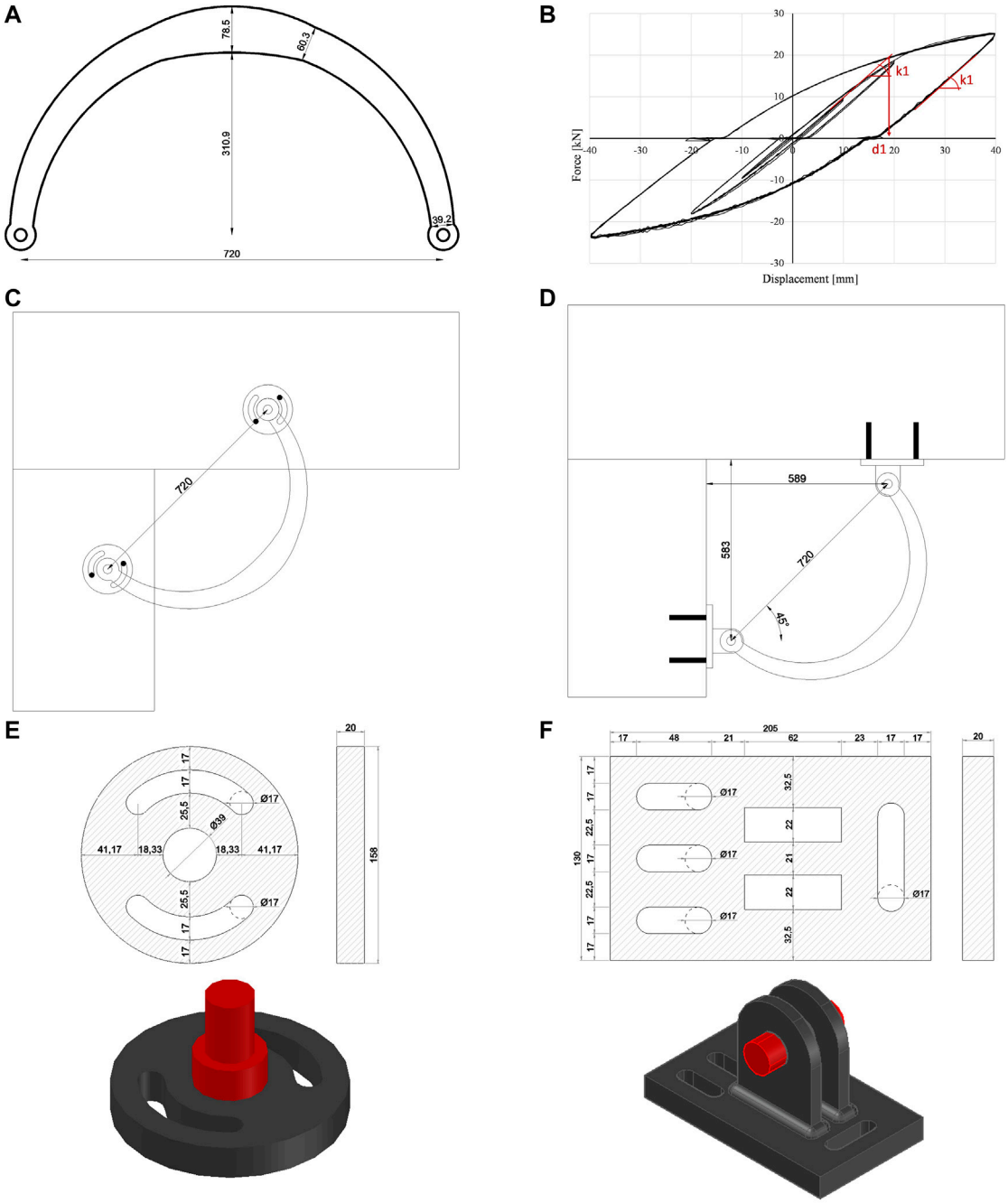

FIGURE 5 | Geometry of the beam-to-column device **(A)**; experimental force-displacement behavior **(B)**; application of the device on beam and column from the side **(C)** and from below **(D)**; geometry of the end-plates **(E, F)**.

d_{bd} design displacement) and the effective damping ξ_{effb} (corresponding to the energy dissipated during the cycles at the design displacement d_{bd}). **Figure 7** shows these parameters.

The maximum design displacement is equal to 121 mm and it was obtained by dividing the displacement at the reference limit d_{lim} by the two coefficients ($\gamma_b = 1.1$ and $\gamma_x = 1.5$). The choice of a design displacement of 40 mm is therefore compatible with the experimental results. The devices tested have successfully passed the required displacement history without failure. According to EN 15129 (2018), the tested devices have a stable behavior with the following design parameters: design displacement d_{bd} equal to 40 mm; displacement at yield d_1 equal to 18.6 mm; first branch stiffness k_1 equal to 1.003 kN/mm; second branch stiffness k_2 equal to 0.268 kN/mm; design effective stiffness k_{eff} equal to

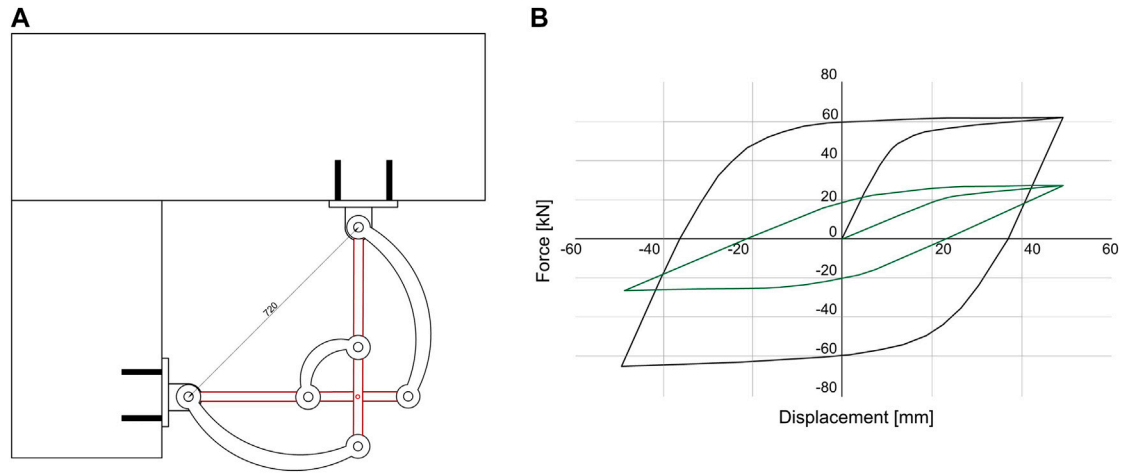

FIGURE 6 | Configuration for the displacement amplification system **(A)** and hysteresis comparison between such system and a single M1 device **(B)**.

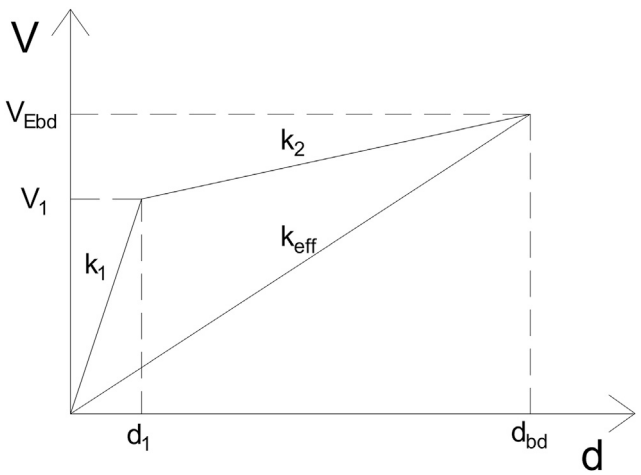

FIGURE 7 | Main parameters describing the hysteretic behavior of the system.

0.595 kN/mm; design effective damping ξ_{eff} equal to 18.91%; design axial load V_{Ebd} at d_{bd} equal to 23.9 kN.

For the definition of the parameter d_1, i.e., the displacement at yielding, a bi-linearization of the curve has been carried out. Specifically, a straight line was drawn from the origin with inclination equal to k_1; the yield strength was taken as the point corresponding to the intersection of such line with the load-displacement curve of the device, **Figure 5B**. According with EN 15129 (2018), the device can be classified as a non-linear dissipative device.

DESIGN METHODOLOGY

The considered device can be implemented in the seismic retrofit of existing precast concrete buildings, where it may be placed at the beam-to-column joint (**Figures 5C,D**) to avoid sliding at the connection and to provide energy dissipation. The device may be also used in new buildings.

According to Eurocode 8 part 3 (CEN, 2005), the retrofit design procedure shall include the following steps: conceptual design, analysis and verification. The conceptual design shall cover the following: selection of techniques and/or materials, as well as of the type and configuration of the intervention, preliminary estimation of dimensions of additional structural parts and preliminary estimation of the modified stiffness of the retrofitted elements.

The design procedure considers the equivalence between the frame with the beam-to-column devices in their actual position (**Figures 8A,B**) and an idealized frame with a lumped rotational spring at each joint (**Figure 8C**).

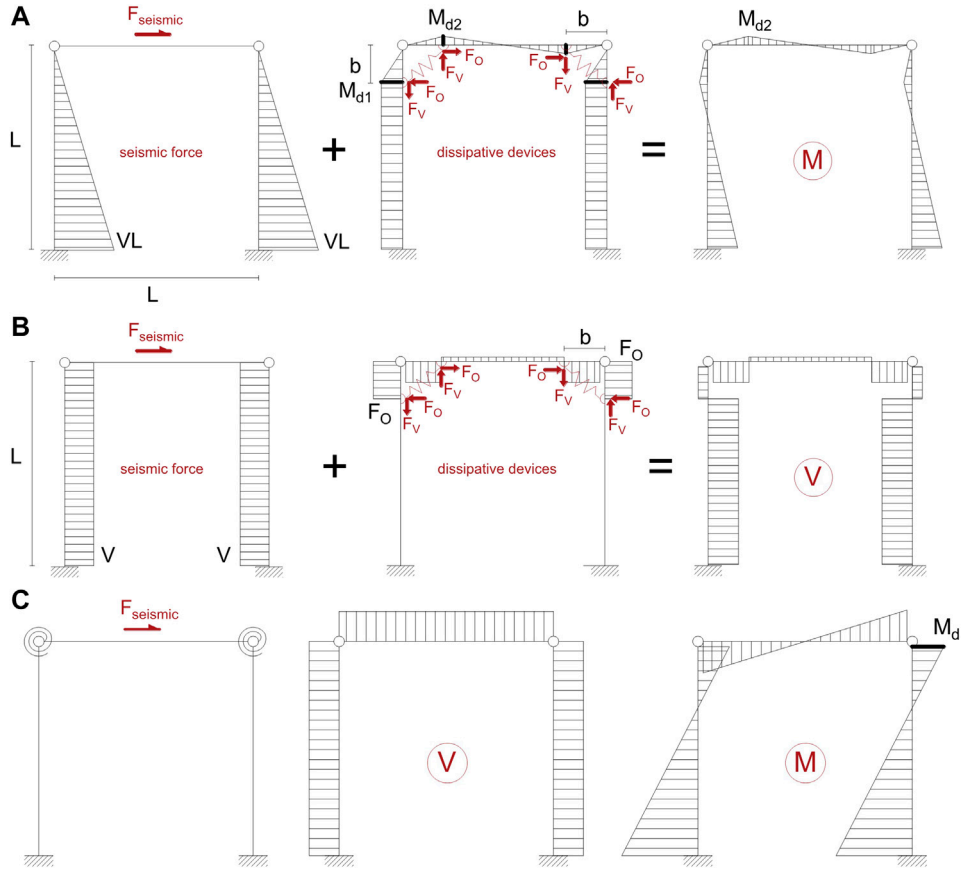

FIGURE 8 | Contribution to the bending moment **(A)** and shear **(B)** diagram of the device in its actual position and in the case of idealized frame with lumped rotational springs at the joints **(C)**.

In **Figures 8A,B**, F_o and F_v are the vertical and horizontal forces of the device, M_d is the moment due to the device and b is the distance between the points of application of the device and the beam-to-column connection, which, in the preliminary design phase, is assumed as a hinge. On the basis of this scheme, it is possible to assess the shear and bending moment in the beam and in the columns before and after placing the device. The following equations may be derived for the bending moment in correspondence to the device on the column and on the beam, respectively:

$$M_{d1} = F_O \cdot b \tag{4}$$

$$M_{d2} = \frac{F_V \cdot b}{L/2} \cdot \left(\frac{L}{2} - b\right) \tag{5}$$

Where L is the length of the beam, F_O and F_V are the horizontal and vertical components associated with the device, respectively. On the basis of the bending moment diagrams and assuming that the dimension b of the device is small in relation to the length of the beam and the height of the column, we obtain that:

$$M_{d2} = F_V \cdot b \tag{6}$$

Therefore, it is possible to replace the actual static scheme with the simplified scheme of **Figure 8B**: the higher the L/b ratio, the better the approximation.

The design procedure consists in defining the required number of devices in each connection. **Figure 9** shows the flow chart of the design procedure. For the design, it is assumed that the crescent-moon device is the only element able to transfer horizontal actions from the beam to the supporting columns, i.e. the contribution of friction is neglected.

The first step of the procedure is the definition of the geometry, the material characteristics and the loading on the column. The probable bending moment capacity at the base of the column, M_{Rd}, is obtained from the geometry of the element, the axial force in the column, the material characteristics and the knowledge level of the existing building and the related confidence factor. The procedure is iterative and starts from the assumption of the development of a plastic hinge at the base of the columns (M_{Rd}) and of the presence of a bending moment at the top of the column due to the additional device (M_d). A first estimate of the shear $V^{(0)}$ and $F_d^{(0)}$ and $M_d^{(0)}$ in the device (i.e., the activation force of the device, aligned to the device connecting points, $F_d^{(0)}$, and the bending moment at the column top, $M_d^{(0)}$, following the scheme in **Figure 8C**) is calculated assuming a linear distribution of the bending moment and an inflection point (i.e., the point at zero moment) equal to 0.8 H (i.e., effective height $H_{eff}^{(0)}$). From $M_d^{(0)}$, it is possible to recalculate the H_{eff} from equilibrium considerations and then derive a new estimation of $V^{(1)}$ and $F_d^{(1)}$. The

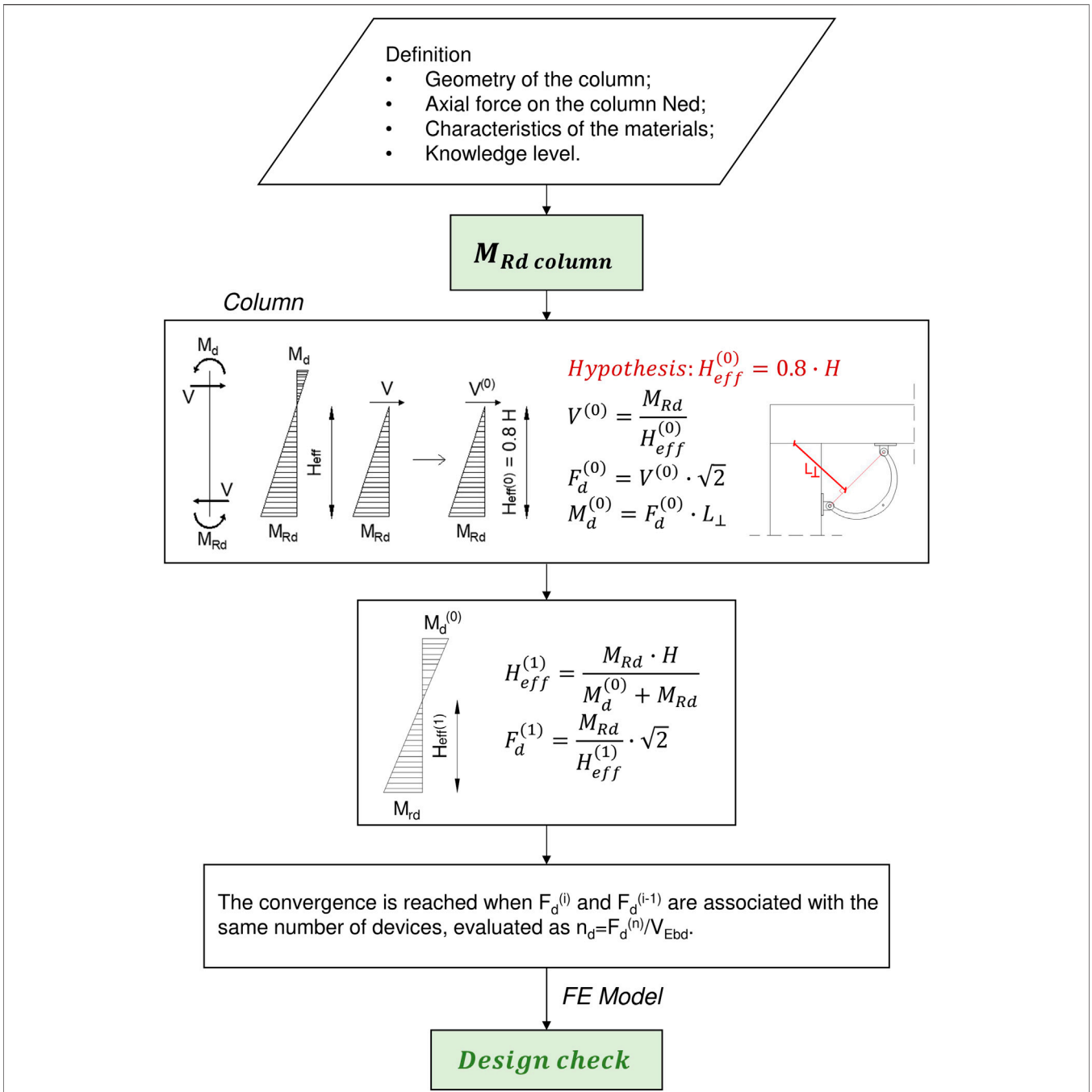

FIGURE 9 | Flow chart of the design procedure.Note: L ⊥ is the distance between the line passing through the device connections and the beam rotation point at the beam-to-column interface.

number of the devices n_d in each beam-to-column connection is calculated with the following equation:

$$n_d^i \geq \frac{F_d^{(i)}}{V_{Ebd}} \tag{7}$$

The convergence is reached when $F_d^{(i)}$ and $F_d^{(i-1)}$ are associated with the same number of devices.

PROCEDURE VALIDATION

A case study (**Figure 10**) has been selected to validate the proposed design methodology. The reference structure is a 4-bay single-story precast RC industrial building with span lengths equal to 20 m along the transverse y-direction and 8 m along the longitudinal x-direction. The building is considered located in an Italian region with high seismicity (L'Aquila)

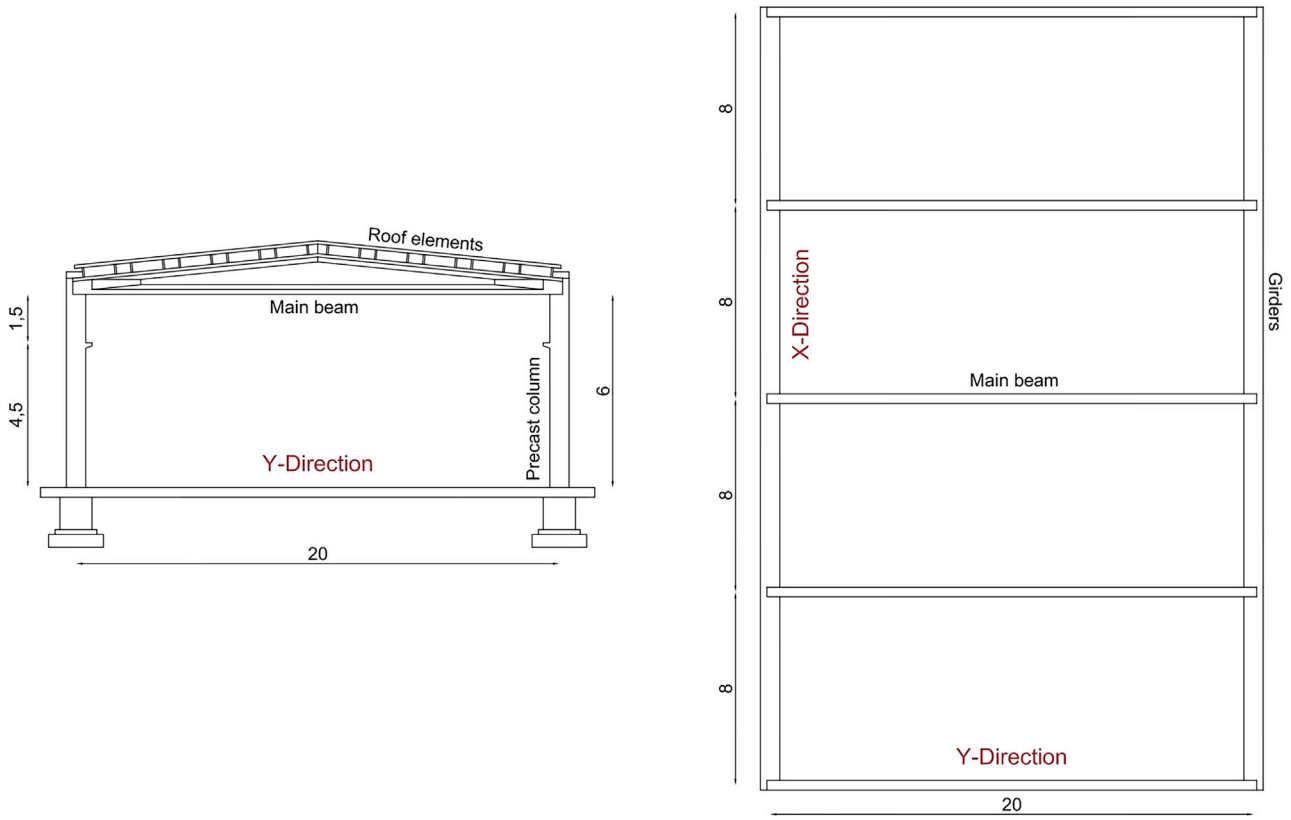

FIGURE 10 | Schematic transverse frame **(left)** and plan view **(right)**.

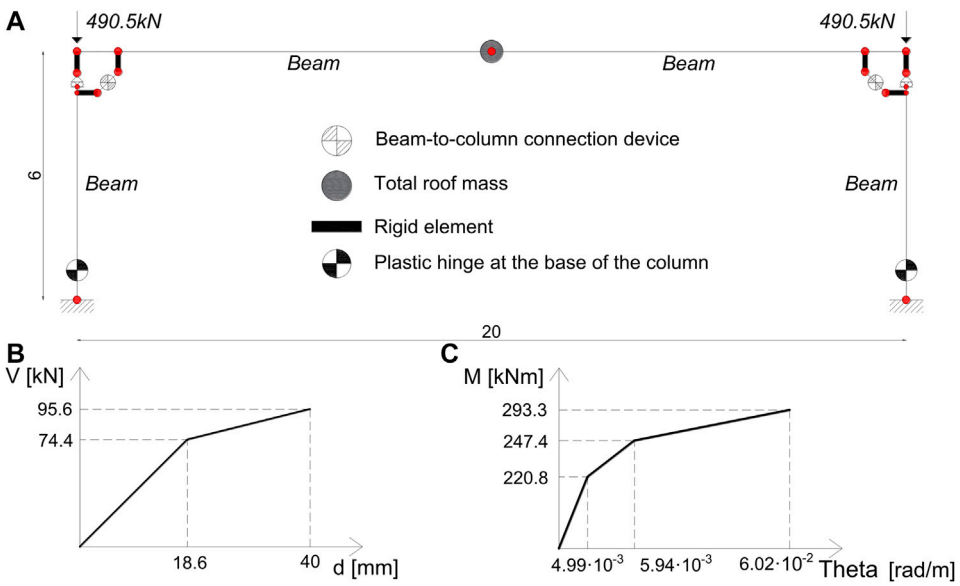

FIGURE 11 | Schematic view of the finite element model **(A)**, total force-displacement behavior of the devices **(B)** and moment-curvature behavior of the plastic hinge at the base of the column **(C)**.

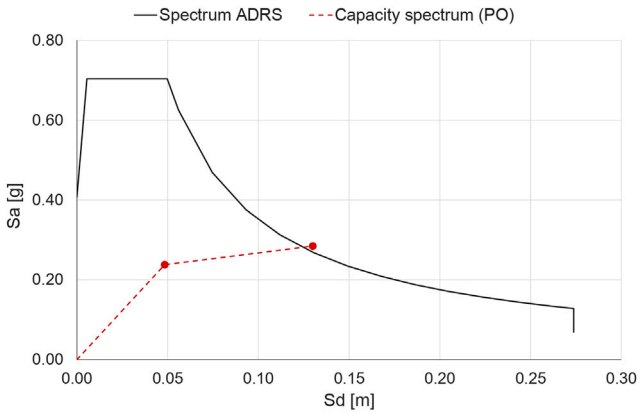

FIGURE 12 | Comparison between capacity spectrum (dashed red line) and ADRS (black line) for the definition of the performance point. Note: S_a and S_d are, respectively, the pseudo acceleration and the displacement spectral values.

with soil class C (NTC, 2018) and ground acceleration on rock equal to 0.261 g.

The columns have a 50 × 50 cm cross-section; the concrete class is C45/55 (45 MPa characteristic cylindrical strength at 28 days) and steel FeB°44K (characteristic yield stress, f_{yk}, equal to 430 MPa). A reinforcement percentage equal to 0.8% in the columns has been assumed; this value is compatible with existing buildings. The average mechanical characteristics of the materials (steel and concrete) were initially defined by assuming a knowledge level equal to LC2 (NTC, 2018; KL2 in; CEN, 2005), which is associated with a confidence factor FC equal to 1.2. This leads to f_{cd} equal to 37.5 MPa and f_{yd} equal to 367 MPa.

Following the proposed methodology a value of $F_d^{(1)}$, i.e., the force required for each connection, equal to 82.3 kN is obtained. Therefore, four M1 devices were selected for each connection, with a total force equal to 95.6 kN. The design displacement of the device is assumed equal to 40 mm.

For the assessment of the in-plane behavior, a single inner portal frame of the considered building has been modeled (**Figure 11A**). The columns are considered fixed at the base. The plastic hinges at the base of the columns are defined in terms of moment-curvature following the modified Takeda hysteresis model in the MidasGEN (2019) software. For the definition of the plastic hinge, the mean values of the materials were used, leading to the diagram shown in **Figure 11C**. In each beam-to-column connection, four dissipative devices are modeled as a single non-linear spring with an elasto-plastic behavior (**Figure 11B**); the total stiffness is equal to 4 kN/mm (**Figure 11B**). The connection is modeled with a roller type constraint following the hypothesis of absence of friction between the beam and the column. The beam and column elements are modeled using beam elements. The mass at the top of the portal frame is equal to 100 t; the vertical roof load transferred to each beam-to-column connection is equal to 490.5 kN.

In-Plane Analysis

The in-plane validation has been carried out by means of static and dynamic non-linear analyses. Regarding non-linear static analyses, the Capacity Spectrum Method (CS) has been applied at the near collapse limit state (NCLS), according to the Italian Building Code (NTC, 2018). A horizontal force at the roof centroid was applied and the friction between beam and column was neglected.

The analysis showed that the design axial deformation of the dissipative device (40 mm) was reached for a roof lateral displacement equal to 130 mm. A bi-linearization of the capacity curve was conducted using an equal energy approach. Starting from the bi-linearized response obtained, it is possible to calculate the associated equivalent viscous damping **Eq. 7**.

$$\xi_{eq} = k\frac{63.7\left(F_y^* \cdot d_{\max}^* - F_{\max}^* \cdot d_y^*\right)}{F_{\max}^* \cdot d_{\max}^*} + 5 = 14.7\% \qquad (8)$$

Where F_y* and d_y* are the yield force and displacement of the bi-linearized curve, respectively; F_{max}* and d_{max}* are the maximum force and displacement of the bi-linearized curve, respectively; the coefficient k takes into account the dissipative capacity of the structure and the characteristics of the hysteresis cycle. The Italian Building Code suggests a value equal to 0.33 for low dissipative structures and 0.66 for high dissipative structures. In the current case, a k equal to 0.33 was assumed due to the limited ductility demand (equal to 2.15) reached at the design displacement. The damped elastic response spectrum corresponding to the NCLS was calculated on the basis of the viscous equivalent damping ξ_{eq}. The bi-linearized capacity curve was converted into the capacity spectrum dividing it by the mass (**Figure 12** dashed red line) and placed in the acceleration-displacement response (ADRS) spectrum (**Figure 12** black line). The intersection of the two curves is the performance point. In the case of no intersection the number of devices is increased.

Response history analyses were conducted to evaluate the dynamic performance of the system. Two sets of ground motions were considered corresponding to the life safety (LSLS) and the near collapse (NCLS) limit states. Each set is composed by three spectrum-compatible ground motions obtained from the SIMQKE-1 algorithm (Venmarcke and Gasparini, 1976). Each ground motion had a duration of 30°s. Mass and Tangent stiffness Rayleigh damping

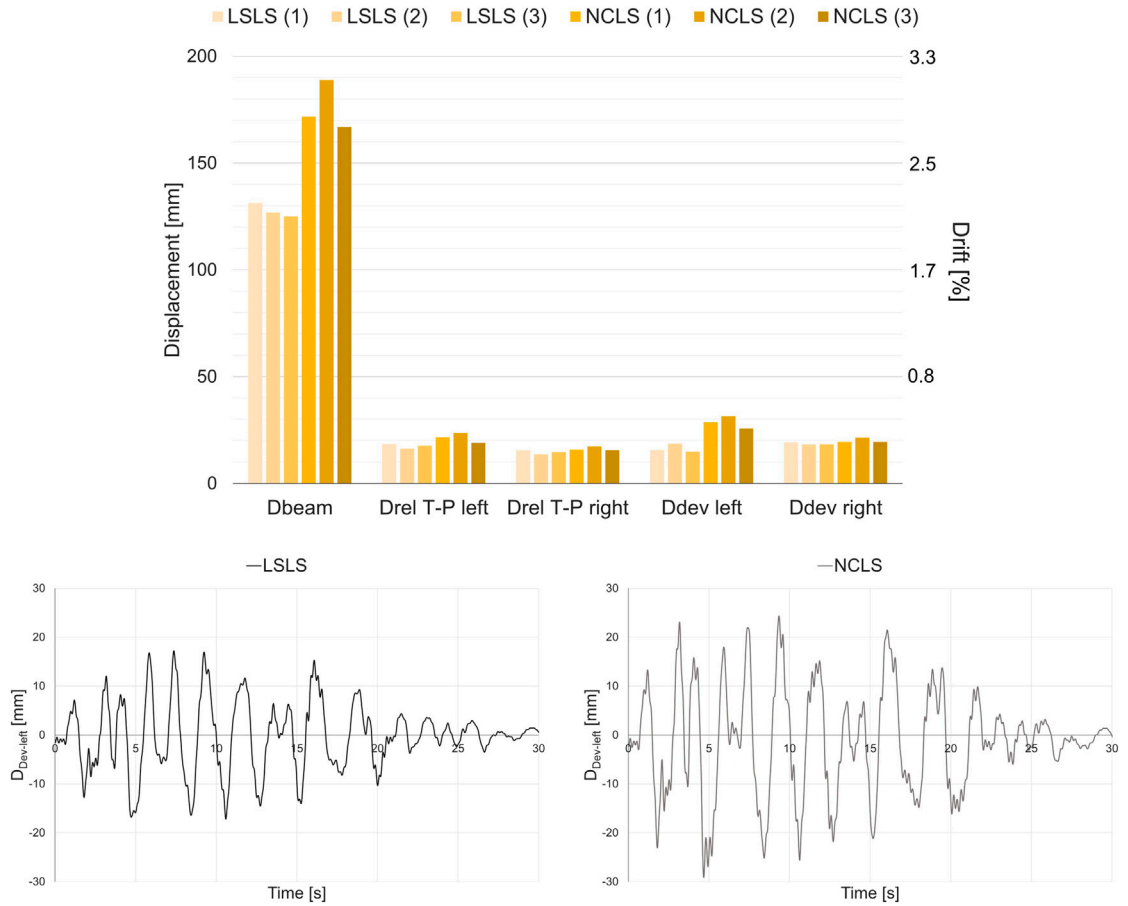

FIGURE 13 | Non-linear response history analyses results.

was assumed based on a damping factor ξ equal to 3% for periods T_1 and T_2 equal to 2.0 and 0.3°s, respectively.

Figure 13 illustrates the main results expressed in terms of displacement at the top of the column (D_{beam}), relative sliding at the beam-to-column interface ($D_{rel\ T\text{-}P\ left}$ and $D_{rel\ T\text{-}P\ right}$) and axial deformation of the devices ($D_{Dev\ left}$ and $D_{Dev\ right}$).

It can be observed that the deformation of the devices is always lower than the displacement limit at NCLS equal to 40 mm for both connections.

Out-of-Plane Analysis

A single column has been modeled as a fixed-end element and loaded in the transverse direction to investigate the effects of the devices on the out-of-plane performance of the system. The beam-to-column interaction (**Figure 14A**) only regarded the rocking of the beam in the transverse direction, while the transverse sliding was neglected (i.e., implicitly assuming a transverse constraint at the base of the beam provided for instance by RC forks). The beam-to-column devices were modeled as nonlinear springs (general links), with a hysteretic behavior defined in terms of force-displacement (**Figure 11B**). The devices were connected to the column through rigid elements to maintain their actual position (**Figure 14**). The contact between the beam and the column was modeled by two compression-only springs. The beam was modeled as a rigid element in the out-of-plane, with a lumped mass corresponding to half of the roof mass placed at the center of gravity of the roof. The gravity loads are first applied to the model as an initial load step before conducting the non-linear dynamic analyses. Second-order geometric effects were included in the model and large displacements were considered. **Figure 14B** shows the response history results in terms of vertical displacements of the beam centroid at the life safety (LSLS) and near collapse (NCLS) limit states. The results clearly show a reduction of the transverse rocking motion of the beam.

CONCLUSION

This paper presented the design and application of a crescent-moon device to be applied at the beam-to-column joint of typical industrial precast reinforced concrete buildings. The device was defined on the basis of the following criteria: kinematic compatibility with the existing system (particularly referring to the beam-to-column connection), energy dissipation capacity,

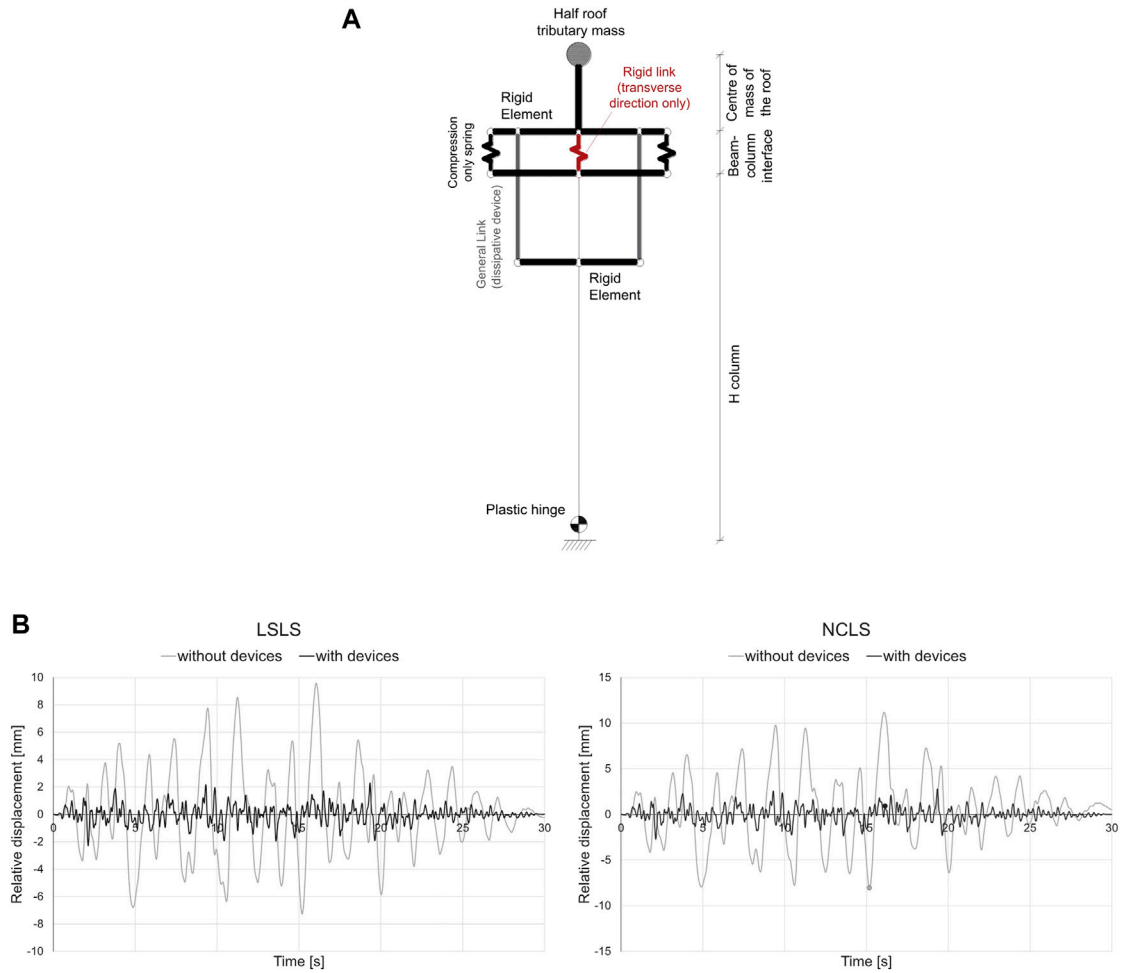

FIGURE 14 | Schematic view of the finite element model **(A)** and response history results of the out-of-plane analysis in terms of device relative displacement **(B)**.

ease of mounting and ease of replacement after seismic events and limited interference with industrial technical systems (e.g., electrical system) often running in the longitudinal direction in close proximity to the beam-to-column joints.

Starting from the definition of the geometry of the element to avoid buckling, experimental tests and finite element analyses were carried out to verify the performance of the investigated device. The analyses allowed to verify its stability, a practically symmetrical behavior in compression and tension and the absence of buckling. On the basis of an experimental campaign, it has been possible to classify the device as "dissipative" according to EN 15129. A simple design methodology was presented and validated by means of non-linear static and non-linear response history analyses considering a precast portal frame resembling a precast industrial building. The application of the device at beam-to-column connections showed its suitability in controlling the sliding of the beam on the column (in the case of friction connections) and also the reduction of out-of-plane rocking movements. To increase the stiffness and the dissipation of the system, an additional configuration has also been presented taking advantage from a lever mechanism to increase the device displacements.

DATA AVAILABILITY STATEMENT

The raw data supporting the conclusions of this article will be made available by the authors upon a reasonable request.

AUTHOR CONTRIBUTIONS

MB: Conceptualization, Methodology, Data curation, Formal analysis, Software, Visualization, Investigation, Validation, Writing—original draft, Writing—review and editing MB: Conceptualization, Methodology, Data curation, Formal analysis, Software, Investigation AB: Conceptualization, Methodology, Visualization, Investigation, Writing—review and editing, Supervision PR: Conceptualization, Methodology, Visualization, Project administration, Writing—review and editing. Supervision. PB: Conceptualization, Writing - review and editing. All authors contributed to the article and approved the submitted version.

REFERENCES

Belleri, A., Cornali, F., Passoni, C., Marini, A., and Riva, P. (2017a). Evaluation of out-of-plane seismic performance of column-to-column precast concrete cladding panels in one-storey industrial buildings. *Earthq. Eng. Struct. Dyn.* 47, 397–417. doi:10.1002/eqe.2956

Belleri, A., Marini, A., Riva, P., and Nascimbene, R. (2017b). Dissipating and re-centring devices for portal-frame precast structures. *Eng. Struct.* 150, 736–745. doi:10.1016/j.engstruct.2017.07.072

Belleri, A. (2017). Displacement based design for precast concrete frames with not-emulative connections. *Eng. Struct.* 141, 228–240. doi:10.1016/j.engstruct.2017.03.020

Belleri, A., and Riva, P. (2012). Seismic performance and retrofit of precast concrete grouted sleeve connections. *Pci. J.* 57 (1), 97–109. doi:10.15554/pcij.01012012.97.109

Belleri, A., Torquati, M., Marini, A., and Riva, P. (2016). Horizontal cladding panels: in-plane seismic performance in precast concrete buildings. *Bull. Earthq. Eng.* 14, 1103–1129. doi:10.1007/s10518-015-9861-8

Belleri, A., Brunesi, E., Nascimbene, R., Pagani, M., and Riva, P. (2015a). Seismic performance of precast industrial facilities following major earthquakes in the Italian territory. *J. Perform. Constr. Facil.* 29 (5), 04014135. doi:10.1061/(ASCE)CF.1943-5509.0000617

Belleri, A., Torquati, M., Riva, P., and Nascimbene, R. (2015b). Vulnerability assessment and retrofit solutions of precast industrial structures. *Earthq. Struct.* 8 (3), 801–820. doi:10.12989/eas.2015.8.3.801

Bosio, M., Belleri, A., Riva, P., and Marini, A. (2020). Displacement-based simplified seismic loss assessment of Italian precast buildings. *J. Earthq. Eng.* 24 (1), 60–81. doi:10.1080/13632469.2020.1724215

Bournas, D. A., Negro, P., and Taucer, F. F. (2014). Performance of industrial buildings during the Emilia earthquakes in Northern Italy and recommendations for their strengthening. *Bull. Earthq. Eng.* 12 (5), 2383–2404. doi:10.1007/s10518-013-9466-z

Brunesi, E., Nascimbene, R., Bolognini, D., and Bellotti, D. (2015). Experimental investigation of the cyclic response of reinforced precast concrete framed structures. *Pci. J.* 60 (2), 57–79. doi:10.15554/pcij.03012015.57.79

Casotto, C., Silva, V., Crowley, H., Nascimbene, R., and Pinho, R. (2015). Seismic fragility of Italian RC precast industrial structures. *Eng. Struct.* 94, 122–136. doi:10.1016/j.engstruct.2015.02.034

CEN (2005). EN 1998-3:2005. Eurocode 8: Design of structures for earthquake resistance, part 3: Assessment and retrofitting of buildings. Brussels, Belgium: European Committee for Standardization. Available at: 305/2011Directive 98/34/EC, Directive 2004/18/EC.

Dal Lago, B., Negro, P., and Dal Lago, A. (2018). Seismic design and performance of dry-assembled precast structures with adaptable joints. *Soil Dyn. Earthq. Eng.* 106, 182–195. doi:10.1016/j.soildyn.2017.12.016

Dal Lago, B., Toniolo, G., and Lamperti Tornaghi, M. (2016). Influence of different mechanical column-foundation connection devices on the seismic behaviour of precast structures. *Bull. Earthq. Eng.* 14 (12), 3485–3508. doi:10.1007/s10518-016-0010-9

Demartino, C., Vanzi, I., Monti, G., and Sulpizio, C. (2018). Precast industrial buildings in Southern Europe: loss of support at frictional beam-to-column connections under seismic actions. *Bull. Earthq. Eng.* 16, 259–294. doi:10.1007/s10518-017-0196-5

EN 15129 (2018). *Anti-seismic device*. Brussels, Belgium: European Committee for Standardization.

Ercolino, M., Bellotti, D., Magliulo, G., and Nascimbene, R. (2018). Vulnerability analysis of industrial RC precast buildings designed according to modern seismic codes. *Eng. Struct.* 158, 67–78. doi:10.1016/j.engstruct.2017.12.005

Ercolino, M., Magliulo, G., and Manfredi, G. (2016). Failure of a precast RC building due to Emilia-Romagna earthquakes. *Eng. Struct.* 118, 262–273. doi:10.1016/j.engstruct.2016.03.054

Francavilla, A. B., Latour, M., Piluso, V., and Rizzano, G. (2020). Design criteria for beam-to-column connections equipped with friction devices. *J. Constr. Steel Res.* 172, 106240. doi:10.1016/j.jcsr.2020.106240

Hsu, H.-L., and Halim, H. (2017). Improving seismic performance of framed structures with steel curved dampers. *Eng. Struct.* 130, 99–111. doi:10.1016/j.engstruct.2016.09.063

Iervolino, I., Spillatura, A., and Bazzurro, P. (2019). "RINTC-e project: towards the assessment of the seismic risk of existing buildings in Italy, RINTC-e: towards seismic risk assessment of existing residential reinforced concrete buildings in Italy," in 7th ECCOMAS Thematic Conference on Computational Methods in Structural Dynamics and Earthquake Engineering, Crete, Greece, June 24–29, 2019.

Magliulo, G., Cimmino, M., Ercolino, M., and Manfredi, G. (2017). Cyclic shear tests on RC precast beam-to-column connections retrofitted with a three-hinged steel device. *Bull. Earthq. Eng.* 15 (9), 3797–3817. doi:10.1007/s10518-017-0114-x

Magliulo, G., Ercolino, M., Petrone, C., Coppola, O., and Manfredi, G. (2014). The Emilia earthquake: seismic performance of precast reinforced concrete buildings. *Earthq. Spect.* 30 (2), 891–912. doi:10.1193/091012EQS285M

MidasGEN (2019). Gyeonggido, Korea: MIDAS Information Technologies Co. Ltd.

Minghini, F., Ongaretto, E., Ligabue, V., Savoia, M., and Tullini, N. (2016). Observational failure analysis of precast buildings after the 2012 Emilia earthquakes. *Earthq. Struct.* 11 (2), 327–346. doi:10.12989/eas.2016.11.2.327

Nastri, E., Vergato, M., and Latour, M. (2017). Performance evaluation of a seismic retrofitted R.C. precast industrial building. *Earthq. Structu.* 12 (1), 13. doi:10.12989/eas.2017.12.1.013

NTC (2018). Aggiornamento delle "Norme tecniche per le costruzioni". Italy: Decreto Ministeriale del..

OPCM 3274. (2003). *Primi elementi in materia di criteri generali per la classificazione sismica del territorio nazionale e di normative tecniche per le costruzioni in zona sismica*. Italy: Presidente Del Consiglio Dei Ministri.

Palanci, M., Senel, S. M., and Kalkan, A. (2017). Assessment of one story existing precast industrial buildings in Turkey based on fragility curves. *Bull. Earthq. Eng.* 15 (1), 271–289. doi:10.1007/s10518-016-9956-x

Palermo, M., Silvestri, S., Gasparini, G., and Trombetti, T. (2015). Crescent shaped braces for the seismic design of building structures. *Mater. Struct.* 48, 1485–1502. doi:10.1617/s11527-014-0249-z

Pollini, A. V., Buratti, N., and Mazzotti, C. (2020). Behavior factor of concrete portal frames with dissipative devices based on carbon-wrapped steel tubes. *Bull. Earthq. Eng.* 19, 553. doi:10.1007/s10518-020-00977-y

Santos, A. F., Santiago, A., Latour, M., and Rizzano, G. (2019). Analytical assessment of the friction dampers behaviour under different loading rates. *J. Constr. Steel Res.* 158, 443–459. doi:10.1016/j.jcsr.2019.04.005

Timoshenko, S. P., and Gere, J. M. (2009). *Theory of elastic stability*. Mineola, NY: Dover Publications Inc. Dover Civil and Mechanical Engineering.

Torquati, M., Belleri, A., and Riva, P. (2018). Displacement-based seismic assessment for precast concrete frames with non-emulative connections. *J. Earthq. Eng.* 24, 1624. doi:10.1080/13632469.2018.1475311

Venmarcke, E. H., and Gasparini, D. A. (1976). *Simulated earthquake motions compatible with prescribed response spectra—SIMQKE-1*. Cambridge, MA: M.I.T. Department of Civil Engineering Research.

Conflict of Interest: PB is the CEO of BIEMME srl. Biemme srl commissioned the research to develop an anti-seismic device to the University of Bergamo through a Scientific Research Contract. The single device presented herein has been certified following UNI EN 15129 under the name 'Mezzaluna M1'. The remaining authors declare the absence of any commercial or financial relationships that could be construed as a potential conflict of interest.

The results presented in the paper are the output of such a contract.

frontiers in Built Environment

REVIEW
published: 26 March 2021
doi: 10.3389/fbuil.2021.630952

Recent Advances in the Research of the Seismic Response of RC Precast Buildings at the University of Ljubljana

Blaž Zoubek†, Anže Babič, Matjaž Dolšek, Matej Fischinger and Tatjana Isaković*

Faculty of Civil and Geodetic Engineering, University of Ljubljana, Ljubljana, Slovenia

Although in Europe, precast concrete buildings had been built for decades, their seismic response was poorly understood, which is reflected in ambiguous code requirements and conservative design approaches. Therefore, this structural system was the main focus of several European research projects in the past 2 decades. The University of Ljubljana was actively involved in these projects. The key results of the work performed at the University of Ljubljana are presented and discussed in this paper. The main contributions include: a) the development of a new capacity model of beam-column dowel connections, which are one of the critical parts of the RC precast structural system, b) new insight into the cyclic behaviour of fastening systems of concrete cladding panels, and new design procedures for the estimation of strength and displacement capacity of cladding fasteners, c) the development of a methodology for seismic fragility analysis of RC precast buildings, and the fragility curves of precast RC building classes, which can be used for the safety-calibration of the new design procedures of RC precast buildings, and d) the development of a relatively simple and economically attractive back-up (strengthening) system to prevent the falling of panels in case of a strong earthquake.

Keywords: precast buildings, dowel beam-to-column connections, precast cladding panels, frictional beam-to-column connections, masonry infills, seismic fragility analysis, seismic restrainers

OPEN ACCESS

Edited by:
Bruno Dal Lago,
University of Insubria, Italy

Reviewed by:
Roberto Nascimbene,
Fondazione Eucentre, Italy
Gennaro Magliulo,
University of Naples Federico II, Italy

****Correspondence:***
Blaž Zoubek
blaz.zoubek@schimetta.at

†Present Address:
Blaz Zoubek,
Schimetta Consult ZT GmbH,
Salzburg, Austria.

Specialty section:
This article was submitted to Earthquake Engineering, a section of the journal Frontiers in Built Environment

Received: *18 November 2020*
Accepted: *27 January 2021*
Published: *26 March 2021*

Citation:
Zoubek B, Babič A, Dolšek M, Fischinger M and Isaković T (2021) Recent Advances in the Research of the Seismic Response of RC Precast Buildings at the University of Ljubljana. Front. Built Environ. 7:630952. doi: 10.3389/fbuil.2021.630952

INTRODUCTION

In Europe, precast industrial buildings most often consist of an assemblage of cantilever columns tied together with beams. Before the early developments of European seismic codes, such systems received relatively little attention from the earthquake engineering community compared to the cast-in-place structures. This was reflected in limited knowledge about several aspects of the seismic response of precast buildings, leading to a quite conservative approach for the design (Fischinger et al., 2014). However, in the last 2 decades, several research projects (ECOLEADER, PRECAST, SAFECAST and SAFECLADDING) provided plenty of experimental and analytical findings, which resulted in the improvement of the design practice governed by the modified provisions in the relevant chapter of current and future versions of Eurocode 8 (EN 1998-1:2004; prEN 1998-1-2_SC8_04-09-2020).

A research team from the University of Ljubljana (UL) actively participated in these projects and cooperated with large consortia of European Associations of precast producers, enterprises and research institutions. The team contributed considerable work with an emphasis on the following subjects: inelastic flexural response of slender cantilever columns, seismic behaviour of beam-to-column dowel connections, seismic behaviour of cladding-to-structure connections, seismic fragility and seismic risk of precast industrial buildings. All these research results offer an important knowledge base for adequate seismic design of modern RC precast buildings. In this paper, recent work on the following four crucial topics will be summarized:

- Cyclic response of beam-to-column dowel connections

One of the key elements in the RC precast structural system is the beam-to-column connection. In Europe, among many different solutions, the dowel beam-to-column connection is most frequently used. In *Beam-to-Column Dowel Connections* Section, an improved procedure for the estimation of the strength capacity of such connections, published in Zoubek et al. (2015), is presented.

- Cyclic response of the typical fastening system of concrete cladding panels

In L'Aquila (2009) and Emilia-Romagna (2012) earthquakes, heavy damage on nonstructural components in RC precast buildings was observed. Particularly vulnerable appeared to be the concrete cladding panels and their connections with the main structural system. Extensive research on typical cladding fastening systems, performed at UL, followed (Zoubek et al., 2013). Experiments and analysis of failure mechanisms of most common beam-to-cladding connections are described in *Typical Fastening Systems of Concrete Cladding Panels* Section.

- Fragility analysis of pre-code RC precast buildings

In order to assess the weaknesses of pre-code single-storey precast buildings, fragility analysis was performed for four classes of such buildings (Babič and Dolšek, 2016): without nonstructural elements, with vertical cladding panels, with horizontal cladding panels and with masonry infills. The results of the analysis can serve to generalize the observations stated in post-earthquake reconnaissance reports, such as insufficient seismic behaviour of beam-to-column connections and fastening systems of concrete cladding panels.

- Strengthening interventions for existing precast buildings with cladding panels

Based on the field reconnaissance reports and recent research (see also *Typical Fastening Systems of Concrete Cladding Panels* and *Seismic Fragility Analysis of Pre-Code RC Precast Buildings with the Consideration of Nonstructural Elements* Sections) it can be concluded that improvements to precast buildings with cladding panels are needed. At the UL, a relatively simple and economically attractive strengthening system has been developed for this purpose. The idea and design of the system are presented in *Strengthening Interventions for Existing Precast Buildings with Cladding Panels* Section.

BEAM-TO-COLUMN DOWEL CONNECTIONS

Common Design Practice and Incomplete Mechanical Models

The dowel connection is the most typical connection between columns and beams in European precast design practice (**Figure 1**). These connections can be subjected to the following types of failure mechanisms (**Supplementary Figure S1**): (A) local failure and (B) global failure.

In most cases, a local failure mechanism is ductile and will usually take place if the distance between the dowel and the edge is sufficiently large. However, when the dowel is positioned closer to the column or beam edge, global failure occurs. In this case, spalling of the concrete between the edge and the dowel is likely to govern the resistance.

Local failure was the subject of several studies (Vintzeleou and Tassios, 1986; Tanaka and Murakoshi, 2011; Zoubek et al., 2013; Magliulo et al., 2014). Consequently, the knowledge has been considerably more extensive in comparison to global failure, where the related analytical and experimental studies were quite limited (Vintzeleou and Tassios, 1986; Fuchs et al., 1995; Capozzi et al., 2012; Psycharis and Mouzakis, 2012). Most of them were carried out on quite simple specimens or models. The critical contribution of the stirrups to the capacity of the dowel connections, as well as to the type of failure, was neglected in Vintzeleou and Tassios (1986), while it was only implicitly considered in Fuchs et al. (1995). Therefore, the results of these

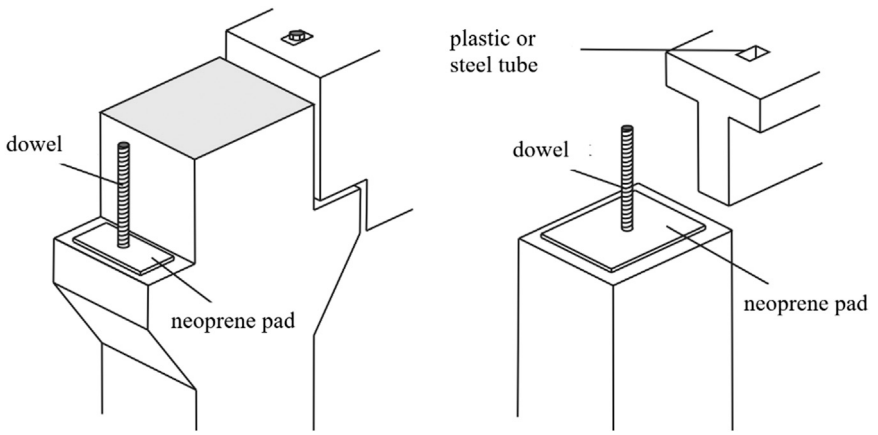

FIGURE 1 | Assembly schemes of typical beam-column dowel connections.

studies cannot be directly applied to beam-to-column dowel connection in RC precast buildings, as the stirrups around the dowel typically have a substantial effect on the strength of the connection and may shift the global failure from brittle to ductile. The procedures suggested in the above-mentioned studies are in most cases, very conservative, leading to unfeasible design solutions.

At the University of Ljubljana, both types of failure of dowel connections were studied, with a particular emphasis on the global type of failure. The procedure is summarized in *A New Approach for the Estimation of the Strength Capacity of Eccentric Dowel Connections* Section.

A New Approach for the Estimation of the Strength Capacity of Eccentric Dowel Connections

A dowel connection is susceptible to the spalling of the concrete between the column or beam edge and the dowel when it is positioned close to the edge of the concrete elements. If there are no stirrups in the region around the dowel, brittle tensile failure typically takes place (solid line in **Figure 2**). However, precast elements are usually reinforced by very compact transverse reinforcement in the critical region around the dowel. In this case, reinforcement influences the stress field and changes the failure type from brittle to ductile (**Figure 2**).

The diameter and spacing of the stirrups determine the influence of the reinforcement on the strength of the connection. If the precast elements are reinforced by a relatively large number of stirrups, the strength is typically higher than the concrete tensile strength. Consequently, the strength of the connection increases after crack formation (**Figure 2**). However, if the number of stirrups is low, the tensile strength of the concrete can, of course, be higher than the strength of the transverse reinforcement. In such situations, the strength of the connection would be reduced after the concrete has cracked (**Figure 2**).

In order to estimate the capacity of dowel connections against global failure, it has been assumed that the strength capacity is mainly provided by transverse reinforcement—the contribution of the concrete is not taken into account. The strength described in this way, as already discussed, may be greater or smaller than the strength given by the concrete's tensile strength.

Considering the crucial role of stirrups, a different approach was implemented from the studies described in *Common Design Practice and Incomplete Mechanical Models* Section. As shown in **Figure 3**, the stirrups were considered explicitly, employing a strut and tie model.

Strut and tie models are already well established. In various codes (ACI 318-08; NZS 3101), they have been widely used, primarily to solve certain problems where the Bernoulli theorem of linear distribution of strains cannot be applied. Strut and tie models typically allow designers to choose how the load is transferred, choosing a certain stirrup arrangement. This arrangement determines an equivalent truss, where the tensile stresses in the stirrups (ties) are in equilibrium with the compressive stresses in the concrete (struts). These stresses should be sustained by both the concrete and the reinforcement.

A FEM numerical model in ABAQUS (ABAQUS, 2011) was developed based on the results of experiments to investigate the stress distribution in dowel connections. It was presented in Zoubek et al. (2013). The equivalent trusses corresponding to different common dowel connection configurations were defined using this model (**Figure 3**).

Typical configurations of the dowel connections are presented in the first column of **Figure 3**. In the second column the corresponding strut and tie model is illustrated. The calculated stresses are shown in the third column. In the final column, a closed expression for the estimation of strength is given. This strength corresponds to the yielding of the first layer of reinforcement. The local ductile failure mechanism is connected to the complete utilization of the compression struts, which is not considered in **Figure 3**.

Let us now analyze the capacities of the connections in more detail on the simple example of a single dowel (**Figure 3**, CASE 1). The equivalent truss consists of stirrups and two compression diagonals (**Figure 4**). The compression diagonals are formed in between the activated vertical corner bars and the dowel

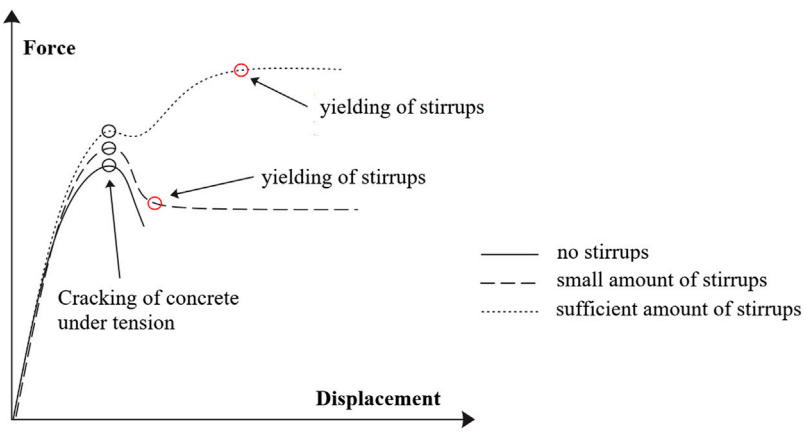

FIGURE 2 | Force–displacement diagram of beam-column dowel connections with eccentrically placed dowel.

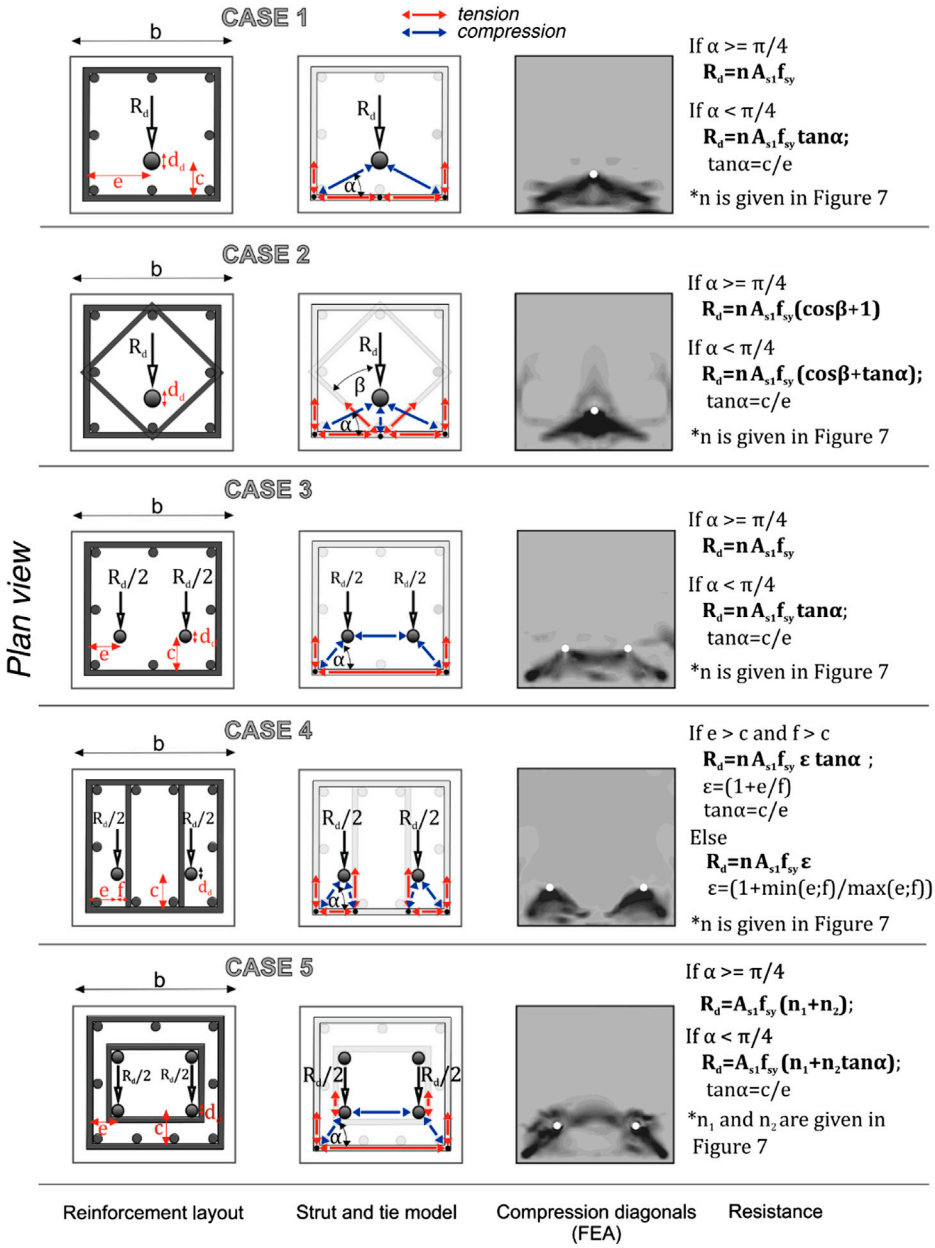

FIGURE 3 | Calculation of the strength capacity of eccentric dowel connection, adopted from Zoubek et al. (2015).

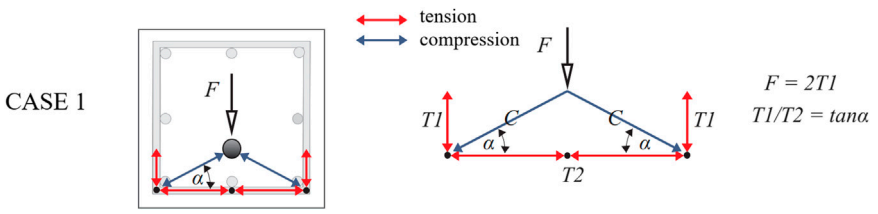

FIGURE 4 | Strut and tie model for a connection with a single eccentric dowel and perimeter hoops [adopted from Zoubek et al. (2015)]

(**Figure 4**). Considering the equilibrium in the dowel, the compression forces C can be expressed as:

$$C = 0.5\ F/\sin\alpha \tag{1}$$

where α is the angle between the compression diagonal and the legs of the stirrups which are perpendicular to the loading direction and F is the force applied to the dowel.

Considering the equilibrium in the corner nodes, the tensile forces which develop in the stirrups can be calculated as:

$$T_1 = C\ \sin\alpha = F/2 \tag{2}$$

$$T_2 = C\ \cos\alpha = F/2/\tan\alpha \tag{3}$$

The force F can thus be expressed as:

$$F = 2\ T_1 \tag{4}$$

$$F = 2\ T_2\ \tan\alpha \tag{5}$$

If the dowel is positioned close to the edge of the concrete element (i.e. $\alpha < \pi/4$), yielding will take place in the legs of the stirrups perpendicular to the loading direction. Thus, the strength capacity can be calculated as:

$$F_{max} = 2\ T_2 \tan\alpha = 2\ A_{s1} f_{sy} \tan\alpha \tag{6}$$

where A_{s1} is the cross-section of a single leg of the perimeter hoop, and f_{sy} is the steel yield strength of the steel.

If the distance between the edge and the dowel is greater (i.e. $\alpha > \pi/4$) yielding will take place in the leg of the stirrups parallel to the direction of loading. The strength capacity can then be expressed as:

$$F_{max} = 2\ T_1 = 2\ A_{s1} f_{sy} \tag{7}$$

The critical region, where the spalling of the concrete is typically observed, is spread along the dowel. Consequently, more than one layer of stirrups may be engaged. The strength of the connection is influenced by all of these stirrups. Based on the experimental data and according to FEA (Zoubek et al., 2013), it has been concluded that the length/height of the critical region can be estimated as:

$$h_{crit} = 2.5\ d_d + c - a, \tag{8}$$

where c is the distance between the dowel axis and the stirrup axis and a is the vertical concrete cover of the outermost stirrup.

Taking into account the vertical distance s between the stirrups, the number of the activated stirrups n can be determined as:

$$n = h_{crit}/s + 1 \tag{9}$$

Finally, the strength capacity of the dowel connection R_d is defined as the maximal force F applied to the dowel when yielding of the first layer of stirrups takes place. It is assumed that the stresses in the other stirrups decrease linearly. Considering the average stress in the stirrups σ_{avg}, the resistance of all stirrups can be calculated as:

$$R_d = R_{max} = 2\ T_2 \tan\alpha = 2\ n\ A_{s1}\ \sigma_{avg} \tan\alpha = n\ A_{s1}\ f_{sy} \tan\alpha \tag{10}$$

if the dowel is positioned close to the edge of the section ($\alpha \le \pi/4$), and

$$R_d = R_{max} = 2\ T_1 = 2\ n\ A_{s1}\ \sigma_{avg} = 2\ n\ A_{s1}\ f_{sy}/2 = n\ A_{s1}\ f_{sy} \tag{11}$$

if the dowel is positioned far from the stirrups ($\alpha \ge \pi/4$).

In **Eqs 10**, **11**, n is the number of activated stirrups, f_{sy} is the yield strength of the steel, A_{s1} is the cross-section of one stirrup's leg and α is the angle marked in **Figure 4**.

TYPICAL FASTENING SYSTEMS OF CONCRETE CLADDING PANELS

Seismic Behaviour of Precast Buildings With Cladding Panels

During the earthquakes in Emilia–Romagna in Italy in 2012, RC precast buildings were amongst most vulnerable types of structures. The damage was observed on structural as well as on nonstructural components. Particularly vulnerable appeared to be the cladding panels and their connections with the main structural system (**Figure 5**). According to Bournas et al. (2013), for example, the collapse of cladding panels was observed in 75% of all precast buildings in the region. Liberatore et al. (2013) reported significant damage to claddings in 50% of 34 surveyed industrial buildings. Many authors (Ioannou et al., 2012; Belleri et al., 2014; Magliulo et al., 2014) emphasized that the cladding fastening systems were designed only for seismic forces perpendicular to the plane of the panel, which are proportional to the local mass of the panels, and for small out-

FIGURE 5 | (left) Collapse of concrete cladding panels, and (right) failure of a typical cladding-to-structure connection during the Emilia earthquakes [adopted from Zoubek et al. (2016a)].

of-plane horizontal loads (e.g. wind loads). At the time, the common opinion was that their poor resistance to the horizontal seismic loads in the plane of the panel was the leading cause of the failure of the fasteners.

According to Belleri et al. (2015), Belleri et al. (2016), the high flexibility of RC precast industrial buildings led to displacement incompatibility between structural elements and concrete panels in the panel plane, which caused many failures of cladding fastening systems. The authors concluded that such systems should possess adequate ductility to accommodate the seismic displacement demand.

Taking into account the lessons learned from the L'Aquila and Emilia earthquakes, the cladding panel connections typically used in RC precast buildings in Europe have been analyzed analytically and experimentally within European project SAFECLADDING (2015). Vertical, as well as horizontal panels, were addressed. The investigated connections were mostly designed to be used in the non-seismic regions. Even though a little was known about their seismic response, they were extensively used in the seismic areas.

Based on the extensive experimental research, which is briefly summarized in *Experiments* Section and thoroughly presented in Zoubek et al. (2016a), the basic mechanisms of the seismic response of typical panels' connections between beams and vertical panels were identified. Considering the observed response, the appropriate numerical models, which can be used in the design practice, were developed and the design procedure, proposed. The estimation formulae for in-plane strength and displacement capacity are given in *Shear Strength and Displacement capacity* Section. Just recently results of research on typical connections between horizontal cladding panels and columns, also performed at the University of Ljubljana, were published in Starešinič et al. (2020). However, these findings are not included in this paper.

Experiments

The study carried out at the University of Ljubljana as part of the SAFECLADDING project initially focused on the connections that are most commonly used to attach vertical panels to precast beams. Such connections consist of a special steel strap (a hammer-head strap), a bolt, a washer, and two steel channels, which are attached to the reinforcement bars before the elements are cast. One of the channels is cast into the panel, while the other is cast into the structural element. The strap is fastened to the channel in the structural element by means of a bolt and a washer (**Figure 6**). The head of the strap is finally fixed inside the steel channel in the panel. In this way, a connection is created between the structural element and the panel.

Within the scope of the study presented in Zoubek et al. (2016a), 16 cyclic tests were performed on hammer-head strap connections. In **Supplementary Table S1** the complete experimental programme is given. In general, the behaviour of the connections in both in-plane directions was analyzed. Thus the following three different types of tests were performed:

- Uniaxial sliding tests: The load was applied in the direction of the vertical channel. Four such uniaxial tests were performed (**Figure 6**).
- Uniaxial shear tests: The load was applied in the direction of the horizontal channel. The hammer-head strap connection was loaded in shear. A total of eight such tests were carried out (4 with cold-formed and 4 with hot-rolled channels).
- Biaxial shear tests: To estimate the effect of out-of-plane force on the in-plane behaviour of the investigated connections, a constant out-of-plane force was simultaneously applied to the panel. Four such tests were carried out.

Figure 7 shows the observed response of the investigated connections with cold-formed channels subjected to a shear loading. At low actuator forces (0.5–1 kN), the strap rotates around the bolt, as shown in **Figure 7** (see Stage 2). At some point (relative displacement of approx. 2–3 cm) the head of the strap becomes stuck inside the channel. Thus, the stiffness of the connection increases abruptly (Stage 2 in **Figure 7**). Yielding occurs in the narrow part of the strap at a shear load of approx. 3 kN. Lastly, the strap fails due to flexural failure in the narrow part (Stage 3 in **Figure 7**).

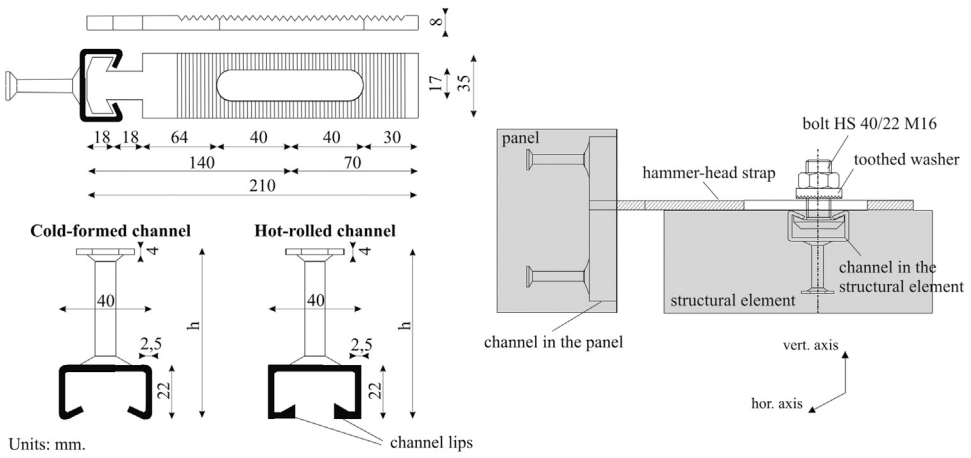

FIGURE 6 | Geometry (left) of the tested connection and (right) of the connection assembly, adopted from Zoubek et al. (2016a).

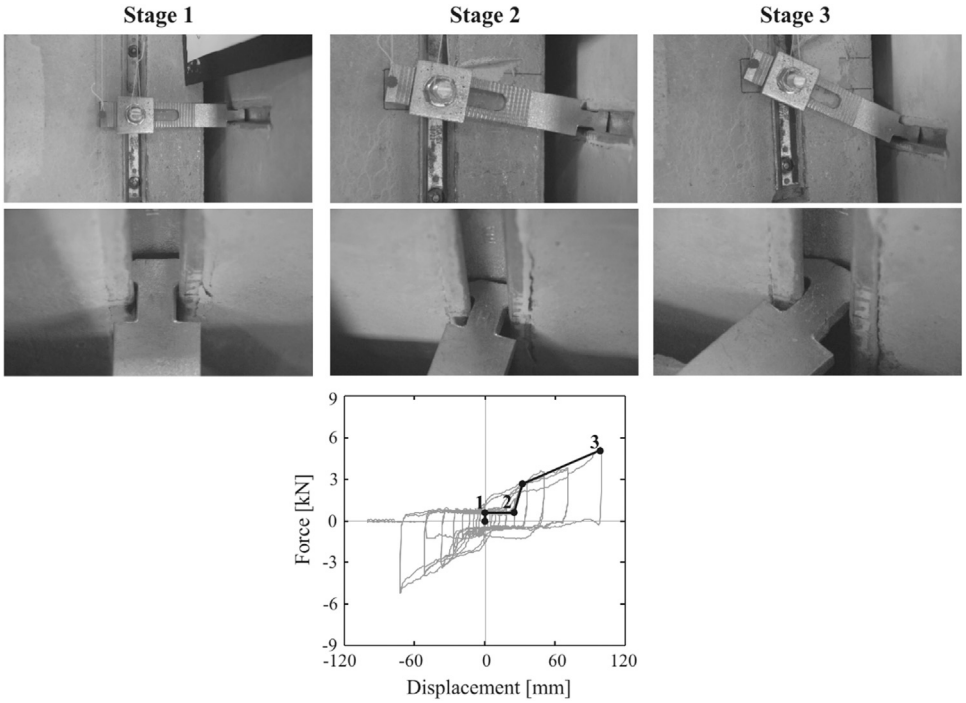

FIGURE 7 | Failure mechanism of the investigated connections, adopted from Zoubek et al. (2016a).

If cold-formed channels were used instead of hot-rolled ones, failure did not occur in the strap, but in the channel. However, the recorded hysteretic loops look very similar.

In some tests, the gap between the panel and the beam closed before the failure of the strap or of the channel. In these cases, the recorded hysteretic behavior of the connection was considerably different. The gap closed at large displacements. Consequently, the friction between the panel and the beam led to an increase in stiffness. However, the strength capacity of the connection itself was not affected because the weakest link was still either the channel or the hammer-head strap, which failed at the same shear force as when the gap was not closed. The gap should therefore be large enough to allow the displacement capacity of connections to be utilized.

Biaxial tests with a constant perpendicular force $P\perp$ were also conducted to determine the effect of an out-of-plane force on the resistance of investigated connections. Even though the mechanism of failure remained the same, the hysteresis clearly show, that in the case of biaxial loading, a higher stiffness can be observed. In these tests, the strap was stuck within the channel already in its initial position. Consequently, there was no sliding of the strap and the stiffness was greater. Surprisingly, the maximal obtained shear force at the failure of the biaxially loaded connections was higher than that recorded in the uniaxial tests.

Shear Strength and Displacement Capacity

An analytical model of the tested connections was developed based on the experimental results. Formulae have been proposed to define the force-displacement envelopes. In this paper, the expressions are presented in their final form and for cold-formed channels only. The derivation of these expressions including the formulae for the hot-rolled channels are given in Zoubek et al. (2016a).

Based on the equilibrium shown in **Figure 8**, the shear strength can be expressed by the following equation:

$$R_{max} = \left[d_u P_\perp + \frac{1}{2R} \sqrt{1 - (d_u/L)^2} \ (R_{ch} - P_\perp) + T_0 \right] \Big/ \sqrt{L^2 - d_u^2} \tag{12}$$

In **Eq. 12**, T_0 is the tightening torque, which was estimated to be equal to M_{fr} (**Figure 8**), R and L are the distances denoted in **Figure 8** (Stage 1), d_u is the ultimate displacement, R_{ch} is the out-of-plane resistance of the channel, which can be obtained from the product specification, and $P\perp$ is the out-of-plane force. **Equation 12** clearly explains how the shear resistance increases with increasing out-of-plane force (see also *Experiments* Section). It should be noted, however, that if the force acts in the opposite direction, the resistance is reduced.

The ultimate displacement d_u can be calculated as a sum of the displacement at which the strap gets stuck within the channel d_{gap} and the displacement d_{ch} due to the deformation of the channel:

$$d_u = d_{gap} + d_{ch} = L\theta_{gap} + L\theta_{ch} = L\left(\theta_{gap} + \theta_{ch}\right), \tag{13}$$

where θ_{gap} and θ_{ch} are the corresponding rotations of the strap. While the rotation θ_{gap} can be estimated on the basis of the geometry of the strap and the channel, θ_{ch} is relatively difficult to evaluate. When the experimental results were compared to the calculated values, the measured deformations of the channel were taken into account.

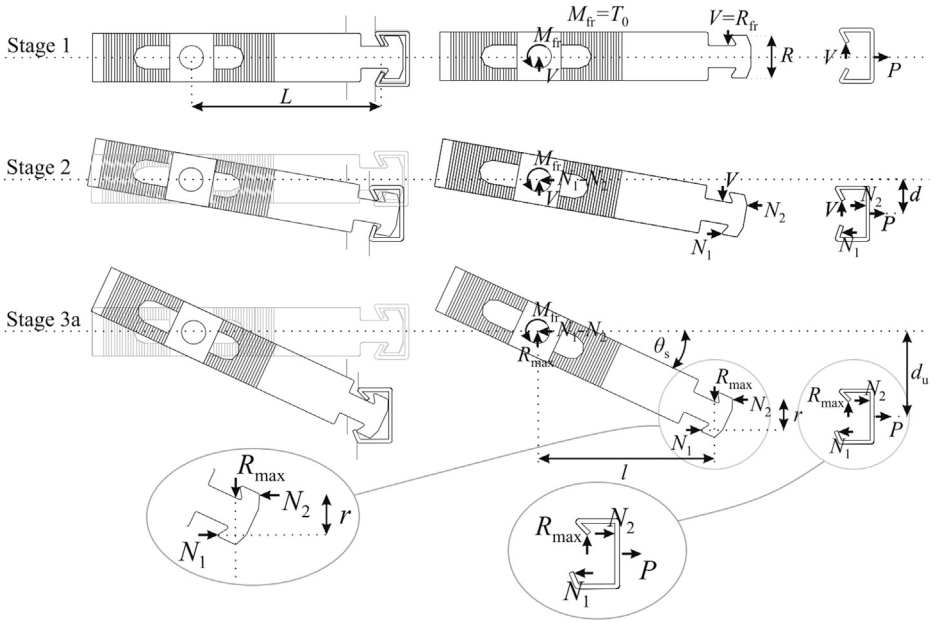

FIGURE 8 | The shear force transfer mechanism in the investigated connections, and the state of equilibrium just before failure, adopted from Zoubek et al. (2016a).

SEISMIC FRAGILITY ANALYSIS OF PRE-CODE RC PRECAST BUILDINGS WITH THE CONSIDERATION OF NONSTRUCTURAL ELEMENTS

Description of the Analyzed Buildings

A large part of existing RC precast buildings was designed and constructed before the implementation of seismic codes. Apart from the deficiencies that are common to all types of pre-code RC buildings, such as the low amount of shear reinforcement, pre-code precast buildings also exhibit other weaknesses. Probably the most critical weakness of pre-code precast buildings is the inadequate design and construction of beam-to-column connections, which in many cases rely only on friction between the column and the beam. Another weakness of such buildings is the lack of a rigid diaphragm, which limits the ability of the structure to transfer lateral loads imposed by the perimeter nonstructural elements to the internal columns.

In this Section, seismic fragility analysis is summarized for four classes of pre-code single-storey precast buildings (i.e. B, V, H and M, **Supplementary Table S2**), which are described in more detail elsewhere (Babič and Dolšek, 2016). The building classes are defined by the statistical distribution of characteristics of the load-bearing structure and nonstructural elements. Characteristics of the load-bearing structure are the same for all building classes, while those of the nonstructural elements vary between the classes. Buildings in class B are without nonstructural elements (bare frame buildings), while buildings in classes V, H and M contain vertical precast panels, horizontal precast panels and masonry infills, respectively (**Supplementary Table S2**).

The load-bearing structures were defined based on previous studies (DOCUP, 2006; Casotto et al., 2015). These studies refer to precast buildings in Northern Italy, which, however, are similar to Slovenian precast buildings (e.g. Isaković et al., 2012). The structures consist of cantilever columns, which support long saddle beams covered by roof elements (**Figure 9**). The beam-to-column connections contain no mechanical elements and rely only on friction. The basic geometric and material parameters are presented in **Figure 9**. The cross-sectional dimensions (equal to 50 cm) and longitudinal reinforcement ratios (with the mean and the standard deviation equal to 1.13% and 0.22, respectively) of the columns were determined based on the building code that was in force at the time of the design (Casotto et al., 2015) and was associated with a design lateral load equal to two per cent of the buildings' self-weight. A low transverse reinforcement ratio was assumed in all parts of columns, resulting in a confinement coefficient equal to 1.00.

The seismic response of the nonstructural elements (**Figure 9**) is mostly dependent on their connections with the structure. Vertical panels are attached to the beams at the top and restrained by a foundation beam at the bottom. The top connection contains the same type of fastenings, as described in *Typical Fastening Systems of Concrete Cladding Panels* Section. On the other hand, horizontal panels are attached to the columns. The connections at the top of the panels contain a steel box element, which is presented in more detail by Starešinič et al. (2020). However, at the bottom, horizontal panels are supported by small corbels that are installed into the columns. Furthermore, masonry infills are placed between the columns. Their connection to the adjacent structural elements relies only on friction, making the infills susceptible to overturning. The uncertain characteristics of nonstructural elements are assumed uniformly distributed. Their minimum and maximum values are reported in Babič and Dolšek (2016). However, the basic geometric and material

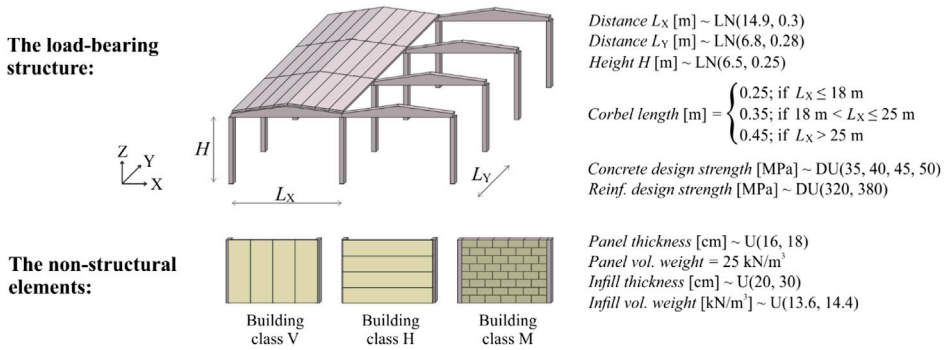

FIGURE 9 | The configuration and basic characteristics of the load-bearing structures (top) and nonstructural elements (bottom). Some parameters are considered constant, while others are uncertain. The uncertain parameters follow either the lognormal (LN), uniform (U) or discrete uniform (DU) distribution.

parameters are also presented in **Figure 9**, while the modeling parameters are given later in **Figure 10**.

Numerical Models of the Analyzed Buildings for Nonlinear Dynamic Analysis

For fragility analysis, a lumped plasticity model of precast buildings was developed using OpenSees software (McKenna and Fenves, 2010). The models were developed to be used in non-linear dynamic analyses considering all three ground motion components. In the case of the load-bearing structures, the same modeling principles were applied for all building classes. The models for building classes V, H and M, however, were expanded to also include the nonstructural elements. A summary of the models is provided in *Load-Bearing Structure, Vertical and Horizontal Panels and Masonry Infills* Sections, while their more detailed description can be found in Babič and Dolšek (2016).

Load-Bearing Structure

The columns were modeled by one-component lumped plasticity elements. At the base of each column, two independent rotational springs were assigned (about both principal directions) (spring A, **Figure 10**). The moment-rotation relationship of the springs was defined according to a previous study (Dolšek, 2010). Moreover, the beams were modeled by elastic elements. At the ends of these elements, nodal masses were applied to represent the mass of the structure. The beam-to-column connections were modeled by 3D contact zero-length elements, which allowed to simulate the support in the vertical direction as well as frictional forces in the horizontal directions. The friction coefficient was determined according to Magliulo et al. (2011), while no cohesion was assigned. The impact between the beams and columns was modeled by an elastic no-tension spring with an initial gap (spring B, **Figure 10**). For the modeling of other elements at the roof level, truss elements with elastic behaviour were used.

Vertical and Horizontal Panels

The effect of vertical panels was modeled by simulating only the response of the fastenings, thus assuming that the deformations in the panels are negligible in comparison to the displacement in the fastenings (**Supplementary Figure S2**, top left). Fastenings were modeled by several springs. Each spring connected the

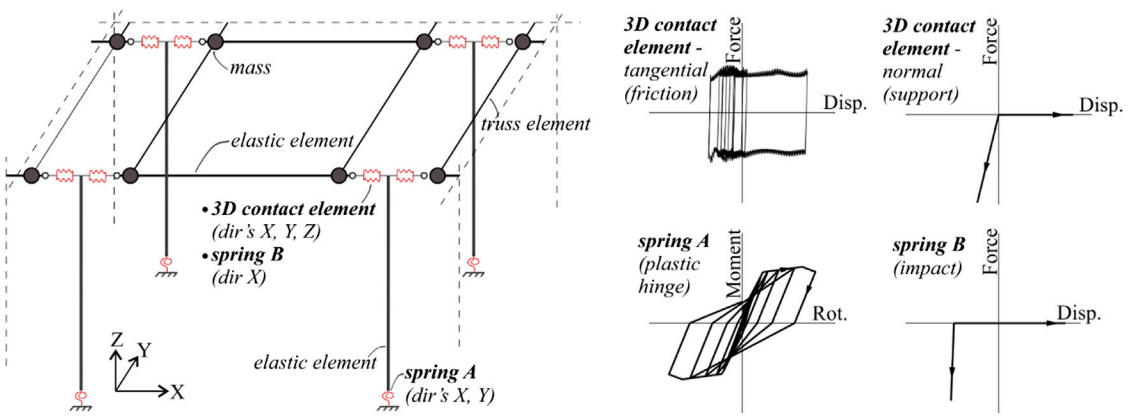

FIGURE 10 | The model of the load-bearing structure (left) and the force-displacement (moment-rotation) relationship of the non-linear elements employed in the model (right).

beams to the nodes that were fixed in the in-plane direction but unrestrained in the out-of-plane direction. The response in the in-plane direction (spring C, **Supplementary Figure S2**) was modeled by three springs in parallel which were calibrated on the basis of cyclic tests (Isaković et al., 2013). This included a perfectly elastic-plastic spring and two elastic-plastic springs with an initial gap. However, in the out-of-plane direction, the response of the fastenings was modeled by an elastic spring (spring E, **Supplementary Figure S2**). Half of the panels' mass was considered in the out-of-plane direction, assuming that the other half is transferred directly to the foundation.

The horizontal panels were modeled by stiff elastic elements (**Supplementary Figure S2**, top right). In order to model the response of the bottom panel-to-column connections in the in-plane direction, two elements in parallel were used. The first element (i.e. a 3D contact element) was used to model the vertical support and friction, while the second element (i.e. a multilinear spring; spring F in **Supplementary Figure S2**) enabled to simulate the impact between the panel and the column, which occurs due to the limited length of the installation gap. In the out-of-plane direction, a stiff elastic spring was employed to prevent significant displacements between the panels and the columns. However, at the top of each panel, several springs were used to model the response of the fastenings. In the in-plane direction, a combination of five springs in parallel was used consisting of a perfectly elastic-plastic spring, and four elastic-plastic springs with an initial gap (spring D, **Supplementary Figure S2**), while in the out-of-plane direction, fastenings were modeled by an elastic spring (spring E, **Supplementary Figure S2**). The mass of each panel was lumped at its centre.

The potential failure of the fastenings installed in the vertical and horizontal panels (either in the in-plane or out-of-plane direction) was also modeled. The failure criteria were defined by the ultimate displacements (**Supplementary Figure S2**), which are described in more detail in Babič and Dolšek (2016). If any of the failure criteria for a given fastening was met, the panel that was attached by that fastening was removed from the model, so that its impact on the seismic response of the building was disregarded during the remaining part of the analysis.

Masonry Infills

A combination of stiff elastic elements and rigid constraints was used to model the masonry infills (**Supplementary Figure S3**). The masses of the infills were lumped at their centres. In the out-of-plane direction, the rocking of the infills was enabled by making use of elastic-no tension springs (spring G, **Supplementary Figure S3**). Moreover, the connections between the infills and the columns at the top were modeled by 3D impact zero-length elements. These elements enabled to simulate the friction in the out-of-plane direction as well as the in-plane non-linear response of the infills. The friction was modeled as in the case of the 3D contact zero-length elements (**Figure 10**), while the in-plane response of the infills was modeled by a bi-linear spring defined according to Panagiotakos and Fardis (1996). The potential failure of the infills was also considered. The failure criteria included the in-plane failure (associated with the exceedance of the infills' in-plane strength) and out-of-plane failure (corresponding to the out-of-plane rotation exceeding the overturning rotation). If any of the failure criteria were met, the infill was immediately removed from the model.

Methodology for Fragility Analysis of the Investigated Building Classes

The methodology for fragility analysis was developed by Babič and Dolšek (2016) as a part of the seismic stress test, which was developed within the EU-funded project STREST. It is based on the methodology proposed by Casotto et al. (2015), where the basis for the seismic fragility analysis is a building class sample. The sample of each building class consisted of 100 buildings. The load-bearing structures were determined through simulated design (Casotto et al., 2015) considering the variations in the geometric and material properties. The sample values were obtained with the Monte Carlo simulation, which was also used to generate a sample of the nonstructural elements. A numerical model was then defined for each building from the building class sample. The performance of the sampled buildings was analyzed for 70 ground motions adopted from Casotto et al. (2015).

In each simulation, two types of damage states, i.e. the nonstructural and the structural damage state were determined. The nonstructural damage was defined by one of the four damage states, which corresponded to different portions of the dislocated nonstructural elements:

- DS-0—no nonstructural element was dislocated.
- DS-1—at least one nonstructural element was dislocated.
- DS-2—at least half of the nonstructural elements were dislocated.
- DS-3—all nonstructural elements were dislocated.

However, the structural damage was defined by one of the three damage states:

- DS-NS—the structure suffered no or slight damage.
- DS-M—the structure suffered moderate damage, which occurred if 1) the yield rotation was exceeded in at least one column, or 2) the sliding was initiated in at least one beam-to-column connection.
- DS-C—the structure collapsed, which occurred if 1) the rotation in at least one column exceeded the ultimate rotation (EN 1998-3:2005), or 2) the relative beam drift in at least one beam-to-column connection exceeded the sliding capacity (i.e. the distance from the edge of the beam to the edge of the corbel).

Dependency between the nonstructural and the structural damage was accounted for by considering that all the nonstructural elements were dislocated in the case of structural collapse.

Based on data obtained with the simulations of seismic performance, the percentages of sample buildings meeting the designated damage states were determined for each ground motion separately. The regression analysis was then carried out to obtain the parameters of the fragility curves, i.e. the

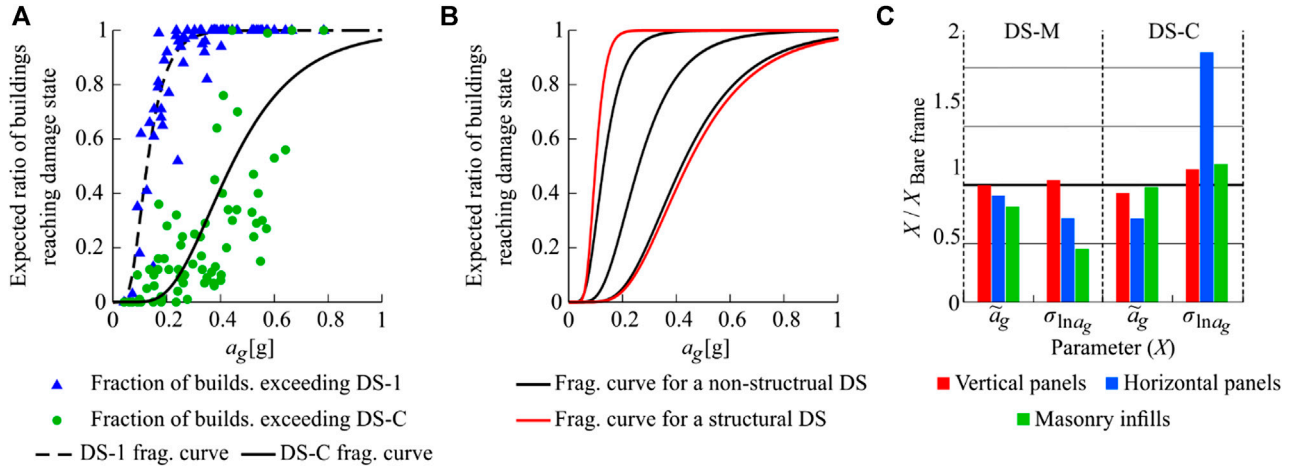

FIGURE 11 | (A) Ratios of buildings from building class H exceeding DS-1 and DS-C with the corresponding fragility curves, **(B)** all fragility curves of building class V, and **(C)** fragility parameters (median and logarithmic standard deviation) of buildings classes V, H and M normalized to the fragility parameters of building class B.

median seismic intensities corresponding to the onset of the damage states and the associated logarithmic standard deviations. As the intensity measure, the geometric mean of the peak ground acceleration in horizontal directions was used. In the regression analysis, lognormal distribution was assumed for the fragility curves, and their parameters were estimated by the maximum likelihood method (Baker, 2015). In **Figure 11A**, simulation data and the corresponding fragility curves are shown for two damage states, and building class V. An illustration of all fragility curves for this building class is presented in **Figure 11B**.

Results and Discussion

Fragility curves for nonstructural damage states depended on the type of nonstructural elements (**Supplementary Table S3**). This was most significant in the case of damage state DS-1, where $\tilde{a}_g$ for buildings with vertical panels exceeded $\tilde{a}_g$ for buildings with horizontal panels and masonry infills for approximately 250% and 120%, respectively. However, the differences became smaller as the degree of damage increased. In the case of damage state DS-2, $\tilde{a}_g$ for building class V was 110% greater than $\tilde{a}_g$ for building class H and 70% greater than $\tilde{a}_g$ for building class M. In the case of DS-3, the differences further reduced to 34% and 20%, respectively.

The type of nonstructural elements also impacted fragility curves for the structural damage states (**Supplementary Table S3**; **Figure 11C**). While the vertical panels had no significant impact on moderate damage, the addition of the horizontal panels and masonry infills reduced both $\tilde{a}_g$ and $\sigma_{\ln a_g}$. In the case of horizontal panels, the fragility parameters were reduced for approximately 10% and 30%, respectively, while the reductions amounted to about 20% and 50% when considering the masonry infills. Furthermore, in the case of damage state DS-C, the addition of vertical panels and masonry infills led to a small reduction of $\tilde{a}_g$ and a slight increase of $\sigma_{\ln a_g}$. Both of these changes in fragility parameters lead to a higher probability of collapse (Cornell, 1996). However, the impact of horizontal panels was more significant. Their inclusion in the structure decreased $\tilde{a}_g$ for approximately 25% and increased $\sigma_{\ln a_g}$ for about 100%.

The impact of nonstructural elements on the structural fragility can be explained by the simulated seismic response of buildings. From these simulations, it was observed that the largest rotations in the plastic hinges of the columns occurred in perimeter columns in buildings with horizontal panels. The large rotations in this type of buildings can be attributed to the inertial forces induced by the panels' mass. In general, a part of these inertial forces is transmitted directly to the foundations of the perimeter columns, while the remaining part is transmitted to other columns through the roof elements. However, the part of the forces transmitted to the other columns can be only as large as the strength of the beam-to-column connections. Because the beam-to-column connections in the analyzed buildings rely solely on friction, their strength is relatively low. Therefore, a large part of the inertial forces induced by the panels was transmitted directly to the foundation, which meant that these inertial forces acted more locally than in the case of precast structures with strong beam-to-column connections. This resulted not only in the concentration of rotations in the perimeter columns but also in the increase of displacements in the perimeter beam-to-column connections. Moreover, it was observed that masonry infills increased the stiffness in the in-plane direction and thus reduced the rotations at the bases of the columns. However, this increased the demand in the beam-to-column connections at the perimeter. Consequently, relative displacements in the beam-to-column connections of the precast buildings with masonry infills were larger than those observed in the bare frame buildings. Lastly, the vertical panels impacted the seismic response mostly with their mass. In this case, the panels-induced inertial forces acted on the structure above the beam-to-column connection, which increased the displacements in the connections, but had a small effect on the rotations in the columns.

The results of the fragility analysis were used in the seismic risk evaluation of pre-code RC precast buildings in Tuscany, Italy (Pitilakis et al., 2018). It was found that the seismic risk was too high, which signals the importance of strengthening interventions for this type of buildings. The results, discussed above, showed that the strengthening interventions should be focused on improving the seismic behaviour of the connections between the precast elements. This includes strengthening of the beam-to-column connections and increasing the in-plane stiffness of the connections between the roof elements. However, it also encompasses the strengthening of the connections between the structural and nonstructural elements and/or reducing the damaging consequences of the failure of such connections. For this reason, special seismic restrainers were developed at the University of Ljubljana, which help to prevent the cladding panels from causing damage after their dislocation from the structure. The seismic restrainers are presented in *Strengthening Interventions for Existing Precast Buildings with Cladding Panels* Section.

STRENGTHENING INTERVENTIONS FOR EXISTING PRECAST BUILDINGS WITH CLADDING PANELS

Seismic Restrainers

Based on the field reconnaissance reports and relevant research (see also *Typical Fastening Systems of Concrete Cladding Panels* and *Seismic Fragility Analysis of Pre-Code RC Precast Buildings with the Consideration of Nonstructural Elements* Sections) it can be assumed that improvements to RC precast structures with concrete cladding panels and the design of new connection types are needed. Withing the framework of the SAFECLADDING project (2015) several advanced solutions have been developed. However, the research was not limited to new types of fastening systems, but also concentrated on the protection of the existing RC precast structures. For instance, an economically appealing and simple strengthening device (seismic restrainer) has been developed at the University of Ljubljana (**Figure 12**), which was first described in Zoubek et al. (2016b). Its use is not limited only to existing precast buildings. It could also be used to prevent the falling of panels in new structures.

The concept of restrainers in seismic engineering is not an entirely new one. In the 1971 San Fernando earthquake in California, several simply supported multi-span bridges collapsed due to the excessive displacements which took place at supports and expansion joints (Randall et al., 1999). In order to limit the risk of superstructure unseating, the California Department of Transportation (CALTRANS) has since installed seismic restrainers in bridges (Randall et al., 1999). In Northern America commonly used restrainers connect girders to the bent cap. In 1999 Randall et al. published an extensive study on design procedures for such restrainer systems. The available literature contains many other related works by different authors (e.g. Saiidi et al., 2001; DesRoches et al., 2003; Hayashikawa et al., 2006). In these studies, a large part of effort was dedicated to the development of design rules. Unfortunately, the outcomes of these studies do not directly apply to RC precast buildings, where the restrainers would be activated upon the failure of the primary cladding-to structures fastening system, when considerable relative displacement between the structure and the panel is developed. Seismic restrainers in bridges are activated already at small longitudinal movements of the superstructure to prevent its unseating. In short, initial and boundary conditions are significantly different. New design procedures for the estimation of forces in restrainers in precast structures are therefore needed. These are summarized in the following sections.

Development of Restrainers for Cladding in Precast Structures

To protect the concrete cladding panels in case of a an earthquake, a back-up fastening system is proposed. The system is based on the use of a synthetic fiber rope or steel restrainer (**Figure 12**). Due to the limited distance between the panels and the bare frame in RC precast buildings, the rope would be normally rather short (less than 70 cm). The distance between the main structural systems and the concrete panels in precast buildings is normally limited. Therefore the length of the ropes/

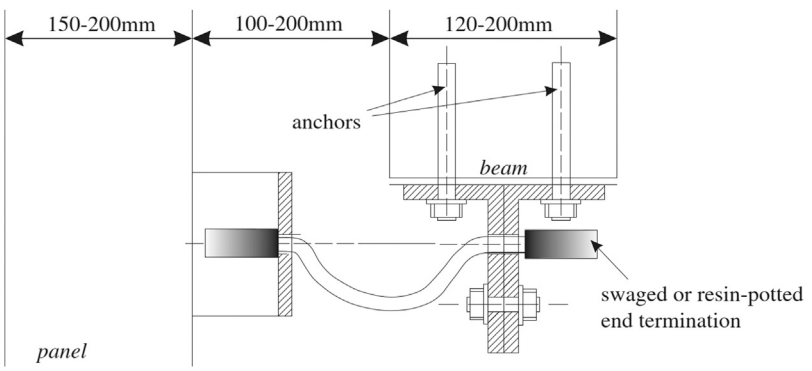

FIGURE 12 | A scheme of a restrainer system as a strengthening solution for the protection of cladding panels upon the failure of the primary cladding-to-structure connections [adapted from Zoubek et al. (2016b)].

restrainers would be relatively short (up to 100 cm). They are designed to be long enough to be triggered only in the case of failure of the primary cladding-to-structure connections occur and should not attach the panels to the structure. Therefore, they should have no influence on the response of a structure and panels as long as the primary cladding-to-structure connections are in operation.

As described in Zoubek et al. (2016b), the ropes/restrainers are connected to angular and omega steel profiles which are fastened to the panels and structural elements. The ropes are anchored in the profiles by means of resin-potted or swaged terminations. The gap between the panels and RC precast beams with realistic dimensions of the elements is illustrated in **Figure 12**. It is important that all system components presented here should be designed to withstand the expected seismic loads. At the University of Ljubljana, tensile tests on steel wire ropes with different swaged end terminations and synthetic fiber ropes with resin-potted terminations were performed (Isaković et al., 2015). In **Supplementary Table S4**, all tested combinations are given. Three 8–12 mm steel wire ropes and four different 8 mm synthetic fiber ropes were loaded in tension until failure. **Supplementary Figure S4** shows the recorded stiffness and strength. Failure of the restrainer occurred, in most of the tests, due to the insufficient strength of the rope termination.

The tests described above were performed on the restrainers attached to the T and omega profiles (as shown in **Figure 12**), which were fixed to the actuators. The anchors used for fixing the profiles to concrete elements were not investigated. Their performance was examined in the Slovenian national project Seismic Resilience and Strengthening of Precast Industrial Buildings with Concrete Claddings. However, the results of this research are not presented in this paper. Withing the framework of the above-mentioned project, also full-scale shaking table tests on a RC precast structure with concrete cladding panels were performed.

Seismic Demand on a Restrainer

Restrainers used to prevent the falling of concrete cladding panels are triggered for time periods of about 0.1 s [for a detailed analysis see Zoubek et al. (2016b)]. The dynamic behaviour of the panels and the primary structure at the time of their activation is relatively complicated. In this paper some equations derived in Zoubek et al. (2016b) are given which can be used to estimate the maximum expected impact forces in a restrainer system. It is important to note that they can be applied only in the case of short restrainers (**Figure 13**, left). When long restrainers are used (**Figure 13**, right), higher maximum forces may occur due to the additional angular acceleration of the panel induced by gravity G. In this second cases, it would be therefore important to take into account the P-Δ effect. If the influence of the P-Δ effect can be neglected, the dynamic response of the system can be described with acceptable accuracy by employing a relatively simple analytical model defined in **Figure 14**.

As demonstrated in **Figure 14**, the equilibrium of forces acting on the system can be written as

$$f_D + f_E + f_I = 0 \tag{14}$$

where f_D is the damping force, f_E is the force in the restrainers, and f_I is the inertial force of the panel.

The inertial force f_I can be calculated as the product of the panel mass per restrainer m_p and the panel acceleration in the direction perpendicular to the panel plane $\ddot{u}_p$ [**Figure 13** (left)]:

$$f_I = m_p \ddot{u}_p \tag{15}$$

By applying Hooke's law the force in the restrainer f_E can be simply calculated:

$$f_E = k_{res} \ddot{u}_r \tag{16}$$

where k_{res} is the restrainer stiffness and u_r is the relative displacement equal to the deformation of the restrainer.

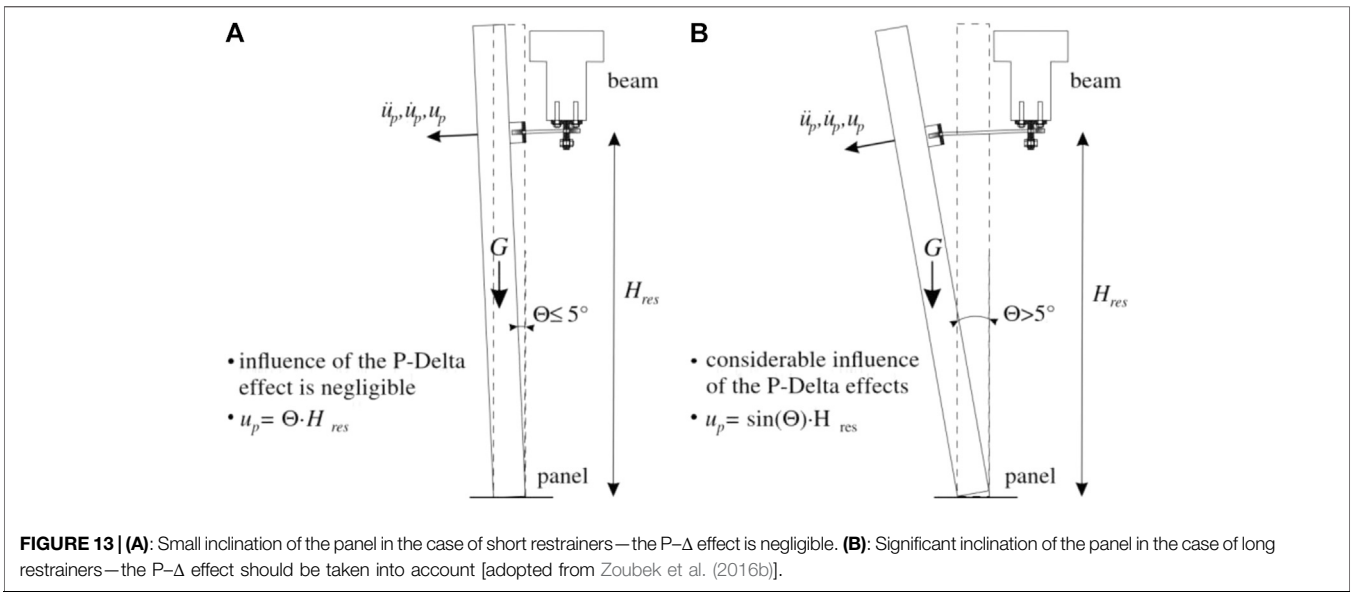

FIGURE 13 | (A): Small inclination of the panel in the case of short restrainers—the P–Δ effect is negligible. **(B)**: Significant inclination of the panel in the case of long restrainers—the P–Δ effect should be taken into account [adopted from Zoubek et al. (2016b)].

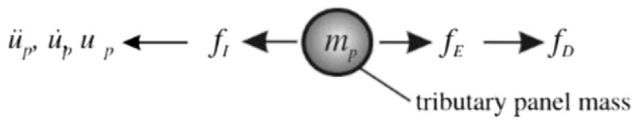

FIGURE 14 | A mathematical model used to calculate the maximum forces in a restrainer system: $\ddot{u}_p$, $\dot{u}_p$, and u_p are the acceleration, velocity and displacement of the panel at the level of the restrainer, and f_D, f_E and f_I are the damping, internal and inertial forces.

If the damping of the secondary system does not have any considerable effect on the tensile forces in the restrainers, one can assume $f_D = 0$. The simplification is reasonable while a relatively small amount of mechanical energy can be converted through damping in a short period of time when the restrainers are triggered (Fajfar, 1984).

Considering **Eqs 15**, **16** and assuming $f_D = 0$, **Eq. 14** takes the following form:

$$m_p \ddot{u}_p + k_{res} u_r = 0 \tag{17}$$

Let us now express the relative acceleration $\ddot{u}_r$ as the difference between the absolute acceleration of the structure $\ddot{u}_s$ and the absolute acceleration of the panel $\ddot{u}_p$:

$$\ddot{u}_p - \ddot{u}_s = \ddot{u}_r \tag{18}$$

Taking into account the relationship defined in **(18)**, **Eq. 17** can be rewritten as follows:

$$m_p \ddot{u}_r + k_{res} u_r = -m_p \ddot{u}_s \tag{19}$$

The solution of **Eq. 19** can be written as:

$$u_r(t) = A \sin(\omega t) + B \cos(\omega t) + f_0 / k_{\text{res}} \tag{20}$$

Where

$$\omega = \sqrt{\frac{k_{\text{res}}}{m_p}} \tag{21}$$

$$f_0 = -m_p \ddot{u}_s \tag{22}$$

While the oscillation period of the main structure is probably approx. ten times longer than the impact duration (Zoubek et al., 2016b), it can be assumed that the acceleration of the main structure (beam) $\ddot{u}_s = a_s$ is invariant during the time when the restrainer is triggered. Therefore, f_0 can also be considered constant. This assumption is confirmed in Zoubek et al. (2016b), based on the results of the performed non-linear time history analysis.

The constants A and B in **Eq. 20** can be calculated by considering the initial conditions just before the impact:

$$u_r(0) = 0, \quad \dot{u}_r(0) = v_{r0} \tag{23}$$

The coeffcients A and B are thus equal to:

$$A = \frac{v_{r0}}{\omega}, \quad B = -f_0 \Big/ k_{\text{res}} \tag{24}$$

Taking into account **Eqs 20**, **24** the relative displacement u_r can be expressed as:

$$u_r = \frac{v_{r0}}{\omega} \sin(\omega t) + f_0 \Big/ k_{res} (1 - \cos(\omega t)) \tag{25}$$

The tensile force in the restrainer can be evaluated as:

$$F_{res} = k_{res} u_r = v_{r0} \sqrt{m_p k_{res}} \sin(\omega t) + f_0 (1 - \cos(\omega t)) \tag{26}$$

Function given in **Eq. 26** has a maximum:

$$F_{res}^{max} = f_0 \left(1 - \frac{f_0}{\sqrt{f_0^2 + f_v^2}} \right) + f_v \sqrt{1 - \frac{f_0^2}{f_0^2 + f_v^2}} \tag{27}$$

where $f_v = \sqrt{k_{res} m_p} v_{r0}$.

The stiffness k_{res} can be measured or obtained from the technical specification of the used product. The stiffness of the synthetic fiber ropes tested at the University of Ljubljana was approx. 2MN/m (Isaković et al., 2015). By taking into account the number of installed restrainers, the corresponding panel mass per restrainer m_p can be estimated. In contrast to these two variables, the estimation of the acceleration of the main structure during the activation of the restrainer a_s and of the relative velocity between the structure and the panel at the beginning of the activation of the restrainer v_{r0} are obviously not trivial tasks. In **Figure 15**, where the results of the non-linear time history analysis and the

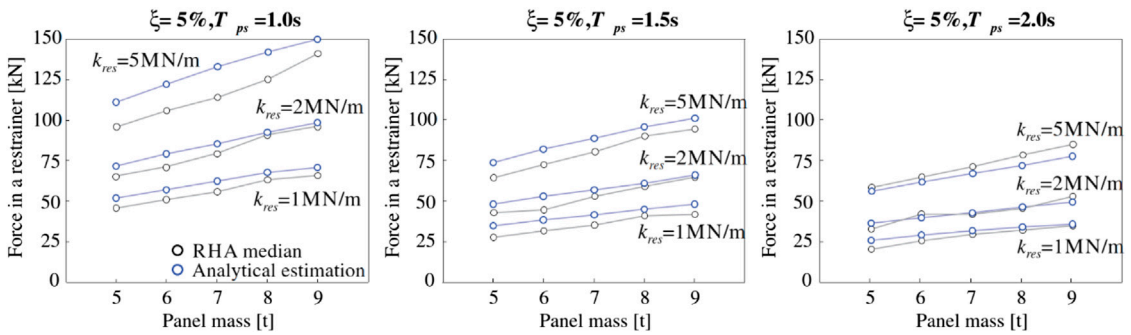

FIGURE 15 | The match between the maximal forces in a restrainer obtained by using the proposed analytical expression and the results of the response history analysis (RHA).

estimations calculated with the proposed formula are compared, the velocity v_{r0} is taken from the results of the performed numerical analysis. The acceleration a_s is simply evaluated from the Eurocode 8 (EN 1998-1:2004) response spectrum.

The results from response history analysis, presented in Zoubek et al. (2016b), were compared with the results obtained with the proposed analytical expressions. The comparison was made for varying panel masses, natural periods of the main structural system and restrainer stiffnesses. Since there are two restrainers per panel, 1/4 of the whole panel mass was taken as a corresponding mass m_p. The relative velocity v_{r0} was calculated as the product of the ratio $\dot{u}_{r,max}/\dot{u}_{s,max}$, obtained from the response history analysis and presented in Zoubek et al. (2016b) and the maximum velocity of the primary structure $\dot{u}_{s,max}$, estimated as the spectral velocity $S_v(T_{ps})$. $S_v(T_{ps})$ was calculated using the Eurocode 8 (EN 1998-1:2004) design spectrum:

$$S_v\left(T_{ps}\right) = S_a\left(T_{ps}\right)\frac{T_{ps}}{2\pi}, \tag{28}$$

where $S_a(T_{ps})$ is the spectral acceleration to the period T_{ps}.

The acceleration of the main structure a_s, was also calculated as the spectral acceleration $S_a(T_{ps})$ according to the EC8 (EN 1998-1:2004) design acceleration spectrum:

$$a_s = S_a\left(T_{ps}\right) \tag{29}$$

The match between the results obtained by using the proposed analytical formula (blue lines) and the numerically obtained results (black lines), as reported in Zoubek et al. (2016b), is illustrated in **Figure 15**. The graphs show relatively good agreement between the results, regardless of the period of vibration of the main structure T_{ps}, restrainer stiffness k_{res} or the panel mass.

CONCLUSION

In the last 2 decades, seismic response of RC precast buildings has been the subject of intense research, supported by European research programmes and precast producers. The University of Ljubljana contributed considerable experimental and analytical work. In this paper, only a few of the most important results and findings from the last few years are gathered and briefly presented. The main contributions include:

- Development of the new capacity model of beam-column dowel connections, which are one of the key parts of RC precast structural system. Most importantly, the new model explicitly considers the contribution of stirrups in the critical region around the dowel, where precast elements are typically reinforced by quite compact transverse reinforcement.
- The new insight into the cyclic behaviour of fastening systems of concrete cladding panels and new design procedures for the estimation of strength and displacement capacity of cladding fasteners. This knowledge represents a basis for the adequate design of the cladding fasteners, which can prevent the failure of concrete cladding panels and further prevent human casualties and enormous financial losses due to the terminated services.
- Development of a methodology for seismic fragility analysis of RC precast buildings, and the fragility curves of precast RC building classes, which can be used for performing seismic stress test of portfolio of RC precast buildings and for the safety-calibration of the new design procedures of RC precast buildings.
- Development of a relatively simple and economically attractive back-up (strengthening) system to prevent the falling of panels in case of a strong earthquake. The system is based on the use of a loose steel or synthetic fiber rope restrainer. In order to measure their resistance to shock loading, several tensile tests in varying configurations were performed. Furthermore, analytical formulae for the estimation of the seismic demand have been proposed.

AUTHOR CONTRIBUTIONS

All authors listed have made a substantial, direct, and intellectual contribution to the work and approved it for publication. Sections Beam-to-Column Dowel Connections, Typical Fastening Systems of Concrete Cladding Panels and Strengthening Interventions for Existing Precast Buildings with Cladding Panels are the work of authors BZ, TI, and MF. Section Fragility Analysis of Pre-Code RC Precast Buildings with the Consideration of Nonstructural Elements is the work of authors AB and MD.

FUNDING

The presented research was mainly supported by the two large EU projects: (a) SAFECAST project "Performance of Innovative Mechanical Connections in Precast Building Structures under Seismic Conditions" (Grant Agreement No. 218417-2), and (b) SAFECLADDING project – "Improved Fastening systems of Cladding Wall Panels of Precast Buildings in Seismic Zones" (Grant Agreement No. 314122), both in the Seventh Framework Programme (FP7) of the European Commission. Both projects were led by the associations of the precast producers in Europe and the Politecnico di Milano. The leading persons in this research were in particular Professor Giandomenico Toniolo and Dr. Antonella Colombo. The presented results are also based on the work conducted within the Earthquake Engineering research program (evidence number P2-0185), which is supported by the Slovenian Research Agency.

SUPPLEMENTARY MATERIAL

The Supplementary Material for this article can be found online at: https://www.frontiersin.org/articles/10.3389/fbuil.2021.630952/full#supplementary-material.

REFERENCES

ABAQUS. (2011). *ABAQUS Theory manual.* Dassault Systèmes.version 6.11-3.

ACI 318-08. (2008). *Building code requirements for structural concrete and commentary*. Farmington Hills, Michigan, USA: American Concrete Institute.

Babič, A., and Dolšek, M. (2016). Seismic fragility functions of industrial precast building classes. *Eng. Struct.* 118, 357–370.

Baker, J. W. (2015). Efficient analytical fragility function fitting using dynamic structural analysis. *Earthq. Spectra* 31 (1), 579–599. doi:10.1193/021113eqs025m

Belleri, A., Brunesi, E., Nascimbene, R., Pagani, M., and Riva, P. (2014). Seismic performance of precast industrial facilities following major earthquakes in the Italian territory. *J. Perform. Constr. Facil.* 29 (5), 04014135.

Belleri, A., Torquati, M., Marini, A., and Riva, P. (2016). Horizontal cladding panels: in-plane seismic performance in precast concrete buildings. *Bull. Earthq. Eng.* 14 (4), 1103–1129. doi:10.1007/s10518-015-9861-8

Belleri, A., Torquati, M., Riva, P., and Nascimbene, R. (2015). Vulnerability assessment and retrofit solutions of precast industrial structures. *Earthq. Struct.* 8 (3), 801–820. doi:10.12989/eas.2015.8.3.801

Bournas, D. A., Negro, P., and Taucer, F. F. (2013). Performance of industrial buildings during the Emilia earthquakes in Northern Italy and recommendations for their strengthening. *Bull. Earthq. Eng.* 12 (5), 2383–2404. doi:10.1007/s10518-013-9466-z

CALTRANS. (2008). *Memo to designers.* Sacramento, CA: California Department of Transportation.

Capozzi, V., Magliulo, G., and Manfredi, G. (2012). Nonlinear mechanical model of seismic behaviour of beam-column pin connections, in 15th world conference on earthquake engineering, Portugal, Lisbon, 24–28 Sept 2012.

Casotto, C., Silva, V., Crowley, H., Nascimbene, R., and Pinho, R. (2015). Seismic fragility of Italian RC precast industrial structures. *Eng. Struct.* 94, 122–136. doi:10.1016/j.engstruct.2015.02.034

CEN-TC250-SC8_N0966 (2020). *prEN 1998 -1-2:2020 Eurocode 8: design of structures for earthquake resistance Part 1-2: rules for new buildings*.

Cornell, C. A. (1996). "Calculating building seismic performance reliability: a basis for multi-level design norms", in *Proceedings of the 11th World conference on earthquake engineering (Acapulco)*.

DesRoches, R., Pfeifer, T., Leon, R. T., and Lam, T. (2003). Full-scale tests of seismic cable restrainer retrofits for simply supported bridges. *J. Bridge Eng.* 8 (4), 191–198. doi:10.1061/(asce)1084-0702(2003)8:4(191)

DOCUP. (2006). *Programma DOCUP Toscana 2000–2006. Misura 2.8.3: Riduzione del rischio sismico nelle aree produttive. Regione Toscana, Direzione Generale Politiche Territoriali, Ambientali e per la Mobilità Coordinamento Regionale Prevenzione Sismica: Report.* (In Italian).

Dolšek, M. (2010). Development of computing environment for the seismic performance assessment of reinforced concrete frames by using simplified nonlinear models. *Bull. Earthq. Eng.* 8 (6), 1309–1329. doi:10.1007/s10518-010-9184-8

EN 1998-1:2004. (2004). *Eurocode 8: design of structures for earthquake resistance – Part 1: general rules, seismic Actions and rules for buildings*. Brussels: European Committee for Standardization.

EN 1998-3:2005. (2005). *Eurocode 8: design of structures for earthquake resistance—Part 3: assessment and retrofitting of buildings*. Brussels: European Committee for Standardization.

Fajfar, P. (1984). *Dynamics of structurescivil engineering and geodesy*. Ljubljana, Slovenia: University of Edvard Kardelj in Ljubljana, Faculty of architecture.

Fischinger, M., Zoubek, B., and Isaković, T. (2014). "Seismic response of precast industrial buildings," in *Perspectives on European earthquake engineering and seismology*. Editor A. Ansal (Cham: Springer), 131–177.

Fuchs, W., Eligehausen, R., and Breen, J. E. (1995). Concrete capacity design (CCD) approach for fastening to concrete. *ACI Struct. J.* 92 (1), 73–94.

Hayashikawa, T., Julian, D. R., and Galindo, C. M. (2006). "Critical performance of unseating prevention cable restrainers under level II earthquakes", in *Proceedings of the Annual conference of Japan society for civil engineers (Kyoto)*.

Ioannou, I., Borg, R., Novelli, V., Melo, J., Alexander, D., Kongar, I., et al. (2012). *The 29th May 2012 Emilia Romagna Earthquake. EPICentre field observation report No. EPI-FO-290512*. College London, United Kingdom: Department of Civil, Environmental and Geomatic Engineering, University.

Isaković, T., Fischinger, M., Karadogan, F., Kremmyda, G. D., Dal Lago, B., Pegan, A., et al. (2012). *Catalogue on the existing cladding panel systems and connections in precast buildings with the identification of their possible seismic deficiencies, SAFECLADDING, Deliverable 1.1*. Brussels: European Commission.

Isaković, T., Zoubek, B., and Fischinger, M. (2015). "*Report and card files on the tests performed on existing connections – update*", in *SAFECLADDING, Deliverable, 1.3*. Ljubljana, Slovenia: University of Ljubljana.

Isaković, T., Zoubek, B., Lopatič, J., Urbas, M., and Fischinger, M. (2013). "*Report and card files on the tests performed on existing connections*". in *SAFECLADDING, Deliverable, 1.2*. Ljubljana, Slovenia: University of Ljubljana.

Liberatore, L., Sorrentino, L., Liberatore, D., and Decanini, L. D. (2013). Failure of industrial structures induced by the Emilia (Italy) 2012 earthquakes. *Eng. Fail. Anal.* 34, 629–647. doi:10.1016/j.engfailanal.2013.02.009

Magliulo, G., Capozzi, V., Fabbrocino, G., and Manfredi, G. (2011). Neoprene-concrete friction relationships for seismic assessment of existing precast buildings. *Eng. Struct.* 33 (2), 532–538. doi:10.1016/j.engstruct.2010.11.011

Magliulo, G., Ercolino, M., Petrone, C., Coppola, O., and Manfredi, G. (2014). The Emilia earthquake: seismic performance of precast reinforced concrete buildings. *Earthq. Spectra* 30 (2), 891–912. doi:10.1193/091012eqs285m

McKenna, F., and Fenves, G. L. (2010). *Open system for earthquake engineering simulation (OpenSees)*. Berkeley, USA: Pacific Earthquake Engineering Research Center. http://opensees.berkeley.edu. Accessed November 10, 2020).

NZS 3101. (2006). *Concrete structures standard. Part 1 – The design of concrete structures and Part 2 – commentary*. Wellington, New Zealand: Standards New Zealand.

Panagiotakos, T. B., and Fardis, M. N. (1996). "Seismic response of infilled RC frame structures", in *Proceedings of the 11th World conference on earthquake engineering (Acapulco)*.

Pitilakis, K., Argyroudis, S., Fotopoulou, S., Karafagka, S., Kakderi, K., Selva, J., et al. (2018). "A multi-level stress test methodology: application to six critical infrastructures in Europe", in *Proceedings of the 16th European conference on earthquake engineering (Thessaloniki)*.

Psycharis, I. N., and Mouzakis, H. P. (2012). Shear resistance of pinned connections of precast members to monotonic and cyclic loading. *Eng. Struct.* 41, 413–427. doi:10.1016/j.engstruct.2012.03.051

Randall, M., Saiidi, M., Maragakis, E., and Isaković, T. (1999). *Restrainer design procedures for multi-span simply-supported bridges. Technical report MCEER-99-001*. Reno: Civil Engineering Department, University of Nevada.

SAFECLADDING. (2015). Safecladding Project – improved fastening systems of cladding wall panels of precast buildings in seismic zones. www.safecladding.eu. Accessed January 15, 2016.

Saiidi, M., Randall, M., Maragakis, E., and Isakovic, T. (2001). Seismic restrainer design methods for simply supported bridges. *J. Bridge Eng.* 6, 307–315. doi:10.1061/(asce)1084-0702(2001)6:5(307)

Starešinič, G., Zoubek, B., Gams, M., Isaković, T., and Fischinger, M. (2020). Modelling in-plane dynamic response of a fastening system for horizontal concrete facade panels in RC precast buildings. *Eng. Struct.* 224, 111210.

Tanaka, Y., and Murakoshi, J. (2011). Reexamination of dowel behavior of steel bars embedded in concrete. *ACI Struct. J.* 108 (6), 659–668.

Vintzeleou, E. N., and Tassios, T. P. (1986). Mathematical model for dowel action under monotonic and cyclic conditions. *Mag. Concr. Res.* 38 (134), 13–22.

Zoubek, B., Fischinger, M., and Isaković, T. (2016a). Cyclic response of hammer-head strap cladding-to-structure connections used in RC precast building. *Eng. Struct.* 119, 135–148. doi:10.1016/j.engstruct.2016.04.002

Zoubek, B., Fischinger, M., and Isakovic, T. (2015). Estimation of the cyclic capacity of beam-to-column dowel connections in precast industrial buildings. *Bull. Earthq. Eng.* 13 (7), 2145–2168. doi:10.1007/s10518-014-9711-0

Zoubek, B., Fischinger, M., and Isakovic, T. (2016b). Seismic response of short restrainers used to protect cladding panels in RC precast buildings. *J. Vib. Control.* 24 (4), 645–658. doi:10.1177/1077546316659780

Zoubek, B., Isakovic, T., Fahjan, Y., and Fischinger, M. (2013). Cyclic failure analysis of the beam-to-column dowel connections in precast industrial buildings. *Eng. Struct.* 52, 179–191. doi:10.1016/j.engstruct.2013.02.028

Conflict of Interest: The authors declare that the research was conducted in the absence of any commercial or financial relationships that could be construed as a potential conflict of interest.

frontiers in Built Environment

ORIGINAL RESEARCH
published: 06 April 2021
doi: 10.3389/fbuil.2021.638509

Unbonded Post-tensioned Precast Concrete Walls With Rocking Connections: Modeling Approaches and Impact Damping

Dimitrios Kalliontzis[1] *and Maryam Nazari*[2]*

[1]Department of Civil and Environmental Engineering, University of Houston, Houston, TX, United States, [2]Department of Civil Engineering, California State University, Los Angeles, CA, United States

Over the past two decades, precast concrete members have been utilized in seismically resilient structures. In developing these structures, different techniques have been used for connecting the precast members to the foundation. In building construction, unbonded post-tensioning (PT) tendons can anchor a precast wall to the foundation, resulting in the so-called rocking wall system. The rocking wall system develops a dry connection with the foundation and provides moment resistance by means of the PT tendons. The PT tendons remain elastic when the wall is subjected to design-level ground motions to preserve the re-centering capability of the wall. Moreover, the structural damage is concentrated near the wall toes and can be minimized with proper detailing of the toes. Rocking wall systems can consist of a Single precast Rocking Wall (SRW), which uses no supplemental damping, or walls with supplemental damping in the form of viscous or hysteretic energy dissipating devices. In addition to the supplemental damping, rocking walls dissipate the seismic energy through their impacts on the foundation base, their inherent viscous damping, and the hysteresis of concrete near the wall base. While the investigation of rocking walls continues to gain interest, there is no widely accepted means of modeling their dynamic behavior. This paper investigates two popular approaches for modeling rocking walls with and without supplemental damping: the finite element method and analytical modeling. The ability of the two approaches to capture the local and global responses of the walls is evaluated against shake table tests of walls with multiple-level intensity base motions. Next, the behavior characteristics of the two modeling approaches and their ability to simulate impact damping are discussed.

Keywords: rocking wall, analytical modeling, finite element method, impact damping, precast concrete

OPEN ACCESS

Edited by:
Andrea Belleri, University of Bergamo, Italy

Reviewed by:
Roberto Nascimbene, Fondazione Eucentre, Italy
Ekkachai Yooprasertchai, King Mongkut's University of Technology Thonburi, Thailand

***Correspondence:**
Maryam Nazari
mnazar12@calstatela.edu

Specialty section:
This article was submitted to Earthquake Engineering, a section of the journal Frontiers in Built Environment

Received: *06 December 2020*
Accepted: *11 February 2021*
Published: *06 April 2021*

Citation:
Kalliontzis D and Nazari M (2021) Unbonded Post-tensioned Precast Concrete Walls With Rocking Connections: Modeling Approaches and Impact Damping. Front. Built Environ. 7:638509. doi: 10.3389/fbuil.2021.638509

BACKGROUND

Unbonded Post-tensioned Precast Concrete Walls

Figure 1A shows an unbonded post-tensioned precast concrete wall with a rocking connection to the foundation base, named as the Single Rocking Wall (SRW). Under seismic lateral loads, the bottom corner of the SRW uplifts as the wall experiences a rocking motion. Seismic shear forces are transferred from the wall to the foundation through friction and the post-tensioning (PT) force enhances re-centering of the wall, following a seismic excitation.

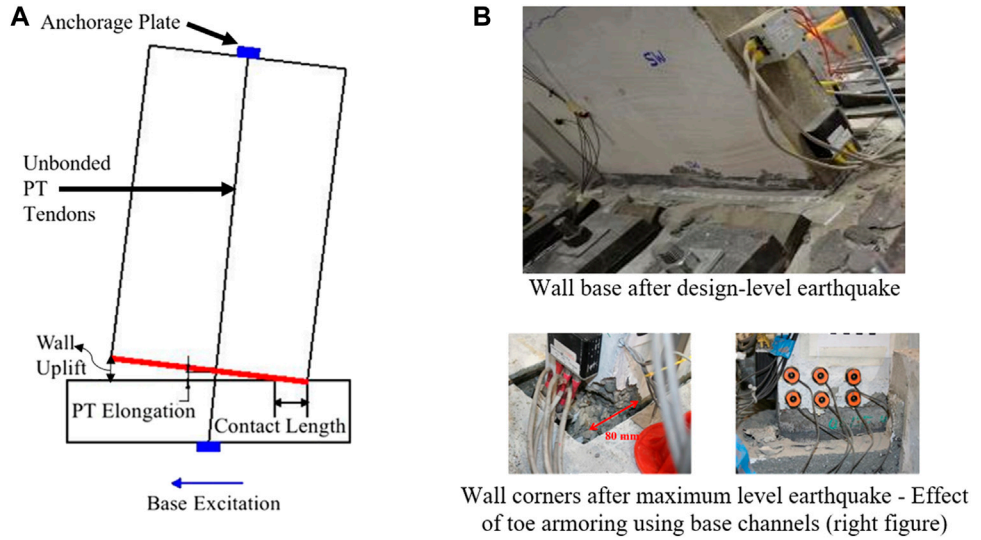

FIGURE 1 | Single rocking wall (SRW) (Nazari et al., 2017): **(A)** System setup; **(B)** Damage status after earthquakes.

During the rocking motion, the PT tendons remain elastic and damage of the wall due to concrete nonlinearity is limited to the bottom toes of the wall, as shown in **Figure 1B** (Kurama et al., 1999; Perez et al., 2004; Twigden, 2016; Nazari et al., 2017; Kalliontzis and Sritharan, 2020). Due to the limited hysteretic action in SRWs, these walls have been viewed as inadequate to efficiently dissipate the absorbed seismic energy. This observation has been formalized in ACI ITG-5.1 (2008) and, subsequently, in ACI 550.6 (2019) which require a minimum energy dissipation ratio as part of the acceptance criteria for precast concrete rocking walls. This ratio is defined as the area enclosed by the hysteresis loop in the force-displacement curve for a cycle over the area of the circumscribing parallelogram. This ratio shall not be less than 12.5%, which exceeds the ratio provided by SRWs. More recently, a performance-based design approach for precast concrete rocking walls has also been presented by Mpampatsikos et al. (2020).

To improve the hysteretic damping of SRWs, different wall systems have been developed utilizing supplemental damping devices. For example, Priestley et al. (1999) developed the jointed wall system where two or more precast concrete walls are connected horizontally with special stainless U-shaped Flexural Plates (UFPs). Though adequate hysteretic damping can be provided through the UFPs, the jointed wall system has not found its way to practice because it provides reduced moment capacity compared to monolithic reinforced concrete walls and the fabrication of UFPs is uneconomical. Restrepo and Rahman (2000) investigated a different concept where partially de-bonded mild steel bars cross the rocking connection of the walls to dissipate the absorbed seismic energy through axial yielding of the bars. This system, named as the hybrid wall system, can provide improved moment capacity and adequate hysteretic energy dissipation. One disadvantage of the hybrid wall system is the inability to inspect and, if needed, replace the mild steel bars in the aftermath of a seismic event. To facilitate replaceability of the supplemental damping devices, Marriott et al. (2008) investigated the use of external energy dissipators across the rocking connection. More recently, Sritharan et al. (2015) developed the PreWEC (PREcast Wall with End Columns) system where replaceable and cost-effective Oval-shaped connectors, namely O-connectors, are utilized. The O-connectors join the wall horizontally with two end or side columns, as shown in **Figures 2A,B**, respectively. Under seismic lateral loads, the O-connectors undergo inelastic deformations through vertical relative movements of the connector legs, providing hysteretic damping to the PreWEC. As shown experimentally by Sritharan et al. (2015), the O-connectors can be designed to produce different levels of hysteretic damping for the PreWEC and moment capacity that is comparable to monolithic reinforced concrete walls.

Damping Behavior

In the above-referenced studies, the lateral behavior of the walls was characterized through quasi-static testing, which inhibited the energy dissipation produced by viscous damping and wall impacts on the foundation. Though dynamic tests were also performed (e.g., Marriott et al., 2008), the individual contribution of different damping mechanisms was not assessed.

More recently, research studies used free vibration and shake table tests of walls to investigate the dynamic sources of energy dissipation. In Kalliontzis et al. (2016), Nazari et al. (2017), and Nazari and Sritharan (2020), appropriate test conditions were established by excluding the supplemental damping devices. Using shake table tests of four SRWs, Nazari et al. (2017) and Nazari and Sritharan (2020) quantified an average value of 1.5% equivalent damping ratio due to wall impacts and 4.2% due to hysteretic action and inherent viscous damping combined, which was based on lateral drift responses in the range of 1.4–2.6%. A different approach of quantifying impact damping experimentally was followed by Kalliontzis et al. (2016) utilizing the coefficient of restitution model proposed by

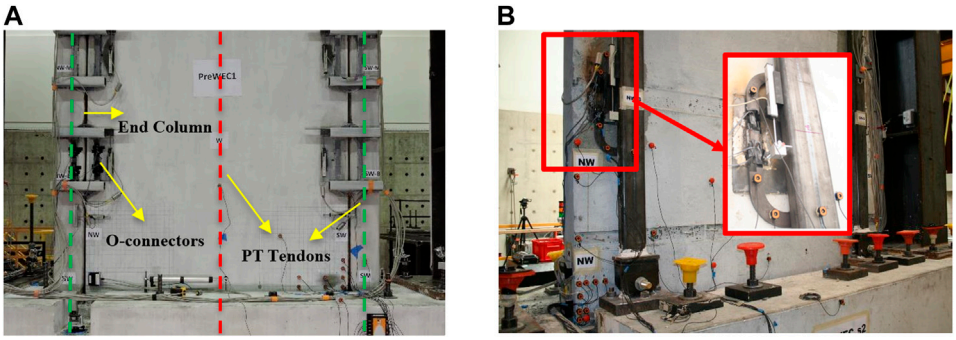

FIGURE 2 | PreWEC (PREcast wall with end columns) system: **(A)** Connectors at the ends of the wall panel; **(B)** Connectors on the sides of the wall panel.

Housner (1963). Kalliontzis et al. (2016) tested three precast concrete members in free vibration, which included one SRW, and recorded the kinetic energy losses of the three members during the impacts. Using the experimental measurements, a generalized formula was developed for the coefficient of restitution, r. The generalized formula, r_g, is an improved version of the formula proposed by Housner (1963) for free-standing rigid blocks:

$$r_g = \left[\frac{1 + \frac{MR_{cm}^2}{I_{cm}} \times \left(1 - (\sin\alpha)^2 \times (1 + k^2)\right)}{1 + \frac{MR_{cm}^2}{I_{cm}} \times \left(1 - (\sin\alpha)^2 \times (1 - k^2)\right)}\right], \quad (1)$$

where $\alpha = \tan^{-1} L_w/(2H_{CG})$ with L_w and H_{CG} being the wall base length and height measured from the foundation base to the center of gravity of the wall, respectively; M is the total mass of the wall; I_{cm} is the mass moment of inertia of the wall about its center of gravity; R_{cm} is the distance of the center of gravity from the bottom corner of the wall; and $k = 0.72$. Later, the accuracy of **Eq. 1** was confirmed experimentally for precast concrete members with and without unbonded post-tensioning (Kalliontzis et al., 2020; Kalliontzis and Sritharan, 2020).

However, **Eq. 1** may be impractical for use in design procedures, where the expression of impact damping in terms of an equivalent viscous damping ratio, ζ, is preferred. For SRWs, Kalliontzis and Sritharan (2021) proposed that r_g can be correlated to ζ as follows:

$$\zeta_{impact} = -0.15 \times ln(r_g), \quad (2)$$

Nazari and Sritharan (2018) observed experimentally that the impact damping may be less significant in walls with supplemental damping devices, such as the PreWECs. They indicated that only 1.14% of the 16.3% total ζ in PreWECs is provided by impact, which is significantly smaller than the relative contribution of impact in SRWs. Nazari and Sritharan (2018) and Nazari and Sritharan (2019) developed a simplified equation to estimate the ζ provided by the O-connectors in PreWECs:

$$\zeta_{conn.D\%} = \frac{N_{conn.} \times F_{c,ave} \times \left(l_{con} - \frac{\Delta_{c,y}}{D\%}\right)}{\pi \times V_{D\%} \times H_{seismic}}, \quad (3)$$

where $N_{conn.}$ is the total number of connectors; $V_{D\%} \times H_{seismic}$ is the moment resistance of the PreWEC at the drift ratio $D\%$, $V_{D\%}$ is the seismic base shear and $H_{seismic}$ is the effective height of $V_{D\%}$; $F_{c,ave}$ is the average of the connector yield strength and the connector force at $D\%$; $\Delta_{c,y}$ is the yield displacement of connectors; and l_{con} is the distance to the center of the connector leg attached to the uplifting end of the wall panel measured from the neutral axis of the wall base.

Modeling Approaches

Following the experimental observations, researchers attempted to reproduce the behaviors of the different wall systems using modeling approaches. One approach was the use of existing finite element platforms with frame element models in the form of distributed or lumped plasticity models or with three-dimensional models (e.g., Marriott et al., 2008; Henry 2011; Belleri et al., 2013; Kalliontzis and Sritharan, 2014; Twigden 2016; Nazari et al., 2017; Kalliontzis and Sritharan, 2018; Nazari and Sritharan, 2018). In the existing finite element platforms, all damping components (e.g., hysteretic, inherent viscous, and impact damping) were lumped into single or multiple continuous energy dissipating elements, with the damping terms being tailored based on the experimental data of individual walls. Moreover, energy loss due to impact was implemented with continuous damping, which neglected that impacts are short-time events, as shown experimentally by Kalliontzis et al. (2016) and Nazari et al. (2017). Some of these models showed good accuracy for lateral drift responses of walls up to 4–5% (Nazari et al., 2017; Nazari and Sritharan 2018).

To improve modeling of impact damping in the finite element method, researchers utilized the numerical damping generated by the Hilber-Hughes-Taylor (HHT) time-integration scheme, which was shown to dissipate seismic energy in short-time intervals, thus closely simulating the impact damping (Vassiliou et al., 2016; Aghagholizadeh, 2020). Outside existing finite element platforms, frame elements have been developed with methodologies to incorporate instantaneous or short-time impact energy loss (Diamantopoulos and Fragiadakis, 2019; Avgenakis and Psycharis, 2020). Although, these latter studies were validated with analytical models of free-standing rigid

blocks, their accuracy with respect to experiment data of precast concrete walls with or without supplemental damping devices was not examined.

Kalliontzis and Sritharan (2020) and Kalliontzis et al. (2020) enhanced the capabilities of the simple analytical model proposed by Housner (1963) to simulate the seismic behavior of rocking walls. In Kalliontzis et al. (2020), a dynamic analysis approach was developed for SRWs to represent the different damping components individually, which included an event-based approach for capturing impact damping. The proposed dynamic analysis approach is generalized, in that it is independent of a specific wall problem, so that it can be applied to various wall geometries, designs, and materials. It is computationally efficient and has been verified with experiments of precast concrete as well as masonry SRWs. Until this research study, the generalized dynamic analysis approach (GDAA) has not been investigated with respect to walls with supplemental damping devices (e.g., PreWEC).

RESEARCH SIGNIFICANCE

This paper is an effort to understand and compare the accuracy of the finite element and analytical models for simulating unbonded post-tensioned precast concrete walls with and without supplemental damping. For this purpose, the finite element model (FEM) developed by Nazari et al. (2017) and the generalized dynamic analysis approach (GDAA) by Kalliontzis et al. (2020) are compared against shake table tests of walls without (i.e., SRWs) and with supplemental damping (i.e., PreWECs). To enable these comparisons, the GDAA is enhanced with the capability to model the supplemental damping in the PreWECs and the lateral inertia effects induced by floor systems. For this purpose, a constitutive model for the O-connectors is also developed. Next, the behavior characteristics of the two modeling approaches and their ability to simulate impact damping are discussed.

REVIEW OF SHAKE TABLE TESTS OF ROCKING WALLS

A total of eight unbonded post-tensioned precast concrete walls were tested using the National Earthquake Engineering Simulation (NEES) shake table facility at the University of Nevada, Reno by Nazari et al. (2015). The walls were designed as part of the lateral load resisting system of a 6-story office building located in Los Angeles, CA, which is considered as a high seismic region per ASCE 7-16 (2016). These walls were scaled by a factor of 5/18 with respect to the original wall sizes in the 6-story office building. The different test units, including four SRWs and four PreWECs, were designed with variation in the initial post-tensioning stress, the external energy dissipation capacity, and the base moment-to-shear ratio.

From the above-referenced database, the shake table test results of one SRW, namely SRW2, and one PreWEC, namely PreWEC-2, were used in the present research study to compare with the FEM and the GDAA. The SRW2 and PreWEC-2 had an average shear resistance near 175 kN. The key design variables of the SRW2 and the PreWEC-2 are noted in **Table 1**. **Figure 3** shows the fabrication and design details of the wall panels.

Figure 4 shows the experimental test setup for the two walls. The two walls were placed on a uniaxial shake table and were connected to an external mass-rig system, which was placed adjacent to the table and was horizontally aligned with the walls. The mass-rig system was connected to the walls through a pin-ended rigid beam, simulating the transfer of horizontal inertia forces from the floor systems of the 6-story office building to the walls. The horizontal inertia forces by the mass-rig system corresponded to an effective weight of 267 kN and were transferred to the wall at an effective height ($H_{seismic}$) of 4.27 m, which were computed based on a single degree of freedom model of the building, developed following the recommendations by Priestley et al. (2007).

The seismic performance of the SRWs and PreWECs was evaluated by exciting the shake table into a series of ground motions with different levels of intensities. The present study employed the following two shake table excitations:

(1) A short duration motion, namely **Eq. 4**s, which is a spectrum-compatible motion representing the strong portion of the 1994 Northridge earthquake-Sylmar station, with the Peak Ground Acceleration (PGA) of 0.71 g.
(2) A long duration motion, which corresponds to the earthquake record at the 1995 Kobe-Takatori station, with the PGA of 0.62 g.

The amplitudes of these records were scaled by a factor of 2.88 and 3.6, respectively, to meet the design basis (EQ-III) and maximum considered (EQ-IV) earthquake events for the scaled walls. The time step of the ground motion records was decreased by a factor of 5/18 to meet the scale. More information about the scaling procedure, the acceleration response spectra of the scaled ground motions, and the recorded shake table motions are presented in Nazari et al. (2015) and Nazari et al. (2017).

DESCRIPTION OF THE MODELS

Two approaches were employed for modeling the experimental responses of the SRW2 and PreWEC-2. The first approach is a Finite Element Model (FEM) that was developed using OpenSees (McKenna et al., 2000). The FEM is a lumped-plasticity model, which uses a nonlinear rotational spring at the wall base to simulate the moment vs. rotation behavior of the wall base section. This model has the capability of capturing the global behavior of different rocking wall systems, which is key for use in performance-based seismic analysis. In this model, the energy dissipation of the rocking wall systems due to impact is represented by an equivalent viscous damping ratio, which was derived based on the experimental study reported in Nazari et al. (2017) and Nazari and Sritharan (2018). The supplemental damping by

TABLE 1 | Summary of design variables for SRW2 and PreWEC-2.

Wall ID	Post-tensioning parameters			Total number of O- connectors, damping ratio at design drift (%)	Shear resistance at 2% drift (kN)[a] design/measured
	No., dia.(mm) of PT tendon	Initial PT stress (MPa), force (kN)			
		Design	Measured		
SRW2	6, 12.7	0.64 f_{pu}[b], 702	0.5 f_{pu}, 547	N/A	206/187
PreWEC-2	3, 15.2	0.56 f_{pu}, 440	0.53 f_{pu}, 418	8, 15.3%	182/183

[a]*Following the SA method (Aaleti and Sritharan 2009); using design/measured parameters.*
[b]f_{pu} *= tensile strength of tendon = 1862 MPa.*

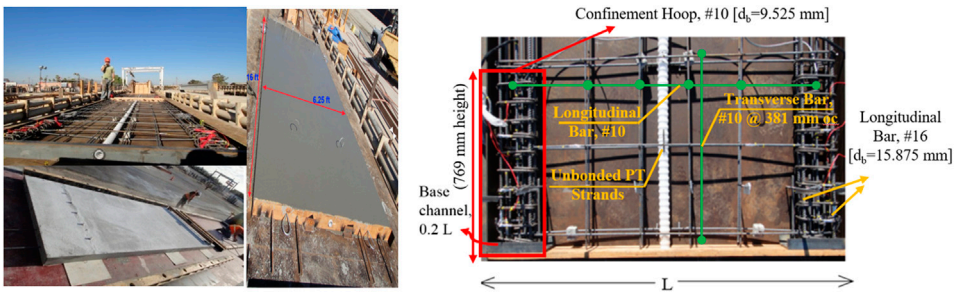

FIGURE 3 | Fabrication and design details of the wall panels.

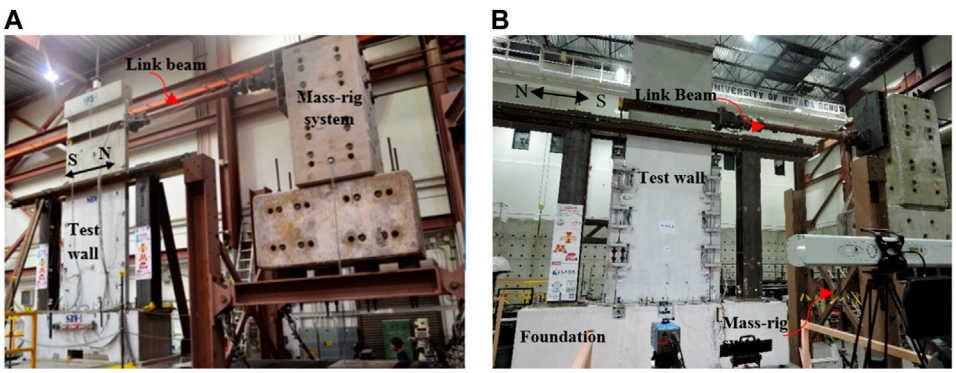

FIGURE 4 | Shake table test setups at UNR: **(A)** SRW; **(B)** PreWEC (Nazari and Sritharan, 2020).

the O-connectors is modeled with a lumped-plasticity element at the wall-to-foundation interface.

The second approach is an analytical model, named in this research study as the Generalized Dynamic Analysis Approach (GDAA). This model was developed by Kalliontzis et al. (2020) with the capability of capturing both the global and local (i.e., contact length at the rocking connection and post-tensioning forces) behaviors of SRWs. The GDAA is extended in this research study for modeling the PreWECs and the lateral inertia effects induced by floor systems.

Finite Element Method

The Finite Element Model (FEM) was developed to simulate the lateral seismic responses of SRWs and PreWECs for the purpose of performance-based analysis up to lateral drift ratios of 4–5%, within which the walls experience little damage at their bottom toes and the material nonlinearity in the PT tendons is limited. A schematic view of the FEM as developed in OpenSees (OS) is presented in **Figure 5**. The FEM is composed of a linear elastic beam-column element representing the concrete wall. As shown in **Figure 5**, a seismic mass was assigned to the top node of the beam-column element to simulate the horizontal inertial load provided by the mass-rig system in the experiments. The bottom node of the element was connected to the foundation base through one and two rotational springs for the SRW2 and the PreWEC-2, respectively. For the SRW, a single spring was used to simulate the re-centering and moment vs. rotation behavior of the wall base with the uniaxial SelfCentering material in OS. The key properties of the SelfCentering material were selected to match

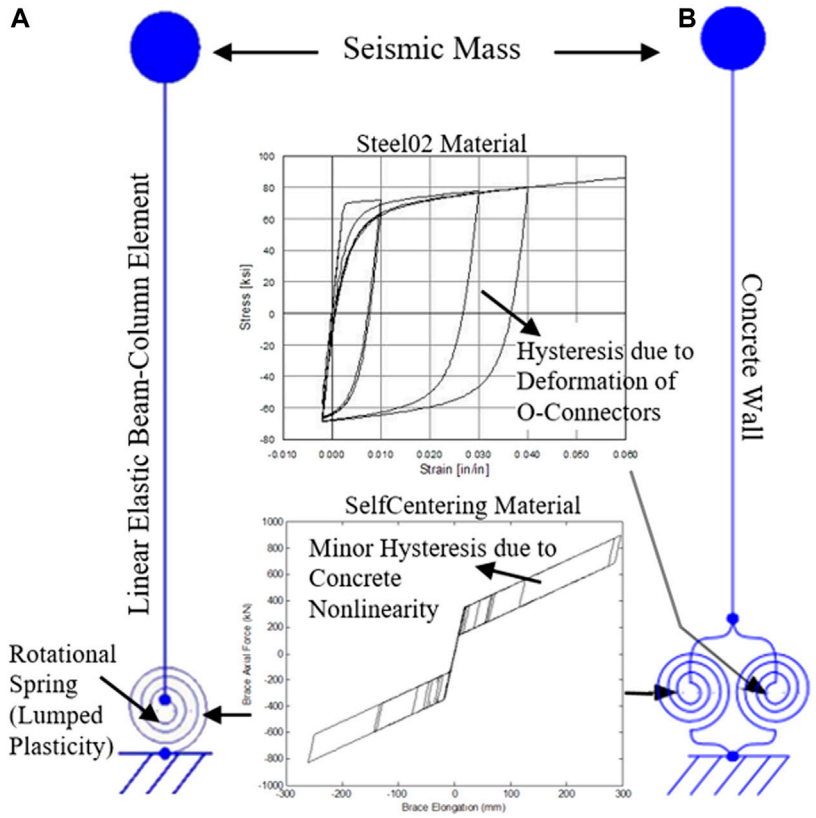

FIGURE 5 | Finite element model (FEM): **(A)** SRW; **(B)** PreWEC.

the back-bone moment-rotation curve of the wall base as defined by the Simplified Analysis method of Aaleti and Sritharan (2009). The area enclosed by the hysteretic curve of the SelfCentering material is controlled by a beta factor, which represents the hysteretic energy dissipation of the system due to concrete nonlinearity as a ratio of the yield force. A beta factor of 0.2 and 0.3 was respectively suggested to model the walls with relatively no damage and higher damage in the toe regions (Nazari et al., 2017). In this study, both SRW2 and PreWEC-2 were modeled using a beta factor of 0.2. As shown in **Figure 5B**, an additional rotational spring was used for the PreWEC-2 to simulate the O-connectors with the OS Steel02 material model. The yield and ultimate strengths of the OS Steel02 material model corresponded to the respective yield and ultimate moment resistances provided by the O-connectors in the PreWEC-2.

In addition to the hysteretic damping in the moment-rotation curve of the wall base and the O-connectors, a tangent stiffness proportional Rayleigh damping was included to simulate the impact energy dissipation. The assigned damping values were 3 and 2%, respectively for the SRW2 and the PreWEC-2, which were derived based on the experimental data as follows: average equivalent damping ratios of 1.5 and 1.0% were calculated experimentally for the SRW2 (Nazari et al., 2017) and the PreWEC-2 (Nazari and Sritharan, 2018), respectively, using the Jacobson's secant stiffness approach (Priestley, 2002). Next, these values were multiplied by a modification factor of 2 to represent the tangent stiffness-based damping as defined by Priestley et al. (2007).

Analytical Modeling

The GDAA was developed to simulate the seismic behavior of SRWs. Three damping components are included in the GDAA: 1) inherent viscous damping of the SRWs; 2) hysteretic damping due to damage of the wall toes and yielding of the unbonded post-tensioning steel; and 3) impact damping, which is implemented with an event-based approach. The GDAA simulates the rocking response of SRWs with respect to the foundation base and first-mode flexural response of the wall body. For the purpose of this paper, the flexural response is eliminated from the formulation of GDAA, because it is small in unbonded post-tensioned precast concrete walls (Nazari et al., 2017; Nazari and Sritharan, 2018; Kalliontzis et al., 2020; Kalliontzis and Sritharan, 2020).

Figure 6A presents an SRW as modeled by the GDAA, excluding flexure of the wall body. The wall has a height of H_w, a base length of L_w, and a wall thickness of t_w. It is post-tensioned with unbonded tendons that are placed at a distance η_{pT} from the wall centerline. It is assumed that a top mass is attached at the wall top with a height of H_s, length of L_s, and thickness t_s. The top mass simulates the load stub commonly used in test configurations of SRWs but can be neglected otherwise.

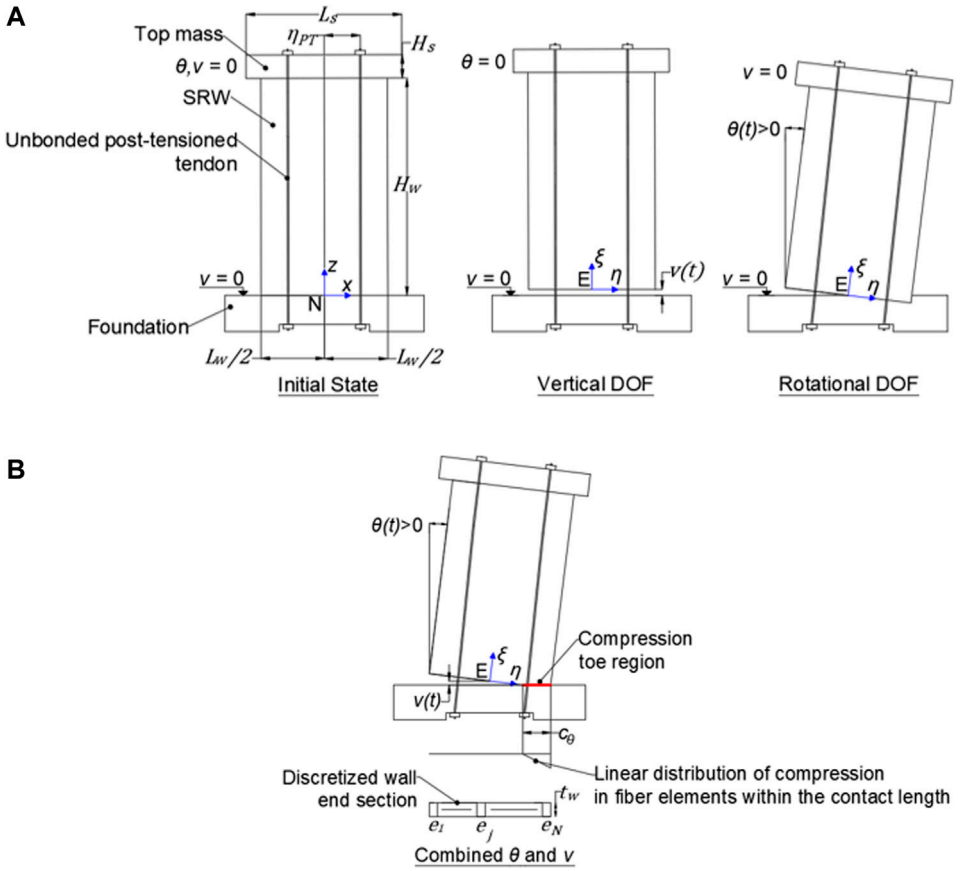

FIGURE 6 | (A) A single rocking wall (SRW) modeled by the generalized dynamic analysis approach (GDAA); **(B)** Combined rotational θ and vertical v motions of a SRW as per the GDAA.

The SRW is restrained against torsional and out-of-plane deformations, while the friction mechanism at the rocking connection prevents horizontal sliding of the SRW. Shear responses are neglected because they are insignificant in SRWs. The foundation is assumed to be a capacity-protected member. Hence all inelastic deformations are concentrated at the base of the SRW.

The dynamic motion of the SRW is calculated with respect to the inertia frame $N\{x, z\}$ that originates at the middle of the foundation top surface, as shown in **Figure 6A**. A moving frame $E\{\xi, \eta\}$ rotates and translates with the midpoint of the bottom face of the wall. The dynamic motion of the SRW is described with two degrees of freedom, excluding flexure of the wall body: 1) θ which describes the rotation of the SRW with respect to the inertia frame $N\{x, z\}$; and 2) v which describes the vertical motion of point E, and is measured with respect to $N\{x, z\}$. In the GDAA, the horizontal translation of the midpoint of the wall base is neglected, which is a reasonable approximation for modeling SRWs to a range of lateral drifts ratios up to 10%.

To capture the compressive deformations of the wall base, the base section is discretized into N number of fibers, as shown in **Figure 6B**. The fibers that are located within the contact length c_θ at an instant of the dynamic motion are subjected to a linear distribution of compressive deformations, while the fibers outside the contact length are subjected to zero deformation, except for the residual deformation induced in the preceding wall response cycles.

Equation of Motion

The equation of motion of the GDAA for SRWs was developed by Kalliontzis et al. (2020) using the extended Hamilton's principle (Baruh 1999):

$$\delta \int (K - V + W)dt = 0, \tag{4}$$

where δ is the variation operator; K is the kinetic energy of the SRW; V is the potential energy of the SRW; and W is the total work produced by the unbonded tendons, the fibers of the wall base section, and the inherent viscous damping forces.

Excluding flexure of the wall body, the equation of motion of the GDAA becomes

$$\begin{bmatrix} -I_5 & I_9 \sin\theta \\ I_9 \sin\theta & -(M+M_s) \end{bmatrix} \begin{pmatrix} \ddot{\theta} \\ \ddot{v} \end{pmatrix} + \begin{pmatrix} 0 \\ (I_9 \cos\theta)\dot{\theta}^2 \end{pmatrix} + \begin{pmatrix} I_9 \sin\theta \\ -(M+M_s) \end{pmatrix} g + \begin{pmatrix} -\sum_{j=1}^{N} C_j \eta_{C_j} \cos\theta - \sum_{i=1}^{N_{PT}} \frac{F_{PT_i}}{\cos^2\theta}\left(v\sin\theta - \eta_{PT_i}\right) \\ \sum_{j=1}^{N} C_j - \sum_{i=1}^{N_{PT}} \frac{F_{PT_i}}{\cos\theta} \end{pmatrix} + \begin{pmatrix} \sum_{j=1}^{N} -c_{ri}\left(-\dot{v} + \dot{\theta}\eta_{C_j}\cos\theta\right)\eta_{C_j}\cos\theta \\ \sum_{j=1}^{N} c_{ri}\left(-\dot{v} + \dot{\theta}\eta_{C_j}\cos\theta\right) \end{pmatrix} = \begin{pmatrix} I_9 \cos\theta \\ 0 \end{pmatrix} \ddot{u}_{gx}, \quad (5)$$

In **Eq. 5**, $\dot{\theta}$ and $\ddot{\theta}$ are the rotational velocity and acceleration of the SRW, respectively; $\dot{v}$ and $\ddot{v}$ are the vertical velocity and acceleration of point E in **Figure 6A**; the parameters I_5 and I_9 represent constants of integration over the total mass of the SRW, respectively, and are defined in the Appendix of this paper; M and M_s are the masses of the SRW and top mass, respectively, as shown in **Figure 6A**; g is the acceleration of gravity; $\ddot{u}_{gx}$ is the horizontal ground acceleration; N is the number of fibers in the wall base section; and N_{PT} is the number of PT tendons in the SRW.

Moreover, C_j is the compressive force of the jth fiber, which is computed as $C_j = f_{c,j} \times dx_j \times t_j$, where $f_{c,j}$, dx_j, and t_j denote the fiber's compressive stress, length, and thickness, respectively. The value of $f_{c,j}$ is calculated with the constitutive model for the concrete fibers that is described in the following section. F_{PT_i} is the tensile force of the ith PT tendon, which is computed as $F_{PT_i} = f_{s,i} \times A_{s,i}$, where $f_{s,i}$ and $A_{s,i}$ are the tensile stress and area of the tendon, respectively. The value of $f_{s,i}$ is obtained with the constitutive model for the PT tendons that is described in the following section. The parameters η_{C_j} and η_{PT_i} denote the distances of the fibers and PT tendons, respectively, from the z-axis of the inertia frame $N\{x, z\}$ as shown in **Figure 6A**. The parameter c_{ri} is the material damping coefficient in a fiber of the wall base section of precast concrete SRWs as defined by Kalliontzis et al. (2020).

The GDAA formula of **Eq. 5** is enhanced in this paper to account for 1) the horizontal seismic mass provided by the mass-rig system at the effective height of $H_{seismic}$ = 14 ft, as shown in the test setup of **Figure 4**; and 2) the contribution by the O-connectors. The horizontal coordinate of the seismic mass with respect to the inertia frame $N\{x, z\}$ is computed as

$$x_{seismic} = L_{seismic} + H_{seismic} \sin\theta, \quad (6)$$

where $L_{seismic}$ is the horizontal distance from the centerline of the wall to the center of gravity of the seismic mass (i.e., mass-rig system) in the test setup of **Figure 4**. Using **Eq. 6**, the horizontal velocity of the seismic mass becomes

$$\dot{x}_{seismic} = \dot{\theta}(H_{seismic} \cos\theta), \quad (7)$$

The kinetic energy of the seismic mass, $K_{seismic}$, can be computed as

$$K_{seismic} = \frac{1}{2} M_{seismic} \dot{x}^2_{seismic}, \quad (8)$$

where $M_{seismic}$ is the seismic mass induced by the mass-rig system. The time integral of the variation in $K_{seismic}$ is computed as

$$\int \delta K_{seismic} dt = \int M_{seismic} H^2_{seismic} \left[-\ddot{\theta}(\cos\theta)^2 + \dot{\theta}^2 \left(\frac{\sin 2\theta}{2} \right) \right] \delta\theta dt, \quad (9)$$

The seismic mass contributes to the potential energy due to the horizontal ground excitation, $V_{\ddot{u}_{gx},seismic}$, with

$$\int \left[-\delta V_{\ddot{u}_{gx},seismic} \right] dt = \int \left[-(M_{seismic} H_{seismic} \cos\theta) \ddot{u}_{gx} \right] \delta\theta dt, \quad (10)$$

The variation of the work produced by the O-connectors, W_0, is computed as

$$\delta W_0 = -\sum_{i=1}^{N_0} F_{0,i} \delta\Delta_{0,i}, \quad (11)$$

where N_0 is the total number of O-connectors in the PreWEC; $F_{0,i}$ is the force developed in the ith O-connector; and $\Delta_{0,i}$ is the deformation of the ith O-connector produced by the relative vertical displacement of the connector legs. The value of $F_{0,i}$ is determined with the constitutive model described in the next section. The deformation $\Delta_{0,i}$ is taken as equal to the vertical displacement of the wall panel at the location of the ith O-connector, neglecting the vertical movement of the end columns and the relative horizontal movement between wall and columns:

$$\Delta_{o,i} = v - \eta_{o,i} \sin\theta + \xi_{o,i}(\cos\theta - 1), \quad (12)$$

where $\eta_{o,i}$ and $\xi_{o,i}$ are the coordinates of the ith O-connector with respect to the $E\{\xi, \eta\}$ frame defined in **Figure 6A**. The time integral of the variation of W_0 is computed as

$$\int \delta W_o dt = \int \begin{bmatrix} \delta\theta & \delta v \end{bmatrix} \begin{bmatrix} \sum_{i=1}^{N_o} F_{o,i}\left(\eta_{o,i}\cos\theta + \xi_{o,i}\sin\theta\right) \\ -\sum_{i=1}^{N_o} F_{o,i} \end{bmatrix} dt, \quad (13)$$

Using **Eqs 9**, **10**, **13**, **Eq. 5** is modified to include the effects of the horizontal seismic mass and the O-connectors:

$$\begin{bmatrix} -I_5 - M_{seismic}H_{seismic}^2\cos^2\theta & I_9\sin\theta \\ I_9\sin\theta & -(M+M_s) \end{bmatrix}\begin{pmatrix} \ddot{\theta} \\ \ddot{v} \end{pmatrix}$$

$$+\begin{pmatrix} M_{seismic}H_{seismic}^2\left(\frac{\sin 2\theta}{2}\right)\dot{\theta}^2 \\ (I_9\cos\theta)\dot{\theta}^2 \end{pmatrix}+\begin{pmatrix} I_9\sin\theta \\ -(M+M_s) \end{pmatrix}g$$

$$+\begin{pmatrix} -\sum_{i=1}^{N}C_j\eta_{Cj}\cos\theta-\sum_{i=1}^{N_{PT}}\frac{F_{PT_i}}{\cos^2\theta}\left(v\sin\theta-\eta_{PT_i}\right)+\sum_{i=1}^{N_o}F_{o,i}\left(\eta_{o,i}\cos\theta+\xi_{o,i}\sin\theta\right) \\ \sum_{j=1}^{N}C_j-\sum_{i=1}^{N_{PT}}\frac{F_{PT_i}}{\cos\theta}-\sum_{i=1}^{N_o}F_{o,i} \end{pmatrix}$$

$$+\begin{pmatrix} \sum_{j=1}^{N}-C_{ri}\left(-\dot{v}+\dot{\theta}\eta_{Cj}\cos\theta\right)\eta_{Cj}\cos\theta \\ \sum_{j=1}^{N}C_{ri}\left(-\dot{v}+\dot{\theta}\eta_{Cj}\cos\theta\right) \end{pmatrix}=\begin{pmatrix} (I_9+M_{seismic}H_{seismic})\cos\theta \\ 0 \end{pmatrix}\ddot{u}_{gx}, \quad (14)$$

Using **Eq. 14**, the seismic behavior of the SRW2 and PreWEC-2 was computed in this investigation. The contribution of O-connectors is eliminated from **Eq. 14** (i.e., $F_{o,i} = 0$) for modeling the SRW2.

Constitutive Models

This section describes the constitutive models used for the concrete fibers of the wall base section, the PT tendons, and the O-connectors.

Concrete Fibers

The compressive stress-strain loading and reloading curves for the concrete fibers are computed with the constitutive model described by Kalliontzis et al. (2020). The compressive strain in a concrete fiber of the wall base section shown in **Figure 6B** is obtained as.

$$\varepsilon_c = \frac{-v+\eta_C\sin\theta}{Z_c}, \quad (15)$$

where Z_c is the compression zone height, defined as $Z_c = 0.06(H_w + H_s)$ as in Kalliontzis et al. (2020). The concrete strength of a fiber is equal to the average concrete strength, $f'_{c,ave}$, calculated based on the unconfined and confined concrete areas shown in **Figure 3**.

$$f'_{c,ave} = \frac{A_c f_c^{'} + A_{cc,1}f'_{cc,1} + A_{cc,2}f'_{cc,2}}{A_g}, \quad (16)$$

where f'_c is the unconfined concrete strength; and $f'_{cc,1}$ and $f'_{cc,2}$ are the confined concrete strengths corresponding to the confined regions of the wall toes and the middle region of the wall, respectively. The values of $f'_{cc,1}$ and $f'_{cc,2}$ were computed with the theoretical model of Mander et al. (1988). Moreover, A_c, $A_{cc,1}$, and $A_{cc,2}$ are the respective areas corresponding to the three above-referenced concrete regions; and A_g is the gross-sectional area of the wall base. Accordingly, the calculated values of $f'_{c,ave}$ were 67.7 and 43.3 MPa for the SRW2 and PreWEC-2, respectively.

PT Tendons

The tensile loading and reloading stress-strain behaviors of the PT tendons are modeled with the constitutive model described by Kalliontzis et al. (2020). The strain in the PT tendons is obtained by adding the initial strain due to prestressing to the tendon elongation induced by the wall uplift over the unbonded length of the tendon:

$$\varepsilon_P = \varepsilon_{Pi} + \frac{v-\eta_{PT}\sin\theta}{\cos\theta L_u}, \quad (17)$$

where ε_{Pi} is the initial strain due to prestressing; and L_u is the unbonded length of the tendon.

O-Connectors

A phenomenological hysteretic law is proposed in this research study for the O-connectors. The law was calibrated with data of the O-connector tests by Nazari et al. (2015). The O-connectors are modeled as nonlinear axial springs. The backbone force-deformation curve of the springs consists of a linear and a nonlinear branch, as given in the following expression:

$$F_{0,backbone} = \begin{Bmatrix} E_0\Delta_0 & \Delta_0 < 2\,\text{mm} \\ 2E_0 + E_0(\Delta_0 - 2)\left[Q_0 + \frac{1-Q_0}{A_0}\right] & \Delta_0 \geq 2\,\text{mm} \end{Bmatrix}, \quad (18)$$

where E_0 is the elastic stiffness of the force-deformation curve, taken to be $E_0 = 0.175$ kN/mm for the O-connectors tested by Nazari et al. (2015); Δ_0 is the axial deformation of the springs computed with **Eq. 12**; and Q_0 and A_0 are numerical parameters defined as

$$Q_0 = \frac{\frac{E_{sec}}{E_0} - \alpha_0}{1-\alpha_0} \text{ and } A_0 = \left[1 + \left|\frac{E_0(\Delta_0 - 2)}{f_{ch,0} - 2E_0}\right|^{1.5}\right]^{1/1.5}, \quad (19)$$

where E_{sec} denotes the slope of the secant line that connects the first point with the end point of the nonlinear branch of **Eq. 18**. The first point of the nonlinear branch is the last point of the linear branch and the end point is located at the ultimate deformation of 91.5 mm with the corresponding force of 40 kN, as in the O-connectors tested by Nazari et al. (2015). The parameters $f_{ch,0}$ and α_0 in **Eq. 19** are computed with the M-P algorithm of Chang and Mander (1994). To compute the values of $f_{ch,0}$ and α_0 in this algorithm, the tangent modulus of the backbone curve at the end point of the nonlinear branch is used, which can be assumed to be zero or given a small value of 0.01 MPa to facilitate numerical convergence. The backbone force-deformation curve for the O-connectors is plotted in **Figure 7A**.

The hysteretic behavior of the O-connectors is described in **Figure 7B**. Once a load reversal takes place on the backbone curve, the resultant force-deformation curve is linear up to the zero resistance, $F_0 = 0$, which is given by the following expression:

$$F_0 = F_{0,1} - E_0(\Delta_{0,1} - \Delta_0), \quad (20)$$

where $F_{0,1}$ and $\Delta_{0,1}$ are the force and deformation values at the first point of the reversal curve, as shown in **Figure 7B**. If loading continues toward the negative direction of deformations, the response follows a nonlinear curve which is defined as

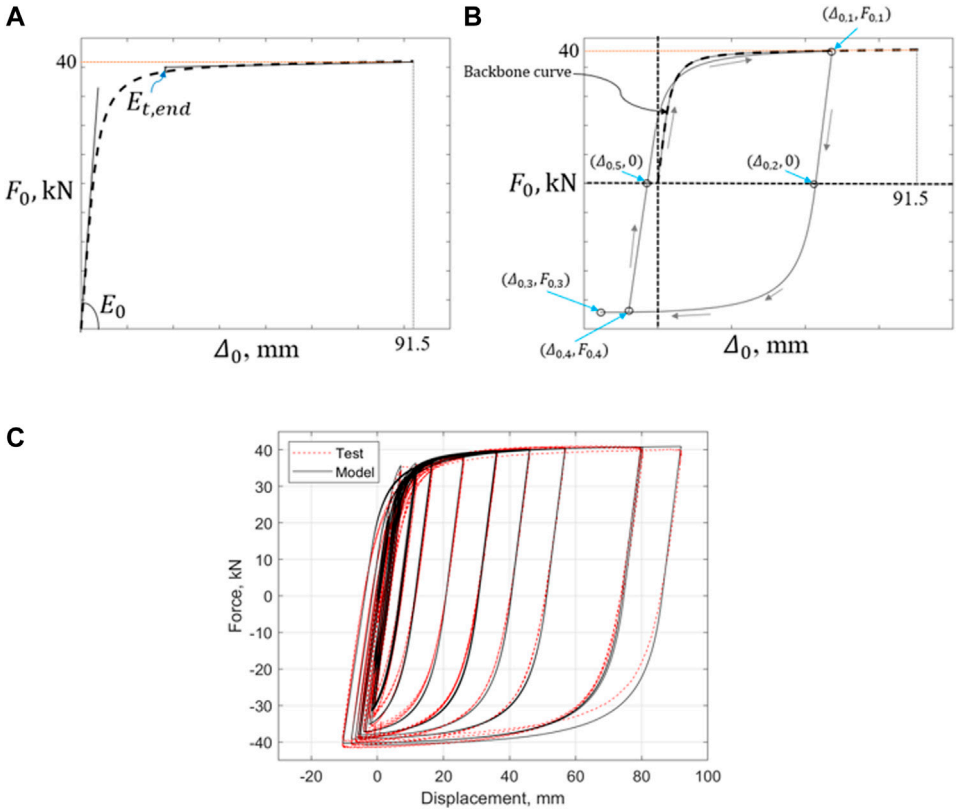

FIGURE 7 | Force-deformation curves for the O-connectors; **(A)** Backbone curve; **(B)** Hysteretic curve; **(C)** Comparison of hysteretic law with the test data by Nazari et al. (2015).

$$F_0 = E_0\left(\Delta_0 - \Delta_{0,2}\right)\left[Q_0 + \frac{1-Q_0}{A_0}\right] \geq -40\,\text{kN}, \tag{21}$$

with $\Delta_{0,2} = \Delta_{0,1} - F_{0,1}/E_0$. In **Eq. 21**, the parameters Q_0 and A_0 are computed using **Eq. 19**, where the factor "1.5" is substituted with the following expression: $0.95 + 0.4(1 - \Delta_{0,1}/91.5)$. In this case, the value of E_{sec} is computed as $E_{sec} = F_{0,3}/(\Delta_{0,3} - \Delta_{0,2})$, where $F_{0,3}$, $\Delta_{0,3}$, and $\Delta_{0,2}$ are shown in **Figure 7B**. The point $(\Delta_{0,3}, F_{0,3})$ is computed as

$$\Delta_{0,3} = -0.5 - \frac{F_{0,1}}{20} \text{ and } F_{0,3} = -40 + \left(1 - \frac{\Delta_{0,1}}{91.5}\right), \tag{22}$$

If loading toward the negative direction continues beyond the deformation $\Delta_{0,3}$, the force-deformation response is computed with **Eq. 21** until $\Delta_0 = -91.5$ mm. The O-connector is assumed to fracture for deformations larger than 91.5 mm in magnitude for both the positive and negative directions of loading. Reloading toward the positive direction at a deformation of magnitude lower than 91.5 mm follows the linear branch of **Eq. 23** up to the force resistance $F_0 = 2E_0$:

$$F_0 = F_{0,4} - \left(E_0 - 10\frac{F_{0,4}}{40}\sqrt{|\Delta_{0,4}|}\right)\left(\Delta_0 - \Delta_{0,4}\right), \tag{23}$$

where $(\Delta_{0,4}, F_{0,4})$ is the first point of the reloading curve in the hysteretic response of **Figure 7B**. For $F_0 > 2E_0$, the reloading continues with the following nonlinear curve:

$$F_0 = E_0\left(\Delta_0 - \Delta_{0,5}\right)\left[Q_0 + \frac{1-Q_0}{A_0}\right] \leq 40\,kN, \tag{24}$$

where Q_0 and A_0 are defined in **Eq. 19**. In this case, the target point for **Eq. 24** is (91.5 mm, 40 kN) and the factor "1.5" in **Eq. 19** is substituted with the following expression:

$$\left\{\begin{array}{ll} \min\left[1.25 + 0.9\left(1 - \frac{|F_{0,4}|}{40}\right), \frac{2.5}{\Delta_{0,5}}\right] & \Delta_{0,5} > 0 \\ 1 - \frac{\Delta_{0,5}}{1.5} & \Delta_{0,5} \leq 0 \end{array}\right\}. \tag{25}$$

The proposed hysteretic law is compared with the O-connector test data in **Figure 7C**.

Impact Event

Rocking walls dissipate part of their kinetic energy during impact on the foundation base. The GDAA models the impact with an event-based approach, which computes the post-impact response of the wall with impulse-momentum equations. It is assumed that the impacts occur when either of the points of the wall base with

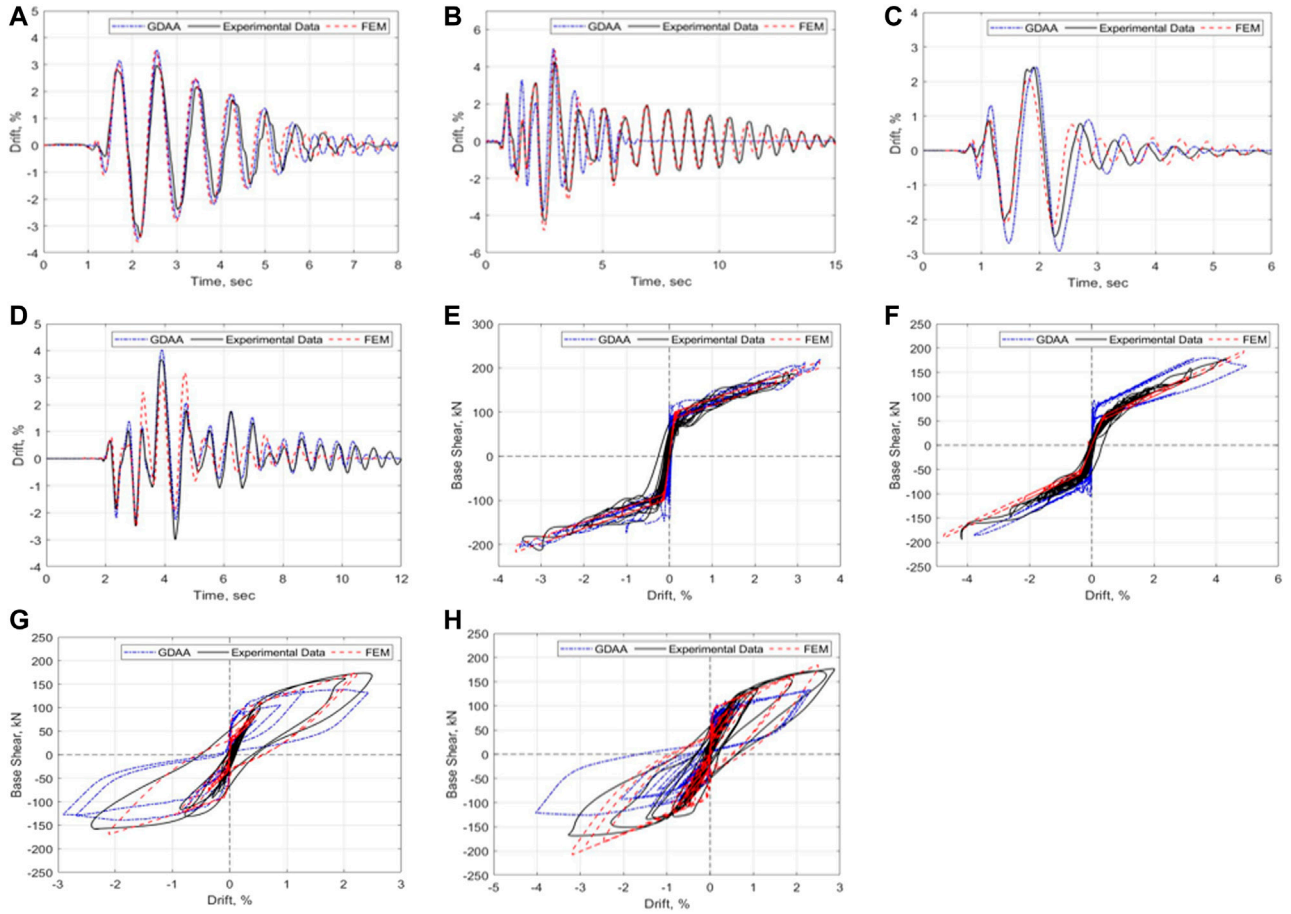

FIGURE 8 | Global responses of FEM and GDAA in comparison with the experimental data: **(A)** Time history of lateral drift, SRW2-Sylmar; **(B)** Time history of lateral drift, SRW2-Takatori; **(C)** Time history of lateral drift, PreWEC2-Sylmar; **(D)** Time history of lateral drift, PreWEC2-Takatori; **(E)** base shear vs. lateral drift, SRW2-Sylmar; **(F)** Base shear vs. lateral drift, SRW2-Takatori; **(G)** Base shear vs. lateral drift, PreWEC2-Sylmar; **(H)** Base shear vs. lateral drift, PreWEC2-Takatori.

coordinates $\eta = \pm 0.72L_w/2$ establish contact with the foundation while the wall is in a re-centering trajectory. Details on the impact formulation can be found in Kalliontzis et al. (2020).

COMPARISONS BETWEEN EXPERIMENTAL AND MODEL RESPONSES

The shake table responses of the SRW2 and PreWEC-2 are compared with those computed using the FEM and the GDAA. As discussed previously, the FEM is a lumped-plasticity model which can compute the global responses of the SRW2 and PreWEC-2, including the maximum and residual lateral drifts, the absolute acceleration, the base shear and moment resistance due to the shake table excitations. Hence local wall responses, such as the wall contact length at the rocking interface and the variation of PT stress are not computed. If computing these local responses is of interest, the use of GDAA, is recommended. This point is discussed below.

Figure 8 presents the global responses of the FEM and GDAA in comparison with the test data. **Figures 8A–D** present the lateral drift time histories. In all cases, the models adequately captured the maximum drift responses and the drift variations as a function of time. Using the GDAA, some deviations from the experimental responses were observed for the SRW2 during the Takatori ground motion and the PreWEC-2 during the Sylmar ground motion. The FEM also deviated from the experimental response of the PreWEC-2 during the Takatori ground motion. Both the GDAA and the FEM were able to capture the decay of motion during the free vibration of SRW2 (i.e., after the first 2.5 s in **Figure 8A**). On the other hand, the FEM was able to better capture the response of the SRW2 in **Figure 8B** after the first 6 s. The inaccuracy exhibited by the GDAA in this response is partly attributed to the overestimation of the hysteretic action at the compression toes of the wall panel after the wall drift reached a value of 5%.

Figures 8E–H present the base shear-lateral drift response of the test units, using the two modeling approaches. The comparisons between the two models and the experimental results are satisfactory for the responses of the SRW2 (**Figures 8E,F**). The FEM shows good accuracy for the PreWEC-2 for both ground motions, while the GDAA overestimates the re-centering

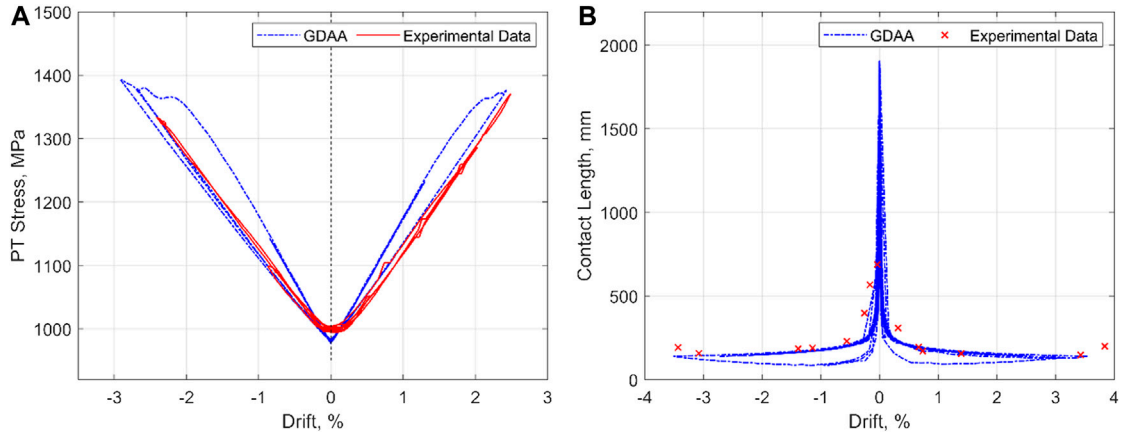

FIGURE 9 | Local responses of GDAA in comparison with the experimental data during Sylmar: **(A)** Variation of PT Stress, PreWEC-2; **(B)** Variation of Contact Length, SRW2.

capability of PreWEC-2 during the Takatori ground motion. This deviation is attributed to the estimation of the O-connector deformation, Δ_0, in **Eq. 12** which neglected the vertical movement of the end columns and the relative horizontal movement between wall and columns. Considering these movements, it is believed that the computed responses by GDAA could improve.

As noted previously, one advantage of using the GDAA as opposed to the FEM described in this paper is the capability to compute the local wall responses. As an example, **Figure 9** compares typical local responses computed by the GDAA against the test data. Variations of the PT stress vs. the lateral drift are plotted in **Figure 9A** for the PreWEC-2, showing that the GDAA provides a good accuracy for this variable. Next, **Figure 9B** compares the GDAA's estimates of contact length between the wall panel and the foundation with the corresponding experimental data for the SRW2. It is shown that the GDAA adequately reproduces the experimental contact lengths.

Overall, the FEM satisfactorily reproduced the global behavior of the SRW2 and the PreWEC-2 for ground motions of different intensities. This model can be used for performance-based analysis of rocking wall systems, when estimating the global behavior of the walls is of interest, up to the lateral drift ratios of 4–5%. On the other hand, when estimation of the local wall responses is of interest, the GDAA may be used, because of its ability to compute these responses with good accuracy.

MODEL BEHAVIOR CHARACTERISTICS

As described in *Finite Element Method*, the FEM was developed to model the rocking wall responses up to lateral drift of 4–5% where no significant wall base damage or material nonlinearity in the PT tendons can occur, in accordance with the design requirements (ACI ITG-5.1 2008, SEAOC 2000). Because of its capability to capture these local responses, the GDAA may be used for modeling the wall responses at larger lateral drifts. Based on the assumptions made in the development of the FEM and the GDAA, key behavior characteristics of the two models are discussed below.

Wall Degradation

When subjected to large lateral drifts, the lateral stiffness and strength of the unbonded post-tensioning precast concrete walls may degrade due to yielding of the unbonded tendons and concrete damage at the compression toes. To examine the behavior of the FEM and GDAA in cases where wall degradation may occur, the horizontal component of the 1994 Northridge earthquake as recorded in the Sylmar-Converter Station (PEER 2020 NGA record sequence number or RSN—1084), was used to excite the FEM and the GDAA for the case of SRW2.

Figure 10 presents the responses of the SRW2 as modeled by the FEM and the GDAA. The two models agree well in their lateral drift time histories during the first 7.5 s of the ground excitation. Subsequently, the GDAA computes lateral drifts as high as ±9.4% while the FEM computes a decaying motion for the SRW2, eventually reaching a zero drift at about 15 s from the beginning of the excitation. The discrepancy between the two models stems from the different approaches in computing the global wall behavior. The FEM uses a predefined global hysteretic law that does not experience strength degradation (see **Figure 5**), while the GDAA computes the global behavior as a function of the local responses at the wall-to-foundation contact and in the PT tendons, which accounts for the strength degradation of the wall. As the SRW2 experiences large lateral drifts, the tendon yields, which reduces the residual prestress, as shown in **Figure 10C**. Moreover, due to the concrete damage at the compression toes, the neutral axis depth at the wall base shifts toward the centerline of the wall, because an increased contact length is required to transfer the vertical compression forces from the wall base to the foundation base. This is explained in **Figure 10D**, which shows that the contact length increases at

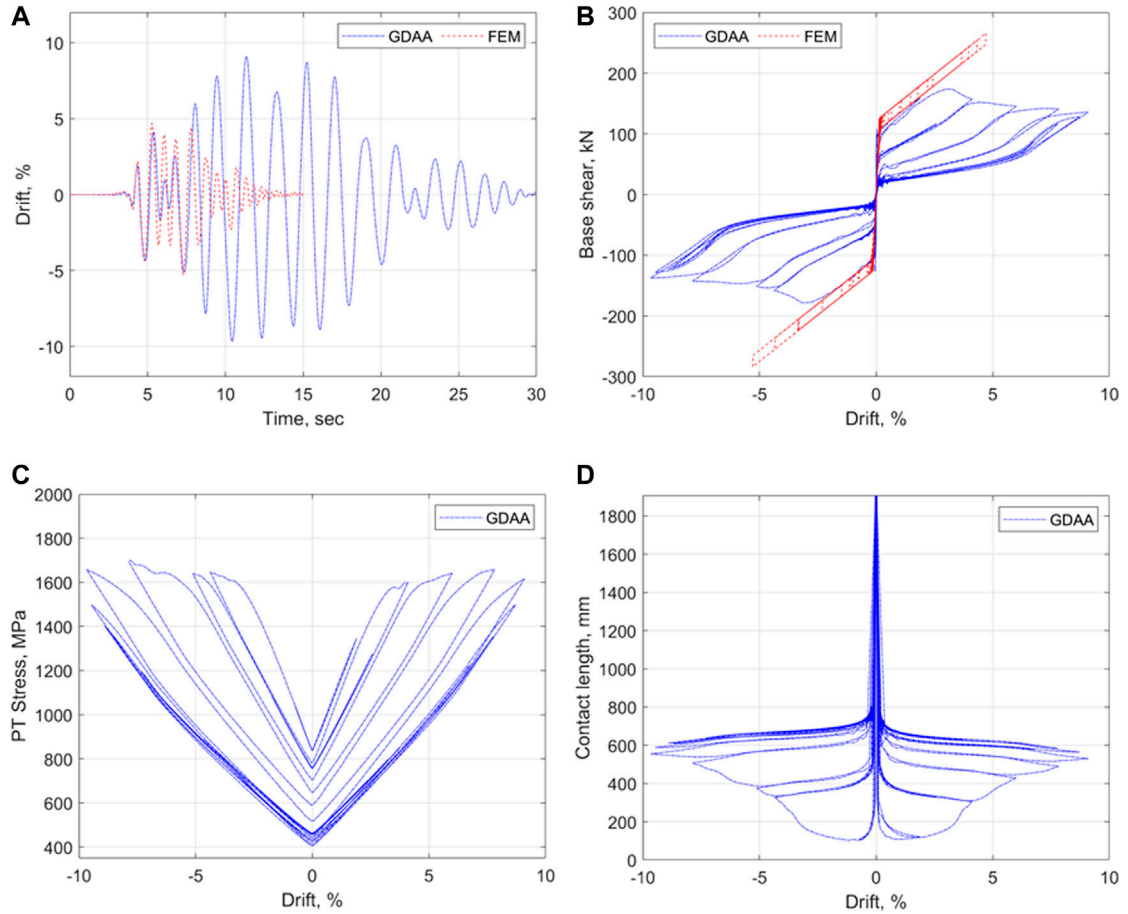

FIGURE 10 | Responses of SRW2 to the horizontal component of Sylmar as modeled by the GDAA and the FEM: **(A)** Time history of lateral drift; **(B)** base shear vs. lateral drift; **(C)** PT Stress vs. lateral drift; **(D)** Contact Length vs. lateral drift.

drifts larger than 3%. The local degradations of the PT tendon and the wall base result in a global degradation of the wall in the GDAA. This is reflected in the base shear vs. drift response of **Figure 10B** showing that the lateral strength of the wall decreases with increasing lateral drift beyond the value of 3%. At the lateral drift of 9.4%, the lateral strength of SRW2 has reduced by 23.4%.

On the other hand, the base shear vs. drift response of the FEM, shown in **Figure 10B** is based on a predefined hysteretic law that does not account explicitly for the local behaviors described previously. This law produces a different global behavior of the wall than the GDAA.

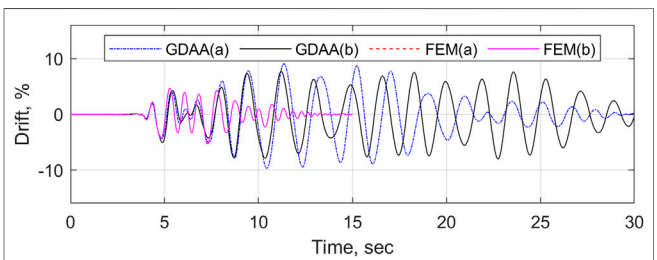

FIGURE 11 | Lateral drift time histories of the FEM and the GDAA for **(a)** the horizontal component of Sylmar alone; and **(b)** the horizontal and vertical components of Sylmar combined.

Vertical Ground Excitation

The effect of vertical components of ground motions on the rocking behavior has been considered in previous analytical research studies of free-standing rigid blocks (e.g., Yim et al., 1980; Dimentberg et al., 1993; Shi et al., 1996; Makris and Zhang 1999; Linde et al., 2020). Most research studies on unbonded post-tensioned precast concrete walls have been limited to horizontal components of the ground motions. This section investigates the responses of the SRW2 to the horizontal and vertical components of the 1994 Northridge earthquake as modeled by the GDAA and the FEM.

The responses of the FEM and the GDAA were calculated considering 1) the horizontal component of the 1994 Northridge earthquake alone; and 2) the horizontal and vertical components of the 1994 Northridge earthquake combined. The lateral drift time histories for the two cases

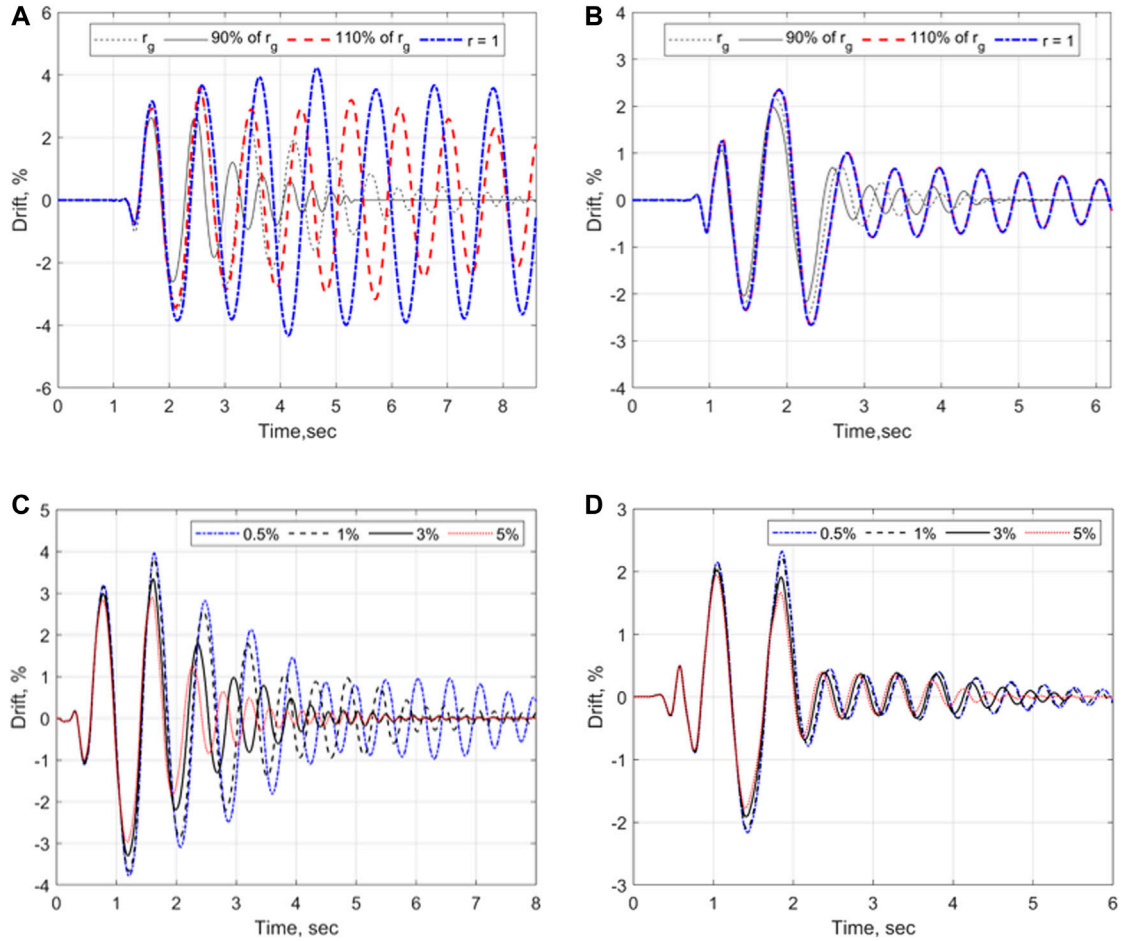

FIGURE 12 | Lateral drift time histories by the GDAA and FEM, respectively for various values of r and ζ_{impact}, during Sylmar: **(A)** GDAA-SRW2; **(B)** GDAA-PreWEC-2; **(C)** FEM-SRW2; **(D)** FEM-PreWEC-2.

TABLE 2 | Design parameters of case study walls.

case study	Length of the wall panel (m), wall aspect ratio (i.e., height[a]/length)	No., dia.(mm) of PT tendon, initial PT stress (MPa)	Moment, kN-m/Shear, kN, resistance at 2% drift[b]
A (SRW2)	1.91, 2.8	6, 12.7 strand, 923.9 (0.5 f_{pu}[c])	769.4, 180.3
B	1.33, 4.0	6, 12.7 strand, 1,270.7 (0.68 f_{pu})	771.1, 180.7
C	1.52, 3.5	6, 12.7 strand, 937 (0.5 f_{pu})	768.1, 180
D	1.78, 3.0	5, 12.7 strand, 845.3 (0.45 f_{pu})	769.2, 180.2
E	2.13, 2.5	4, 12.7 strand, 754.3 (0.41 f_{pu})	772.8, 181.0
F	2.67, 2.0	3, 12.7 strand, 635.7 (0.34 f_{pu})	767.7, 179.9

[a]*Height of the wall panels remained unchanged, i.e., 5.33 m.*
[b]*Following the SA method (Aaleti and Sritharan, 2009).*
[c]f_{pu} *= tensile strength of tendon = 1862 MPa.*

are plotted in **Figure 11**. Because the FEM is a lumped plasticity model, it does not account explicitly for the interaction between the axial and rocking behaviors, which is necessary to capture the inertia effects of the SRW2 induced by the vertical ground excitation. Hence the responses of the FEM to the cases **(a)** and **(b)** were identical, suggesting that the model had no sensitivity to the vertical ground excitation. Because the GDAA uses a fiber-based sectional analysis at the wall base, its behavior was influenced by the vertical ground excitation. This is shown in **Figure 11** where the drifts

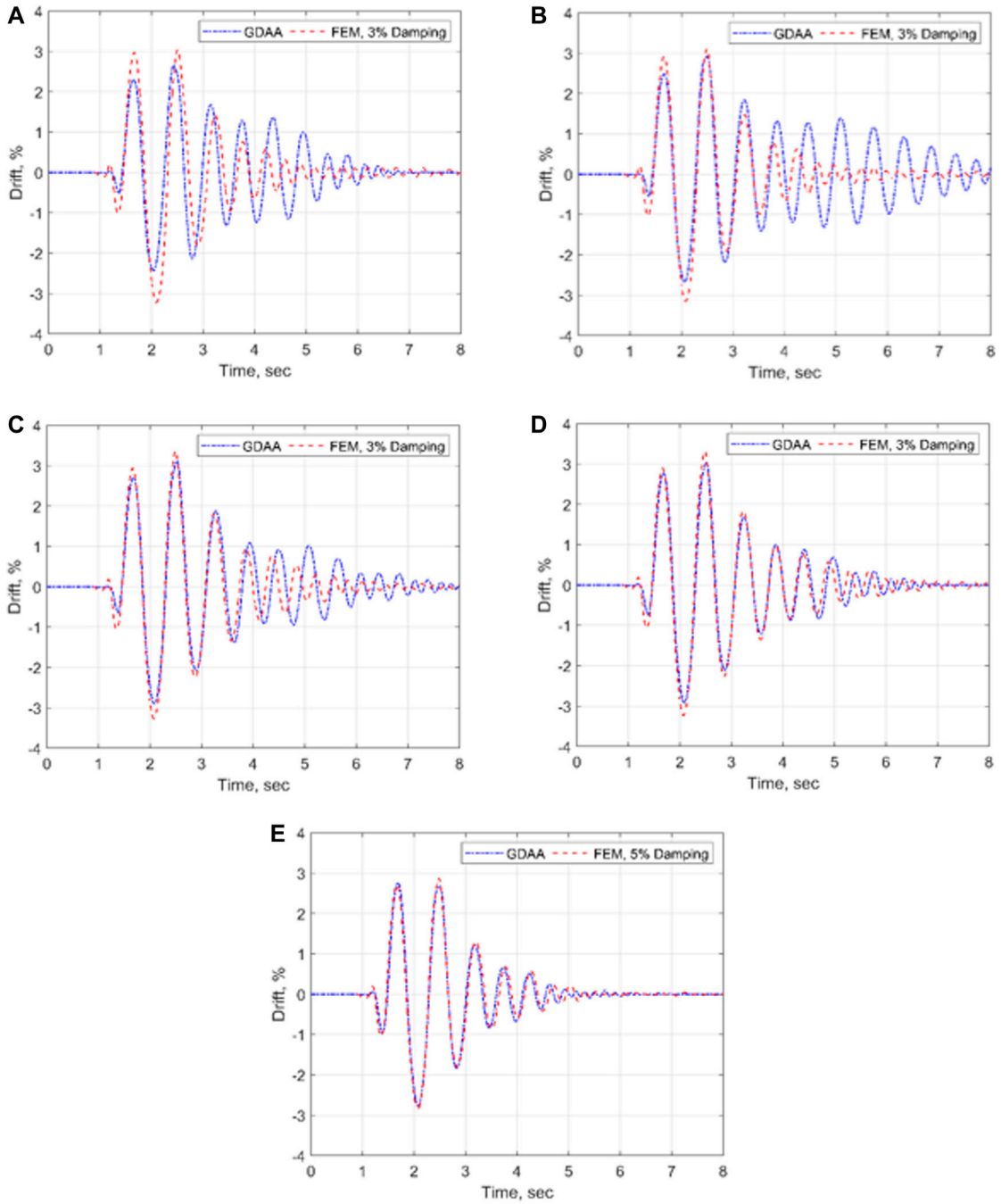

FIGURE 13 | Lateral drift time histories of case study SRWs during Sylmar–the FEM with selected damping ratios vs the GDAA: **(A)** Case B, with aspect ratio of 4; **(B)** case C, with aspect ratio of 3.5; **(C)** Case D, with aspect ratio of 3; **(D)** Case E, with aspect ratio of 2.5; **(E)** Case F, with aspect ratio of 2.

computed by the GDAA are different between cases (**a**) and (**b**). Based on these analytical data, the presence of a vertical ground excitation may influence the seismic behavior of the SRW2. The accuracy of this analytical observation, however, needs to be verified experimentally in future research studies.

IMPACT DAMPING

The impact damping influences the seismic behavior of SRWs, as observed experimentally by Nazari and Sritharan (2020) and by Kalliontzis and Sritharan (2020). However, the sensitivity of

rocking wall models to the numerical simulation of impact damping has not received adequate attention. This is investigated in this section using the FEM and the GDAA.

The seismic response of the SRW2 to the Sylmar excitation (i.e., namely **Eq. 4s**, as per *Review of Shake Table Tests of Rocking Walls*) was computed using the GDAA by varying the r_g of **Eq. 1** by ±10% and assuming $r = 1$ (or no impact damping). These responses are compared in **Figure 12A** with the numerical solution of **Figure 8A**, showing that a small change in the assumed value of r caused a significant change to the maximum response and the decay of motion of the SRW2. For example, decreasing r_g by 10% (i.e., $r = 90\%r_g$) caused a 27.6% decrease in the maximum drift, while increasing r_g by 10% (i.e., $r = 110\%r_g$) caused an 8.4% increase in the maximum drift. Assuming no impact damping, (i.e., $r = 1$), resulted in an overly conservative response with long oscillations for the SRW2 and an increase in the maximum drift by 26.5% with respect to the numerical solution of **Figure 8A**. The sensitivity of SRW2 to impact damping was also explored with the FEM in **Figure 12C** by varying the equivalent viscous damping ratio (ζ_{impact}) from 0.5 to 5%. The numerical results of the FEM confirm that accurate estimation of impact damping is required for accurate modeling of the SRW2.

Modeling of the impact damping can also influence the dynamic behavior of walls with supplemental damping devices, such as the PreWEC. This is discussed in **Figures 12B,D** with the use of GDAA and FEM, respectively. For example, **Figure 12B** shows that neglecting impact damping (i.e., $r = 1$) increased the maximum drift by 11%, while decreasing r by 10% (i.e., $r = 90\%r_g$) reduced the maximum drift by 8.8%. Similar conclusions are made by the FEM in **Figure 12D**.

Modeling Impact Damping in the FEM

Based on the above discussion, accurate modeling of impact damping is important for capturing the experimental behavior of rocking walls. While the use of a generalized coefficient of restitution, r, approach (e.g., **Eq. 1**) in the GDAA has been shown to provide good accuracy, this approach cannot be implemented with the FEM. As discussed in *Finite Element Method*, impact damping in the FEM used a 3% tangent stiffness proportional Rayleigh damping, which was derived based on shake table tests of four SRWs, all of them having an aspect ratio equal to 2.8.

To investigate modeling of impact damping in the FEM for walls with different aspect ratios, five additional case study SRWs were designed by varying the wall aspect ratio from 2.0 to 4.0, as shown in **Table 2** (i.e., cases B–F). The five SRWs were designed following the Simplified Analysis Method by Aaleti and Sritharan (2009) to match the moment capacity of SRW2 at the 2% design drift. **Table 2** presents the design parameters of the case study SRWs.

Next, the seismic responses of the five SRWs were computed with the FEM by calibrating the tangent stiffness proportional Rayleigh damping to achieve an adequate comparison with the corresponding responses by the GDAA. The selected seismic excitation in this case was the Sylmar excitation (i.e., namely **Eq. 4s**, as per *Review of Shake Table Tests of Rocking Walls*) because both the FEM and the GDAA showed good accuracy in capturing the experimental response of SRW2 to this excitation, as shown previously in **Figure 8A**.

Figure 13 presents the comparison of the seismic responses of the five case study SRWs obtained by the FEM and the GDAA. The FEM used a 3% tangent stiffness proportional Rayleigh damping for the Cases B-E, which is the same as recommended in *Finite Element Method*; however, this ratio was increased to 5% for case F, which had the smallest aspect ratio of 2.0. As shown in **Figures 13A,B**, for slender walls (i.e., Cases B and C), the FEM did not reproduce accurately the free vibration phase of the GDAA (i.e., after the first 2.5 s of the time history); however, the FEM captured the maximum drift of the GDAA satisfactorily. Moreover, **Figures 13C,D** show that the FEM accurately reproduced the lateral drift time histories of the GDAA with the aspect ratio of 3.0 and less (i.e., case D and E) using the damping ratio of 3%. Using the larger damping ratio of 5%, the FEM was able to capture the response of case F by the GDAA, as shown in **Figure 13E**.

CONCLUSION

Modeling of unbonded post-tensioned precast concrete walls with rocking connections was discussed in this research study. Two modeling approaches were investigated, namely 1) a Finite Element Model (FEM), which was developed based on lumped plasticity to capture the global wall responses up to lateral drift ratios of 4–5%; and 2) a Generalized Dynamic Analysis Approach (GDAA), which is an analytical model developed to capture both the global and local wall responses up to lateral drift ratios of 10%. The accuracy of the two models was evaluated with shake table tests of unbonded post-tensioned precast concrete walls without (SRW2) and with (PreWEC-2) supplemental damping devices. The following conclusions were made:

- Both the FEM and the GDAA satisfactorily reproduced the experimental global behaviors of the SRW2 and the PreWEC-2.
- The GDAA was capable of computing the experimental local responses of the SRW2 and the PreWEC-2, including the variation of the post-tensioning force and the contact length of the wall to the foundation base. Because the FEM is a lumped plasticity model, it cannot compute these local responses. The use of a fiber-based modeling approach can be investigated for improving the FEM in future research studies.
- While the FEM satisfactorily reproduced the global behavior of the walls up to the drifts of 4–5%, the GDAA may be preferred for computing wall responses to larger drifts, because of its ability to simulate concrete damage and yielding of the PT tendons.
- It was shown that the use of a fiber-based sectional analysis in the GDAA provided the capability to capture the effect of vertical ground excitations to the wall responses and that vertical excitations may alter the seismic behavior of the walls.
- The FEM and the GDAA corroborated that small variations of the impact damping can influence the seismic behavior

of unbonded post-tensioned precast concrete walls significantly. The GDAA captured impact damping with an event-based approach, while the FEM used a tangent stiffness-based equivalent impact damping ratio of 3% for SRWs, which was derived based on shake table test data.

- Results of a case study analysis on five SRWs with different aspect ratios confirmed the accuracy of the FEM's 3% impact damping for walls with aspect ratios of 2.5 and higher. It was found that an equivalent damping ratio of 5% is more suitable for modeling SRWs with lower aspect ratios.

DATA AVAILABILITY STATEMENT

The original contributions presented in the study are included in the article/Supplementary Material, further inquiries can be directed to the corresponding author.

AUTHOR CONTRIBUTIONS

DK: Modeling and Analysis (GDAA), Results and Discussions, Writing. MN: Modeling and Analysis (FEM), Comparison with the Shake Table Data, Results and Discussions, Writing.

REFERENCES

Aaleti, S., and Sritharan, S. (2009). A simplified analysis method for characterizing unbonded post-tensioned precast wall systems. *Eng. Struct.* 31 (12), 2966–2975. doi:10.1016/j.engstruct.2009.07.024

ACI 550.6-19 (2019). *Acceptance criteria for special unbonded post-tensioned precast structural walls based on validation testing and commentary*. Farmington Hills, MI: American Concrete Institute.

ACI Innovation Task Group 5.1 (2008). *Acceptance criteria for special unbonded post-tensioned precast structural walls based on validation testing and commentary*. Farmington Hills, MI: American Concrete Institute.

Aghagholizadeh, M. (2020). A finite element model for seismic response analysis of vertically-damped rocking-columns. *Eng. Struct.* 219, 110894. doi:10.1016/j.engstruct.2020.110894

ASCE 7-16 (2016). *Minimum design loads for buildings and other structures*. Reston, VA: ASCE.

Avgenakis, E., and Psycharis, I. N. (2020). An integrated macroelement formulation for the dynamic response of inelastic deformable rocking bodies. *Earthq. Eng. Struct. Dyn.* 49 (11), 1072–1094. doi:10.1002/eqe.3279

Baruh, H. (1999). *Analytical dynamics*. New York, NY: McGraw-Hill.

Belleri, A., Torquati, M., and Riva, P. (2013). "Finite element modeling of rocking walls," in 4th ECCOMAS thematic conference on computational methods in structural dynamics and earthquake engineering, Kos Island, Greece, June 12–14, 2013.

Chang, G. A., and Mander, J. B. (1994). Seismic energy based on fatigue damage analysis of bridge columns: part 1—evaluation of seismic capacity. NCEER technical report no. NCEER-94-0006. Buffalo, NY State University of New York.

Diamantopoulos, S., and Fragiadakis, M. (2019). Seismic response assessment of rocking systems using single degree-of-freedom oscillators. *Earthq. Eng. Struct. Dyn.* 48 (7), 689–708. doi:10.1002/eqe.3157

Dimentberg, M. E., Hou, Z. K., Noori, M. N., and Zhang, W. (1993). *Non-Gaussian response of a single-degree-of-freedom system to a periodic excitation with random phase modulation.Recent development in the mechanics of continua (special volume)*. New York, NY: ASME.

Henry, R. S. (2011). Self-centering precast concrete walls for buildings in regions with low to high seismicity. PhD thesis. Auckland (New Zealand): University of Auckland.

Housner, G. W. (1963). The behavior of inverted pendulum structures during earthquake excitations. *Bull. Seismol. Soc. Am.* 53 (2), 403–417.

Kalliontzis, D., Schultz, A. E., and Sritharan, S. (2020). Generalized dynamic analysis of structural single rocking walls (SRWs). *Earthq. Eng. Struct. Dyn.* 49 (7), 633–656. doi:10.1002/eqe.3257

Kalliontzis, D., and Sritharan, S. (2014). "A finite element approach for modelling controlled rocking systems," in Proceedings of the 2nd European Conference on earthquake Engineering and seismology, Turkey, Istanbul, August, 2014.

Kalliontzis, D., and Sritharan, S. (2018). Characterizing dynamic decay of motion of free-standing rocking members. *Earthq. Spectra* 34 (2), 843–866. doi:10.1193/011217eqs013m

Kalliontzis, D., and Sritharan, S. (2020). Dynamic response and impact energy loss in controlled rocking members. *Earthq. Eng. Struct. Dyn.* 49 (4), 319–338. doi:10.1002/eqe.3240

Kalliontzis, D., Sritharan, S., and Schultz, A. (2016). Improved coefficient of restitution estimation for free rocking members. *J. Struct. Eng.* 142 (12), 06016002. doi:10.1061/(asce)st.1943-541x.0001598

Kalliontzis, D., and Sritharan, S. (2021). Seismic behavior of unbonded post-tensioned precast concrete members with thin rubber layers at the jointed connection. *PCI J.* 66 (1), 60–76. doi:10.15554/pcij66.1-02

Kurama, Y., Sause, R., Pessiki, S., and Lu, L.-W. (1999). Lateral load behavior and seismic design of unbonded post-tensioned precast concrete walls. *ACI Struct. J.* 96 (4), 622–632.

Linde, S. A., Konstantinidis, D., and Tait, M. J. (2020). Rocking response of unanchored building contents considering horizontal and vertical excitation. *ASCE J. Struct. Eng.* 146 (9). doi:10.1061/10.1061/(asce)st.1943-541x.0002735

Makris, N., and Zhang, J. (1999). Rocking response and overturning of anchored equipment under seismic excitation. Report No. PEER-99/06. Berkeley (United States): University of California.

Mander, J. B., Priestley, M. J. N., and Park, R. (1988). Theoretical stress-strain model for confined concrete. *J. Struct. Eng.* 114 (8), 90–103. doi:10.1061/(ASCE)0733-9445(1988)114:8(1804)

Marriott, D., Pampanin, S., Bull, D., and Palermo, A. (2008). Dynamic testing of precast, post-tensioned rocking wall systems with alternative dissipating solutions. *Bull. N.Z. Natl. Soc. Earthqu. Eng.* 41 (2), 90–103. doi:10.5459/bnzsee.41.2.90-103

McKenna, F., Fenves, G., and Scott, M. (2000). *Open system for earthquake engineering simulation*. Berkeley, CA: University of California.

Mpampatsikos, V., Bressanelli, M. E., Belleri, A., and Nascimbene, R. (2020). A non-dimensional parametric approach for the design of PT tendons and mild steel dissipaters in precast rocking walls. *Eng. Struct.* 212, 110513. doi:10.1016/j.engstruct.2020.110513

Nazari, M., Aaleti, S., and Sritharan, S. (2015). *Shake table testing of single rocking walls and PreWECs @ UNR*. Network for Earthquake Engineering Simulation (distributor). doi:10.4231/D3H98ZF0B(SRW2) and doi:10.17603/DS2WK5B(PreWEC-2)

Nazari, M., Sritharan, S., and Aaleti, S. (2017). Single precast concrete rocking walls as earthquake force-resisting elements. *Earthq. Eng. Struct. Dyn.* 46 (5), 753–769. doi:10.1002/eqe.2829

Nazari, M., and Sritharan, S. (2018). Dynamic evaluation of PreWEC systems with varying hysteretic energy dissipation. *ASCE J. Struct. Eng.* 144 (10), 04018185. doi:10.1061/(ASCE)ST.1943-541X.0002169

Nazari, M., and Sritharan, S. (2020). Influence of different damping components on dynamic response of concrete rocking walls. *Eng. Struct.* 212, 110468. doi:10.1016/j.engstruct.2020.110468

Nazari, M., and Sritharan, S. (2019). Seismic design of precast concrete rocking wall systems with varying hysteretic damping. *PCI J.* 64 (5), 58–76. doi:10.15554/pcij64.5-04

Pacific Earthquake Engineering Research Center (PEER) (2020). Next generation attenuation (NGA) database. Available at: http://peer.berkeley.edu/nga/ (Accessed December 08, 2020).

Perez, F. J., Pessiki, S., and Sause, R. (2004). Experimental and analytical lateral load response of unbonded post-tensioned precast concrete walls. ATLSS report No. 04-11. Bethlehem (United States): Lehigh University.

Priestley, M., Calvi, G. M., and Kowalsky, M. J. (2007). Displacement-based seismic design of structures. *Building* 23 (33), 1453–1460.

Priestley, M. J. N. (2002). Direct displacement-based design of precast/prestressed concrete buildings. *PCI J.* 47 (6), 66–79. doi:10.15554/pcij.11012002.66.79

Priestley, M. J. N., Sritharan, S., Conley, J. R., and Pampanin, S. (1999). Preliminary results and conclusions from the PRESSS five-story precast concrete test building. *PCI J.* 44 (6), 42–67. doi:10.15554/pcij.11011999.42.67

Rahman, A. M., and Restrepo, J. I. (2000). Earthquake resistant precast concrete buildings: seismic performance of cantilever walls prestressed using unbonded tendons. Research Report 2000-5. Christchurch (New Zealand): University of Canterbury.

Shi, B., Anooshehpoor, A., Zeng, Y., and Brune, J. N. (1996). Rocking and overturning of precariously balanced rocks by earthquake. *Bull. Seismological Soc. Amer.* 86 (5), 1364–1371.

Sritharan, S., Aaleti, S., Henry, R. S., Liu, K. Y., and Tsai, K. C. (2015). Precast concrete wall with end columns (PreWEC) for earthquake resistant design. *Earthq. Eng. Struct. Dyn.* 44 (12), 2075–2092. doi:10.1002/eqe.2576

Twigden, K. M. (2016). Dynamic response of unbonded post-tensioned concrete walls for seismic resilient structures. PhD Thesis. Auckland (New Zealand): University of Auckland.

Vassiliou, M. F., Mackie, K. R., and Stojadinović, B. (2016). A finite element model for seismic response analysis of deformable rocking frames. *Earthq. Eng. Struct. Dyn.* 46 (3), 447–466. doi:10.1002/eqe.2799

Yim, C. S., Chopra, A. K., and Penzien, J. (1980). Rocking response of rigid blocks to earthquakes. *Earthq. Eng. Struct. Dyn.* 8, 565–587. doi:10.1002/eqe.4290080606

Conflict of Interest: The authors declare that the research was conducted in the absence of any commercial or financial relationships that could be construed as a potential conflict of interest.

APPENDIX: CONSTANTS I_5 AND I_9 IN EQUATION OF MOTION OF GDAA

$$I_5 = M\left(\frac{L_w^2}{12} + \frac{H_w^2}{3}\right) + M_s\left[\frac{L_s^2}{12} + \frac{H_s^2}{3}\left(\left(1 + \frac{H_w}{H_s}\right)^3 - \left(\frac{H_w}{H_s}\right)^3\right)\right] \tag{A1}$$

$$I_9 = \mathrm{M}\frac{H_w}{2} + M_s\frac{H_s}{2}\left[\left(1 + \frac{H_w}{H_s}\right)^2 - \left(\frac{H_w}{H_s}\right)^2\right] \tag{A2}$$

frontiers in Built Environment

ORIGINAL RESEARCH
published: 20 April 2021
doi: 10.3389/fbuil.2021.629956

Influence of Modelling Assumptions on the Seismic Risk of Industrial Precast Concrete Structures

Michele Egidio Bressanelli[1], Davide Bellotti[2], Andrea Belleri[1], Francesco Cavalieri[2], Paolo Riva[1] and Roberto Nascimbene[3]*

[1]Department of Engineering and Applied Sciences, University of Bergamo, Dalmine, Italy, [2]European Centre for Training and Research in Earthquake Engineering, Pavia, Italy, [3]University School for Advanced Studies (IUSS), Pavia, Italy

This research evaluates the influence of different modelling assumptions on the global and local seismic risk assessment of code-conforming precast reinforced concrete buildings, specifically single-story industrial buildings. In particular the modelling of the system mass, the overhead crane, the beam-to-column and roof-to-beam connections and the cladding system are investigated. For this purpose, a case study resembling a new industrial building designed in accordance with the current Italian building code was selected. Typical dowel beam-to-column connections were considered and the influence of various modelling strategies investigated: perfect hinges, linear elastic connections and non-linear connections with a degrading hysteretic force-displacement model which was calibrated from available data on experimental tests. Three different types of roof-to-beam connections were investigated removing the assumption of rigid diaphragm, namely hot-rolled, cold-formed and socket welded connections. Initially, simplified planar models of single frames were considered to evaluate the influence of the different modelling strategies, then 3D models of the entire building were analyzed. Multiple-stripe non-linear dynamic time history analyses allowed to evaluate displacements, drifts, deformations and ultimate curvatures of the main elements and connections for various intensity measure levels. The seismic risk was assessed in terms of failure rate considering the collapse of both the columns and of the connections. The results show that the beam-to-column connections fail right after reaching yielding due to their low displacement ductility, leading to the loss of support of the beam and therefore increasing the collapse rate of the investigated structural typology.

Keywords: precast industrial buildings, modelling assumptions, seismic risk, beam-to-column connections, dowel connections, overhead crane

OPEN ACCESS

Edited by:
Massimo Latour,
University of Salerno, Italy

Reviewed by:
Alessia Monaco,
Polytechnic University of Turin, Italy
Saverio Spadea,
University of Dundee, United Kingdom

****Correspondence:***
Andrea Belleri
andrea.belleri@unibg.it

Specialty section:
This article was submitted to Earthquake Engineering, a section of the journal Frontiers in Built Environment

Received: *16 November 2020*
Accepted: *18 February 2021*
Published: *20 April 2021*

Citation:
Bressanelli ME, Bellotti D, Belleri A, Cavalieri F, Riva P and Nascimbene R (2021) Influence of Modelling Assumptions on the Seismic Risk of Industrial Precast Concrete Structures. Front. Built Environ. 7:629956. doi: 10.3389/fbuil.2021.629956

INTRODUCTION

The last earthquakes in Italy, particularly the ones that struck Emilia Romagna region (Northern Italy) in 2012, highlighted major vulnerabilities in reinforced concrete (RC) precast industrial buildings designed before the entry into force of modern anti-seismic provisions and accurate seismic zonation of the Italian territory (Belleri et al., 2015a; Belleri et al., 2015b; Ercolino et al., 2016; Bournas et al., 2014; Magliulo et al., 2014; Minghini et al., 2016; Nastri et al., 2017; Palanci et al., 2017; Savoia et al., 2012; Toniolo and Colombo, 2012). The main collapses observed were due to failure of the RC fork supporting the beams, the development of short columns due to ribbon glazing, or to the

loss of support of the main structural elements due to under-designed or friction-based connections (Brunesi et al., 2015; Casotto et al., 2015; Demartino et al., 2018; Titi et al., 2018; Bosio et al., 2020). On the beam-to-column faying surface, a neoprene bearing pad is generally included both for spreading the vertical load and to allow for thermal expansions; the neoprene pads lead to a reduction of the coefficient of friction from 0.5, typical of concrete-to-concrete contact, to values also in the order of 0.1 (Magliulo et al., 2011), therefore facilitating relative displacements during earthquakes. Another observed failure is the fall of perimetral cladding elements, generally RC precast panels, due to the failure of their mechanical connections, which were under-designed to sustain the in-plane deformation demand and the out-of-plane loads arising in the system as the results of flexible diaphragms (Scotta et al., 2015; Belleri et al., 2016; Belleri et al., 2017a; Dal Lago et al., 2018).

In Italy, in the field of industrial buildings, RC precast buildings are broadly employed given their capability of covering large spaces, the high-quality standards on materials and elements, and the reduction of construction time if compared with ordinary RC buildings. Precast industrial structures are also characterized by a low displacement ductility if compared with typical RC buildings due to the higher inter-story height. They are commonly built following simple structural schemes, with columns fixed at the base and behaving as cantilever beams placed into socket foundations or connected to the foundation through mechanical devices (Belleri and Riva, 2012; Dal Lago et al., 2016). In modern precast buildings, the beams are generally simply supported and dowel connections are employed (Clementi at al., 2016; Magliulo et al., 2014; Zoubek et al., 2015; Kremmyda et al., 2017). In general, one or two dowels are embedded in the upper part of the column and inserted in pass-through holes, filled with mortar, within the beam. The adopted connections play a crucial role in the seismic response of precast buildings (Bressanelli et al., 2019; Cimmino et al., 2020): beam-to-column connections, in particular, influence the global response of the structure, altering substantially its behavior in terms of deformability and ductility.

The present work aims to assess the influence of different finite element modelling approaches on the probability of failure of precast industrial buildings. At this regard, a case study resembling a typical precast industrial building was selected and a multiple-stripe analysis was carried out. The current research is part of an Italian national project, namely RINTC (Bracchi et al., 2019; Cantisani and Della Corte, 2019; Iervolino et al., 2019; Magliulo et al., 2019; Ragni et al., 2019; Ricci et al., 2019), aiming at assessing the failure rate of various construction typologies designed in accordance with modern anti-seismic regulations (specifically the Italian building code, NTC18, 2018), therefore estimating the implicit risk of code-conforming buildings. Specifically, the comparison of the collapse rates of the investigated comprehensive 3D model with models accounting for simplified assumptions (such as those used in the RINTC project) allows validating the simplifying assumptions, such as in the case of the dowel beam-to-column connections, in order to obtain good estimates of the structural failure rate while reducing the computational effort.

Starting from the work of Bressanelli et al. (2019) and Magliulo et al. (2018), this research moves further by: investigating two different hysteretic models for the beam-to-column connections, such as the hysteretic uniaxial material model (Sousa et al., 2020) and the Modified Ibarra-Medina-Krawinkler Deterioration model (Lignos and Krawinkler, 2011); explicitly modelling the cladding panels in a pendulum configuration; removing the hypothesis of rigid diaphragm by introducing the roof elements and three types of beam-to-roof connections, namely hot-rolled, cold-formed and welded; explicitly modelling the overhead crane and the oscillating payload. The building collapse rates obtained from the comprehensive 3D model allowed to validate the collapse rates obtained from previous simplified analyses.

CONSIDERED CASE STUDY

The considered case study is a single-story four-bay precast RC industrial building supposed located at L'Aquila (Italy). The span length along the transverse x-direction and the longitudinal y-direction are 15 and 6 m, respectively (**Figure 1**). The structural elements have been designed according with the Italian building code (NTC18, 2018). For further structural verifications, not available or not fully addressed in the Italian building code, Eurocode 2 (CEN, 2004), Eurocode 3 (CEN, 2004), CNR 10018/99 and CNR 10025/98 provisions were considered, particularly in respect to dowel capacity. Other details regarding the geometry of the selected case study may be found in Magliulo et al. (2019).

The lateral force resisting system is constituted by precast RC square columns (60 × 60 cm) fixed at the base. The concrete grade is C45/55 (characteristic cylindrical strength at 28 days equal to 55 MPa) and the steel grade is B450C (characteristic yield stress equal to 450 MPa). The columns have a longitudinal reinforcement ratio equal to 2.5% and are connected through dowels to double-tapered prestressed beams. The dowel connection is considered effective only in the transverse direction due to the presence of a RC fork at the top of the column inhibiting the beam movements in the longitudinal direction. The height of the column is 6 m, a corbel supporting the overhead crane is located at height equal to 4.5 m. The beams are double-tapered with 10% slope and they are characterized by a I-shaped cross-section with varying web dimensions. The longitudinal gutter beams, hatched in **Figure 1B**, have a rectangular cross section (0.3 × 0.5 m) and provide a support to the cladding system. The roof is made by precast double-tee elements. A cast in place RC topping (5 cm thickness) is considered when evaluating the influence of a rigid diaphragm. The cladding system consists of vertical precast panels connected to the longitudinal girder beams; the panel weight per unit surface is 4 kN/m^2. An overhead-crane with a pay load equal to 80 kN is also considered with HE400A runway beams. For this structural typology, the structural behavior factor

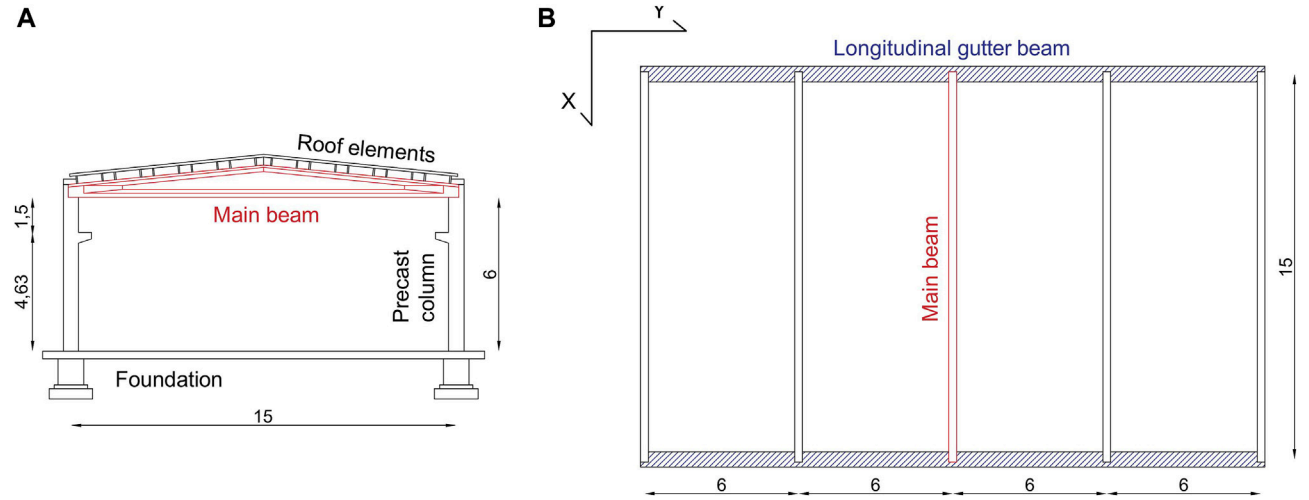

FIGURE 1 | Building cross section **(A)** and plan view **(B)**. Note: the dimensions are expressed in meters.

considered in the design is equal to 2.5 for "low ductility class" (NTC18, 2018).

MODELLING AND ANALYSIS

Numerical models were created in the OpenSees software (McKenna et al., 2000). Initially a planar frame was taken as reference and simplified models were developed to preliminary evaluate the seismic influence of modelling assumptions, such as the mass location, i.e. distributed or lumped in a single point at the centre of the plane diaphragm, the beam-to-column connection, i.e. perfectly hinged or with a non-linear hysteresis, and the presence of an overhead crane.

Subsequently, 3D models were created to validate the results of the planar models and to investigate additional aspects such as the roof-to-beam connections and the precast cladding system; the latter was considered both as lumped masses at the panel-to-structure connections or explicitly modelled. For all the analyses a tangent stiffness Rayleigh damping was adopted with 5% relative damping at 0.5 and 2s. No damping was applied at the connection level which were modelled as zero-length elements.

2D Simplified Models

Nine simplified numerical models representative of a portal frame were developed for preliminary multiple-stripe analyses:

– Model SA1: non-linear beam-to-column connections and distributed masses;
– Model SA2: hinged beam-to-column connections and distributed masses;
– Model SA3: non-linear beam-to-column connections with Coulomb friction and distributed masses;
– Model SA4: non-linear beam-to-column connections and lumped mass;
– Model SA5: hinged beam-to-column connections and lumped mass;
– Model SA6: non-linear beam-to-column connections, distributed masses and crane model;
– Model SA7: non-linear beam-to-column connections with Coulomb friction, distributed masses and crane model;
– Model SA8: elastic-perfectly-plastic beam-to-column connections and distributed masses;
– Model SA9: linear elastic beam-to-column connections and distributed masses.

The columns were fixed at the base. The main beams and the girders were modelled with elastic elements; a constant cross section was assigned to the double-tapered beams as the mean value of the variable height and width. The cladding panels were only included in terms of mass and gravity loads applied to the main structure. This is in accordance with the hypothesis that the cladding panels are connected to the structure with an isostatic pendulum connection arrangement (Toniolo and Dal Lago, 2017). The non-linear behavior of the structural elements was modelled considering a lumped plasticity approach with plastic hinges at the column bases and elastic column elements. The column curvature and the yielding moment were obtained from a fiber analysis of the column cross-section. The plastic hinge was modelled with a zero-length element considering the Modified Ibarra-Medina-Krawinkler Deterioration Model with peak-oriented hysteretic response (Fischinger et al., 2008): effective yield moment M_y equal to 1256 kNm, effective stiffness Ke equal to 4.37·104 kN/m and cyclic deterioration parameter λ equal to 2.734.

The seismic masses were lumped at the centre of the roof diaphragm or distributed to the various elements. In the first case, the lumped mass (M_C) was equal to 44.6 kN/g and 35.6 kN/g in the horizontal and vertical direction, respectively. The lower value in the vertical direction was due to the absence of the cladding panel mass which does not participate in the seismic response in

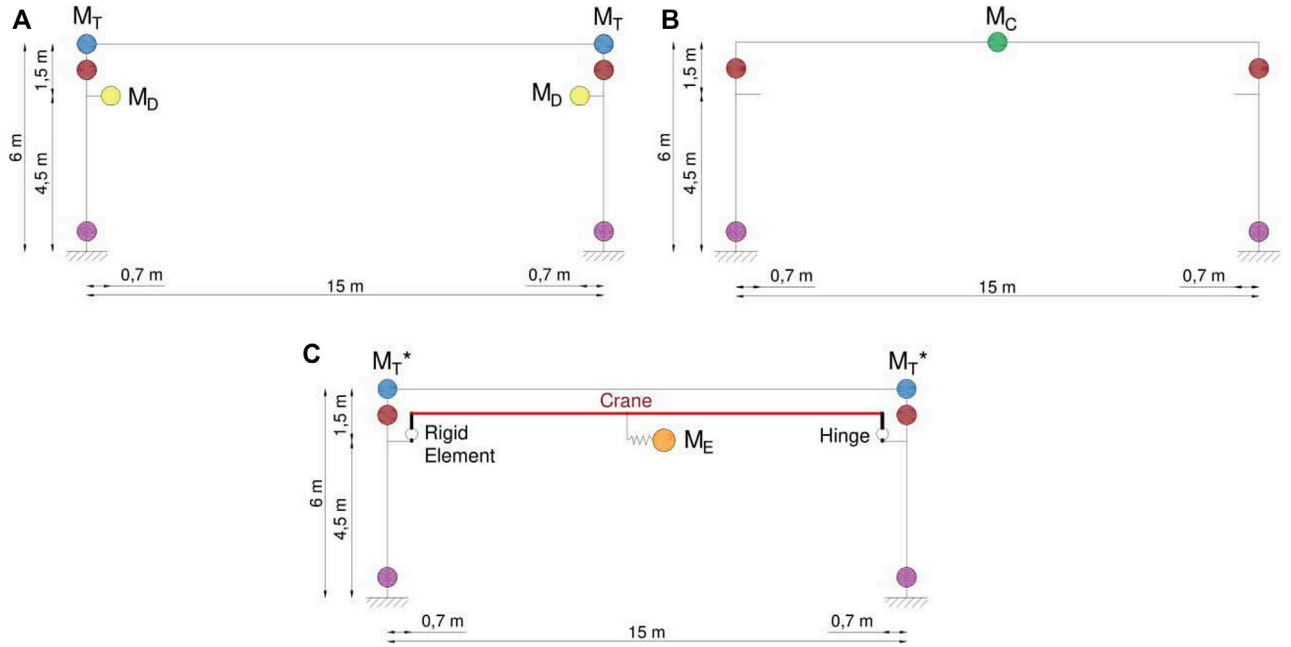

FIGURE 2 | Simplified models with distributed masses **(A)**, lumped mass at the centre of the roof **(B)** and distributed masses and crane load **(C)**. Note: The purple circle represents the plastic hinge at the base of the column, the red circle indicates the position of the beam-to-column connection, the yellow circle represents the mass M_D at the corbel position, the green circle represents the lumped mass M_C, the orange circle represents the mass of the payload crane M_E and the blue circle indicates the roof mass M_T (in the model (C) the blue circle represents the mass M_T minus the mass of the crane, indicated as M_T*).

this direction. In the second case, two sets (M_D and M_T) of distributed masses were defined: the mass M_D (1.329 kN/g), placed at each corbel, corresponds to an equal distribution among the columns of the crane mass (5 kN/g) and of 80% of the crane payload; the mass M_T, placed at the top of each column, is the mass of the roof system equal to 28.9 kN/g and 37.90 kN/g in the vertical and horizontal direction, respectively. In the case of explicit modelling of the overhead crane, the crane payload (M_E) was set equal to 8 kN/g.

The influence of the overhead crane modelling was assessed in two ways: in the first case, the crane was modelled only in terms of mass (M_D in the case of model with distributed masses or as part of M_C in the case of model with lumped mass in the diaphragm centroid); in the second case, the overhead crane was modelled with an elastic element with adequate stiffness connected to the runway beams, while the mass M_E of the payload was connected to the middle of the overhead crane through an elastic spring with stiffness equal to $M_E \cdot g/R$ (Belleri et al., 2017b). R is the assumed length of the cable, equal to half the column height (i.e. 3 m). The simplified models are represented in **Figure 2**.

Beam-to-Column Connection

Different types of beam-to-column connection modelling were considered (Kramar et al., 2010; Soroushian, 1987; Zoubek et al., 2014; Capozzi et al., 2011): hinged, elastic, elastic-perfectly plastic and non-linear hysteresis (**Figure 3**). All types of connections have been modelled as zero-length elements at the top of the column. The non-linear beam-to-column connections were designed following a shear demand resulting from capacity design and a shear strength resulting from the following formulation (Tassios and Vintzeleou, 1987; Psycharis and Mouzakis, 2012; Kremmyda et al., 2017):

$$V_{Rm} = n \cdot \alpha \cdot d_b^2 \sqrt{f_{ym} \cdot f_{cm}} \quad (1)$$

where n represents the number of dowels, d_b the dowel diameter, f_{ym} is the mean yielding value of the dowels, f_{cm} is the concrete mean

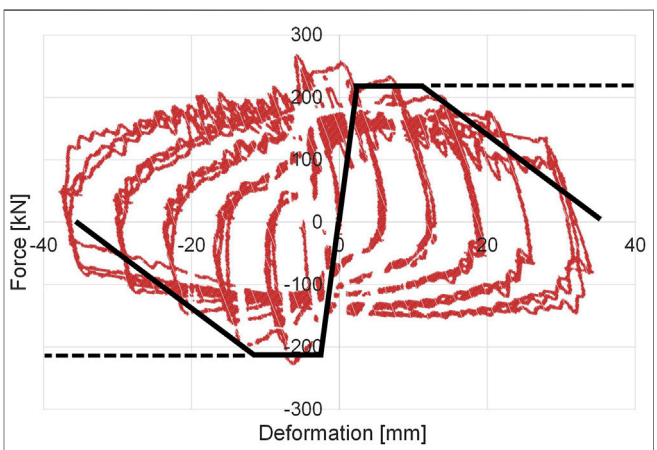

FIGURE 3 | Comparison of the analytical and experimental force-displacement diagrams of the dowel connection. Note: the red dots indicate the experimental results (Kremmyda et al., 2014), the black lines indicate the analytical model used in the finite element analysis.

compression strength and α is a reduction factor (Magliulo et al., 2014; Zoubek et al., 2015). For this specific case, f_{ym} is equal to 816 MPa and f_{cm} is equal to 60 MPa. The connections have been designed with a coefficient α equal to 1.6 according to CNR10018 (1999) and CNR10025 (1998) and have been checked against failure with the formulation provided in the design guidelines of the Safecast project (Negro and Toniolo, 2012) with a coefficient α equal to 0.9. The design process led to two steel dowels with 24 mm diameter for each joint. The stiffness of the beam-to-column dowel's connection was derived according to Ferreira and El Debs (2000):

$$\lambda = \frac{1}{K} = \left[\frac{nE_s \cdot \pi \cdot d_b^4}{64} \cdot \left(\frac{t_n^3}{12} + \frac{1}{3.5 \cdot a_g^3} + \frac{1}{3.5 \cdot a_{cls}^3}\right)^{-1} + \frac{G_n \cdot (b \cdot h)_n}{t_n}\right]^{-1} \quad (2)$$

where the subscripts *n*, *cls*, and *g* indicate neoprene, concrete and grout, respectively. The yield displacement was computed as:

$$d_y = \lambda \cdot F_y \quad (3)$$

with F_y derived from **Equation 1** (i.e., V_{Rm}). The resulting yield displacement of the considered beam-to-column connection is 2.8 mm.

The beam-to-column connection hysteresis was defined in accordance with the experimental results of cyclic tests reported in Kremmyda et al. (2014): the capping displacement was conservatively assumed equal to half the dowel diameter, i.e. 12 mm, while the ultimate displacement capacity equal of 1.5 times the dowel diameter, i.e. 36 mm. The OpenSees hysteretic uniaxial material model according with Sousa et al. (2020) and the Modified Ibarra-Medina-Krawinkler Deterioration model (Lignos and Krawinkler, 2011) were adopted and compared. For the hysteretic uniaxial material model, the following parameters were considered (according to Fischinger et al., 2013): damage1 equal to 0, damage 2 equal to 0.06, pinchX and pinchY equals to 0.5 and beta equal to 0. Such parameters allow adjusting the strength degradation, pinching effects and unloading stiffness of the constitutive model. **Figure 3** shows the comparison of the analytical and experimental force-displacement diagrams of the dowel connection.

Finally, the possible presence of friction in the beam-to-column connection was considered using a Coulomb model with friction coefficient μ equal to 0.1337 and initial stiffness k_{init} equal to 490 kN/m, corresponding to the lateral stiffness of the neoprene pad.

3D Complete Models

3D models of the entire reference building were developed. As for the simplified models, the beams (both the transversal main beams and the longitudinal secondary beams) were modeled as elastic elements. The columns were modeled following the same lumped plasticity approach of the planar models with the same parameters of the "Krawinkler-Ibarra-Medina Deterioration Model with Peak-Oriented Hysteretic Response" (Fischinger et al., 2008). The seismic masses were lumped at the centre of the roof diaphragm or distributed to the various elements as before. In the first case, the lumped mass (M_C) was equal to 425.3 and 287.5 kN/g in the horizontal and vertical direction, respectively. The lower value in the vertical direction was due to the absence of the cladding panel mass which were considered directly supported by the ground. In the second case, a distributed masses approach was adopted with the same mass values of the planar model previously described.

The beam-to-column connection was modeled in three different ways: perfectly hinged, linear elastic and non-linear hysteresis connections. The Krawinkler-Ibarra-Medina Deterioration hysteretic model was selected in the 3D models on the basis of the results obtained from the planar frame analyses. The presence of the overhead crane was considered either only in terms of masses (models MA1, MA2, MB1, MB2, MC1, and MC2) or with an explicit modeling (models MA3, MB3, MC3, and ME1). **Figure 4** shows the model of the overhead crane with the same parameters adopted in the simplified models.

The precast cladding system was modelled either in terms of lumped masses or by two explicit modeling approaches. In the first explicit modelling approach (MC4 model), the whole cladding system was modelled by placing a single beam element with 15 subdivisions (12 and 19.2 kN/g·m mass per unit length in the transverse and longitudinal direction, respectively) hinged connected to the ground and to the roof centroid. In the second explicit modelling approach, model ME1 in **Figure 5**, the cladding panels of each bay were modelled by a single element hinged connected at the ground and at the center line of each span, similarly to what carried out in the first explicit modelling approach. The related distributed mass per unit length was in accordance with a RC panel thickness of 12 cm.

The considered models are:

– Model MA1: hinged beam-to-column connections and distributed masses;
– Model MA2: hinged beam-to-column connections and lumped mass;
– Model MA3: hinged beam-to-column connections, distributed masses and explicit modeling of the overhead crane;
– Model MB1: elastic beam-to-column connections and distributed masses;
– Model MB2: elastic beam-to-column connections and lumped mass;
– Model MB3: elastic beam-to-column connections, distributed masses and explicit modeling of the overhead crane;
– Model MC1: non-linear beam-to-column connections and distributed masses;
– Model MC2: non-linear beam-to-column connections and lumped mass;
– Model MC3: non-linear beam-to-column connections, distributed masses and overhead crane;
– Model MC4: non-linear beam-to-column connections, distributed masses, overhead crane and cladding panels;
– Model MD1: hot rolled beam-to-roof element connections and distributed masses;
– Model MD2: cold formed beam-to-roof element connections and distributed masses;

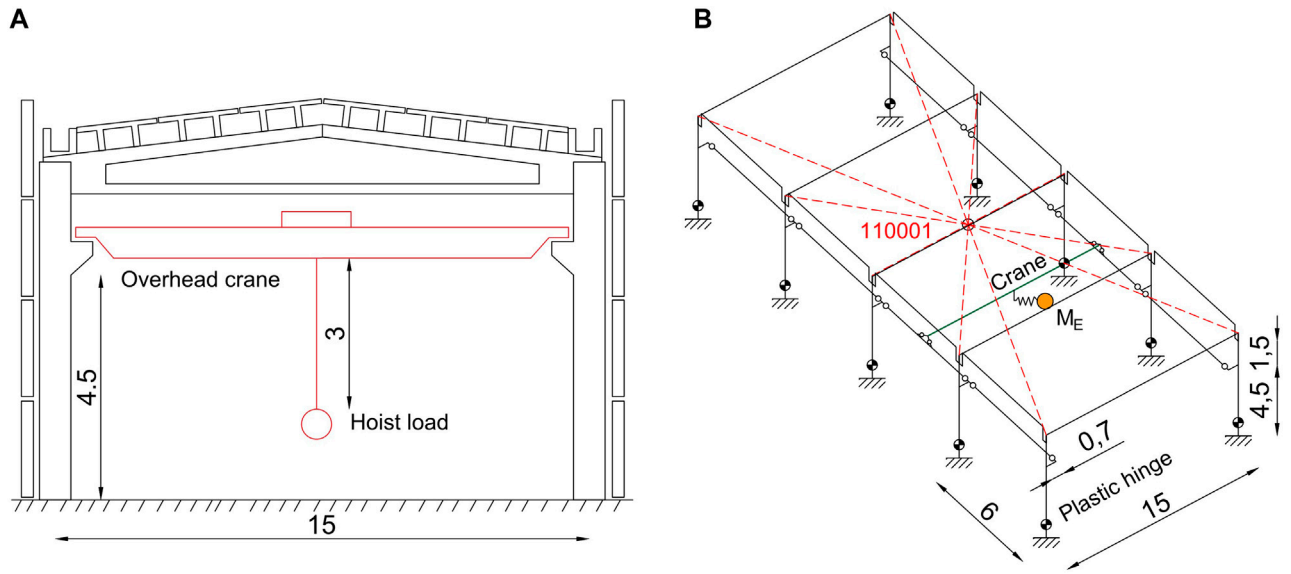

FIGURE 4 | Building section drawing with overhead crane **(A)** and schematic view of models MA3, MB3 and MC3 **(B)**. Note: in the right figure, the empty dots indicate the position of the hinges in the modelled structure with OpenSees and the number 110001 in the centre indicates the degree of constraints of the diaphragm floor, i.e. no relative displacements in the horizontal plane.

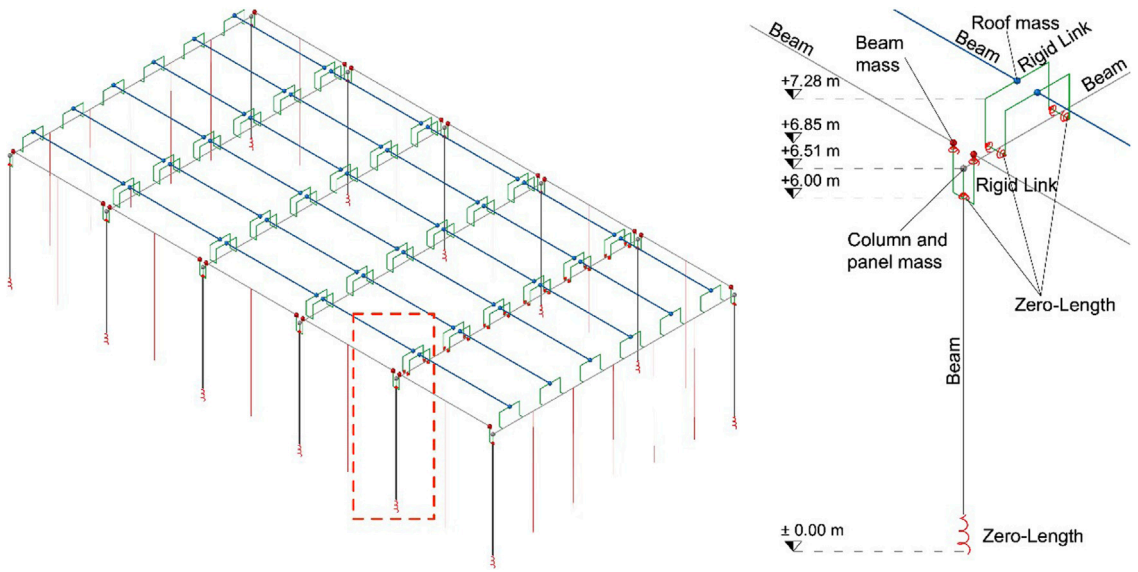

FIGURE 5 | Schematic view of models ME1 and detail of the connections (close-up on the dashed red box). Note: in the left-side figure the red vertical lines indicate the position of the elements introduced to capture the seismic effects of the cladding system.

– Model MD3: welded beam-to-roof element connections and distributed masses;
– Model MD4: rigid beam-to-roof element connections and distributed masses;
– Model ME1: non-linear beam-to-column connections, distributed masses, hot-rolled beam-to-roof element connections and cladding panels.

Roof Element-to-Beam Connections

Two possible roof modeling methods were considered: a rigid diaphragm approach and the explicit modeling of the roof elements and of their connections (Dotreppe et al., 2006; Felicetti et al., 2008a; Beconcini et al., 2008; Felicetti et al., 2008b; Beconcini et al., 2009; Dal Lago et al., 2012). In the latter case, the double-tee roof elements were modeled as

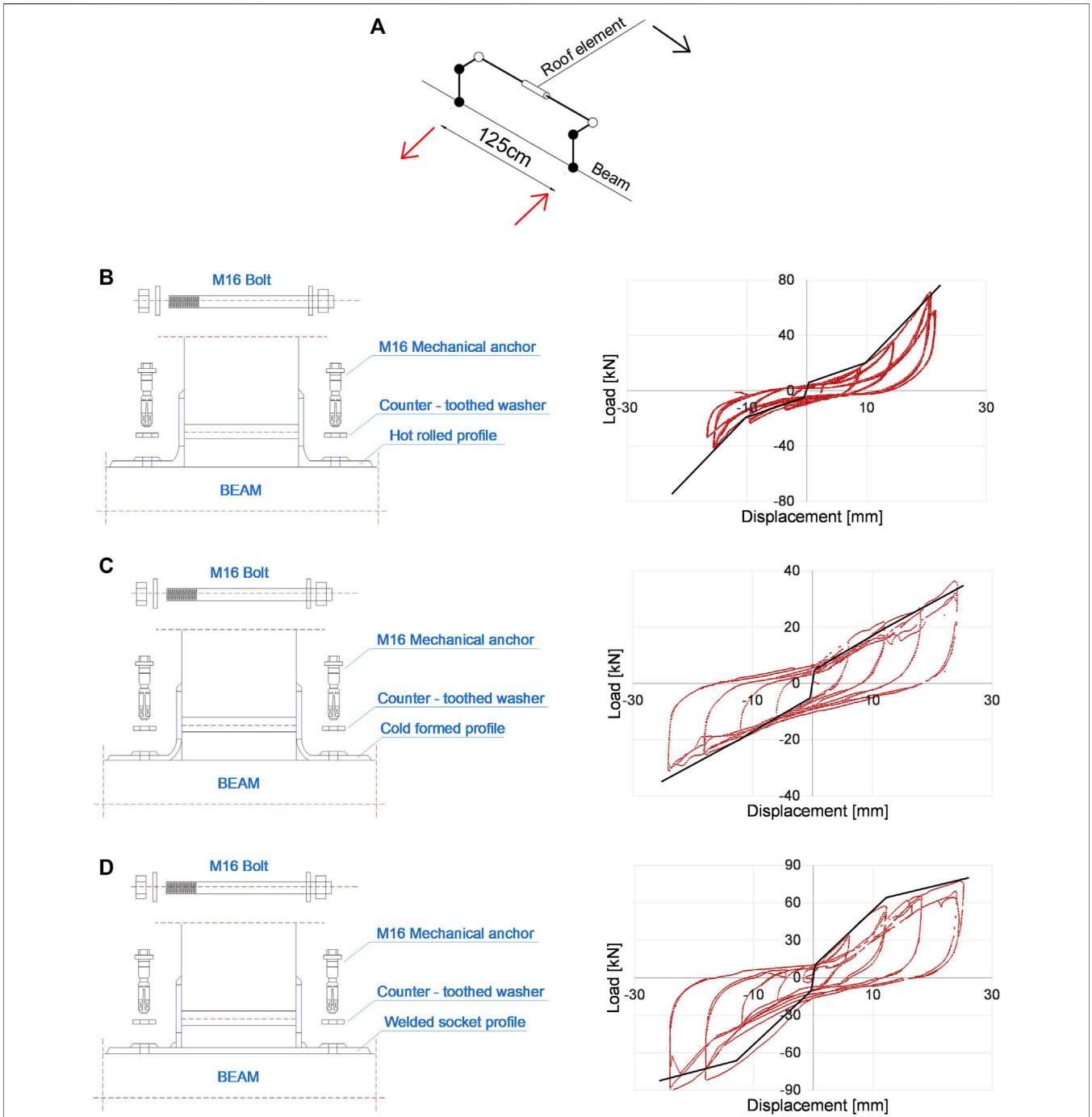

FIGURE 6 | (A) Rigid link arrangement for the connection of the roof double-tee beam element to the supporting beam; the empty dots indicate the position of the hinges, the full dots indicate the position of the rigid connections and the thick lines indicate the rigid link in the modelled structure with OpenSees.Considered connections: hot-rolled **(B)**, cold-formed **(C)** and socket welded **(D)**.

beams connected to the main beam by means of rigid links (**Figure 6A**) which behaves as a cylindrical hinge in the vertical plane and a rigid connection in the horizontal plane. The in-plane stiffness of the roof is associated with the torque that is transferred to the base of the links, which represent the ribs of the double-tee roof elements; such stiffness is directly related to the stiffness of the roof element-to-beam connections. This modelling approach is able to capture the real in-plane stiffness of the roof for both new and existing buildings.

The connection between the double-tee roof element and the beam is made by two steel angle profiles located at the base of each rib of the roof element. Three types of connections were considered

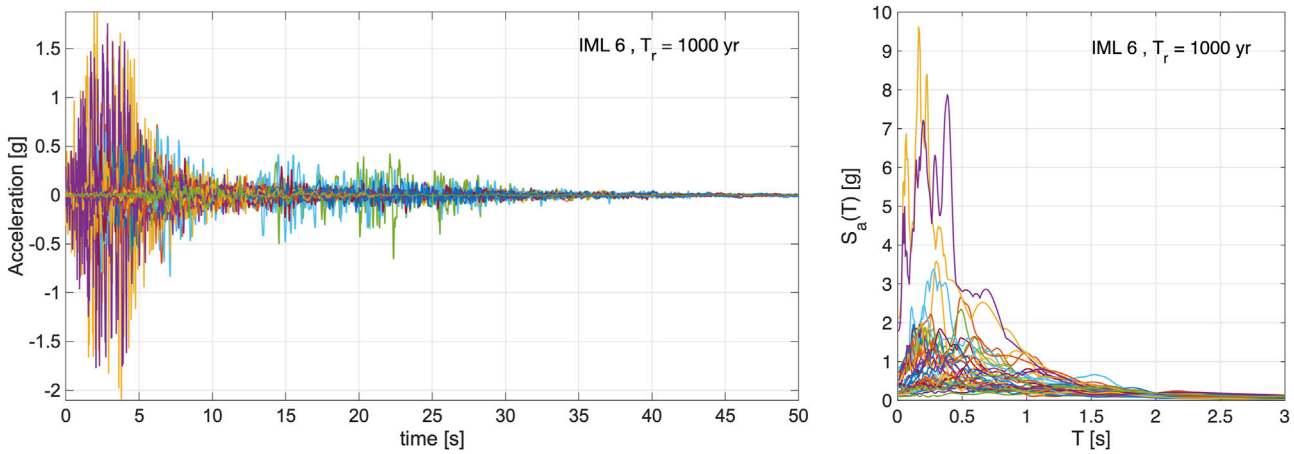

FIGURE 7 | Selected scaled records (both components) for the stripe at Tr = 1,000 years, in terms of **(left)** time histories and **(right)** response spectra.

(Dal Lago and Ferrara, 2018): hot rolled, cold formed and welded socket with M16 anchor bolts. The hysteresis of the connections was analytically reproduced using the non-linear OpenSees solver combined with Matlab (Matlab, 2019) (**Figure 6**). The connections were modeled in OpenSees through a MultiLinear Material in terms of load and relative displacement.

The connection failure occurs when the maximum displacement recorded in the experimental tests is reached. The roof element remains connected to the beam after the collapse, but with a connection stiffness equal to zero. At this regard, the relative displacement of the two nodes of the connection was checked in a step-by-step basis during the analysis: if such displacement exceeds the allowable displacement, the zero-length element associated with the connection is removed and a new zero-length elastic element with stiffness approximately equal to zero is placed between the two nodes.

Regarding the connection modelling, zero-length elements are placed at the base of the vertical rigid links of the roof elements (**Figure 6A**). In the longitudinal direction, i.e. along the roof element, the hysteresis depicted in **Figure 6** was considered, while in the transverse direction an elastic behaviour with high stiffness was implemented.

Definition of the Seismic Input

The multiple-stripe analysis (MSA) method (Jalayer, 2003; Jalayer and Cornell, 2009) was adopted herein among the available approaches used to retrieve fragility curves and associated collapse probabilities. Within MSA, a number of nonlinear dynamic analyses were carried out with records scaled at ten increasing levels (i.e., the stripes) of $Sa(T_1)$ [0.011; 0.026; 0.049; 0.08; 0.124; 0.184; 0.27; 0.379; 0.572; 1.077] g, corresponding to return periods T_r [10; 50; 100; 250; 500; 1,000; 2,500; 5,000; 10,000; 100,000] years, respectively. The fundamental period of the considered precast structure is T_1 = 2s. Hazard-consistent record selection was employed. In particular, at each stripe, both horizontal components of 20 records were selected through disaggregation of seismic hazard and matched with target spectra conditioned on the ten intensity measure (IM) levels, using the Conditional Spectrum method (Baker, 2011).

Figure 7 shows the time-histories and response spectra of both components of the 20 records selected at the 6th stripe (i.e., intensity measure level, IML, 6), related to a 1,000-years return period, scaled at $Sa(T_1)$ = 0.184 g. The considered values of $Sa(T_1)$ are those related to the site of L'Aquila, with soil type C and topographic category T_1, according to the Italian code (NTC18, 2018). These values, as well as the ones related to other Italian sites and soil types considered within the RINTC project (RINTC Workgroup, 2018), can be found in the work by Cimmino et al. (2020). The selected records were extracted from the Italian accelerometric archive (Luzi et al., 2008) and from the NGAwest2 database (Ancheta et al., 2014).

NUMERICAL RESULTS

2D Simplified Models

The failure rate of the building could be associated with both local collapses (i.e. related to the loss of support of the beam) and global collapse. Considering local collapses, different assumptions apply based on the type of the beam-to-column connection modelling. For non-linear modeling, the failure is considered related to the achievement of the maximum relative displacement of the connection, set herein equal to $1.5 \cdot d_b$ (where d_b is the diameter of the dowel), i.e. 36 mm. As it will be highlighted in the following, it is worth to note that the beam displacement increases in such a way to lead to the loss of support after the failure of the connection. For linear modelling, the failure is considered when reaching the shear capacity, equal to 230 kN (V_{max}). Regarding the global collapse, the failure was considered related to a lateral displacement corresponding to a 50% reduction of the total base shear, obtained from a non-linear static analysis. Depending on these considerations, **Figure 8** shows the number of analyses leading to a local collapse for each seismic intensity and for each model.

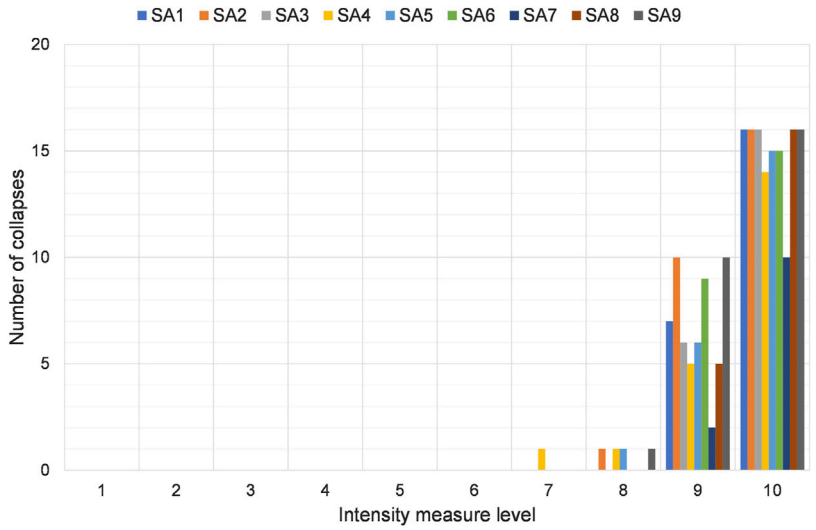

FIGURE 8 | Number of analyses leading to local collapses in the 2D models.

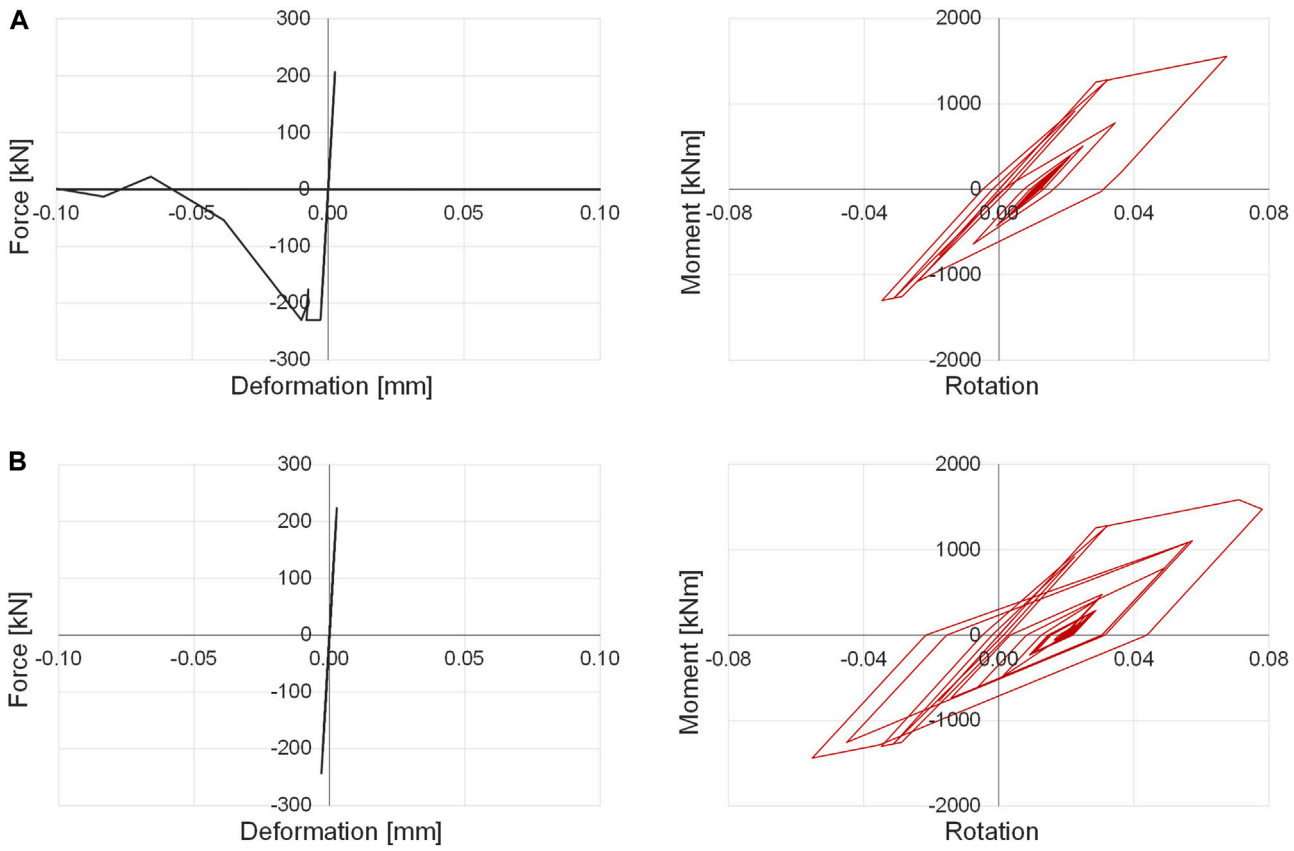

FIGURE 9 | Time history results in the case of elastic **(A)** and non-linear **(B)** beam-to-column connection. The left-side refers to the beam-to-column connection hysteresis, while the right side refers to the base column plastic hinge.

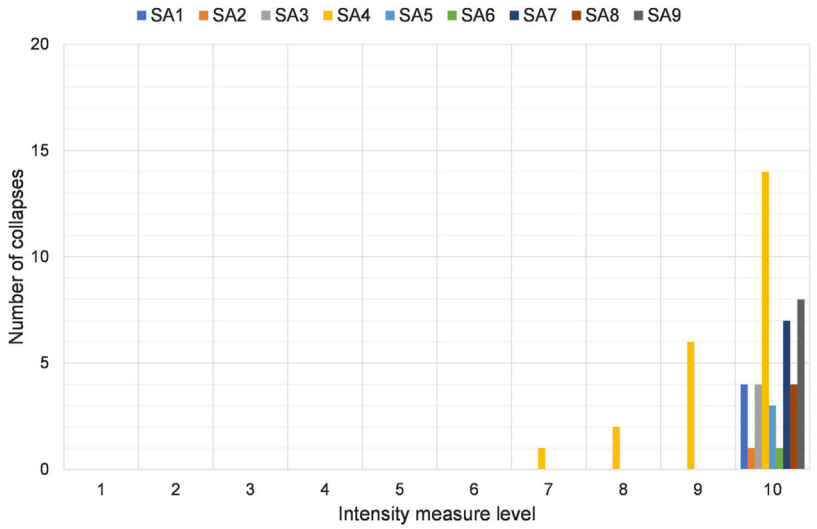

FIGURE 10 | Number of analyses leading to a global collapse in the 2D models.

The models with non-linear beam-to-column connections shown in **Figure 8** refer to modelling with the Krawinkler-Ibarra-Medina deterioration model. The use of the hysteretic uniaxial material model, in place of the aforementioned degradation model, causes a limited increase in the number of collapses in the case of lumped masses due to the increased stress in the dowels (model SA4). The other models are characterized by a similar number of collapses. For this reason, the Krawinkler-Ibarra-Medina deterioration model was used in the analyses of the 3D models. Two possible failure conditions have been considered when the beam-to-column connection hysteresis is accounted for: the relative displacement corresponding to the loss of support of the beam, and the failure of the beam-to-column connection. It is observed that the only difference among these two types of failure conditions occurs only for the seismic intensity level 9 in Model SA3 (i.e. Krawinkler-Ibarra-Medina deterioration model for the beam-to-column connection, Coulomb's friction and distributed masses), where seven collapses are recorded instead of six. These results show that the connections move directly from the elastic stage (or yield stage) to its failure by developing high relative displacements leading to the loss of support of the beam. It is also noted that there are no cases in which the beam-to-column connection is in the softening zone. This was also observed by introducing a strain hardening in the post-yield range.

The results of two different models of the beam-to-column connection are showed on the left side of **Figure 9**, a non-linear (a) and an elastic (b) connection, respectively. The same figure, on the right side, shows the corresponding moment-rotation curves of the plastic hinges at the base of the column. In the case with elastic beam-to-column connection (a), the demand on the column is greater than in the case with a non-linear connection (b) because in such model the connection can reach higher values (exceeding its capacity 230 kN).

Figure 10 shows the number of analyses leading to global failure for each seismic intensity and for each model. The global results for the models SA2, SA5, SA8, and SA9 are not significant because they are characterized by beam-to-column connections modelled with hinged, elastic-plastic or perfectly elastic models. In general, global collapses occur only at the highest seismic intensity. An exception is observed for Model SA4 (non-linear beam-to-column connections, lumped masses at the centre of the roof), where the lumping of the mass at the roof center caused an increase of the demand both in local and global terms.

3D Complete Models

Initial evaluations were carried out on models MA, MB and MC. Non-linear static analyses were performed with a lateral load distribution according to the fundamental mode of vibration in each of the principal directions. **Figure 11** shows the capacity curves of the 3D complete models. In **Figure 11B** (corresponding to a capacity curve for a loading direction perpendicular to the main beams) a lower initial stiffness is observed in the lumped mass models (A2, B2 and C2) as a result of the different height of the lateral loads. This difference is not observed in the transverse direction.

Figure 12 shows the number of analyses leading to a local collapse for each seismic intensity and for each model. The same local failure assumptions made in the previous section were considered.

For the higher seismic intensities, it is possible to observe a clear correlation, in terms of number of local collapses, between the various models. In general, the number of collapses increases for models with lumped masses (MA2, MB2, MC2) compared with models with distributed masses (MA1, MB1, MC1). This trend is even more significant at the seismic intensity level 9 with $Sa(T_1)$ equal to 0.572 g. For the lower seismic intensities, the local behavior of the connections is generally similar among the various models. The models with elastic beam-to-column

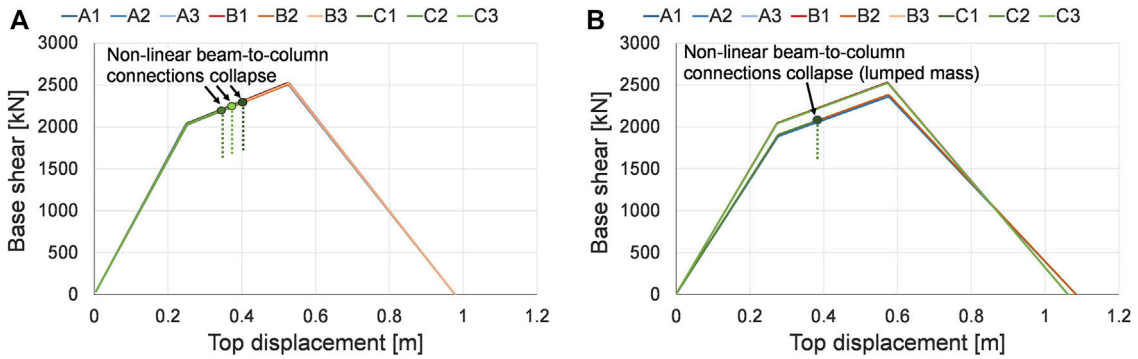

FIGURE 11 | Capacity curves of the 3D complete models in the transverse **(A)** and longitudinal **(B)** direction.

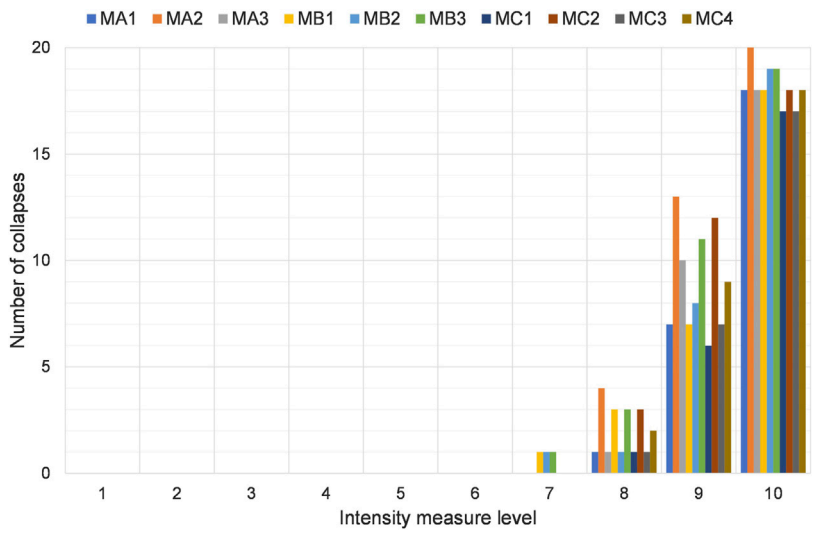

FIGURE 12 | Number of analyses leading to a local collapse in the 3D models (MA, MB and MC).

connections are the only ones showing collapses at seismic intensity level 7, where Sa(T_1) is equal to 0.27 g.

Considering global collapses (**Figure 13**), the models are characterized by similar results. The collapses are slightly higher in models characterized by a lumped mass at the centre of the roof diaphragm (MA2, MB2, MC2). Models with non-linear beam-to-column connections and lumped masses, i.e. MC2, or distributed masses and overhead crane load, i.e. MC3, are the only ones with global collapses for lower seismic intensities. The results obtained from the analysis of 3D models confirm the results previously obtained for the simplified planar models.

As well as for simplified models, also for the complete 3D models there is a direct transition of the beam-to-column connections from the elastic field to failure. To highlight this aspect, the non-linear behavior of the beam-to-column connection has been divided into four fields (**Figure 14A**): elastic (A), plastic (B), softening (C) and failure (D). For the three highest seismic intensities, the number of cases falling inside these fields are reported in **Figure 14B**. The results clearly show that the beam-to-column connections moves directly from the elastic (A) or plastic (B) field to failure (D).

With regard to the modelling of the beam-to-roof connection, i.e. MD models, the obtained results are reported in **Figure 15**. **Figure 15A** indicates the number of local collapses of the beam-to-roof connection. MD4 is not represented because it is characterized by rigid roof element-to-beam connections. **Figure 15B** indicates the number of global collapses of columns in the x-direction, i.e. the transverse direction. For the global assessment, the maximum displacement capacity is that corresponding to a 50% reduction of the shear at the base of the column (0.818 m). For the local assessment, the maximum capacity is that corresponding to the maximum relative displacement of the roof-to-beam connections, herein assumed equal to 24 mm. When the relative displacement between the roof element and the supporting beam exceeds the support length, the

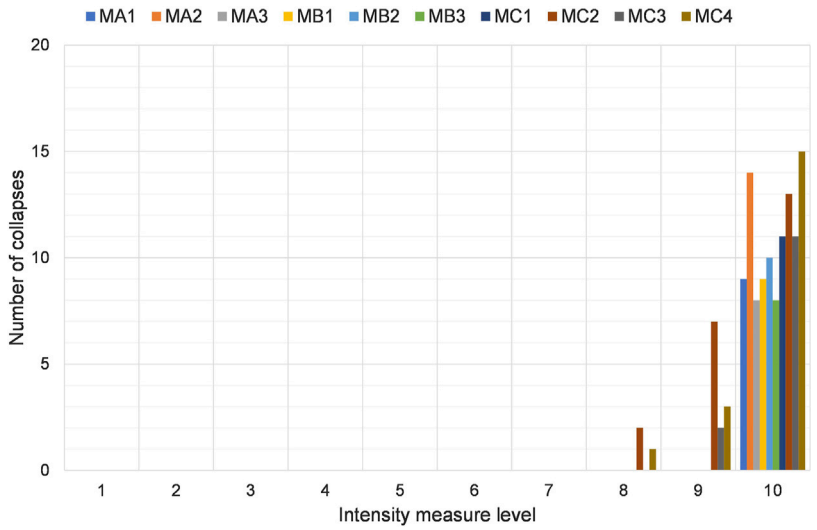

FIGURE 13 | Number of analyses leading to a global collapse in the 3D models (MA, MB and MC).

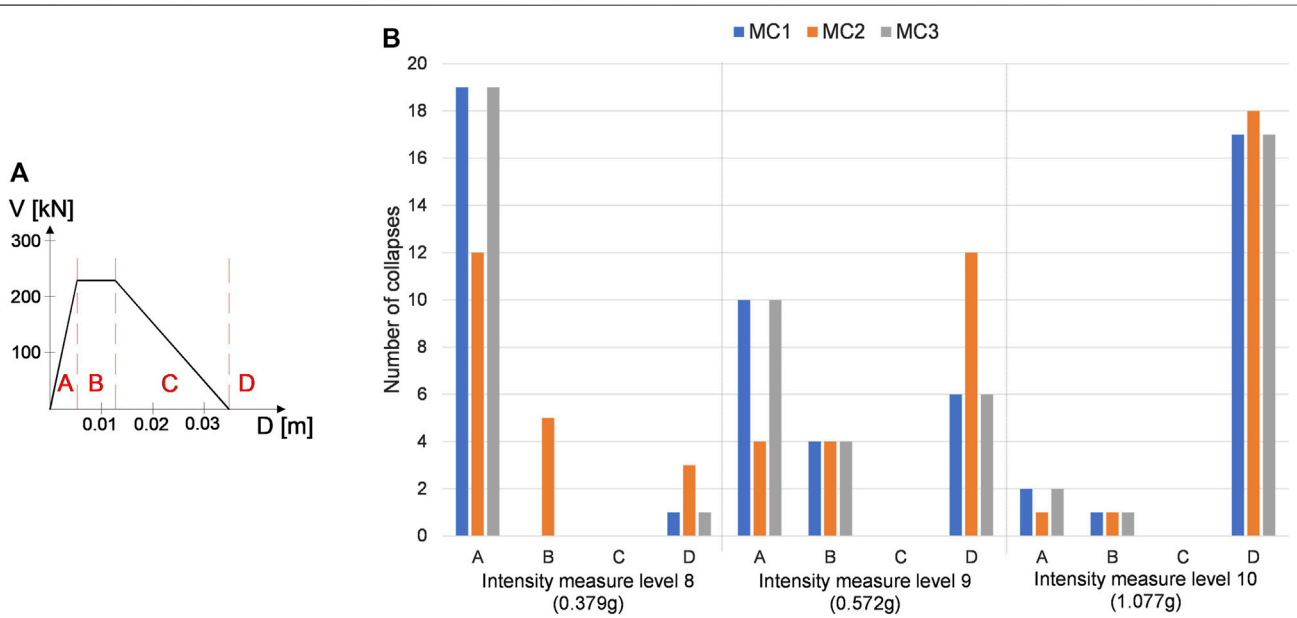

FIGURE 14 | Subdivision of the Krawinkler-Ibarra-Medina deterioration model of the beam-to-column dowel's connection **(A)** and evolution of the number of collapses for the dowel's connection in the tri-dimensional complete models **(B)**.

double-tee unit is considered collapsed and the analysis is stopped. In terms of number of collapses, it is observed that for the present case study there is no significant difference between flexible or rigid diaphragm and that failure at the column base generally foregoes failure at the roof element-to-beam connections.

The last considered model (ME1) is characterized by the simultaneous presence of: beam-to-column connections modelled with the Ibarra-Medina-Krawinkler deterioration model; roof-to-beam connections modelled with a multilinear model; distributed masses at the top of the columns; precast cladding system located along the perimeter of the structure. The results of the analyses are reported in **Figure 15**. The models with the roof elements show collapses for seismic intensities 9 and 10 with $Sa(T_1)$ equal to or greater than 0.572 g. Therefore, the modelling of the cladding system along the perimeter of the structure has led to global and local collapses (at the roof-to-beam connections) for the intensity measure level 9, unlike the MD models where the only collapses occurred for intensity level 10. The analyses also showed that the roof-to-beam connections

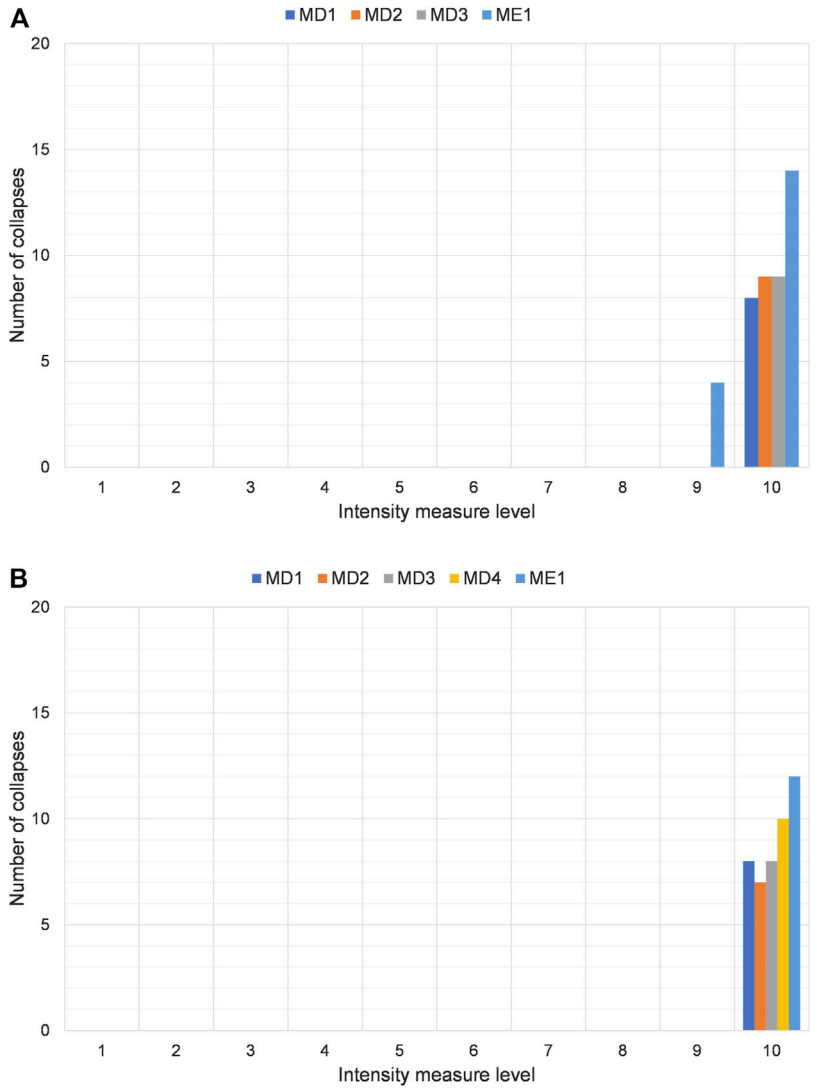

FIGURE 15 | Total number of analyses leading to a local **(A)** and global **(B)** collapse for models MD1, MD2, MD3, MD4 and ME1 (20 ground motions were considered for each intensity measure level).

adopted are effective both in terms of capacity and stiffness, because there are collapses in these connections only for the highest intensity levels.

Finally, the rate of collapses associated with the most comprehensive model (ME1) is obtained from the following equation (Suzuki and Iervolino, 2019):

$$\lambda_f = \int_0^{x_{T_r=10^5}} P\left[failure \middle| IM = x\right] |d\lambda_x| + 10^{-5} \quad (4)$$

where the addition of 10^{-5} is due to the lack of information in the hazard curve beyond 100,000 years; therefore, this formulation leads to a conservative estimate. The fragility parameters of the intensity measure were derived through the R2R_EU software (Baraschino et al., 2020) using the maximum likelihood estimation. The obtained failure rate λ_f is equal to 6.9×10^{-5} in the case of global collapse and 1.1×10^{-4} in the case of collapse of the connections, the corresponding values obtained from previous research with simplified 3D models are 5.8×10^{-5} (Suzuki and Iervolino, 2019) and 1.7×10^{-4} (Iervolino et al., 2018). Therefore, the collapse rate estimation considering local collapse is slightly overestimated compared to the results obtained from detailed models, while the collapse rate estimation considering global collapse is slightly underestimated. It is worth noting that these differences are reasonable and in the same order of magnitude. Therefore, the previous formulation of the building models is suitable for the collapse rate evaluation. The main advantage of detailed 3D models is related to the possibility of detecting local damages in a more comprehensive way suitable, for instance, for a detailed loss assessment (Bosio et al., 2020).

CONCLUSION

The present paper investigated the influence of finite element modelling in the evaluation of the collapse rate of precast industrial buildings, referring in particular to beam-to-column and beam-to-roof connections. A single-story precast industrial building was selected as reference structure and modelled in OpenSees with different assumptions: the overhead crane (modelled explicitly or present only in terms of masses) and the distribution of the overhead crane mass (i.e. equally distributed on each column corbel and with or without accounting for the payload); the beam-to-column connections (i.e. elastic, hinged or dowel connection with a non-linear model); the masses acting on the structure (distributed or lumped at the center of the roof diaphragm); the beam-to-roof connections (i.e. hot-rolled, cold-formed and socket welded). Non-linear dynamic analyses with increasing intensity were carried out for $Sa(T_1)$ ranging from 0.011 to 1.077 g. Each intensity level consists of twenty pairs of ground motions acting in both horizontal directions. Simplified planar models and complete three-dimensional models were considered.

The analyses showed that the complete three-dimensional models reflect the results of the simplified planar models as regards the different modelling of the mass, the beam-to-column connections and the overhead crane. In the case of beam-to-column connections with non-linear hysteresis, it was observed a direct transition of the connections from the elastic or plastic range to the collapse, with no cases in the softening range.

Moving from models with distributed masses toward models with a lumped mass at the roof diaphragm centroid causes a slight increase in the number of collapses, both in global and local terms. The explicit model of the payload of the overhead crane provided limited influence on the results.

The beam-to-roof connections modelling allowed to capture the actual in-plane stiffness of the diaphragm and it is suitable for both existing and new buildings models. The results showed that in the present case study the different types of beam-to-roof connections considered did not affect the results and that the collapse of the connections was generally anticipated by the collapse of the columns.

Regarding beam-to-column connections, various collapses were observed for high intensity levels. The analyses of the model with linear elastic beam-to-column connections and distributed masses showed collapses of several connections for $Sa(T_1)$ equal or higher than 0.379 g. While, in the case of non-linear beam-to-column connections, a high number of collapses is observed only in the case of a lumped mass at the roof level, which causes an increase of the connections demand. It is worth observing that, despite capacity design was used for the design of these connections, various collapses were recorded. This result reflects the fact that the design formulation for the connections was taken from an aged Italian co-normative document while the actual capacity used in the analyses was obtained from a stricter formulation taken from a more recent European design guideline report.

Finally, the collapse rate for the most representative three-dimensional model was provided considering both for global and local collapses. The obtained values allowed to validate the collapse rate previously obtained with simplified models. The comprehensive model formulation is also suitable to detect local vulnerabilities and to assess losses in a more detailed manner.

DATA AVAILABILITY STATEMENT

The raw data supporting the conclusions of this article will be made available by the authors, upon reasonable requests.

AUTHOR CONTRIBUTIONS

MB: Conceptualization, Methodology, Formal analysis, Visualization, Investigation, Validation, Writing - original draft, Writing - review and editing. DB: Conceptualization, Methodology, Formal analysis, Investigation, Writing - review and editing. AB: Conceptualization, Methodology, Formal analysis, Visualization, Investigation, Writing - review and editing, Supervision. FC: Conceptualization, Methodology, Formal analysis, Investigation, Writing - review and editing. PR: Conceptualization, Methodology, Writing - review and editing. RN: Conceptualization, Methodology, Writing - review and editing.

FUNDING

This research study has been funded by the Italian Department of Civil Protection, in the framework of the national project DPC-ReLUIS-EUCENTRE WP3 (RINTC) 2019–2021; however, opinions and conclusions do not necessarily reflect those of the funding entity.

REFERENCES

Ancheta, T. D., Darragh, R. B., Stewart, J. P., Seyhan, E., Silva, W. J., Chiou, B. S. J., et al. (2014). NGA-West2 database. *Earthqua. Spectra.* 30 (3), 989. doi:10.1193/070913EQS197M

Baker, J. W. (2011). Conditional mean spectrum: tool for ground-motion selection. *J. Struct. Eng.* 137 (3). doi:10.1061/(ASCE)ST.1943-541X.0000215

Baraschino, R., Baltzopoulos, G., and Iervolino, I. (2020). R2R-EU: software for fragility fitting and evaluation of estimation uncertainty in seismic risk analysis. *Soil Dyn. Earthqu. Eng.* 132, 106093. doi:10.1016/j.soildyn.2020.106093

Beconcini, M. L., Croce, P., Del Corso, R., Formichi, P., Previdero, M., and Taccola, R. (2009). "Analisi sperimentale del comportamento statico e ciclico di connessioni tegolo-trave di strutture prefabbricate," in 25° Convegno nazionale AICAP, Pisa.

Beconcini, M. L., Croce, P., and Formichi, P. (2008). "Comportamento sismico di connessioni tegolo-trave in strutture prefabbricate." in 17° Convegno CTE, Roma.

Belleri, A., Brunesi, E., Nascimbene, R., Pagani, M., and Riva, P. (2015a). Seismic performance of precast industrial facilities following major earthquakes in the Italian territory. *J. Perform. Construct. Facil.* 29 (5). doi:10.1061/(ASCE)CF.1943-5509.0000617

Belleri, A., Torquati, M., Riva, P., and Nascimbene, R. (2015b). Vulnerability assessment and retrofit solutions of precast industrial structures. *Earthqua. Struct.* 8 (3), 801. doi:10.12989/eas.2015.8.3.801

Belleri, A., Cornali, F., Passoni, C., Marini, A., and Riva, P. (2017a). Evaluation of out-of-plane seismic performance of column-to-column precast concrete cladding panels in one-storey industrial buildings. *Earthquake Engng Struct. Dyn.* 47, 397. doi:10.1002/eqe.2956

Belleri, A., Labò, S., Marini, A., and Riva, P. (2017b). The influence of Overhead cranes in the seismic Performance of industrial Buildings. *Front. Built Environ.* 3. doi:10.3389/fbuil.2017.00064

Belleri, A., and Riva, P. (2012). Seismic performance and retrofit of precast concrete grouted sleeve connections. *PCI J.* 57 (1), 97. doi:10.15554/pcij.01012012.97.109

Belleri, A., Torquati, M., Marini, A., and Riva, P. (2016). Horizontal cladding panels: in-plane seismic performance in precast concrete buildings. *Bull. Earthqu. Eng.* 14, 1103. doi:10.1007/s10518-015-9861-8

Bosio, M., Belleri, A., Riva, P., and Marini, A. (2020). Displacement-based simplified seismic loss assessment of Italian precast buildings. *J. Earthqu. Eng.* 24 (Suppl. 1), 60. doi:10.1080/13632469.2020.1724215

Bournas, D. A., Negro, P., and Taucer, F. F. (2014). Performance of industrial buildings during the Emilia earthquakes in Northern Italy and recommendations for their strengthening. *Bull. Earthquake Eng.* 12 (5), 2383–2404. doi:10.1007/s10518-013-9466-z

Bracchi, S., Cattari, S., Degli Abbati, S., Lagomarsino, S., Magenes, G., Mandirola, M., et al. (2019). "RINTC-e project: towards the seismic risk of retrofitted existing Italian URM buildings." in 7th ECCOMAS Thematic Conference on Computational Methods in Structural Dynamics and Earthquake Engineering, Crete, Greese, 24–26 June 2019

Bressanelli, M. E., Belleri, A., Riva, P., Magliulo, G., Bellotti, D., and Dal Lago, B. (2019). "Effects of modeling assumptions on the evaluation of the local seismic response for RC precast industrial buildings." in 7th International Conference on Computational Methods in Structural Dynamics and Earthquake Engineering Methods in Structural Dynamics and Earthquake Engineering – COMPDYN, Crete, Greece, 24–26 June 2019, 182–195.

Brunesi, E., Nascimbene, R., Bolognini, D., and Bellotti, D. (2015). Experimental investigation of the cyclic response of reinforced precast concrete framed structures. *PCI J.* 60 (2), 57. doi:10.15554/pcij.03012015.57.79

Cantisani, G., and Della Corte, G. (2019). "RINTC-e: seismic risk of pre-code single-story non-residential steel buildings in Italy."in 7th ECCOMAS Thematic Conference on Computational Methods in Structural Dynamics and Earthquake Engineering. Crete, Greece, 24–26 June 2019, doi:10.7712/120119.7323.19971

Capozzi, V., Magliulo, G., and Manfredi, G. (2011). "Prove a taglio su connessioni trave pilastro spinottate nelle strutture prefabbricate." in 14° Convegno ANIDIS.

Casotto, C., Silva, V., Crowley, H., Nascimbene, R., and Pinho, R. (2015). Seismic fragility of Italian RC precast industrial structures. *Eng. Structures* 94, 122. doi:10.1016/j.engstruct.2015.02.034

CEN, 2004 (2004). *Eurocode 2, Design of concrete structures - Part 1-1: general rules and rules for buildings*. European Standard. Brussels, Belgium.

Cimmino, M., Magliulo, G., and Manfredi, G. (2020). Seismic collapse assessment of new European single-story RC precast buildings with weak connections. *Bull. Earthqu. Eng.* 18, 6661–6686. doi:10.1007/s10518-020-00952-7

Cimmino, M., Magliulo, G., and Manfredi, G. (2020). Seismic collapse assessment of new European single-story RC precast buildings with weak connections. *Bull. Earthquake Eng.* 1–26. doi:10.1007/s10518-020-00952-7

Clementi, F., Scalbi, A., and Lenci, S. (2016). Seismic performance of precast reinforced concrete buildings with dowel pin connections. *J. Building Eng.* 7, 224. doi:10.1016/j.jobe.2016.06.013

CNR 10018 (1999). Apparecchi di appoggio per le costruzioni. *Bollettino Ufficiale Del. CNR*.

CNR 10025 (1998). Istruzioni per il progetto, l'esecuzione ed il controllo delle strutture prefabbricate in calcestruzzo. *Bollettino Ufficiale Del. CNR*.

Dal Lago, B., and Ferrara, L. (2018). Efficacy of roof-to-beam mechanical connections on the diaphragm behaviour of precast decks with spaced roof elements. *Eng. Struct.* 176, 681–696. doi:10.1016/j.engstruct.2018.09.027

Dal Lago, B., Lamperti, M., and Toniolo, G. (2012). "Comportamento a strappo di estremità di tegoli prefabbricati con connessioni meccaniche." in 19° Congresso CTE.

Dal Lago, B., Negro, P., and Dal Lago, A. (2018). Seismic design and performance of dry-assembled precast structures with adaptable joints. *Soil Dyn. Earthqu. Eng.* 106, 182. doi:10.1016/j.soildyn.2017.12.016

Dal Lago, B., Toniolo, G., and Lamperti, M. (2016). Influence of different mechanical column foundation connection devices on the seismic behaviour of precast structures. *Bull. Earthqu. Eng.* 14 (12), 3485–3508. doi:10.1007/s10518-016-0010-9

Demartino, C., Vanzi, I., Monti, G., and Sulpizio, C. (2018). Precast industrial buildings in Southern Europe: loss of support at frictional beam-to-column connections under seismic actions. *Bull. Earthqu. Eng.* 16, 259–294. doi:10.1007/s10518-017-0196-5

Dotreppe, J. C., Colinet, G., and Kaiser, F. (2006). "Influence of the deformability of connections in the analysis of precast concrete frames." in Fédération Internationale du Béton, Proceedings of the 2nd fib congress, Naples, Italy.

Ercolino, M., Magliulo, G., and Manfredi, G. (2016). Failure of a precast RC building due to Emilia-Romagna earthquakes. *Eng. Struct.* 118, 262–273. doi:10.1016/j.engstruct.2016.03.054

Felicetti, R., Lamperti, M., Toniolo, G., and Zenti, C. L. (2008). "Analisi sperimentale del comportamento sismico di connessioni tegolo-trave di strutture prefabbricate." in 17° Convegno CTE, Roma.

Felicetti, R., Toniolo, G., and Zenti, C. L. (2008). Amsterdam. "Experimental investigation on the seismic behaviour of connections in precast structures." in Proceedings of the International FIB symposium

Ferreira, A., and El Debs, M. K. (2000). "Deformability of a beam-column connection with elastomeric cushion and dowel bar to beam axial force." in The Second International Symposium on Prefabrication, Helsinki, Finland.

Fischinger, M., Kramar, M., and Isaković, T. (2008). Cyclic response of slender RC columns typical of precast industrial buildings. *Bull. Earthqu. Eng.* 6, 519–534. doi:10.1007/s10518-008-9064-7

Fischinger, M., Zoubek, B., and Isakovic, T. (2013). "Seismic behaviour of the beam-to-column dowel connections: macro modelling." in 4th ECCOMAS Thematic Conference on Computational Methods in Structural Dynamics and Earthquake Engineering.

Iervolino, I., Spillatura, A., and Bazzurro, P. (2019). "RINTC-e project: towards the assessment of the seismic risk of existing buildings in Italy, RINTC-e: towards seismic risk assessment of existing residential reinforced concrete buildings in Italy." in 7th ECCOMAS Thematic Conference on Computational Methods in Structural Dynamics and Earthquake Engineering.

Iervolino, I., Spillatura, A., and Bazzurro, P. (2018). Seismic reliability of code-conforming Italian buildings. *J. Earthqu. Eng.* 22 (S2), 5–27. doi:10.1080/13632469.2018.1540372

Jalayer, F., and Cornell, C. A. (2009). Alternative non-linear demand estimation methods for probability-based seismic assessments. *Earthqu. Eng. Struct. Dyn.* 38 (8), 951. doi:10.1002/eqe.876

Jalayer, F. (2003). Direct probabilistic seismic analysis: implementing non-linear dynamic assessments. [Ph.D. Dissertation]: Stanford University.

Kramar, M., Isakovic, T., and Fischinger, M. (2010). "Experimental investigation of "pinned" beam-to-column connections in precast industrial buildings. " in Proceedings of the Fourteenth European Conference on Earthquake Engineering. Ohrid, Republic of Macedonia, 30 August–3 September 2010 Republic of Macedonia.

Kremmyda, G. D., Fahjan, Y. M., Psycharis, I. N., and Tsoukantas, S. G. (2017). Numerical investigation of the resistance of precast RC pinned beam-to-column connections under shear loading. *Earthqu. Engng Struct. Dyn.* 46 (9), 1511–1529. doi:10.1002/eqe.2868

Kremmyda, G. D., Fahjan, Y. M., and Tsoukantas, S. G. (2014). Nonlinear FE analysis of precast RC pinned beam-to-column connections under monotonic and cyclic shear loading. *Bull. Earthqu. Eng.* 12, 1615–1638. doi:10.7712/120113.4611.c1443

Lignos, D. G., and Krawinkler, H. (2011). Deterioration modeling of steel components in support of collapse prediction of steel moment frames under earthquake loading. *J. Struct. Eng.* 137 (11), 1291–1302. doi:10.1061/(asce)st.1943-541x.0000376

Luzi, L., Hailemikael, S., Bindi, D., Pacor, F., Mele, F., and Sabetta, F. (2008). ITACA (Italian ACcelerometric Archive): a web portal for the dissemination of Italian strong-motion data. *Seismological Res. Lett.* 79 (5), 716–722. doi:10.1785/gssrl.79.5.716

Magliulo, G., Bellotti, D., Cimmino, M., and Nascimbene, R. (2018). Modeling and seismic response analysis of RC precast Italian code-conforming buildings. *J. Earthquake Eng.* 22, 140–167. doi:10.1080/13632469.2018.1531093

Magliulo, G., Bellotti, D., Di Salvatore, C., and Cavalieri, F. (2019). "RINTC-e project: towards the seismic risk of low and pre-code single-story RC precast buildings in Italy." in 7th ECCOMAS Thematic Conference on Computational Methods in Structural Dynamics and Earthquake Engineering. Crete, Greece. doi:10.7712/120119.7110.20034

Magliulo, G., Capozzi, V., Fabbrocino, G., and Manfredi, G. (2011). Neoprene-concrete friction relationships for seismic assessment of existing precast buildings. *Eng. Struct.* 33 (2), 532. doi:10.1016/j.engstruct.2010.11.011

Magliulo, G., Ercolino, M., Petrone, C., Coppola, O., and Manfredi, G. (2014). The Emilia earthquake: seismic performance of precast reinforced concrete buildings. *Earthqua. Spectra* 30 (2), 891. doi:10.1193/091012EQS285M

Magliulo, G., Ercolino, M., Petrone, C., Coppola, O., and Manfredi, G. (2014). The Emilia earthquake: seismic performance of precast reinforced concrete buildings. *Earthqua. Spectra* 30 (2). doi:10.1193/091012eqs285m

Matlab (2019). *MATLAB R2019b*. Natick, MA: The MathWorks Inc.

McKenna, F., Fenves, G. L., Scott, M. H., and Jeremic, B. (2000). OpenSees: open system for earthquake engineering simulation. Berkeley: Pacific earthquake engineering research center, University of California. Available at: http://opensees.berkeley.edu (Accessed April 8, 2021).

Minghini, F., Ongaretto, E., Ligabue, V., Savoia, M., and Tullini, N. (2016). Observational failure analysis of precast buildings after the 2012 Emilia earthquakes. *Earthqua. Struct.* 11 (2), 327–346. doi:10.12989/eas.2016.11.2.327

Nastri, E., Vergato, M., and Latour, M. (2017). Performance evaluation of a seismic retrofitted R.C. precast industrial building. *Earthqua. Struct.* 12 (1), 13. doi:10.12989/eas.2017.12.1.013

Negro, P., and Toniolo, G. (2012). Design guidelines for connections of precast structures under seismic actions. *JRC Scientific Pol. Rep.* doi:10.2777/37605

NTC08 (2008). *Norme tecniche per le costruzioni*.Decreto Ministeriale del 14/01/2008Suppl. ord. n. 30 alla G.U. n. 29 del 04/02/2008

NTC18. (2018). Aggiornamento delle "Norme tecniche per le costruzioni". Decreto Ministeriale del 17/01/2018. Suppl. ord. n. 8 alla G.U. n. 42 del 20/02/2018.

Palanci, M., Senel, S. M., and Kalkan, A. (2017). Assessment of one story existing precast industrial buildings in Turkey based on fragility curves. *Bull. Earthquake Eng.* 15 (1), 271–289. doi:10.1007/s10518-016-9956-x

Psycharis, I. N., and Mouzakis, H. P. (2012). Shear resistance of pinned connections of precast members to monotonic and cyclic loading. *Eng. Structures* 41, 413. doi:10.1016/j.engstruct.2012.03.051

Ragni, L., Cardone, D., Conte, N., Dall'Asta, A., Di Cesare, A., Flora, A., et al. (2019). "RINTC-e project: the seismic risk of existing Italian RC buildings retrofitted with seismic isolation."in 7th ECCOMAS Thematic Conference on Computational Methods in Structural Dynamics and Earthquake Engineering.

Ricci, P., Manfredi, V., Noto, F., Terrenzi, M., De Risi, M. T., Di Domenico, M., et al. (2019). "RINTC-e: towards seismic risk assessment of existing residential reinforced concrete buildings in Italy." in 7th ECCOMAS Thematic Conference on Computational Methods in Structural Dynamics and Earthquake Engineering.

RINTC Workgroup (2018). Results of the 2015-2017 Implicit seismic risk of code-conforming structures in Italy (RINTC) project. ReLUIS report, Rete dei Laboratori Universitari di Ingegneria Sismica (ReLUIS). Naples, Italy. doi:10.1080/13632469.2018.1543697

Savoia, M., Mazzotti, C., Buratti, N., Ferracuti, B., Bovo, M., Ligabue, V., et al. (2012). Damages and collapses in industrial precast buildings after the Emilia earthquake. *Ingegne. Sismi.* 29, 120–131.

Scotta, R., De Stefani, L., and Vitaliani, R. (2015). Passive control of precast building response using cladding panels as dissipative shear walls. *Bull. Earthqu. Eng.* 13, 3527–3552. doi:10.1007/s10518-015-9763-9

Soroushian, P. (1987). Behavior of bars in dowel action against concrete cover. *Struct. J.* 84 (2), 170–176.

Sousa, R., Batalha, N., and Rodrigues, H. (2020). Numerical simulation of beam-to-column connections in precast reinforced concrete buildings using fibre-based frame models. *Eng. Struct.* 203, 109845. doi:10.1016/j.engstruct.2019.109845

Suzuki, A., and Iervolino, I. (2019). Seismic fragility of code-conforming Italian buildings based on SDoF approximation. *J. Earthqu. Eng.*, 1. doi:10.1080/13632469.2019.1657989

Tassios, T. P., and Vintzeleou, E. N. (1987). Behavior of dowels under cyclic Deformations. *Aci Struct. J.* 84 (1), 18–30. doi:10.14359/2749

Titi, A., Biondini, F., and Toniolo, G. (2018). Seismic assessment of existing precast structures with dry-friction beam-to-column joints. *Bull. Earthqu. Eng.* 16, 2067–2086. doi:10.1007/s10518-017-0271-y

Toniolo, G., and Colombo, A. (2012). Precast concrete structures: the lessons learned from the L'Aquila earthquake. *Struct. Concrete* 13 (2), 73. doi:10.1002/suco.201100052

Toniolo, G., and Dal Lago, B. (2017). Conceptual design and full-scale experimentation of cladding panel connection systems of precast buildings. *Earthqu. Eng. Struct. Dyn.* 46 (14), 2565. doi:10.1002/eqe.2918

Zoubek, B., Fahjan, Y., Fischinger, M., and Isaković, T. (2014). Nonlinear finite element modelling of centric dowel connections in precast buildings. *Eng. structures* 14 (4), 463–477. doi:10.12989/cac.2014.14.4.463

Zoubek, B., Fischinger, M., and Isakovic, T. (2015). Estimation of the cyclic capacity of beam-to-column dowel connections in precast industrial buildings. *Bull. Earthqu. Eng.*13 (7), 2145–2168. doi:10.1007/s10518-014-9711-0

Conflict of Interest: The authors declare that the research was conducted in the absence of any commercial or financial relationships that could be construed as a potential conflict of interest.

frontiers in Built Environment

REVIEW
published: 29 April 2021
doi: 10.3389/fbuil.2021.640189

Design Approach for Lateral Capacity of Dowel-Type Steel Connections in Precast Reinforced Concrete Elements

*Giovanni Muciaccia**

Department of Civil and Environmental Engineering, Politecnico di Milano, Milan, Italy

In precast concrete buildings, connections play a key role. Among them and especially in industrial buildings, the ability to transfer a shear force from the beam to the column is often left to steel bars (often a single one) that act as dowels. Despite several research studies carried out in recent years, there is still a lack of agreement regarding the applicability of Eurocode 2 rules for fastening in concrete to such specific design case. More specifically, the role of the edge reinforcement and the effectiveness of multiple reinforcement layers in the proximity of the steel bar do not find a unique interpretation. The present paper aims to review existing design methods, both in codes and in literature, for such connections, aiming to propose a common interpretation of the load-transfer mechanism.

Keywords: anchorage, fastener, dowel, shear, supplementary reinforcement

OPEN ACCESS

Edited by:
Bruno Dal Lago,
University of Insubria, Italy

Reviewed by:
Fabio Minghini,
University of Ferrara, Italy
Emanuele Brunesi,
Fondazione Eucentre, Italy
Tatjana Isakovic,
University of Ljubljana, Slovenia

***Correspondence:**
Giovanni Muciaccia
giovanni.muciaccia@polimi.it

Specialty section:
This article was submitted to Earthquake Engineering, a section of the journal Frontiers in Built Environment

Received: *10 December 2020*
Accepted: *03 March 2021*
Published: *29 April 2021*

Citation:
Muciaccia G (2021) Design Approach for Lateral Capacity of Dowel-Type Steel Connections in Precast Reinforced Concrete Elements. Front. Built Environ. 7:640189. doi: 10.3389/fbuil.2021.640189

INTRODUCTION

Steel dowel connections are universally used to transfer shear forces acting transversal to their axes between two separate elements in reinforced concrete structures. The maximum capacity of the connection is directly linked to the shear resistance of the single shear plane at the joint location between the two connected members.

However, when the dowel is located close to a free edge, the stress field induced in the narrow member is such that the brittle response of the concrete may become dominant.

Such effect was carefully investigated by Vintzeleou and Tassios (1987) in the eighties, who predicted the conditions corresponding to side or bottom splitting of the concrete member. At the same time, due to the local crushing of the concrete in front of the dowel, they capped the dowel capacity by the force generating a plastic hinge in the dowel located within its portion embedded in the concrete. Additionally, the proposed model also accounted for strength degradation due to cyclic loading. In the end, such model indicates that the capacity of the connection is the minimum between the capacity associated with contemporary yielding of the bar and crushing of the concrete and the capacity associated with (side or bottom) splitting of the concrete member (**Figure 1**).

Approximately 10 years later, the concrete capacity design (CCD) approach was proposed (Fuchs et al., 1995) to evaluate the capacity of single or groups of precast or post-installed fasteners in concrete subjected to tension, shear, or their interaction. In shear, the model derives semi-empirically the capacity of the concrete in front of the fastener assuming a failure surface equal to a half-cone (idealized as a half-pyramid for design easiness) and accounting for the effect of the concrete member size (**Figure 2**). The capacity of the connection is evaluated as the minimum

between the capacity given by the cone mechanism and the simple capacity in shear of the steel element section at the concrete surface.

Such model was the basis for the initial provisions of ETAG 001 Annex C (1998), which, after some refinements (CEN/TS 1992-4-2:2009, 2009), represents the basis for the current design model of EN 1992-4 (2018).

None of the methods, at least in their original formulation, accounted for the effects of additional reinforcement in the proximity of the dowel/fastener.

EN 1992-4 (2018) currently considers the beneficial effect of the so-called "anchor reinforcement" in preventing concrete edge breakout to be decisive, while a different design model was developed by Zoubek et al. (2015) on the basis of the one proposed by Vintzeleou and Tassios (1987) for dowel connections in heavily reinforced elements subjected to cyclic loading. Such model was rapidly adopted in the design of precast industrial buildings in the presence of seismic actions.

The present paper compares the provisions provided by the two methods with respect to test results available in literature, aiming to address the inconsistencies between the two approaches and finally suggesting possible improvements and additions. To the author's knowledge, the test results accounted in this paper are the only available ones such as to allow a direct comparison of such methods.

ACCOUNTED DESIGN MODELS IN PRESENCE OF ADDITIONAL REINFORCEMENT IN SHEAR

Eurocode 2 Model

The Eurocode 2 model (EN 1992-4, 2018) accounts for the possibility that the reinforcement can entirely take up shear load if placed according to a simplified strut and tie model under some given conditions (see **Figure 3**). From a physical point of view, it is assumed that the reinforcement is activated after the concrete fails, according to the model previously discussed. This implies that only the reinforcement within the concrete edge breakout body, and if placed at a transversal distance no larger than 0.75 the edge distance, is activated. Additionally, it is required that (i) inside the breakout body, non-welded straight bars are anchored at least 10 times the bar diameter (and four times in the other cases) and (ii) the bars are properly anchored outside the breakout body according to "standard" Eurocode 2 prescriptions.

Against such detailed requirements on the bars parallel to the shear direction, the model is quite vague regarding the verification of the horizontal tie. Even if in the case of stirrups, due to the limitation regarding the transversal "activation band," the verification of the tie is automatically satisfied, in the case of single bars (whether straight or not), there is the need of accounting on surface reinforcement to guarantee the equilibrium. Such requirement is often overlooked when this model is applied, assuming that the existing surface reinforcement is sufficient to prevent any splitting action.

Finally, no specification is given with respect to the concrete strut beside the assumption of a 45° angle of the same strut.

The Zoubek, Fischinger, and Isakovic Model

Relatively recently, Zoubek et al. (2015) developed a model to predict the capacity of beam-to-column dowel connections under cyclic actions. The model was developed on the basis of experimental results obtained in the FP7 SAFECAST project (Toniolo, 2012), and it is currently adopted in the precast industry, such that it will be probably introduced or accounted in the next generation of Eurocodes.

The model distinguishes between "local" and "global" failure modes.

The local failure mode is heavily based on the previously described Vintzeleou and Tassios (1987) model, assuming a fixed position of the plastic hinge in the dowel (at a distance from the surface equal to 2.5 times the dowel diameter) and limiting the maximum contact pressure in front of the dowel to three times the concrete uniaxial compressive strength. The resistance of the dowel R_{du} associated with such failure mode results as follows:

$$\boldsymbol{R_{du}} = d_d^2 \cdot \sqrt{f_c \cdot f_{sy}} \tag{1}$$

where d_d is the dowel diameter, f_c is the concrete cylindrical compressive strength, and f_{sy} is the steel yield strength.

The global failure mode is a strut-and-tie model (**Figure 4**), which accounts for the presence of multiple layers of closed stirrups, in line with the principle designed such as to avoid the occurrence of concrete brittle failure, where (i) the strut varies its inclination, which is always determined by the relative position between the dowel and the bend of the hook, and (ii) the reinforcement layers below the surface one are also activated, if located within a critical region h_{crit}, with an effectiveness that decreases as a function of the depth.

The number of the engaged stirrups n is defined as

$$\boldsymbol{n} = h_{crit}/s + 1 \tag{2}$$

where s is the vertical spacing between the stirrups and h_{crit} is defined as

$$\boldsymbol{h_{crit}} = 2.5 \cdot d_d + c - a \tag{3}$$

with c equal to the distance between the dowel axis and the stirrup axis and a equal to the vertical concrete cover of the outermost stirrup.

In such a model, the strength of the dowel connection is defined as the force that is applied to the dowel when yielding of the first layer of stirrups occurs, while stresses in the other stirrups in the critical region are linearly reduced. As a matter of fact, from a purely computational perspective, such an assumption is equivalent to assume a number of stirrups at yielding equal to n/2.

It is remarked that an explicit evaluation of the concrete strut is not accounted by the author.

Finally, it is interesting to notice that, even though the model was developed to predict the dowel capacity under cyclic actions, it does not account for any degradation of the strength of the materials or any impact on force redistribution as potential effects of the load cycling. In particular, as for the local failure mode, this represents a significant difference with respect to the Vintzeleou and Tassios (1987) model, where the

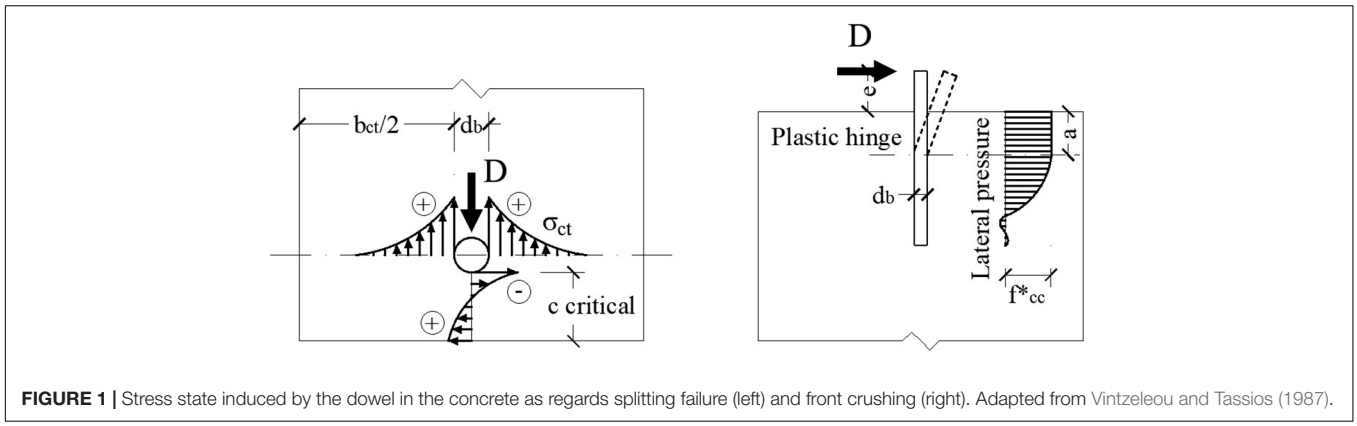

FIGURE 1 | Stress state induced by the dowel in the concrete as regards splitting failure (left) and front crushing (right). Adapted from Vintzeleou and Tassios (1987).

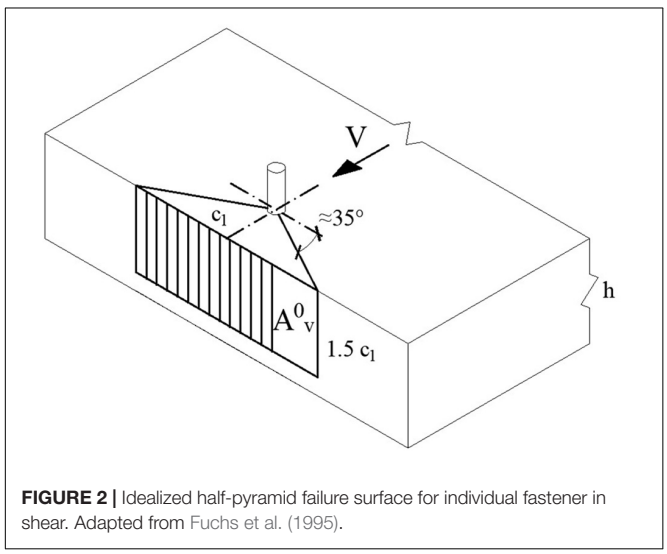

FIGURE 2 | Idealized half-pyramid failure surface for individual fastener in shear. Adapted from Fuchs et al. (1995).

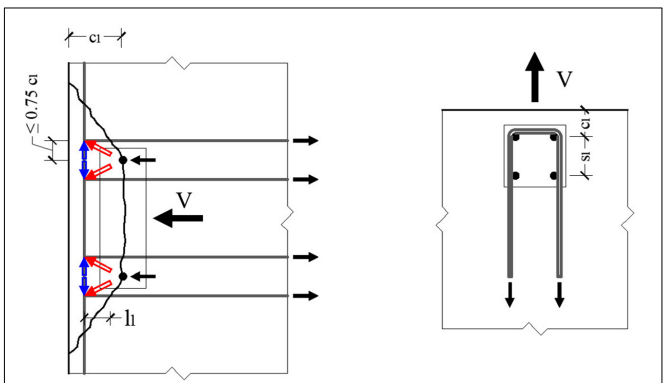

FIGURE 3 | Surface reinforcement to take up shear forces with simplified strut and tie model to design edge reinforcement. Adapted from EN 1992-4 (2018).

influence of cyclic loading on the dowel capacity was estimated in a 50% reduction of the capacity under monotonic loading. Such inconsistency may be solved considering that, if sufficient confinement is provided to concrete along the dowel embedment depth, concrete crushing is not dominant and dowel yielding in shear is attained (Tullini and Minghini, 2016).

Besides, it is the author's opinion that some of the simplified assumptions in the local equilibrium in the Zoubek et al. (2015) model compensate the absence of an explicit reduction factor.

Comparison Between the Described Models

The main features of the previously described models are summarized in **Table 1**. For simplicity, the Eurocode model and the Zoubek et al. models are hereinafter labeled as "fastener" and "dowel," respectively.

It can be noticed how:

(a) both models account for local steel failure, even if in the "dowel" model it is assumed that a plastic hinge develops in the connector within the embedded part contemporary to local concrete crushing;

(b) the "fastener" model does not account for local concrete crushing but for a possible engagement of a wider concrete portion resulting in a half-cone edge breakout;

(c) both models account for the possibility of reinforcement to take up shear load, even if its effectiveness strongly depends on its spatial arrangement;

(d) even though the local concrete crushing in the "dowel" model accounts for a bearing resistance in front of the connector, none of the two models explicitly evaluates the capacity of the concrete strut.

Regarding the last item, it is also noticed that the assumption of a bearing resistance equal to three times the concrete uniaxial compressive strength in the "dowel" model may be unconservative in the case of small edge distances or conservative in the opposite case.

In particular, the way the two models account for the reinforcement effectiveness is discussed with respect to the graphical representation reported in **Figure 5**, based on a typical detailing of reinforcement in precast concrete column (as reported in the same Zoubek et al., 2015).

As it can be seen, both models account for a portion of concrete in front of the connector, which is engaged, but while in the "dowel" model, such portion is defined only to the scope

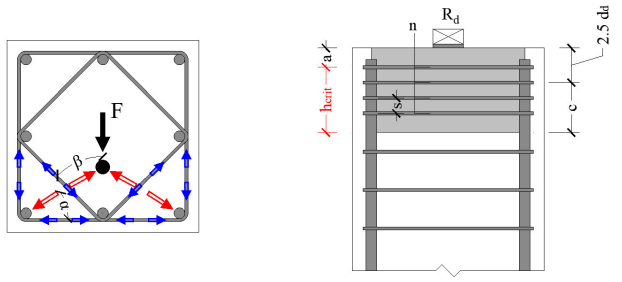

FIGURE 4 | Zoubek et al. model: strut and tie model for a connection with a single dowel (left and center) and schematic representation of the activated stirrups (right). Adapted from Zoubek et al. (2015).

of defining the number of activated stirrups (over a depth equal to the edge distance $c_1 + 2.5$ times the diameter d of the connector), and in the "fastener" model, such portion, as previously mentioned, is assumed to provide a resistance to the breakout actions carried out by the connector.

Additionally, a fundamental difference exists with regards the possibility of engaging the stirrups with respect to the in-plan geometry.

In fact, according to the "fastener" model, the stirrups may be engaged only if they "bend" within the concrete breakout cone (**Figure 5**, bottom center), whose geometry is defined uniquely as a function of the edge distance. If, for the same edge distance, the stirrup corner is located outside of the concrete cone (**Figure 5**, bottom right), then the stirrups are considered as ineffective in resisting the external action.

On the contrary, the "dowel" model simply sets the inclination of the concrete strut as a function of the stirrups corners, starting from the assumption that they are always engaged.

As previously mentioned, none of the models accounts for an explicit verification of the concrete compressive strut. It is the author's opinion that the capacity related to such mechanism cannot be assumed to be automatically accounted by estimating the capacity of other concrete-related failure modes, especially in the case of heavily reinforced elements. However, very few investigations were dedicated to evaluate the strut capacity in this type of connections, as will be discussed later.

TABLE 1 | Main features of the "fastener" and "dowel" models.

Model	Local concrete failure	Local steel failure	Global concrete failure	Reinforcement contribution	Concrete strut
Fastener	No	Yes, in shear and bending at the concrete surface	Yes, by edge breakout	Yes, only the first layer within the edge breakout cone	No
Dowel	Yes, by crushing of the concrete	Yes, by activation of a plastic hinge	No	Yes, multiple layers within a critical region	No

EVALUATION WITH RESPECT TO EXISTING LITERATURE RESULTS

When presenting their "dowel" model, Zoubek et al. (2015) compared its prediction and the ones provided by the "fastener" model (in the version of CEN/TS 1992-4-2:2009, 2009) with existing literature results on precast beam-to-column dowel connections (Fischinger et al., 2012; Psycharis and Mouzakis, 2012) obtained from the University of Ljubljana (UL) and the National Technical University of Athens (NTUA), respectively.

The same results are taken as reference in the comparison that will follow. The reason lies in the fact that Zoubek et al. (2015), when carrying out their comparison, did not account for the following items:

- The capacity related to the concrete edge breakout model should be carried out with respect not to its characteristic value (corresponding to the Eurocode 2 formulation) but rather to its mean values, which can be derived by Hofmann (2005). The ratio between such mean and characteristic values is equal to 1.8.;
- The Eurocode 2 model assumes that the reinforcement may activate after the concrete edge breaks out. However, for low amounts of reinforcement and great edge distances, the capacity provided by the edge breakout mechanism may be higher than the one provided by the reinforcement. Hence, the biggest between the two has to be considered.

The main geometrical parameter and the experimental capacity for the evaluated tests are reported in **Table 2**.

By adopting such refined approach and considering, as for the test results, only the direction for which the lower capacity was detected (which is always the "pull" one, being the connector closer to the edge), the connection capacities are evaluated according to the two approaches. It is recalled that:

- as for the "dowel" model, the capacity is given by the minimum between the "local" (concrete crushing + dowel bending) and the "global" (failure of the tie represented by the reinforcement) mechanisms;
- as for the "fastener" model, the capacity is given by the maximum between the concrete edge breakout and the reinforcement (when considered to be activated) failures.

With respect to the effects of cyclic loading, it is remarked that:

- The "dowel model," as discussed in *The Zoubek, Fischinger, and Isakovic Model* section, does not provide any specific material strength reduction factor;
- The "fastener" model, as formulated in EN 1992-4 (2018), generally accounts for a capacity reduction factor under cyclic (seismic) loading. As for the failure modes relevant in the evaluated tests (concrete edge failure and steel failure of the reinforcement), assuming that both the dowel and the reinforcement have adequate ductility, such factor is taken as unitary, except in the case of concrete edge group failure, where such factor is estimated as 0.85. However, such factor mainly accounts for the

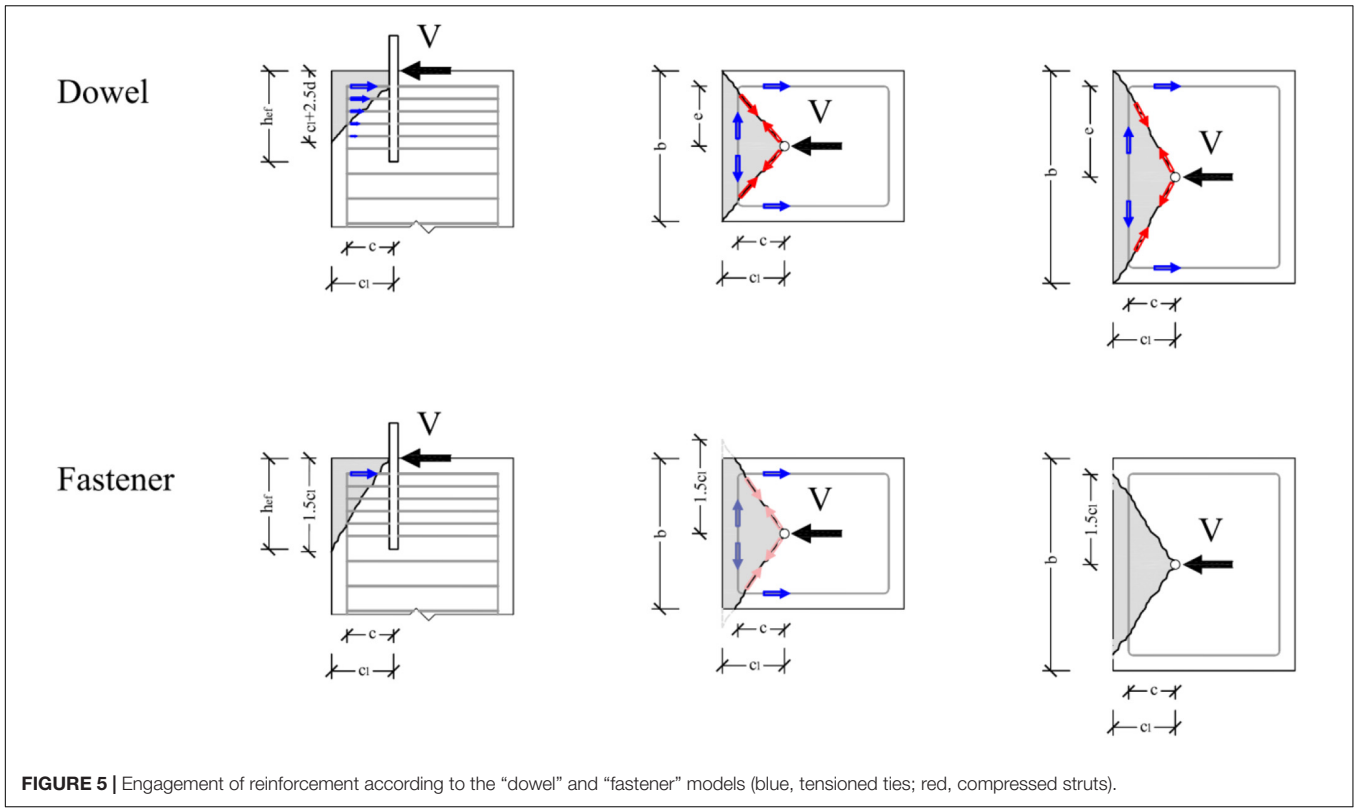

FIGURE 5 | Engagement of reinforcement according to the "dowel" and "fastener" models (blue, tensioned ties; red, compressed struts).

effects of uneven crack distribution, which, in the author's opinion, is not applicable to the considered case, given both the compact geometry and the dense reinforcement. Consequently, to the scopes of the current comparison, no reduction is accounted.

The comparison between the predicted and tested capacities is reported in **Figure 6**.

It can be noticed how the predictions of the two models, globally, are not dramatically different. The mean value and the coefficient of variation (CoV) for the tested vs. predicted ratio are equal to (1.18, 18%) and (1.31, 45%) for the fastener and dowel models, respectively. The dowel model seems to provide a bigger scatter (CoV equal to 45%); this is probably due to the very low predicted capacity associated with the specimen 2D25d100(S7-2) (marked by a circle in **Figure 6**), which was characterized by the presence of ø8 stirrups (instead of ø10 or ø12 as in the other cases). If such specimen is not included, the model prediction significantly improves (1.12 mean and 10% CoV). However, such result stresses one critical aspect

TABLE 2 | Evaluated test results.

Code	d (mm)	b (mm)	e (mm)	c (mm)	a (mm)	c_1 (mm)	s_1 (mm)	d_s (mm)	s_s (mm)	f_{cm} (MPa)	$f_{ym,d}$ (MPa)	$f_{ym,s}$ (MPa)	$V_{u,test,pl}$ (kN)	$V_{u,test,pu}$ (kN)
1D28d250(S1-2)	28	500	215	215	25	250	0	10	40	50	580	560	150	–
1D28d125(S6-2)	28	500	215	90	25	125	0	10	40	50	580	560	95	120
2D25d100(S7-2)	25	500	65	70	70	105	300	8	50	50	540	560	160	–
2D25d100	25	400	65	65	70	100	200	12	50	35	580	560	130	200
2D25d150	25	400	65	115	70	150	200	12	50	30	580	560	175	200
2D25d200	25	400	65	165	70	200	200	12	50	30	580	560	180	200
1D25d100	25	400	165	65	70	100	0	12	50	35	580	560	70	90
2D16d100	16	400	65	65	70	100	200	12	50	35	560	560	70	–
1D32d200	32	400	165	165	70	200	0	12	50	30	560	560	150	–

d, column depth; b, column basis; e, distance between the dowel axis and the stirrup axis in a direction transversal to the applied load; c, distance between the dowel axis and the stirrup axis in a direction parallel to the applied load; a, cover of the first stirrup in direction parallel to the connector axis; c_1, edge distance in direction parallel to the applied load; s_1, spacing between connectors in direction transversal to the applied load; d_s, stirrup diameter; s_s, vertical spacing between stirrups; f_{cm}, concrete compressive strength; $f_{ym,d}$, steel yield strength, dowel; $f_{ym,s}$, steel yield strength, stirrup; $V_{u,test,pl}$, tested capacity in pull direction (toward the closer edge); $V_{u,test,pu}$, tested capacity in push direction (toward the farthest edge).

of the model, which consists in taking the minimum of the capacity associated with the "local" and "global" failure modes and of not considering any mechanism related to a global concrete failure.

It is remarked that, according to the fastener model, in specimens 1D28d125(S6-2) and 1D25d100, the stirrups are not active, since their bend is located outside of the potential concrete edge cone. Additionally, it is remarked that the dowel model is a better predictor when multiple rows are engaged, as for the specimens 2D25d150 and 2D25d200.

ENHANCED FASTENER MODEL

On the basis of the final remark of the previous section, a modification of the fastener model can be proposed to account for a number of engaged stirrups rows higher than one, as considered in its original formulation.

It is noticed that the possibility of activating all the rows within the critical region, as accounted in the dowel model, strongly accounts for a significant redistribution capacity along the depth, which may be impaired by the limited displacement associated with the local failure of the connector.

Consequently, it is proposed to limit the maximum number of activated rows to three, while still adopting a linear decrease of stresses along the depth. Such an assumption is equivalent to consider a maximum increase with respect to the full capacity provided by the first layer equal to 50%.

With reference to the test results reported in **Table 2**, the capacity predicted according to such model is reported in **Figure 7**, jointly with the predictions provided by the standard fastener model.

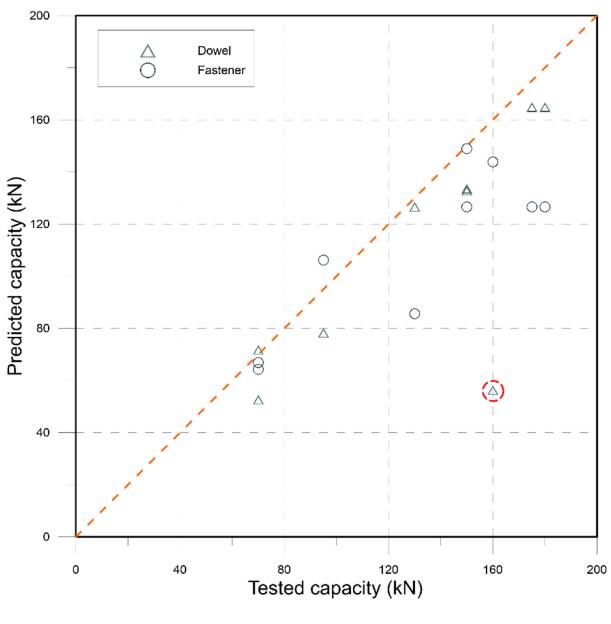

FIGURE 6 | Predicted capacity vs. tested capacity for the "dowel" and "fastener" models.

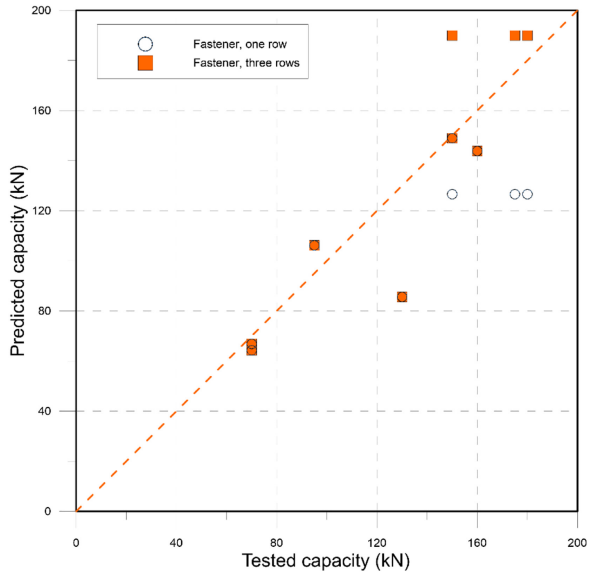

FIGURE 7 | Predicted capacity vs. tested capacity for the "fastener" model accounting for different numbers of engaged rows.

A better agreement of the enhanced model with respect to the considered test results is provided, with a mean value and the coefficient of variation for the tested vs. predicted ratio equal to 1.04 and 18%, respectively.

Additionally, the following modifications are proposed.

As previously discussed, the fastener model does not account for a contribution of the stirrups where these ones bend outside of the edge breakout cone. However, in such case, at least the contribution of the stirrup related to their shear capacity (i.e., a "dowel effect" across the cone crack plane) should be considered.

With respect to the analyzed experimental cases, such contribution is not significant (out of two affected cases, only in one of them the predicted capacity is closer to the tested one). However, it cannot be excluded that such modification can be relevant in other cases.

Finally, it is recalled that none of the discussed models explicitly accounts for a verification of the concrete strut. Relatively recently, Eligehausen et al. (2018) showed how this failure mode may be decisive when dealing with fastener reinforcement, and they proposed an evaluation of the capacity of the concrete strut, which is basically evaluated as a Ψ_{strut} multiplier of the edge breakout capacity:

$$\Psi_{strut} = 2.75 - 1.17 \cdot e/c_1 \tag{4}$$

where e and c_1 are consistent with the definitions adopted in **Table 2**.

Such opportunity should be considered, especially when considering multiple rows of stirrups engaged, which implies a higher force acting in the strut.

It is remarked that the evaluation according to the model proposed by Eligehausen et al. (2018) is carried out for the tests previously discussed, and it is found to be never

decisive. However, it would be prudent to account for it in a robust design model.

Finally, it is noticed that the current comparison is carried out for rectangular stirrups only. In the presence of additional reinforcement layers placed in non-rectangular shapes (for instance, "diamond stirrups"), an additional contribution to the reinforcement capacity may be accounted, directly proportional to the sum of the reinforcement resistance components parallel to the applied shear.

CONCLUSION

The paper reviews the main features of two existing models used to predict the lateral capacity of dowel-type steel connections in precast reinforced concrete elements, namely, the EN 1992-4 (2018) and the Zoubek et al. (2015) models, referred to as "fastener" and "dowel" model, respectively.

It is noticed how the two models, even if they both account for a potential strut-and-tie force transfer mechanism, significantly differ in the way they consider concrete-related failure modes and the capacity associated with the additional reinforcement.

By also comparing the predictions based on the models with existing test results for cases with stirrups arranged in rectangular shapes, as main critical issues, it is noticed how the "fastener" model (i) does not allow to consider multiple rows of stirrups along the member depth and (ii) does not consider any contribution of the stirrup where their corners are located outside of the edge breakout area. On the other side, the "dowel" model, assuming that sufficient confinement is provided along the dowel embedment depth, does not consider any contribution provided by a global failure mechanism in the concrete element (as the "edge breakout failure"), being conservative in the cases where a low reinforcement is present. Additionally, none of the models accounts for an explicit verification of the concrete strut.

However, with respect to the considered test results, no remarkable differences are detected for elements that are not lightly reinforced.

To overcome such potential conflict, it is proposed to enhance the "fastener" model by (i) accounting for a possible increase of the reinforcement capacity in the case of multiple rows up to 50% of the capacity of the most engaged row, (ii) accounting for the capacity associated with "dowel effect" in shear for cases where the stirrup corners are not internal to the volume of the edge concrete cone, and (iii) introducing an explicit verification for the concrete strut.

A validation of the proposed enhancement on a wider test results database is preferred, perhaps involving different shapes and layout of stirrups and building specimens (fullscale or not); however, to the author's knowledge, no additional test results for dowel-type connections in narrow concrete member with multiple layers of closed stirrups are currently available.

AUTHOR CONTRIBUTIONS

The author confirms being the sole contributor of this work and has approved it for publication.

REFERENCES

CEN/TS 1992-4-2:2009 (2009). *Design of Fastenings for Use in Concrete—Part 4–2: Headed Fasteners*. Brussels: CEN.

Eligehausen, R., Asmus, J., and Sharma, A. (2018). Neue Versuche erlauben ein wesentlich verbessertes Modell für die Berechnung des Tragverhaltens und die Bemessung. *Der. Prüfingenieur.* 52, 54–67.

EN 1992-4 (2018). *Eurocode 2–Design of Concrete Structures–Part 4: Design of Fastenings for Use in Concrete*. Brussels: CEN.

ETAG 001 Annex C (1998). *European Technical Approval Guidelines 001 "Metal anchors for use in concrete", Annex C "Design Methods for Anchorages*. Brussels: EOTA.

Fischinger, M., Zoubek, B., Kramar, M., and Isakovic, T. (2012). "Cyclic response of dowel connections in precast structures," in *Proceedings of the 15th World Conference on Earthquake Engineering* (Lisbon), 24–28.

Fuchs, W., Eligehausen, R., and Breen, J. E. (1995). Concrete Capacity Design (CCD) approach for fastening to concrete. *ACI Struct. J.* 92, 73–94. doi: 10.14359/1533

Hofmann, J. E. (2005). *Tragverhalten Und Bemessung von Befestigungen Unter Beliebiger Querbelastung in Ungerissenem Beton*. PhD Dissertation, University of Stuttgart, Stuttgart.

Psycharis, I. N., and Mouzakis, H. P. (2012). Shear resistance of pinned connections of precast members to monotonic and cyclic loading. *Eng. Struct.* 41, 413–427. doi: 10.1016/j.engstruct.2012.03.051

Toniolo, G. (2012). "SAFECAST Project: European research on seismic behavior of the connections of precast structures," in *Proceedings of the 15th World Conference on Earthquake Engineering* (Lisbon), 24–28.

Tullini, N., and Minghini, F. (2016). Grouted sleeve connections used in precast reinforced concrete construction–experimental investigation of a column-to-column joint. *Eng. Struct.* 127, 784–803. doi: 10.1016/j.engstruct.2016.09.021

Vintzeleou, E. N., and Tassios, T. P. (1987). Behavior of dowels under cyclic deformations. *ACI Struct. J.* 84, 18–30. doi: 10.14359/2749

Zoubek, B., Fischinger, M., and Isakovic, T. (2015). Estimation of the cyclic capacity of beam-to-column dowel connections in precast industrial buildings. *Bull. Earthq. Eng.* 13, 2145–2168. doi: 10.1007/s10518-014-9711-0

Conflict of Interest: The author declares that the research was conducted in the absence of any commercial or financial relationships that could be construed as a potential conflict of interest.

frontiers in Built Environment

ORIGINAL RESEARCH
published: 03 May 2021
doi: 10.3389/fbuil.2021.631360

Multi-Stripe Seismic Assessment of Precast Industrial Buildings With Cladding Panels

Krunal Gajera[1], *Bruno Dal Lago*[2]*, *Luca Capacci*[3] and *Fabio Biondini*[3]

[1] DLC Consulting s.r.l., Milan, Italy, [2] Department of Theoretical and Applied Sciences, Università degli Studi dell'Insubria, Varese, Italy, [3] Department of Civil and Environmental Engineering, Politecnico di Milano, Milan, Italy

Following the empirical observation of widespread collapses of cladding panel connections of precast industrial buildings under recent seismic events, new design solutions have been developed in the framework of the European project SAFECLADDING, including isostatic systems effectively decoupling the seismic response of frame structure and cladding panels. The present paper is aimed at evaluating the seismic response and vulnerability of precast frame structures employing pendulum, cantilever, and rocking cladding connection systems. Within the framework of the research project RINTC–Implicit seismic risk of code-conforming structures funded by the Italian Civil Protection Department within the ReLUIS program, the seismic performance of a typical precast industrial building has been assessed with a probabilistic approach based on the results of static and multi-stripe dynamic non-linear analyses. The seismic vulnerability assessment of each structural system has been carried out with reference to life safety and damage limit states considering three sites of increasing seismic hazard in Italy. The effect of distributed panel mass modeling vs. more common lumped mass modeling has been analyzed and critically commented based on the results of demand over capacity (D/C) ratios. Moreover, biaxial seismic D/C ratios have been evaluated for realistic strong hinge connections for cladding panels.

Keywords: seismic vulnerability, precast structures, industrial buildings, probabilistic assessment, panel connection systems, multi-stripe analysis, pushover analysis

OPEN ACCESS

Edited by:
Massimo Latour,
University of Salerno, Italy

Reviewed by:
Saverio Spadea,
University of Dundee, United Kingdom
Fabio Mazza,
University of Calabria, Italy

***Correspondence:**
Bruno Dal Lago
bruno.dallago@uninsubria.it

Specialty section:
This article was submitted to Earthquake Engineering, a section of the journal Frontiers in Built Environment

Received: *19 November 2020*
Accepted: *22 February 2021*
Published: *03 May 2021*

Citation:
Gajera K, Dal Lago B, Capacci L and Biondini F (2021) Multi-Stripe Seismic Assessment of Precast Industrial Buildings With Cladding Panels. Front. Built Environ. 7:631360. doi: 10.3389/fbuil.2021.631360

INTRODUCTION

Since the end of World War II, precast buildings have been widely constructed in Europe and other world regions as industrial and commercial frame buildings and residential panel/block buildings. The typical modern industrial single-story precast frame structure consists of cantilever tall columns restrained at the base with pocket foundations and connected at the top to hinged prestressed beams supporting different typologies of prestressed roof elements. Vertical or horizontal precast concrete panels are connected to load bearing frame elements as perimeter cladding. The cladding-to-structure connections may play a crucial role under seismic action (Biondini et al., 2013). The traditional design approach for the precast structure is based on a bare frame model where peripheral cladding panels are considered as masses only, without any in-plane stiffening contribution. Panels have been often connected to the structure with fixed fastenings proportioned for out-of-plane horizontal actions related to the local mass of single

panels, neglecting any in-plane possible interaction with the frame. Different earthquakes that recently occurred in Southern Europe have shown that this approach is not adequate. Frame structures properly designed and detailed for seismic actions performed satisfactorily (Biondini and Toniolo, 2009), while many cladding panels collapsed after failure of their connections (Toniolo and Colombo, 2012; Belleri et al., 2015a). Surveys from areas where the frame structures were not conceived for seismic strength (Belleri et al., 2015b, 2017), and did not perform satisfactorily, also reported extensive failures of cladding panels and their connections (Bournas et al., 2013; Magliulo et al., 2014; Savoia et al., 2017; Batalha et al., 2019). The SAFECLADDING project was funded by the European Commission to tackle this issue. The project analyzed innovative design solutions to improve the performance of both existing and new precast buildings. Three different cladding connection arrangements were investigated: Isostatic, Integrated, and Dissipative (Biondini et al., 2013; Dal Lago et al., 2018). The cladding solution analyzed in this project is made of external precast concrete panels connected with mechanical devices, which represent since many decades the standard solution for precast buildings. However, it is worth noting that this solution is not representative of the existing heritage of precast structures, since many of them are cladded with infill walls made of masonry or precast concrete stacked panels. In this case, the seismic behavior of the global structural assembly and of the local cladding wall is remarkably different from the case of external panels, with the stiffening effect and the strength being much larger, where the failure mode is usually related to the in-plane-out-of-plane interaction on the cladding wall rather than on its mechanical connections (Asteris et al., 2017; Pasca et al., 2017; Mazza, 2019; Di Domenico et al., 2021).

In this paper, Isostatic systems aimed at decoupling the motion of frame structure and external panels have been addressed. Three different connection arrangements for vertical cladding panels have been considered in the present study: (1) Pendulum, (2) Cantilever, and (3) Rocking. Details about each arrangement and numerical modeling strategies can be found in Dal Lago (2019). Each of these arrangements was previously subjected to seismic testing on full-scale prototype within the SAFECLADDING project (Negro and Lamperti Tornaghi, 2017; Toniolo and Dal Lago, 2017; Dal Lago and Molina, 2018). This paper is aimed at providing indications on the seismic behavior of precast industrial frame structures with Isostatic cladding connection arrangements based on probabilistic seismic vulnerability assessment. The work has been carried out in the framework of the Italian research project RINTC–Implicit seismic risk of code-conforming structures, as part of a wider project conducted by ReLUIS (Italian Laboratories University Network of Earthquake Engineering) and funded by the Italian Department of Civil Protection.

CASE-STUDY BUILDINGS

The considered case-study buildings consist of a reference geometry with Pendulum, Cantilever, and Rocking cladding-to-structure designed for soil type C for three sites in L'Aquila (AQ), Naples (Napoli, NA), and Milan (Milano, MI) with high to low hazard levels, respectively. The Cantilever solution has been investigated both including and neglecting the effect of friction induced by out-of-plane loading during the in-plane sliding of the connection. The considered case-study building reflects a common type of precast industrial buildings across Europe.

Figure 1A shows the 3D view of the frame structure without cladding panels (the same frame arrangement has been previously modeled by Magliulo et al., 2018). **Figure 1B** shows the structural cross section of the building and the schematic plan view of the considered building, with one 15-m-wide bay in the transversal direction (i.e., the X direction) and four 6-m-wide bays in the longitudinal direction (i.e., the Z-direction), the building being cladded by 2.2-m-wide and 6.85-m-tall vertical cladding panels with soft corners (**Figure 1C**).

Each considered case-study building consists of squared section precast columns fixed at the base with isolated pocket foundations. The columns are connected by means of double dowels to the main precast prestressed beam having a variable depth cross section in the longitudinal direction, and by means of bolted connections to the girders having a rectangular cross section, in the longitudinal direction. The roof element consists of the double T section connected with each other through mechanical connections and topped with cast-*in-situ* reinforced concrete slab. The rigid diaphragm effect is hence considered for the case-study buildings, although the roof slab of precast industrial structures is often not topped, which would require its explicit modeling to account for the deformability of roof elements and their connections (Dal Lago et al., 2017, 2019; Dal Lago and Ferrara, 2018). The cladding system consists of vertical precast panels with specific weight of 4 kN/m^2, connected to the roof peripheral beams via different connection arrangements (Pendulum, Cantilever, and Rocking system). The structural elements for the considered case studies are designed (Ercolino et al., 2018; Magliulo et al., 2018) according to the Italian building code NTC08 (MIT (Ministero delle Infrastrutture e dei Trasporti), 2008), which is very similar to Eurocode 8 (CEN, 2005) for soil type C for the three investigated sites. Dowel connections have been designed according to the Italian technical specifications CNR 10025/98 (2000), taken as typical reference for designers. More thorough information on structural details is available in Magliulo et al. (2018).

NUMERICAL MODELING

All the case studies have been modeled in OpenSees (Mazzoni et al., 2006) to perform non-linear static and multi-stripe dynamic analysis. **Figure 2A** shows the 3D view of the numerical model.

The columns are modeled with elastic elements characterized by lumped plasticity at the base. In the OpenSees software, the plastic hinge is implemented with a non-linear spring element characterized by the "Modified Ibarra–Medina–Krawinkler deterioration model with peak-oriented hysteretic response"

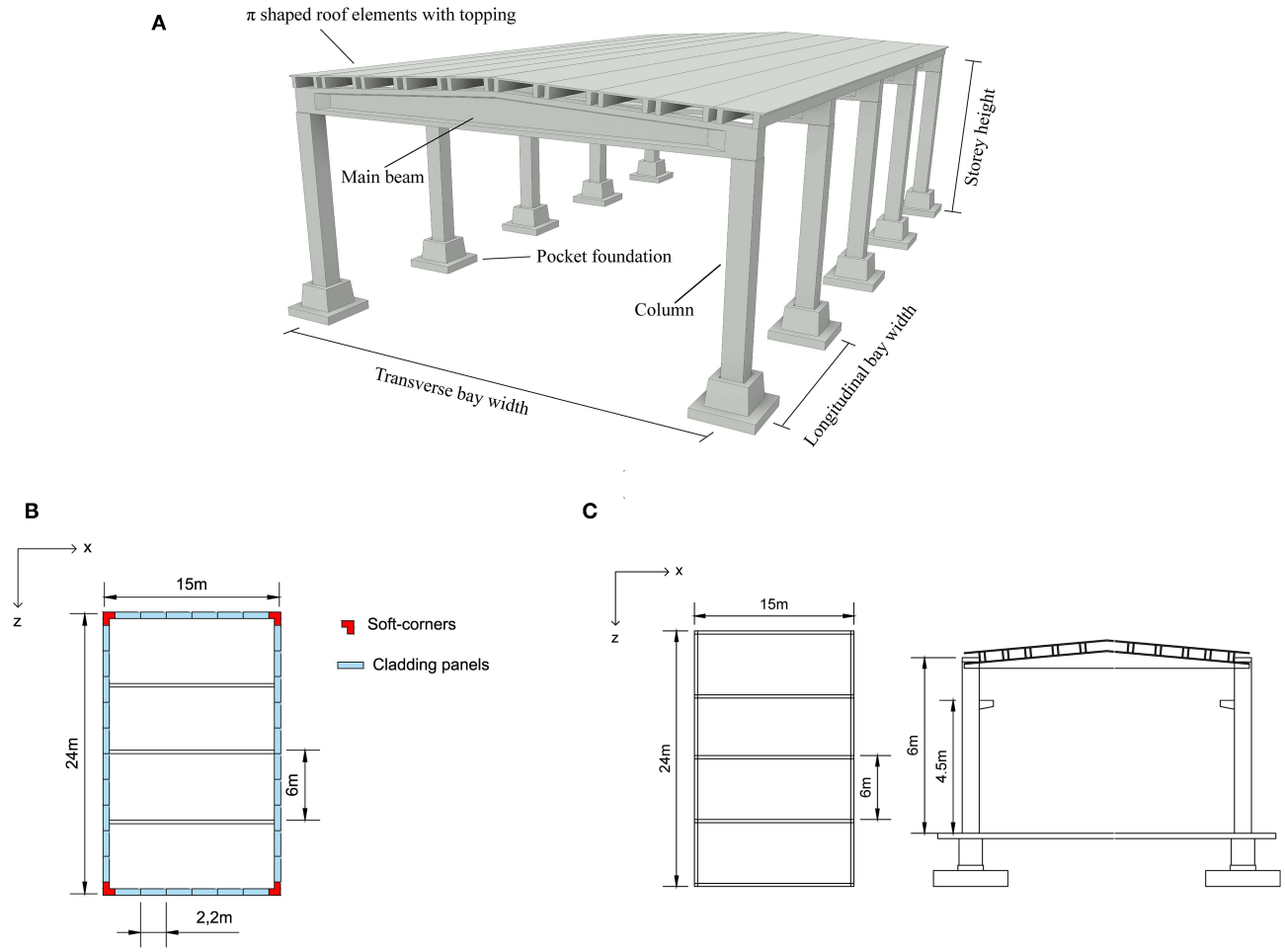

FIGURE 1 | (A) 3D view of the frame structure without cladding panels, **(B)** plan view, and **(C)** transversal cross section of the building.

whose behavior is described by a trilinear backbone curve, which accounts for history-dependent strength and stiffness deterioration based on energy dissipation (Ibarra et al., 2005).

The beams and girder elements are modeled with elastic elements as well; the main double-tapered beams are modeled with a simplified constant cross section, which is characterized by the mean values of site-dependent height and width of the cross sections. This simplification should not result in large modeling errors, since all the horizontal elements are not part of the lateral load-bearing system of the building assembly. The roof elements are not modeled, and rigid diaphragm constraint is applied at the roof level in correspondence to the location of the mean center of gravity of the beams.

The connections between beams and columns are perfectly hinged due to bolted connections. The top column joint, where main and peripheral beams are converging, is modeled such that the main beam can rotate in the transversal plane at its base with respect to the column (**Figure 2B**). As a result, the building is slightly more flexible in the direction of the peripheral beams (z-axis). The geometrical eccentricities (**Figures 2C,D**) of structural elements have been modeled by rigid elements based on the model developed by Ercolino et al. (2018).

The isostatic cladding-to-structure connections (Pendulum, Cantilever, and Rocking) are modeled with following strategies for three considered sites (L'Aquila, Napoli, and Milano).

Pendulum Arrangement

Concerning the pendulum arrangement, the total mass of structural elements as well as panels is lumped to the master node at the center of the roof, where the identification number 1111 in **Figure 3** represents the master node. The lumped masses assigned to the master node were 404.27 tons for both Milano and Napoli buildings, and 408.67 for L'Aquila building. This assumption of null in-plane neither out-of-plane stiffening contribution reflects the kinematics of truss-like panels hinged at both base and top beam. The mass associated to the frame structure was set to 258.29 tons for both Milano and Napoli buildings, and to 262.68 tons for L'Aquila building. The masses associated to the cladding panels in X and Z directions, respectively, were set to 89.83 tons and 56.15 tons for all buildings.

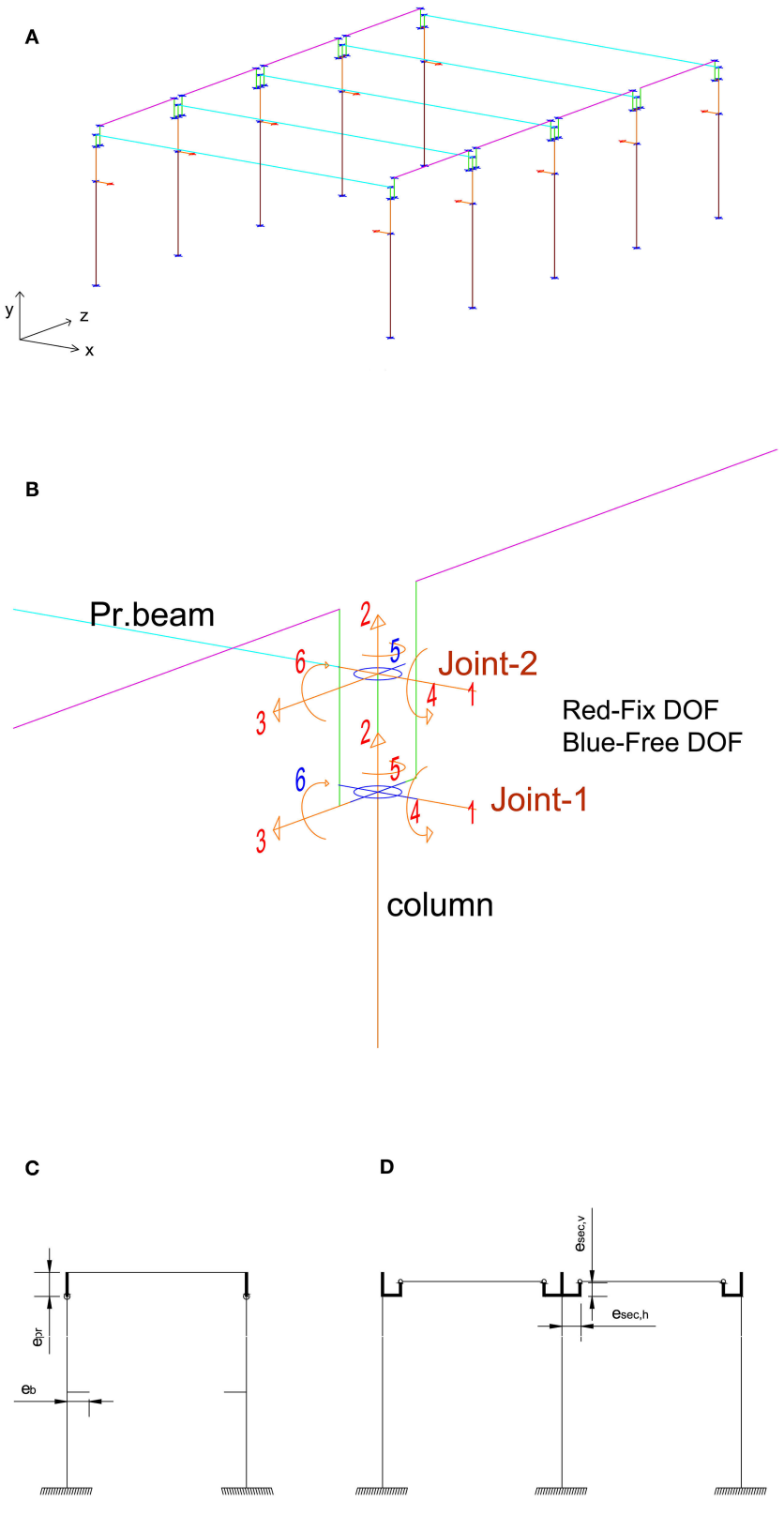

FIGURE 2 | (A) 3D view of the numerical model developed in OpenSees **(B–D)** model joint details.

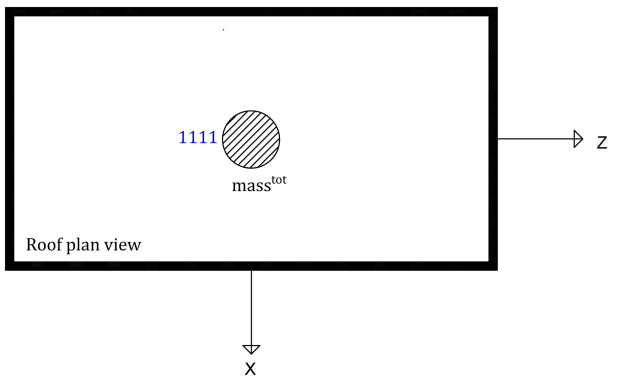

FIGURE 3 | Schematic view of the numerical model assumptions for pendulum arrangement.

Cantilever Arrangement

In the cantilever arrangement, relative horizontal in-plane sliding occurs between the structure and the cladding panel under seismic action, with panels not moving in-plane and rigidly tilting in the out-of-plane direction. Thus, the connector is subjected to multiaxial actions, and horizontal sliding may be hampered by friction (**Figure 4A**). The cantilever arrangement has been modeled with two different strategies, either considering or neglecting the friction forces in the cladding-to-structure connections.

The cantilever model without friction has been developed by modifying the lumped masses at the master node. As shown in **Figure 4B**, two different masses in both directions have been assigned, i.e., in the X direction, the total assigned mass is $mass_{xz,roof} + mass_{x,panel}$ and in the Z direction $mass_{xz,roof} + mass_{z,panel}$.

The cantilever model accounting for friction effects has been modified as illustrated in **Figure 4C**. The lumped mass in the master node is referred to the frame structure in both directions, while the mass of the panels has been assigned to two independent nodes in each horizontal direction. To model the friction between the frame structure and panels, the axially rigid zero-length "flat slider bearing" element has been used in OpenSees. In order to account for such effect, a constant dynamic friction coefficient equal to 0.22 has been set in the model based on the test results obtained by Dal Lago and Lamperti Tornaghi (2018) on a cladding-to-structure sliding connection subjected to multi-axial loading.

Rocking Arrangement

In the rocking arrangement, the panels brace the structure up to a lateral load associated with the scenario in which the overturning moment overcomes the stabilizing one provided by the panel self-weight (**Figure 5A**). After this phenomenon occurs, the panels rigidly rotate providing a restoring force that is slightly decreasing with the displacement due to second-order effects associated with the reduction of the lever arm from the center of mass of the panel to the rotation center located at one of its corners (**Figure 5B**). The lumped mass in the master node is the same as the pendulum case, and the building model has been modified as described in **Figure 5C**.

Two fixed non-linear springs representing the mechanical behavior of the panels (**Figure 5B**) are linked to the master node. Due to progressive contact of the vertical sliders with the channel lips after random tolerance positioning, an initial tolerance gap $\delta_{tol} = 2$ mm is considered in the model covered by a linear branch, which is calibrated following experimental observations reported in Toniolo and Dal Lago (2017), Negro and Lamperti Tornaghi (2017). The shear stiffness of the springs is null. Friction may provide additional actions under seismic motion, but it has been disregarded, supposedly being much less than the restoring force of the panel.

Finally, it is to be remarked that the strongly non-linear idealized behavior of **Figure 5B** is not associated with any dissipation of energy, being the multilinear hysteresis completely elastic.

NON-LINEAR STATIC (PUSHOVER) ANALYSIS

Non-linear static analyses are performed in both of the horizontal X and Z directions for all considered case studies, i.e., three isostatic panel arrangements at each investigated site. **Figure 6** shows the pushover curves for all case studies.

For the examined structural typology, pushover curves depend on the mechanical behavior of frame columns under lateral loading conditions. Consequently, when cross-section design and construction detailing of columns depend on non-seismic actions (e.g., wind forces) and code minimum requirements, pushover curves and roof lateral displacement capacities may match for different case studies, even if they are characterized by different seismic hazard levels.

The pushover curves for each structural typology shown in **Figure 6** are adopted to define the structural capacity threshold for the collapse limit state, to be presented in the following section.

LIMIT STATES

The limit states are defined according to performance-based design criteria and refer to specific Engineering Demand Parameters (EDPs) of seismic performance, related to global and/or local seismic response of the structural and non-structural elements. Therefore, appropriate EDPs are selected to describe the structural demand and compared with threshold values representative of the structural capacity for specific limit states. Demand-over-Capacity (D/C) ratios have been evaluated with respect to the Damage Limit States (DLSs) and Collapse Limit States (CLSs) to carry out seismic response and vulnerability assessment.

Collapse Limit States

This limit state corresponds to the failure of structural elements, which corresponds to the failure of the structure. Two limits state

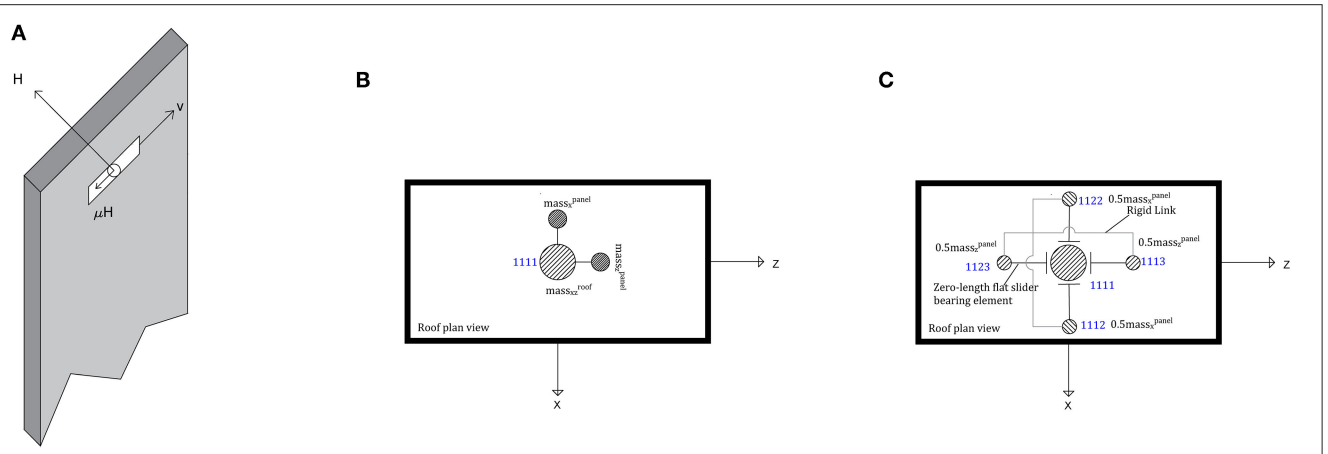

FIGURE 4 | (A) Schematic friction mechanism occurring in the cantilever panels when subjected to multi-axial seismic excitation. **(B)** Cantilever model without friction forces. **(C)** Cantilever model with friction forces.

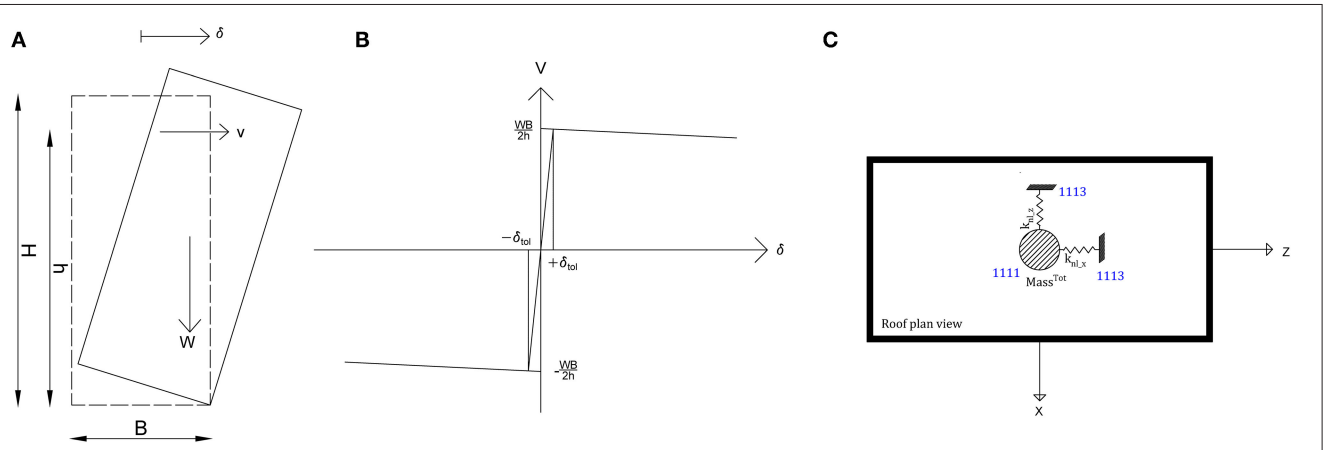

FIGURE 5 | Rocking panel: **(A)** geometry and loads, **(B)** non-linear force–displacement relationship, and **(C)** schematic view of the numerical model assumptions for the Rocking arrangement.

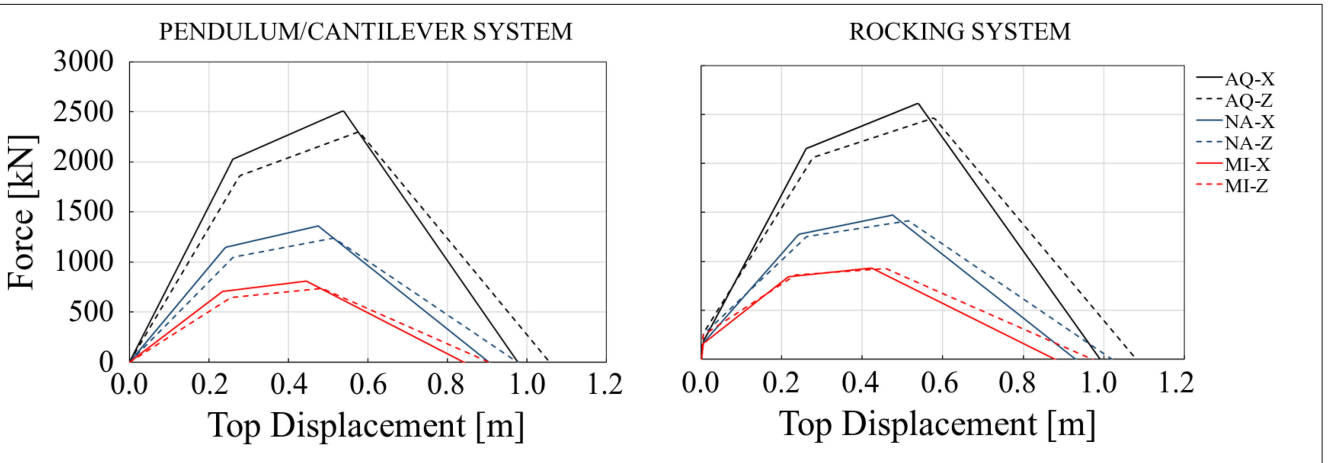

FIGURE 6 | Pushover analysis results for Pendulum and Cantilever panel arrangement.

TABLE 1 | The displacement capacity for all panel arrangement for all sites.

Site	Type of Panel Arrangement	Displacement Capacity [m]		Type of Panel Arrangement	Displacement Capacity [m]	
		X	Z		X	Z
Napoli	Pendulum/ Cantilever	0.69	0.745	Rocking	0.705	0.765
L'Aquila		0.76	0.82		0.765	0.83
Milano		0.645	0.695		0.65	0.715

have been considered as CLS: Global Failure Limit State (GFLS) and Local Failure Limit State (LFLS).

The engineering demand parameter for GFLS representing the global failure of the structure in terms of lateral load resisting behavior is the maximum roof displacement. The corresponding top displacement capacity is evaluated via non-linear pushover analyses (**Figure 6**). The EDP threshold is identified along the softening branch of the pushover curve as the post-peak displacement corresponding to a 50% reduction in base shear, in accordance with the general RiNTC project criteria (Iervolino et al., 2018). **Table 1** shows the displacement capacity threshold for all considered cases.

LFLS is defined by the shear failure of the beam-column dowel connection. The shear strength of the dowel connection has been evaluated with a more recent formulation, outcome of a large experimental program carried out in the framework of the Safecast project, as the minimum of those actions associated with ductile failure of the dowel bars and crushing of surrounding concrete (EUR 27935 EN, 2016). The steel failure resulted critical for the considered joints, where the dowel strength has been computed on the safe side assuming the unconfined concrete strength. The shear strength values of the connections of the different buildings considered are 79.5 kN, 153.4 kN, and 232.0 kN for Milano, Napoli, and L'Aquila, respectively. Details on this calculation and on comparisons with formulas provided by other authors, including Vintzeleou and Tassios (1987) and Zoubek et al. (2015), are available in Cimmino et al. (2020).

Damage Limit States

This limit state corresponds to damage prevention of the non-structural elements, i.e., cladding panels. DLS is relevant in terms of the economic losses, and it causes building use interruption for the repair. Two limit states have been considered as DLS, namely, Standard Damage Limit State (SDLS) and Panel Failure Limit State (PFLS).

The adopted EDP for SDLS is the roof displacement, and the capacity threshold value is set to 1% of inter-story drift in accordance with the provisions of NTC2008 and Eurocode 8. It is to be noted that past studies carried out by Babič and Dolšek (2016) show that at roof displacement of 1% of column height, 50% of traditional panel-to-structure connections fail. These results have been obtained on traditional connections which are characterized by a small displacement capacity (Zoubek et al., 2016), which is however not depending on the height of the building. The limit of 1% of column height to attain DLS is practically too tolerant for traditional cladding connections, and too strict for the innovative panel connections considered in this work, since the latter can easily accommodate much larger displacements.

Despite being a potential source of casualties, the collapse of the cladding panels associated with the failure of their connections with the structure is herein framed as an intermediate damage condition in accordance with the general RiNTC project criteria (Iervolino et al., 2018), since this event does not lead to global failure or jeopardy of the global structural system. The functional limit displacement for each panel arrangement depends on their aspect ratio and has been set to 250 mm for all arrangements, based on attainment of collision for pendulum and rocking arrangements and on the exhaustion of the slider stroke for cantilever arrangement.

NON-LINEAR DYNAMIC MULTI-STRIPE ANALYSIS

The time-history response of the case study buildings depends on the intensity measure of the seismic event, e.g., peak ground acceleration PGA or spectral acceleration at first natural period $S_a(T_1)$. Seismic assessment has been carried out by means of multi-stripe analyses (Jalayer and Cornell, 2003; Jalayer, 2013) at 10 intensity levels associated with the return periods collected in Cimmino et al. (2020) for subsoil type C (not reported here for the sake of brevity). A set of 20 records is selected at each intensity level for the three sites. The ground motion records have been selected based on the conditional mean spectrum approach selecting as reference intensity measure the spectral acceleration at period of 2.0 s (Shome and Cornell, 1999; Jayaram et al., 2011; Lin et al., 2013).

Figure 7 shows the comparison of displacement time-history for the investigated panel arrangements under one of the selected ground motions at the L'Aquila site. The maximum top displacement has been reduced in the rocking system due to the restoring forces provided by the self-weight of the cladding panels. Residual drift after the earthquake is almost zero. The response of the simplified cantilever shows a similar trend to the pendulum system in terms of maximum top displacement and shear. The addition of the friction forces does not introduce a relevant difference in this case either.

The mean values of the D/C ratio for CLS are similar among the investigated panel arrangements. For the sake of brevity, only the D/C curves related to the pendulum arrangement are reported in **Figure 8**. Circle markers are associated with global collapse condition, while square markers refer to local collapse conditions. Structures designed according to different hazard levels are differentiated by the markers' color: Milano in red, Napoli in blue, and L'Aquila in black. The D/C ratios in terms of the shear force in the beam-to-column connections associated with LFLS are always larger than those in terms of the roof displacements associated with GFLS. Only in the case of the L'Aquila site has attainment of the failure limit reached the largest considered return period of 100,000 years, whereas it is never attained in the case of Milano and Napoli. This

indicates that the seismic vulnerability to the seismic action of the panel arrangements is significantly lower than the one assumed for design with a reference return period of $T_R = 475$ years. Therefore, this shows that the Italian building code, which follows the approach of Eurocode 8, overestimates the necessary capacity requirements for these case studies. With reference to another ultimate limit state according to the Italian building code which is the "near collapse limit state" (i.e., SLC) associated with

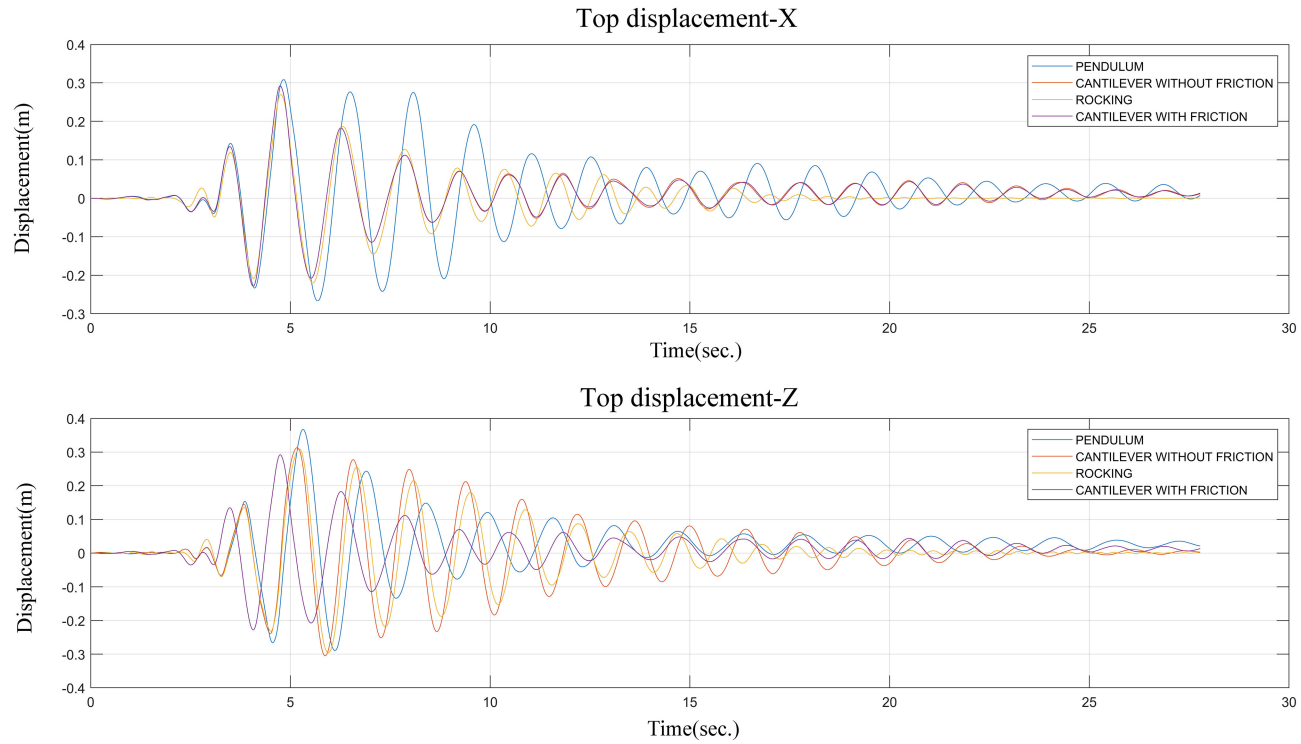

FIGURE 7 | Time-history response of the panel arrangements at the L'Aquila site.

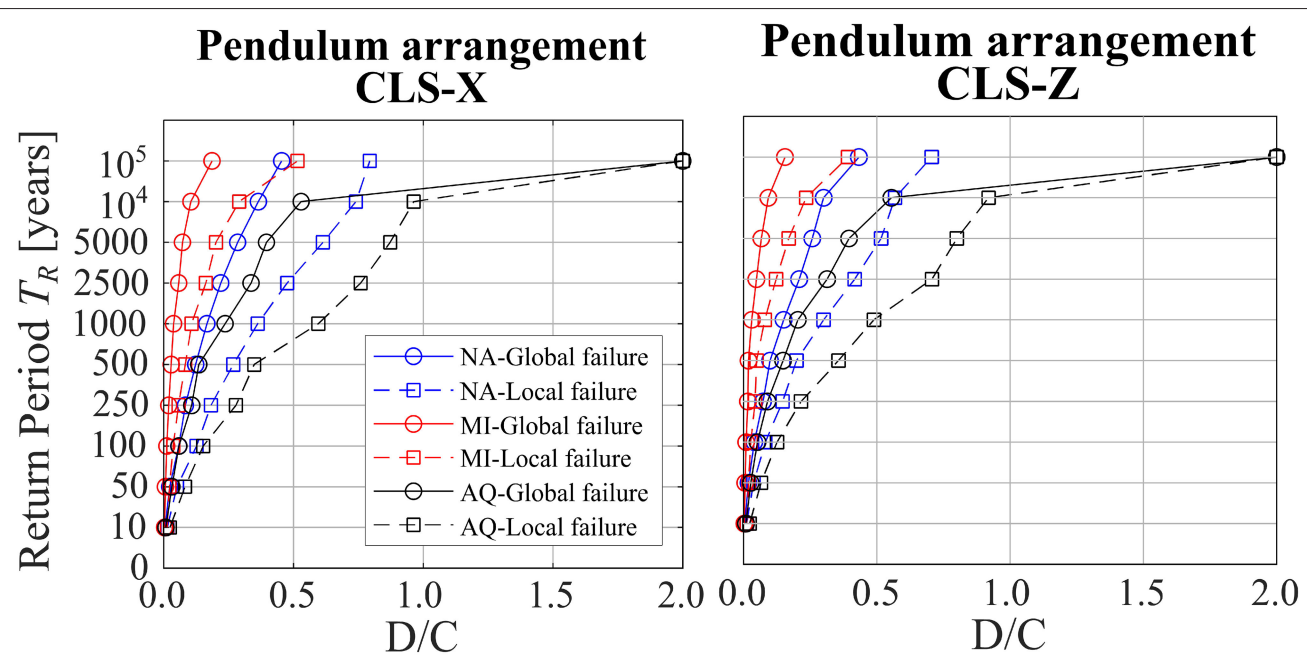

FIGURE 8 | The mean value of D/C ratio with reference to Collapse Limit State for all considered panel arrangement at three considered sites.

a return period of 975 years, the D/C ratio is still significantly lower than 1. It is important to note that the mean D/C ratios increase with the hazard level at each site, showing that the code provisions do not guarantee uniform average safety with respect to the collapse limit state.

Concerning DLS, **Figure 9** shows the comparison of the mean value of the D/C ratio for both Damage limit states with a marker layout similar to the one proposed in **Figure 8**. In general, the D/C ratios for DLS are much larger than those at CLS, mainly due to the intrinsic flexibility of precast industrial frames composed by cantilever columns only acting as a lateral load-resisting system.

According to the Italian build code, design at DLS is referred to a return period of the $T_R = 50$ year. In L'Aquila (high hazard) and Napoli (medium hazard), the mean Standard DLS is attained at a return period of 250 years. As mentioned in the previous section, the standard limit associated with SDLS is severe for the panel arrangements designed with modern connections, as they could easily accommodate small displacements without failure. The second considered damage limit state, the mean Panel DLS is attained at $T_R = 2500$ year in the case of L'Aquila, $T_R =$ 10,000 years in Napoli, and never attained in Milano. As in the case of the Collapse limit state, the D/C ratio increases as the hazard level increases for the same return period. The results conclude that the above-cited codes do not guarantee a uniform distance from the attainment of a damage limit state when varying the seismic hazard. The results of the "Panel Failure limit state" show the effectiveness of the considered panel arrangements.

Even though the mean value of the Demand/Capacity ratio looks similar for different panel arrangements, the maximum response of each panel arrangement differs from each other. **Figure 10** shows the ratio of the maximum value of EDPs at each intensity level of cantilever with friction/cantilever without the friction/Rocking system to that of the Pendulum system.

Figure 10 shows the relevant reduction of the displacement and the shear forces in the rocking system due to the restoring forces which added non-linear elastic hysteresis. This effect is more evident in a weaker frame of a low seismic hazard site, e.g., Milano. The response of the cantilever system is similar to that of the pendulum system.

EFFECT OF SPREAD PANEL MASS MODELING

Upgraded models have been set to investigate the influence of the simplifying assumption of lumped panel mass instead of a more realistic distribution of masses. To this aim, only the pendulum arrangement has been considered. The numerical model has been modified model as described in **Figure 11**, removing the amount of lumped mass associated with the cladding panels from the master node of the roof and implementing two vertical beam elements collecting the spread mass and stiffness of the full lines of panels. The stiffness of a single panel has been modeled which has been assimilated to the one of a 12-cm-thick solid concrete panel, equivalent of typical sandwich panels with the outer suspended layer. The elastic beam elements have been restrained at their base with a flexural hinge with prevented torsion. The element is linked to the master node at its height, enforcing a portion of the panel to behave as a cantilever beyond such location.

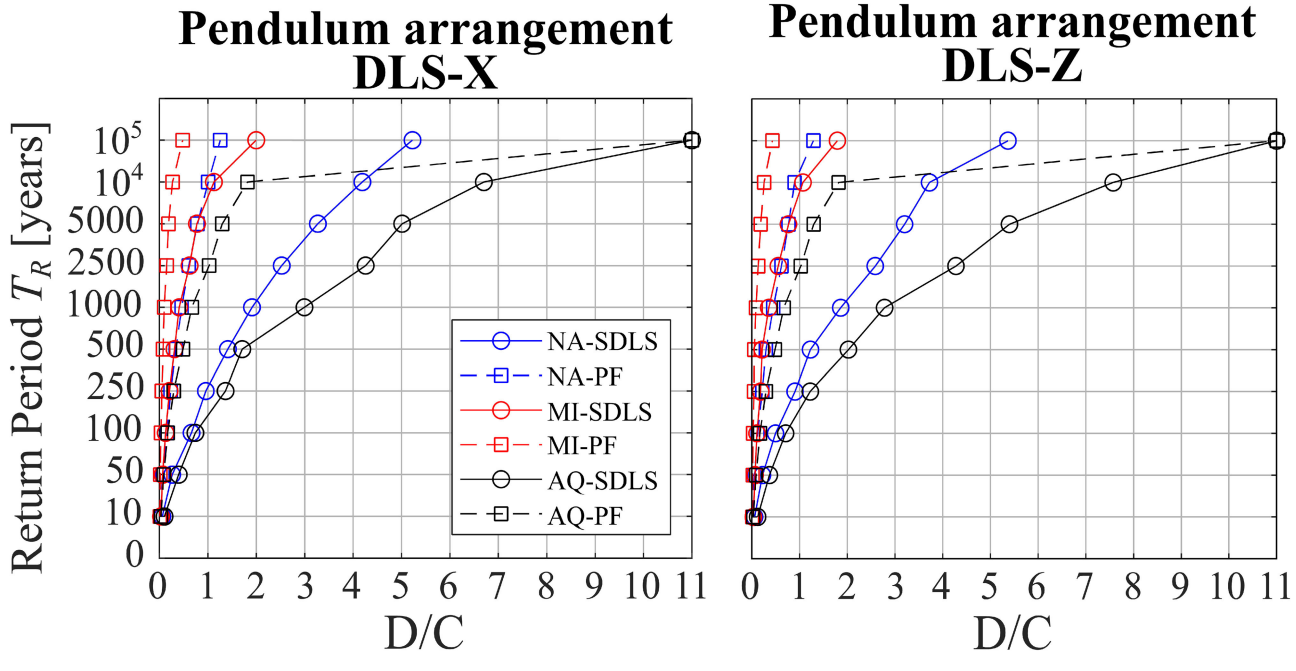

FIGURE 9 | The mean value of D/C ratio with reference to Damage Limit State for all considered panel arrangement at three considered sites.

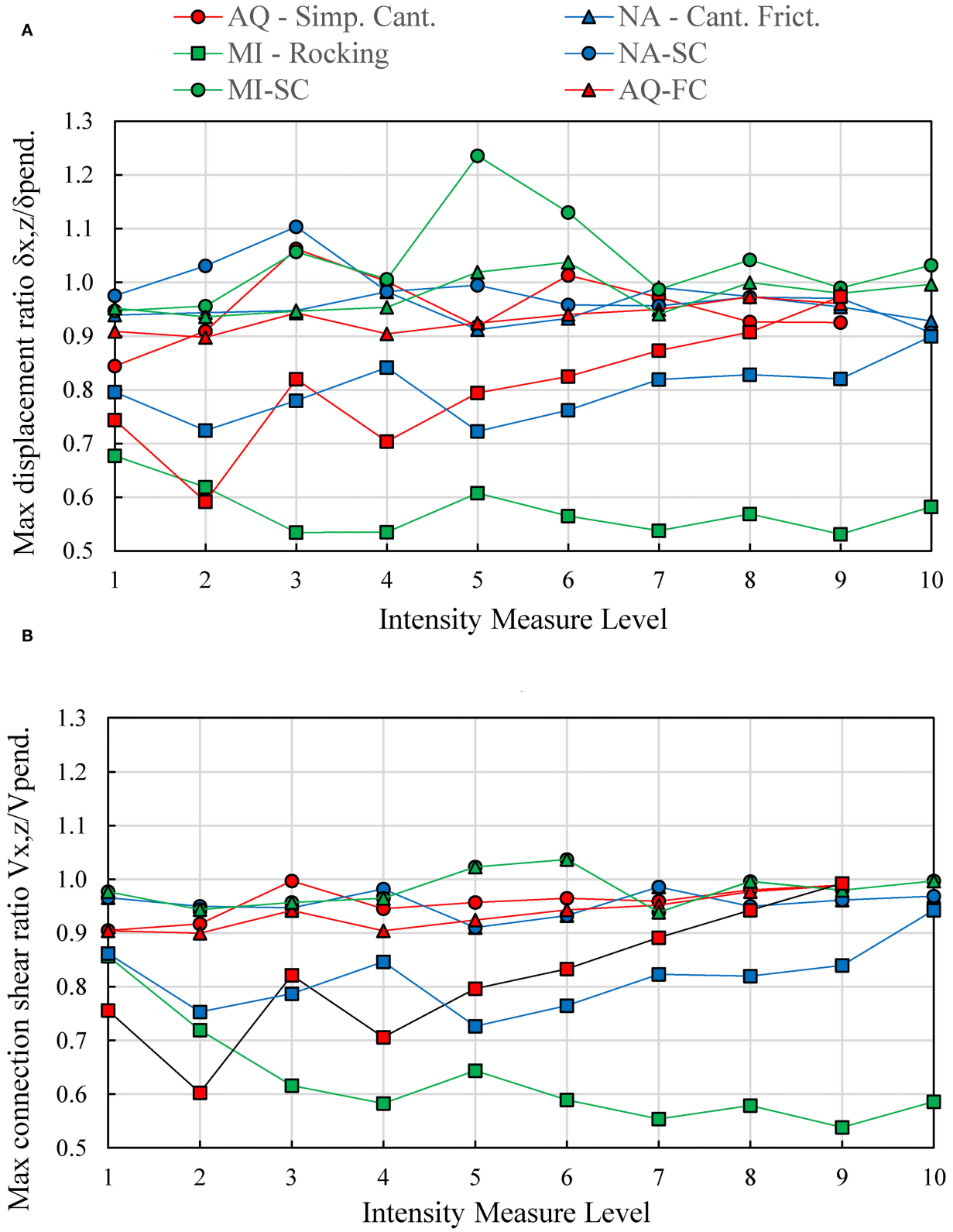

FIGURE 10 | Performance ratio of the other panel connection systems over the pendulum system: **(A)** displacement and **(B)** local shear.

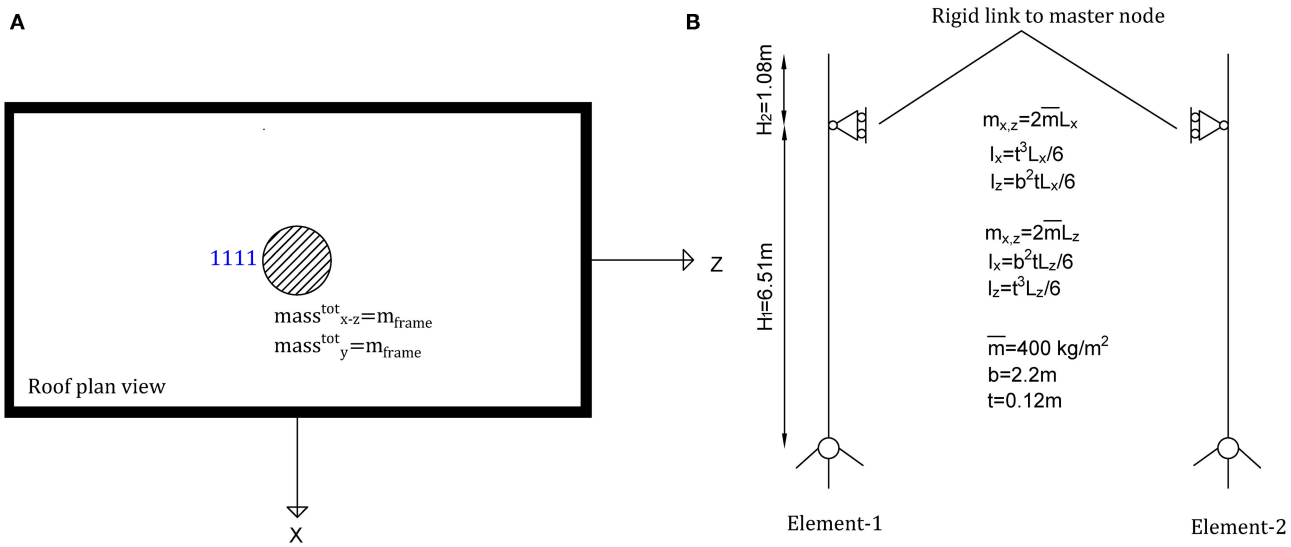

FIGURE 11 | Details of mass modeling: **(A)** lumped frame mass, **(B)** spread mass over elastic beam elements.

TABLE 2 | Fundamental periods calculated in each main direction: comparison with model results for both spread and lumped panel mass assumptions.

	Frame Only		Spread Mass Theoretical			Spread Mass Numerical		Spread Mass Theor/Num		Lumped Mass Numerical		Lumped/Spread	
	T_1 [s]	T_2 [s]	χ [–]	T_1 [s]	T_2 [s]	T_1 [s]	T_2 [s]	T_1 [–]	T_2 [–]	T_1 [s]	T_2 [s]	T_1 [–]	T_2 [–]
Milano	1.83	1.69	1.190	2.18	2.01	2.18	2.01	1.001	0.999	2.41	2.22	1.106	1.104
Napoli	1.54	1.42	1.190	1.83	1.69	1.84	1.70	1.004	1.006	1.96	1.81	1.065	1.065
L'aquila	1.22	1.14	1.187	1.45	1.35	1.45	1.35	1.001	0.998	1.54	1.44	1.062	1.067

In such a model, the single element tilts during the seismic motion in both horizontal directions. Nonetheless, their rotational inertia is taken into consideration with this modeling technique, while it has been disregarded with the simplified assumptions of lumped mass. The theoretical values of the natural periods associated with the main vibration modes in each translational direction are reported in **Table 2** and have been computed according to Foti et al. (2018). The results of the numerical model confirm with remarkable precision the theoretical values (**Table 2**), with differences originating only from numerical rounding. A comparison with the periods from the models with lumped mass is also provided in **Table 2**. The results show that the more realistic spread mass distribution leads to a decrease of the fundamental periods of the order of 6–10%.

The full set of non-linear dynamic analyses previously carried out on the lumped mass model has been repeated with the spread mass model. **Figure 12** represents the statistical description of the ratio between maximum measured displacements (i.e., EDP for GFLS and SDLS) for spread mass models vs. lumped mass models. Sample mean values and standard deviations for such ratios are obtained for each stripe based on the time-history analyses of the 20 ground motions. A large dispersion of ratios can be observed, meaning that the dynamic behavior is remarkably modified by the panel mass modeling technique. Furthermore, the mean ratios highlight an increase of about 10% of the maximum displacements, quantifying the error on the unsafe side made when adopting the simplified assumption of lumped mass distribution.

Within the spread mass model, the in-plane and out-of-plane forces in the panel connections have been recorded as the concentrated horizontal shear actions on the beam elements simulating the panels in correspondence of the link with the roof master node. Considering the shear key connector successfully used in the experimentation related to both pendulum and rocking systems in the Safecladding test program (Negro and Lamperti Tornaghi, 2017; Toniolo and Dal Lago, 2017; Dal Lago and Molina, 2018), whose structural behavior under simple shear and combined shear-axial forces is described in **Figure 13**, the D/C ratios and failure rates could be evaluated. The results, collected in **Figure 14**, show peculiarly low D/C ratios apart from the higher stripes of the L'Aquila site. This is attributable not only to the large strength of the device but also to the low accelerations transmitted by the more flexible frame structures designed at Milano and Napoli sites.

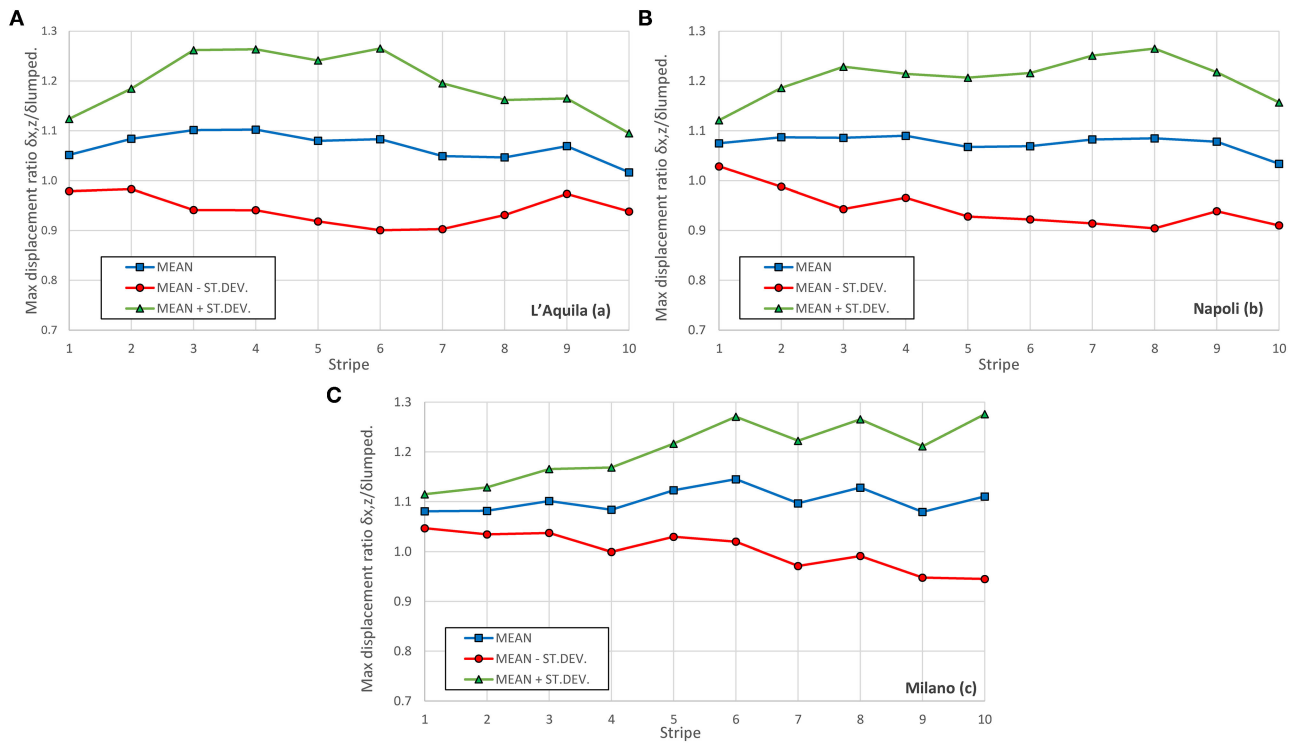

FIGURE 12 | Maximum displacement ratio of results from model with spread panel mass and lumped panel mass for the site: **(A)** Milano, **(B)** Napoli, and **(C)** L'Aquila.

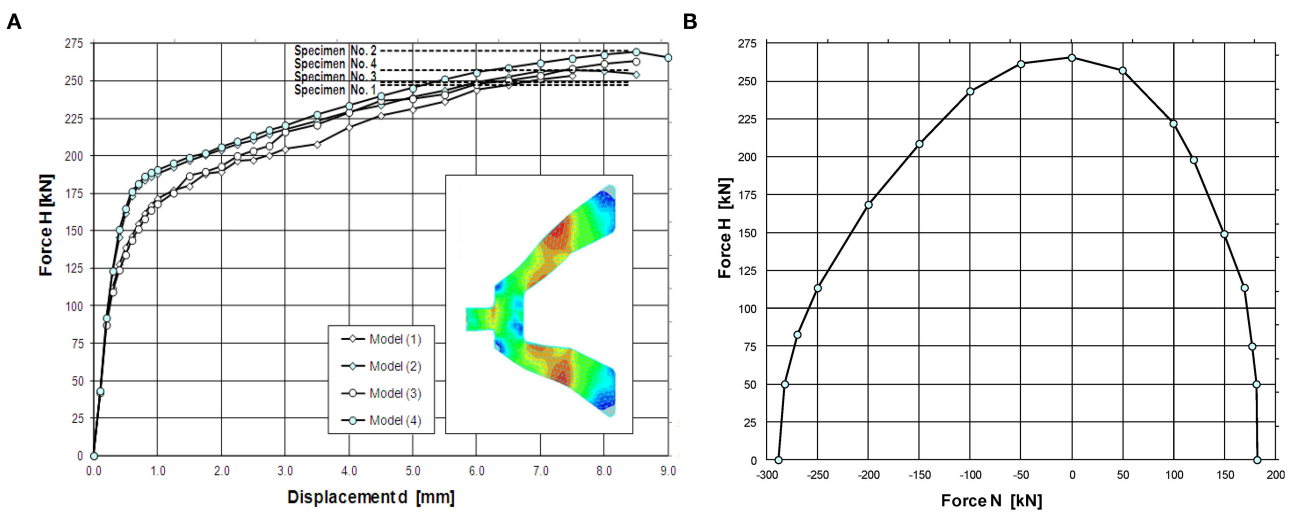

FIGURE 13 | Cladding shear key connection considered: **(A)** numerical shear pushover curves vs. experimental strength and **(B)** shear-axial interaction domain.

CONCLUSIONS

The D/C ratio curves obtained in this work indicate a low vulnerability of well-detailed modern precast industrial frame structures provided with decoupling cladding connections, with combined global/local collapses recorded only for the higher return period of 10^5 years in the site of high seismic hazard of L'Aquila. The seismic behavior of this structural typology is characterized by large deformability and displacement capacity, with the global collapse condition being associated with the leaning of the structure due to second-order effect. However, this behavior makes the structural assembly less performant toward the damage limit state, since the standard damage limitation conditions are overcome

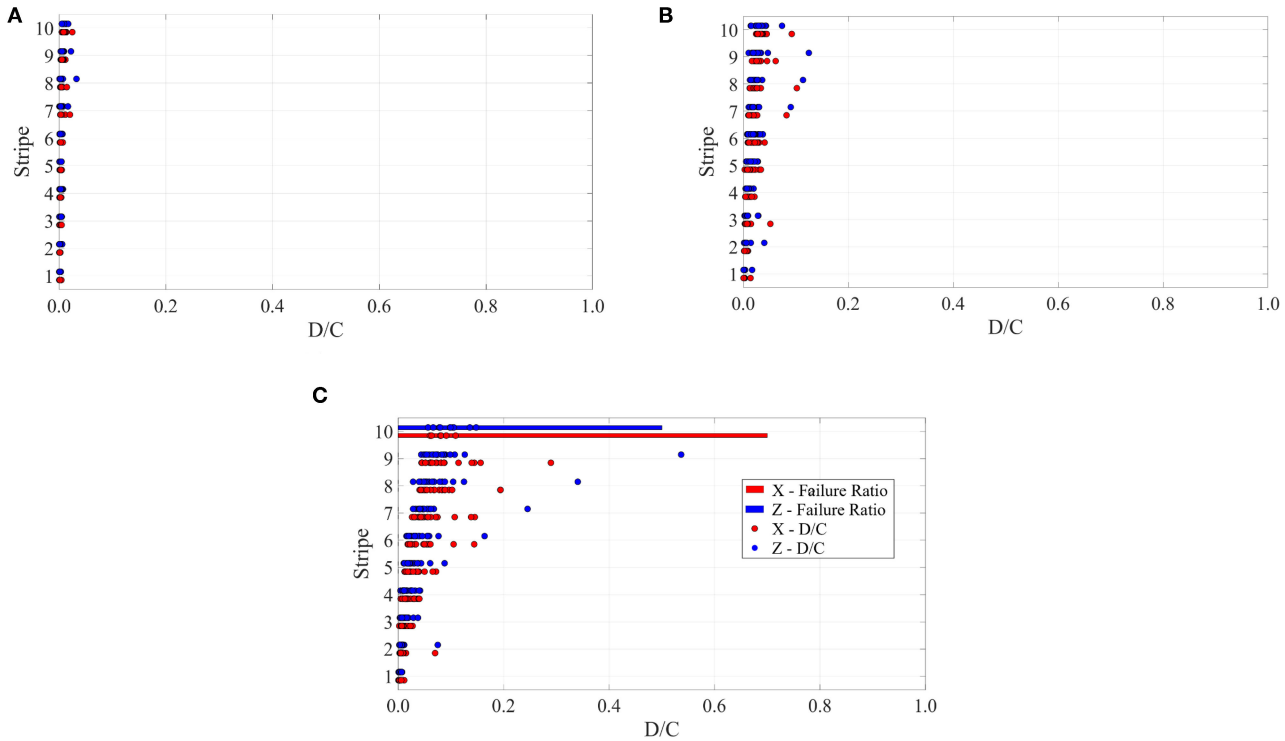

FIGURE 14 | Cladding connection D/C and failure ratios for the site of: **(A)** Milano, **(B)** Napoli, and **(C)** L'Aquila.

with high probability for large return periods in all the considered sites.

The adoption of innovative cladding connections leading to an effective decoupling of the frame structure motion from the lateral stiffness of the cladding panels of precast industrial buildings leads to relevant enhancement in their seismic behavior, with displacement being associated with the failure of these connections about one order of magnitude larger than that associated with more traditional fixed channel connections. The performance in the damage limit state appears to be much better if adopting specific engineering demand parameters related to the failure of the cladding panel connections considered, for instance the no-collision condition for tilting panels (pendulum and rocking arrangements) or the exhaustion of the available stroke for sliding connections typical of the cantilever arrangement.

The rocking arrangement provides the lower maximum drifts, due to the recentering effect provided by the self-weight of the cladding panels, which is more pronounced for weaker frame structures, hence for low seismic hazard areas. The adoption of the common assumption of lumped mass of the cladding panels in the centroid of the roof involving a percentage of the total panel mass related to its tributary area proved not to be fully on the safe side, since the comparison with new models involving a spread panel mass shows that the lumped models provide higher fundamental periods (associated in general with lower accelerations) and systematically lower seismic displacements, with around 10% being the increase in displacement demand when considering spread cladding mass. Moreover, spreading the mass by introducing the panel rotational inertia severely affects the dynamic behavior of the structural system. The maximum loads on one real typology of strong hinged panel-to-structure connection considered are fully compatible with the device strength for all intensity measure levels for the sites of Milano (low hazard) and Napoli (medium hazard), while the demand overcomes the capacity only in the higher-intensity measure level for the site of L'Aquila (high hazard).

The D/C curves computed are more severe for sites with a higher seismic hazard. This result highlights that the current code provisions for the Italian territory do not ensure uniform safety with respect to both collapse and damage limit states as the seismic hazard varies, the safety margin lowering with the hazard. Ongoing developments are concerning the vulnerability analysis of both new and existing buildings with flexible diaphragm and with sophisticated constitutive laws for the existing roof slab and cladding panel connections, also considering the effect of the vertical acceleration. Further developments should also aim to address the seismic risk of structures and systems of structures with a probabilistic life-cycle perspective based on probabilistic frameworks involving performance metrics such as resilience (Capacci and Biondini, 2020; Capacci et al., 2020) as well as economic user cost indicators (Messore et al., 2020).

DATA AVAILABILITY STATEMENT

The raw data supporting the conclusions of this article will be made available by the authors upon request.

AUTHOR CONTRIBUTIONS

KG developed the numerical model, arranged the pre-processing, and carried out post-processing of the results. BDL provided guidance for the underlying modeling assumptions of the considered precast structures and drafted the paper. LC provided guidance for the implementation of the structural model and the development of the multi-stripe seismic risk analyses. FB supervised and coordinated the activities. All authors contributed to the article and approved the submitted version.

FUNDING

This research study was funded by the Italian Department of Civil Protection within the framework of the national project DPC/ReLUIS 2019-2021.

ACKNOWLEDGMENTS

The other members of the working group on precast concrete buildings within the project DPC/ReLUIS 2019-2021, including Andrea Belleri, Davide Bellotti, Gennaro Magliulo, Roberto Nascimbene, and Paolo Riva, are gratefully acknowledged for their cooperation.

REFERENCES

Asteris, P. G., Cavaleri, L., Di Trapani, F., and Tsaris, A. K. (2017). Numerical modelling of out-of-plane response of infilled frames: state of the art and future challenges for the equivalent strut macromodels. *Eng. Struct.* 132, 110–122. doi: 10.1016/j.engstruct.2016.10.012

Babič, A., and Dolšek, M. (2016). Seismic fragility functions of industrial precast building classes. *Eng. Struct.* 118, 357–370. doi: 10.1016/j.engstruct.2016.03.069

Batalha, N., Rodrigues, H., and Varum, H. (2019). Seismic performance of RC precast industrial buildings—learning with the past earthquakes. *Inn. Infrastruct. Solut.* 4:4. doi: 10.1007/s41062-018-0191-y

Belleri, A., Brunesi, E., Nascimbene, R., Pagani, M., and Riva, P. (2015a). Seismic performance of precast industrial facilities following major earthquakes in the italian territory. *ASCE J. Perf. Constr. Fac.* 29:04014135. doi: 10.1061/(ASCE)CF.1943-5509.0000617

Belleri, A., Labò, S., Marini, A., and Riva, P. (2017). The influence of overhead cranes in the seismic performance of industrial buildings. *Front. Built Environ.* 3:64. doi: 10.3389/fbuil.2017.00064

Belleri, A., Torquati, M., Riva, P., and Nascimbene, R. (2015b). Vulnerability assessment and retrofit solutions of precast industrial structures. *Earthq. Struct.* 8, 801–820. doi: 10.12989/eas.2015.8.3.801

Biondini, F., Dal Lago, B., and Toniolo, G. (2013). Role of wall panel connections on the seismic performance of precast structures. *Bull. Earthq. Eng.* 11, 1061–1081. doi: 10.1007/s10518-012-9418-z

Biondini, F., and Toniolo, G. (2009). Probabilistic calibration and experimental validation of the seismic design criteria for one-story concrete frames. *J. Earthq. Eng.* 13, 426–462. doi: 10.1080/13632460802598610

Bournas, D., Negro, P., and Taucer, F. (2013). Performance of industrial buildings during the Emilia earthquakes in Northern Italy and recommendations for their strengthening. *Bull. Earthq. Eng.* 12, 2383–2404. doi: 10.1007/s10518-013-9466-z

Capacci, L., and Biondini, F. (2020). Probabilistic life-cycle seismic resilience assessment of aging bridge networks considering infrastructure upgrading. *Struct. Infrastruct. Eng.* 16, 659–675. doi: 10.1080/15732479.2020.1716258

Capacci, L., Biondini, F., and Titi, A. (2020). Lifetime seismic resilience of aging bridges and road networks. *Struct. Infrastruct. Eng.* 16, 266–286. doi: 10.1080/15732479.2019.1653937

CEN, (2005). *Eurocode 8: Design of Structures for Earthquake Resistance-Part 1: General Rules, Seismic Actions and Rules for Buildings*. Dublin: National Standards Authority of Ireland.

Cimmino, M., Magliulo, G., and Manfredi, G. (2020). Seismic collapse assessment of new European single-story RC precast buildings with weak connections. *Bull. Earthq. Eng.* 18, 6661–6686. doi: 10.1007/s10518-020-00952-7

CNR 10025/98 (2000). *Istruzioni per il progetto, l'esecuzione ed il controllo delle strutture prefabbricate in calcestruzzo: CNR 10025/98 (in Italian)*. Roma : Consiglio nazionale delle ricerche.

Dal Lago, B. (2019). Numerical simulation of seismic tests on precast concrete structures with various arrangements of cladding panels. *Comput. Concr.* 23, 81–95. doi: 10.12989/cac.2019.23.2.081

Dal Lago, B., Bianchi, S., and Biondini, F. (2019). Diaphragm effectiveness of precast concrete structures with cladding panels under seismic action. *Bull. Earthq. Eng.* 17, 473–495. doi: 10.1007/s10518-018-0452-3

Dal Lago, B., Biondini, F., and Toniolo, G. (2018). Seismic performance of precast concrete structures with energy dissipating cladding panel connection systems. *Struct. Concr.* 19, 1908–1926. doi: 10.1002/suco.201700233

Dal Lago, B., and Ferrara, L. (2018). Efficacy of roof-to-beam mechanical connections on the diaphragm behaviour of precast decks with spaced roof elements. *Eng. Struct.* 176, 681–696. doi: 10.1016/j.engstruct.2018.09.027

Dal Lago, B., and Lamperti Tornaghi, M. (2018). Sliding channel cladding connections for precast structures subjected to earthquake action. *Bull. Earthq. Eng.* 16, 5621–5646. doi: 10.1007/s10518-018-0410-0

Dal Lago, B., and Molina, F. J. (2018). Assessment of a capacity spectrum design approach against cyclic and seismic experiments on full-scale precast RC structures. *Earthq. Eng. Struct. Dyn.* 47, 1591–1609. doi: 10.1002/eqe.3030

Dal Lago, B., Toniolo, G., Felicetti, R., and Lamperti Tornaghi, M. (2017). End support connection of precast roof elements by bolted steel angles. *Struct. Concr.* 18, 755–767. doi: 10.1002/suco.201600218

Di Domenico, M., De Risi, M. T., Ricci, P., Verderame, G. M., and Manfredi, G. (2021). Empirical prediction of the in-plane/out-of-plane interaction effects in clay brick unreinforced masonry infill walls. *Eng. Struct.* 227:111438. doi: 10.1016/j.engstruct.2020.111438

Ercolino, M., Bellotti, D., Magliulo, G., and Nascimbene, R. (2018). Vulnerability analysis of industrial RC precast buildings designed according to modern seismic codes. *Eng. Struct.* 158, 67–78. doi: 10.1016/j.engstruct.2017.12.005

EUR 27935 EN (2016). "Design guidelines for wall panel connections," in *SAFECLADDING (Grant agreement n° 314122. Year 2012)*, eds A. Colombo, P. Negro, G. Toniolo, and M. Lamperti Tornaghi (Luxembourg: Publications Office of the European Union), 1–150.

Foti, F., Dal Lago, B., and Martinelli, L. (2018). "Sull'interazione sismica fuori piano tra telai prefabbricati e pannelli di tamponamento/on the seismic out-of-plane interaction between precast frames structures and cladding panels," in *Italian Concrete Days 2018 (ICD2018), Milano/Lecco, Italy, 15th-18th June, Paper No. 42* (Milano/Lecco).

Ibarra, L. F., Medina, R. A., and Krawinkler, H. (2005). Hysteretic models that incorporate strength and stiffness deterioration. *Earthq. Eng. Struct. Dyn.* 34, 1489–1511. doi: 10.1002/eqe.495

Iervolino, I., Spillatura, A., and Bazzurro, P. (2018). Seismic reliability of code-conforming Italian buildings. *J. Earthq. Eng.* 22, 5–27. doi: 10.1080/13632469.2018.1540372

Jalayer, F. (2013). *Direct probabilistic seismic analysis: implementing non-linear dynamic assessments* (Ph.D. thesis dissertation). Stanford University, Stanford, CA, United States.

Jalayer, F., and Cornell, C. A. (2003). A special application of non-linear dynamic analysis procedures in probability-based seismic assessments in the region of global dynamic instability. *Appl. Stat. Probab. Civ. Eng.* 1–2.

Jayaram, N., Lin, T., and Baker, J. W. (2011). A computationally efficient ground-motion selection algorithm for matching a target response spectrum mean and variance. *Earthq. Spectra* 27, 797–815. doi: 10.1193/1.3608002

Lin, T., Haselton, C. B., and Baker, J. W. (2013). Conditional spectrum-based ground motion selection. Part I: hazard consistency for risk-based assessments. *Earthq. Eng. Struct. Dyn.* 42, 1847–1865. doi: 10.1002/eqe.2301

Magliulo, G., Bellotti, D., Cimmino, M., and Nascimbene, R. (2018). Modeling and seismic response analysis of RC precast Italian code-conforming buildings. *J. Earthq. Eng.* 22, 140–167. doi: 10.1080/13632469.2018.1531093

Magliulo, G., Ercolino, M., Petrone, C., Coppola, O., and Manfredi, G. (2014). Emilia earthquake: the sesmic performance of precast RC buildings. *Earthq. Spectra* 30, 891–912. doi: 10.1193/091012EQS285M

Mazza, F. (2019). In-plane-out-of-plane non-linear model of masonry infills in the seismic analysis of r.c.-framed buildings. *Earthq. Eng. Struct. Dyn.* 48, 432–453. doi: 10.1002/eqe.3143

Mazzoni, S., McKenna, F., Scott, M. H., and Fenves, G. L. (2006). Open System for Earthquake Engineering Simulation (OpenSEES) User Command-Language Manual. *Pacific Earthq. Eng. Res. Cent.* 465.

Messore, M. M., Capacci, L., and Biondini, F. (2020). Life-cycle cost-based risk assessment of aging bridge networks. *Struct. Infrastruct. Eng.* 17, 515–533. doi: 10.1080/15732479.2020.1845752

MIT (Ministero delle Infrastrutture e dei Trasporti) (2008). *D.M. 14/01/2008–Norme Tecniche per le Costruzioni*. Rome: MIT.

Negro, P., and Lamperti Tornaghi, M. (2017). Seismic response of precast structures with vertical cladding panels: the SAFECLADDING experimental campaign. *Eng. Struct.* 132, 205–228. doi: 10.1016/j.engstruct.2016.11.020

Pasca, M., Liberatore, L., and Masiani, R. (2017). Reliability of analytical models for the prediction of out-of-plane capacity of masonry infills. *Struct. Eng. Mech.* 64, 765–781. doi: 10.12989/sem.2017.64.6.765

Savoia, M., Buratti, N., and Vincenzi, L. (2017). Damage and collapses in industrial precast buildings after the 2012 Emilia earthquake. *Eng. Struct.* 137, 162–180. doi: 10.1016/j.engstruct.2017.01.059

Shome, N., and Cornell, C. A. (1999). *Probabilistic Seismic Demand Analysis of Non-linear Structures. Technical Report*. Stanford University.

Toniolo, G., and Colombo, A. (2012). Precast concrete structures: the lessons learned from the L'Aquila earthquake. *Struct. Concr.* 13, 73–83. doi: 10.1002/suco.201100052

Toniolo, G., and Dal Lago, B. (2017). Conceptual design and full-scale experimentation of cladding panel connection systems of precast buildings. *Earthq. Eng. Struct. Dyn.* 46, 2565–2586. doi: 10.1002/eqe.2918

Vintzeleou, E. N., and Tassios, T. P. (1987). Behavior of dowels under cyclic deformations. *ACI Struct. J.* 84, 18–30. doi: 10.14359/2749

Zoubek, B., Fischinger, M., and Isaković, T. (2015). Estimation of the cyclic capacity of beam-to-column dowel connections in precast industrial buildings. *Bull. Earthq. Eng.* 13, 2145–2168. doi: 10.1007/s10518-014-9711-0

Zoubek, B., Fischinger, M., and Isaković, T. (2016). Cyclic response of hammer hammer-head strap cladding cladding-to -structure connections used in RC precast buildings buildings. *Eng. Struct.* 119, 135–148. doi: 10.1016/j.engstruct.2016.04.002

Conflict of Interest: BDL is partner—and KG is collaborator—of DLC Consulting srl of Milan, Italy, a Structural Engineering consultant company active in different fields, among which precast concrete structures. The consultant holds several patents, including some concerning cladding panel connections which may be employed to make some of the arrangements investigated in the paper.

The remaining authors declare that the research was conducted in the absence of any commercial or financial relationships that could be construed as a potential conflict of interest.

frontiers in Built Environment

ORIGINAL RESEARCH
published: 20 December 2021
doi: 10.3389/fbuil.2021.639777

Seismic Behavior of Precast Buildings With Dissipative Connections

Lorenzo De Stefani and Roberto Scotta*

DICEA Department of Civil Environmental and Architectural Engineering, University of Padova, Padova, Italy

Recent earthquakes in southern Europe highlighted that the connections of cladding panels to R.C. frames in precast buildings had a major role in the structural collapse. For this reason, there is an urgent need for a review of the design methods for these connections as well as for an improvement in the manufacturing technology. This article aimed to assess the efficiency of dissipative panel-to-structure and roof connections in R.C. precast buildings. A parametric study consisting of linear and non-linear analyses on one case-study building is performed. Different sensitivity analyses are performed varying their mechanical properties (i.e., stiffness, strength, and ductility) to analyze the behavior of the CP/frame connections. The study focuses on dissipative connections with an elastic–plastic behavior, placed between cladding panels (CPs) and frames in precast buildings with stacked horizontal cladding panels. The introduction of dissipative CP/frame connections implies the inclusion of panels in the global seismic resisting system. The "panels + frame" system highlights a high stiffness until the yield strength of the CP/frame connections is reached. The results, obtained from non-linear dynamic analyses (NLDAs), clearly show how the proposed connection improves the structural seismic performance. By contrast, this is no longer true for R.C. precast structures with flexible diaphragms, especially for intermediate columns, far from panels aligned to seismic action. In this case, significant and unexpected axial forces arise on out-of-plane connections between panels and columns. The integration of an efficient diaphragm is essential to prevent these critical issues both on intermediate columns and CP/column connections; it enables the dissipative capacity of the "panels + frame" system, and it significantly limits the forces and displacements of intermediate alignments. Unfortunately, the achievement of a rigid diaphragm is not always feasible in precast buildings. A possible alternative to activate dissipative capacities of the roof diaphragm with limited in-plane stiffness is the use of dissipative connections linking roof beams and main beams. The solutions described in this article can be applied both in the design of new buildings and for the seismic upgrading of existing ones with easy-to-install and low-impact applications.

Keywords: seismic design, precast structures, dissipative connections, elasto-plastic connection, precast and cantilever erection

OPEN ACCESS

Edited by:
Bruno Dal Lago,
University of Insubria, Italy

Reviewed by:
Marianna Ercolino,
University of Greenwich,
United Kingdom
Izuru Takewaki,
Kyoto University, Japan

****Correspondence:***
Lorenzo De Stefani
lorenzo.destefani@dicea.unipd.it

Specialty section:
This article was submitted to Earthquake Engineering, a section of the journal Frontiers in Built Environment

Received: *09 December 2020*
Accepted: *18 October 2021*
Published: *20 December 2021*

Citation:
De Stefani L and Scotta R (2021) Seismic Behavior of Precast Buildings With Dissipative Connections. Front. Built Environ. 7:639777. doi: 10.3389/fbuil.2021.639777

1 INTRODUCTION

The current design of R.C. precast buildings is typically based on bare frame models where perimetral cladding panels are considered only as seismic mass which does not contribute to the global lateral stiffness and resistance (i.e., non-structural elements (NSEs)). Cladding connections are mainly conceived to allow dimensional tolerance during the installation phase and to avoid out-of-plane overturning of the panels. Therefore, the panels are typically linked to the structure with fragile connections designed with local calculations for wind and/or seismic actions, thus evaluating only anchoring forces orthogonal to the plane of the panels.

Recent earthquakes in Italy, in particular L'Aquila 2009 (Menegotto 2009; Colombo and Toniolo 2012a) and Emilia 2012 (Colombo and Toniolo 2012b), have tragically demonstrated the shortcomings of this design approach.

Independent of the theoretical design approach of their connections, cladding panels behave as shear walls modifying the seismic response of precast buildings. The higher stiffness of the resisting system leads to higher global seismic forces than those evaluated with a frame model. Moreover, forces on panel connections are related to the global mass of the building, and they mainly lay in the plane of the panels. Therefore, forces on the connections are completely different from those evaluated with a local design approach.

Furthermore, the seismic force reduction in precast structures can be related on energy dissipation due to the development of plastic hinges at the base of the columns. Very large displacements at the top of the columns are required to activate this energy dissipation, and usually, the displacement capacity of the connections ends before the complete development of the required drift. Therefore, the design of these connections cannot be related with the seismic behavior factor used for the design of the bare structure.

Based on the previous considerations, the need for new technological solutions for connections designed with a consistent conceptual approach is undeniable.

Arnold (1989) proposed the following classification for cladding panels:

- completely separated cladding: not interfering with the lateral stiffness and resistance;
- accidentally participating cladding: characterized by a gap with the structural system too small compared to the seismic demand;
- controlled participating cladding: claddings contribute to the stiffness and damping of the structure (Pinelli et al., 1995, 1996; Craig et al., 1992; National Institute of Standards and Technology, 1998; Shultz et al., 1994; Ferrara et al., 2011);
- fully participating cladding: claddings are fully integrated in the lateral force resisting system (Biondini et al., 2013a; Magliulo et al., 2014).

Moreover, Colombo and Toniolo (2012b) presented some solutions to avoid panel collapse due to connection failure:

- the use of a statically determined support system, making the panels independent from the motion of the structure and allowing their rigid motion;
- the use of an integrated support system, well-proportioned, which makes the panels an effective part of the resisting structure.

The first approach was followed by Dal Lago et al. (2012) who carried out an experimental study of sliding bidirectional connections for efficient statically determined support systems.

Applying the second approach, Biondini et al. (2013a) presented an integrated frame-wall system with dissipative connections for precast building with the vertical panel.

Scotta et al. (2015) proposed an integrated frame-wall system with dissipative connections for precast buildings with horizontal panels. They also highlighted the development of very high axial forces on the out-plane CP/column connections in precast buildings with deformable roof, defining this behavior as the "skew effect."

Belleri et al. (2016) investigated the in-plane performance of the horizontal precast RC panel in one-story precast building.

Biondini et al. (2013b) highlighted the importance of a rigid roof diaphragm for enhancing the effectiveness of the integrated frame/wall support system with dissipative connections.

In this article, a fully stacked arrangement of horizontal CPs is considered. The CPs are placed one on the top of each other, and their weight loads the foundation beam.

Different from the previous work by the same authors (Scotta et al., 2015), a modified constraint pattern of panels is assumed:

- CP/frame connections sliding in the plane of the panels,
- CP/frame connections pinned in the out-of-plane of the panels,
- panel-to-panel fixed connections.

Dissipative connections are introduced between the main beam and the top panel, where the higher relative displacement between panels and frame develops.

Figure 1 represents constraints and in-plane independent movement of the dual structure.

This work demonstrates that the use of this type of CP/frame connections drastically modifies the seismic response of precast buildings, reducing global displacements and generalized stresses on columns compared to the bare frame structure. Moreover, for buildings with flexible diaphragms, the study shows a limited effectiveness in reducing forces on columns of intermediate alignments.

As suggested by Biondini et al. (2013b), a rigid roof floor could be realized to prevent this critical behavior. However, in precast buildings, a rigid diaphragm is not always feasible due to long spans and repetitive large openings at the roof level and for the interferences of suspended plants in existing buildings to be retrofitted.

Therefore, the effectiveness of a possible alternative solution to the rigid roof diaphragm is evaluated: the introduction of ductile elastic-plastic translational connections between roof beams and the main beams (**Supplementary Figure S1**) able to activate a dissipative capacity in the roof diaphragm with limited in-plane stiffness.

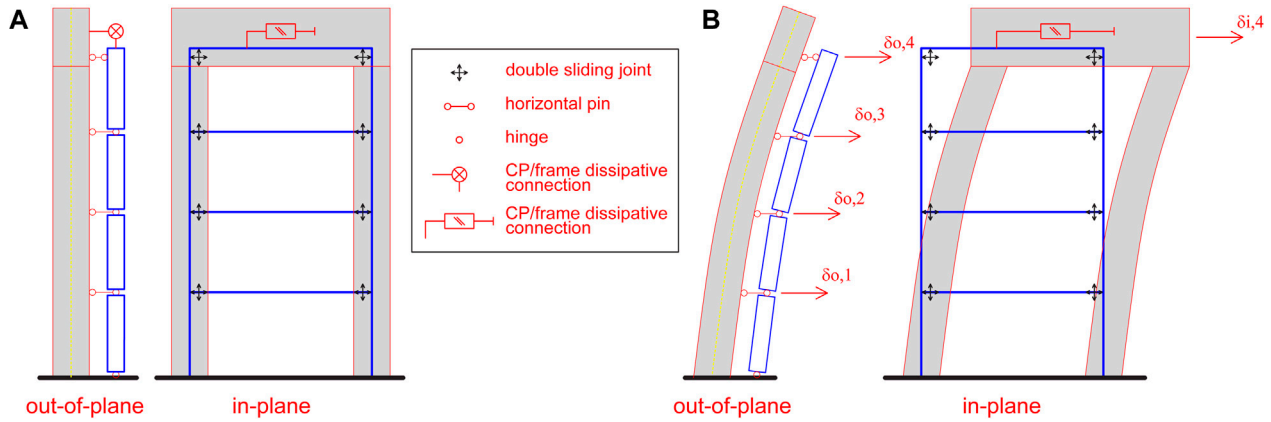

FIGURE 1 | In-plane and out-of-plane constraints and DOF.

2 Description of the Case-Study Building

The case study analyzed is the same presented in Scotta et al., 2015, but with horizontal cladding panels (**Supplementary Figure S2**) and a different restrain system for them (**Figure 1**).

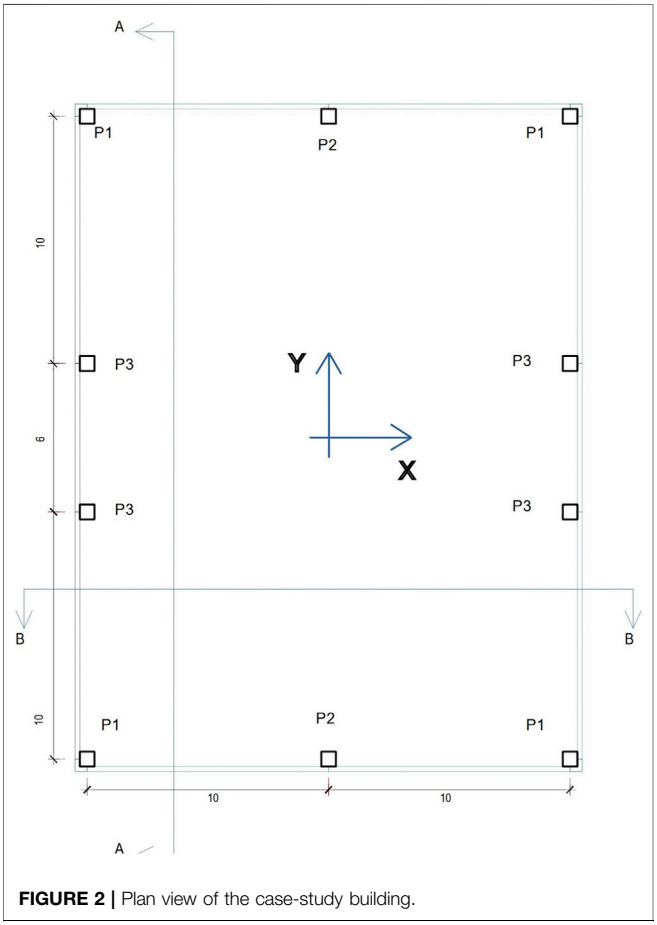

FIGURE 2 | Plan view of the case-study building.

A typical single-story precast RC building with CPs in horizontal configuration is analyzed (**Figure 1**). Its plan dimensions are 20.0 × 26.0 m. The structure is composed by

- 10 columns with a square cross-section 60 × 60 cm and 9.0 m high. Four columns (P1) are located at the corners of the building. Two columns (P2) are in the middle of short sides of the building. Four columns (P3) are placed in the middle of long sides of the building, to support panels and to allow openings;
- 4 main beams with I-section (W x H = 60 × 100 cm) along the *X* direction, simply supported by columns P1 and P2, with a span of 10 m;
- 8 roof beams, with TT 100/250 cm shaped sectiocons, supported by main beams, with free spans of 26 m along the *Y* direction. They are assumed pinned to main beams, creating a deformable roof diaphragm;
- 6 secondary beams (beam-holder panels) with rectangular cross-section (W x H = 0.4 × 0.6 m) supported by columns P3 and P1 on both long sides of the building.

No connections exist between secondary and roof beams. Moreover, no connections are placed between P3 columns and roof beams: P3 columns are simple cantilevers used as horizontal supports of the CPs placed on the long side of the building.

Only self-weight and dead roof loads are considered in the seismic analyses:

- roof beams, TT 100/250 cm (including roof finishing) = 7.8 kN/m^2,
- main beams (average weight) = 9 kN/m,
- secondary beams (beam-holder panel) = 6.0 kN/m,
- cladding panels = 3.25 kN/m^2.

Figures 2, **Supplementary Figure S2** and **Figure 3**, respectively, show floor plan, side views, and vertical sections

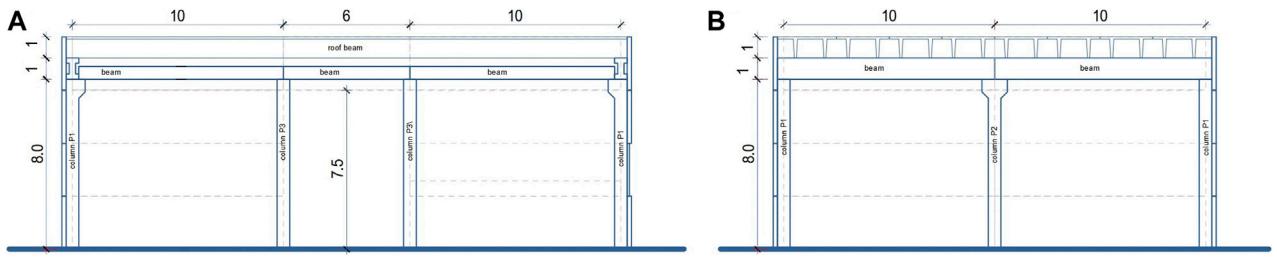

FIGURE 3 | Vertical sections: **(A)** AA, **(B)** BB.

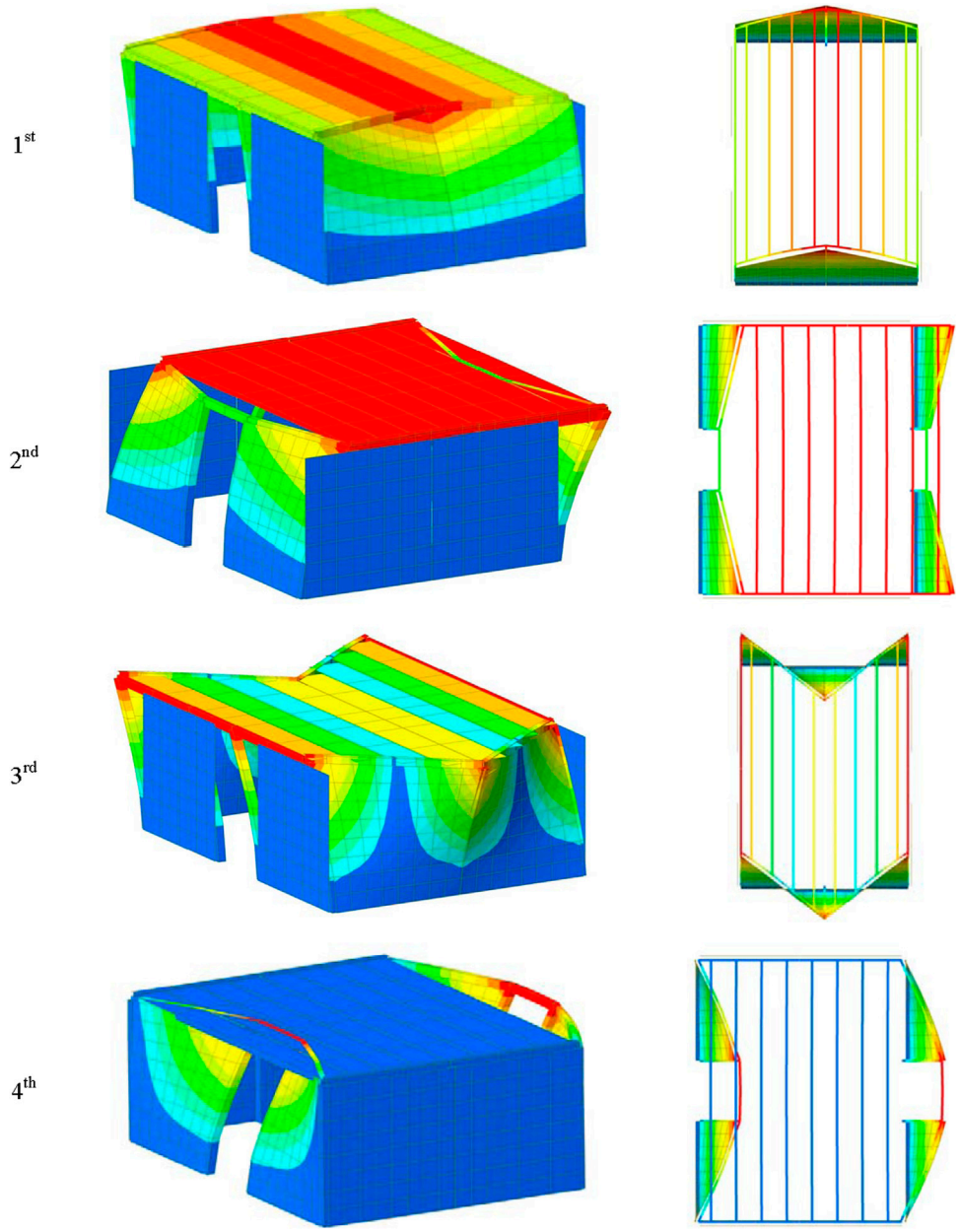

FIGURE 4 | 1st to 4th modal shapes

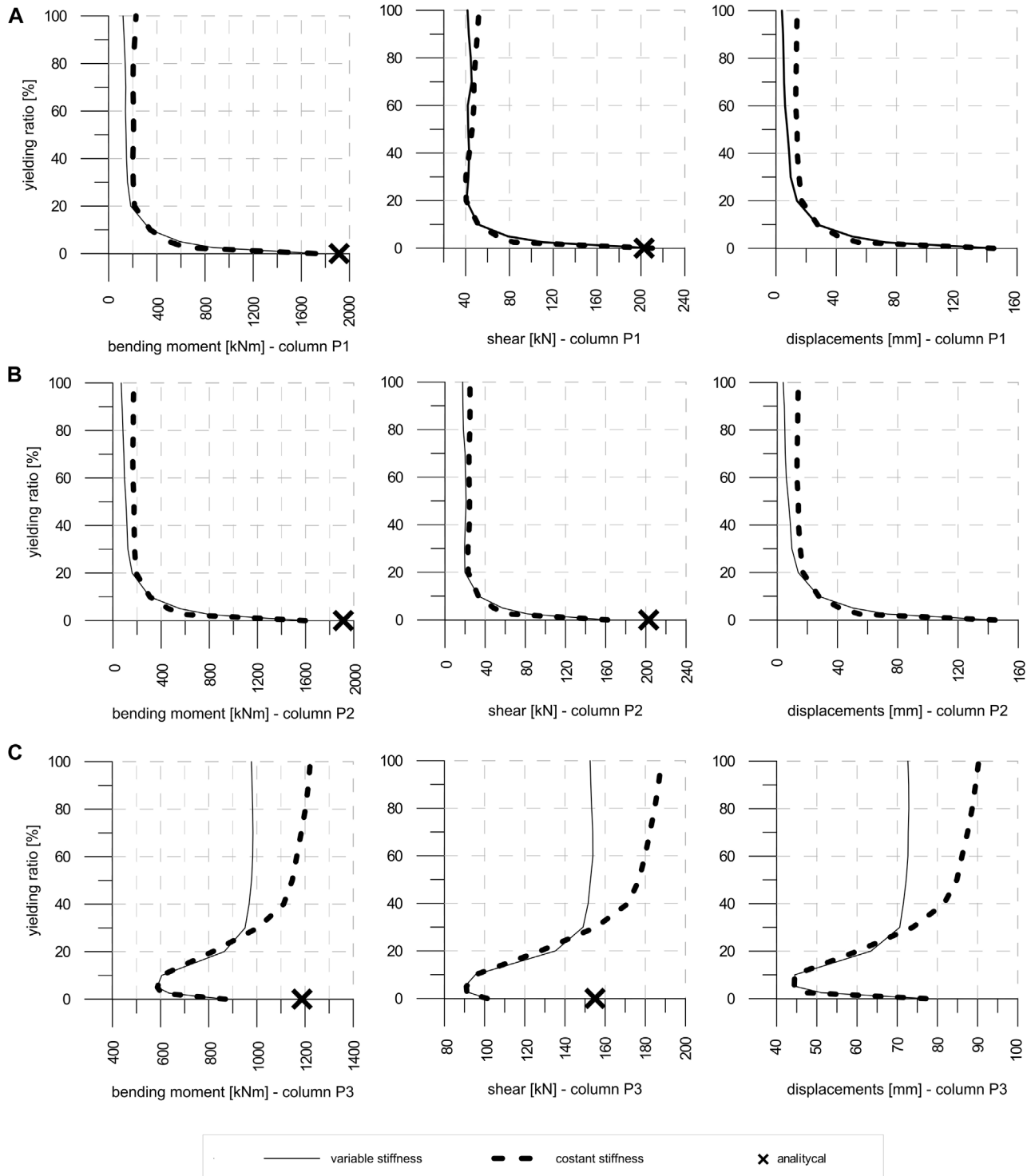

FIGURE 5 | Columns - earthquake along X direction: **(A)** P1; **(B)** P2; **(C)** P3.

TABLE 1 | Elastic-plastic laws parameters for connections.

n	r_y	F_y [kN]	Constant stiffness		Variable stiffness	
			K_{el} [kN/m]	δ_y [mm]	K_{el} [kN/m]	δ_y [mm]
	Yielding ratio	Yielding forces	Stiffness	Yielding displacement	Stiffness	Yielding displacement
# 1	0.025	18.1	80,000	0.226	18,100	1.0
# 2	0.05	36.1		0.451	36,100	
# 3	0.10	72.2		0.903	72,200	
# 4	0.20	144.4		1.805	144,400	
# 5	0.30	216.6		2.708	216,600	
# 6	0.40	288.8		3.61	288,800	
# 7	0.50	361		4.513	361,000	
# 8	0.60	433.2		5.415	433,200	
# 9	0.70	505.4		6.318	505,400	
# 10	0.80	577.6		7.22	577,600	
# 11	0.90	649.8		8.123	649,800	
# 12	1.00	722		9.025	722,000	

of the building. In **Figure 2**, columns are identified with their labels.

3 NUMERICAL FINITE ELEMENT MODELS AND PERFORMED ANALYSES

The structural FE models to simulate the different configurations have been created using Midas Gen software (Gen, 2015). The external restraints and the internal constraints are shown in the kinematic scheme of **Figure 1**.

The common assumptions for all the models are listed below:

- linear elastic beam elements have been used for the vertical (columns) and horizontal (main and roof beams) frame members linked with pinned connections;
- linear elastic plate elements represent the CPs;
- panel-to-panel rotational joints have been modeled using rotational plate-edge releases. Moreover, the hypothesis of the absence of relative displacements between panels was considered due to the high in-plane panel-to-panel friction assumed;
- axial rigid trusses have been used to model CP-to-column connections.

The elastic stiffness of beam elements has been evaluated from their nominal dimensions and considering a concrete elastic modulus equal to E_c = 33 GPa. The contribution of rebars and the cracking effect have been ignored.

Both modal identification and spectral analyses have been performed using an elastic model, assuming pinned connections at the roof level (i.e., the hypotheses normally assumed in design practice), without considering the structural contribution of the CPs (i.e., considering them as NSE). For spectral analyses, used as a reference for the non-linear analyses, the following parameters were assumed to define the elastic seismic spectrum according to Eurocode 8 (CEN-EN-1998-1, 2004):

Soil Type = B, S = 1.2, a_g = 0.187 g → T_B = 0.15 s, T_C = 0.50 s, T_D = 2.00 s, PGA = Sag = 0.225 g

A behavior factor q = 1.0 was assumed.

Three different sensitivity analyses (non-linear dynamic analyses (NLDAs)) were performed to assess the effects of ductile connections placed in the structure.

The first two sensitivity analyses have been used to evaluate the effects of the mechanical parameters of the CP/frame dissipative connections in precast building with deformable roof diaphragm.

The optimal CP/frame dissipative connections found have been used in the third and final sensitivity analysis with the aim to examine the introduction of ductile connections between roof and main beams and create a dissipative roof diaphragm.

The non-linearities of the structural elements were considered according to the different NLDAs performed:

- CP/frame connections;
- columns (plastic hinges at the base of the columns);
- roof/main beams connections;

Seven accelerograms spectrum-compatible with the elastic design spectrum used for spectral analyses were generated for NLDAs using the Simqke1 code (Gasparini and Vanmarcke, 1976).

A duration of 20s was assumed for the seismic action.

The numerical integration was performed using a Newmark scheme with constant acceleration parameters (c = 0.5 and b = 0.25, i.e., without numerical damping) and time-steps of 0.005 s. A Rayleigh-type damping was assumed with a damping ratio equal to ξ = 5%, a coefficient for proportional mass equal to α = 0.242 and a coefficient for proportional stiffness equal to β = 0.0015.

Results from NLDAs have been averaged over the seven accelerograms.

The following paragraphs summarize the mechanical properties assumed in the non-linear models.

The yielding ratio r_y of CP/frame connections has been defined as: $r_y = F_y / F_{el,max}$,
where

- F_y is the yield strength of connections;

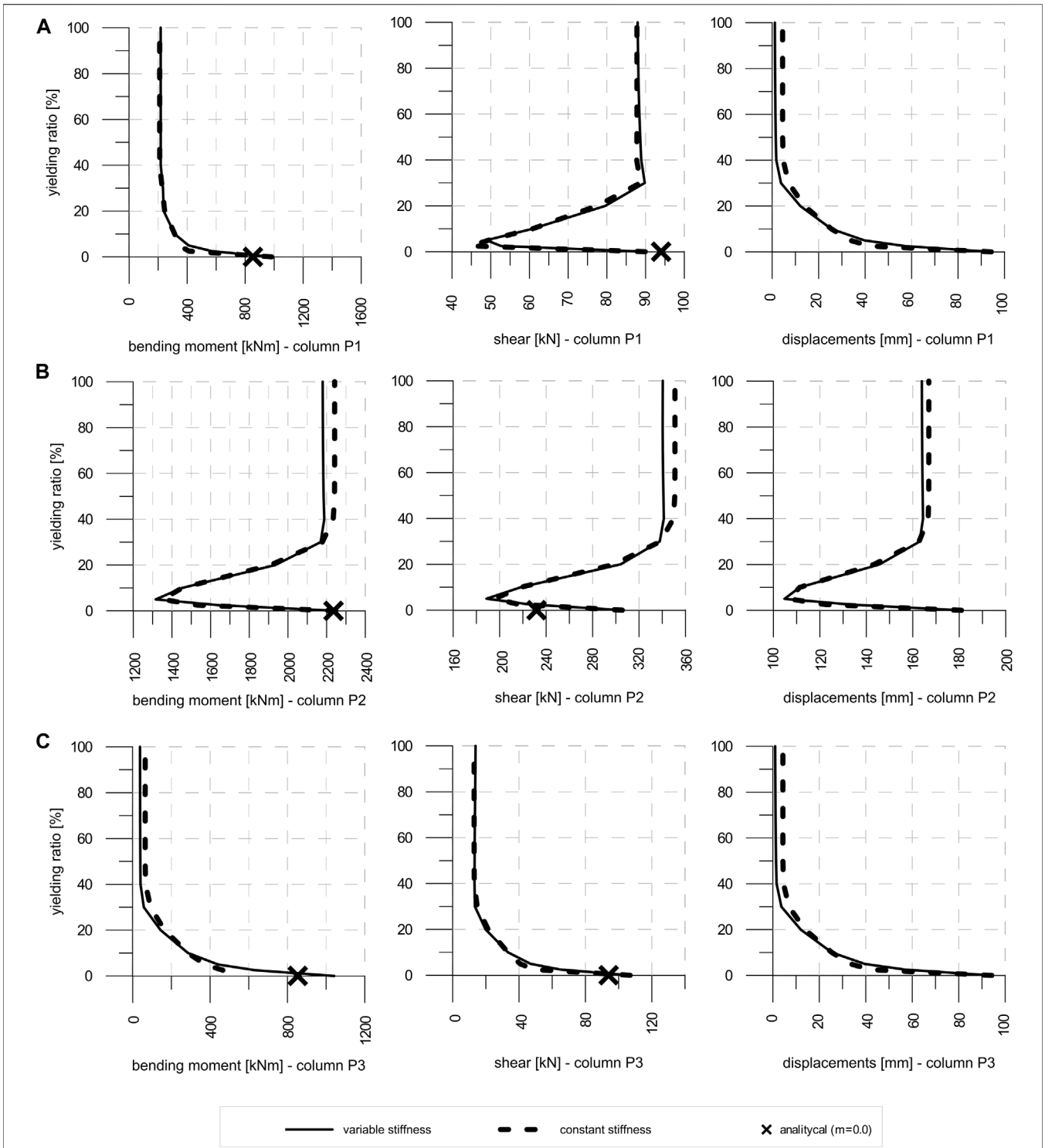

FIGURE 6 | Columns – earthquake along Y direction : **(A)** P1; **(B)** P2; **(C)** P3.

- $F_{el,max}$ = 722 kN, is the maximum force on CP/frame connections derived from a reference elastic spectral analysis and assuming K_{el} = 80,000 kN/m.
- F_y = 0 implies no-interaction between CPs and frame (lack of CP/frame connections) which is typical for statically determined structures and usually adopted in the design.

TABLE 2 | Variables adopted in the sensitivity analyses.

Sensitivity analyses		Column behavior	CP-frame connection		Roof-frame connection
			Behavior	r_y	
Sensitivity analyses varying CP/frame connection's characteristics with linear column	1st	Linear	Elastic–plastic (K = 80,000 kN/m)	0–100 (%)	Pinned (deformable roof)
			Elastic–plastic (δ_y = 1 mm)	0–100%	Pinned (deformable roof)
Sensitivity analyses varying CP/frame connection's characteristics with non-linear column	2nd	Non-linear	elastic–plastic (K = 80,000 kN/m)	0–100%	Pinned (deformable roof)
			Elastic–plastic (δ_y = 1 mm)	0–100%	Pinned (deformable roof)
Sensitivity analyses varying CP/frame connection's characteristics and roof/frame connection's characteristics with non-linear column	3rd	Non-linear	elastic	100	Pinned (deformable roof)
		Non-linear	Elastic–plastic (δ_y = 1 mm)	10	Pinned (deformable roof)
		Non-linear	Elastic–plastic (δ_y = 1 mm)	10	Elastic–plastic (F_y = 10 kN, δ_y = 1 mm)

TABLE 3 | Natural frequencies and modal participation.

Mode	Period [sec]	Frequency [Hz]	Modal participation factor DX [%]	Modal participation factor DY [%]	Modal participation factor RX [%]	Modal participation factor ry [%]	Modal participation factor RZ [%]
1	1.725	0.580	0	75.95	26.10	0	0
2	1.073	0.587	77.21	0	0	27.87	0
3	0.690	1.449	0	3.93	0.80	0	0
4	0.454	2.204	3.76	0	0	0.57	0

Results refer to spectral analysis and are labeled as "analytical results."

Values of CP/frame connections parameters are listed in **Table 1** for the whole investigated range of r_y. The non-linear laws of connections are assumed to be bilinear elastic-plastics with hardening and unloading phase parallel to the elastic branch.

r_y has been modified to evaluate the different behavior of two limit conditions: rigid-elastic strong connections ($r_y = 1$) and high ductility connections (r_y <<).

First Sensitivity Analyses

The following properties were chosen for NLDAs:

- deformable roof (pinned connections between roof beams and main beams);
- linear elastic column;
- elastic–plastic CP/frame connections with hardening behavior (plastic stiffness K_{pl} equal to 1% of the elastic stiffness K_{el}: $K_{pl} = K_{el}/100$);

The sensitivity analyses consider the variation of the yielding ratio of CP/frame connections, $0.0 \leq r_y \leq 1.0$, and two alternatives for their elastic stiffness:

- constant stiffness K_{el} = 80,000 kN/m with variable yielding displacement δ_y (see **Supplementary Figure S3A**)
- variable stiffness K_{el} with constant yielding displacement δ_y = 1.0 mm (see **Supplementary Figure S3B**).

2nd Sensitivity Analyses

The following properties were selected for NLDAs:

- deformable roof (pinned connections between roof beams and main beams);
- non-linear column with lumped plasticity ("Takeda" type hinges placed at the base of the columns);
- elastic–plastic CP/frame connections with hardening behavior ($K_{pl} = 0.01 \cdot K_{el}$).

The analyses were performed with the same range of yielding ratio r_y used in the first sensitivity analyses, but under the hypothesis of constant yielding displacement δ_y = 1 (i.e., variable elastic stiffness of the connection, according to **Supplementary Figure S3B**).

Third Sensitivity Analyses

The following properties were chosen for NLDAs:

- non-linear column with lumped plasticity ("Takeda" type hinges placed at the base of the columns);
- elastic–plastic CP/frame connections with hardening behavior ($K_{pl} = K_{el}/100$) with two alternative characteristics:
  ι. δ_y = 1.0 mm and r_y = 1,00 → K_{el} = 722,000 kN/m
  ιι. δ_y = 1.0 mm and r_y = 0,10 → K_{el} = 80,000 kN/m

Concerning the roof connections, two different cases were analyzed:

- deformable roof (pinned connections between roof beams and main beams);
- roof-to-main beam connections with elastic-perfect plastic behavior (yielding force F_y = 10 kN and yielding displacement δ_y = 1 mm → K_{el} = 10,000 kN/m).

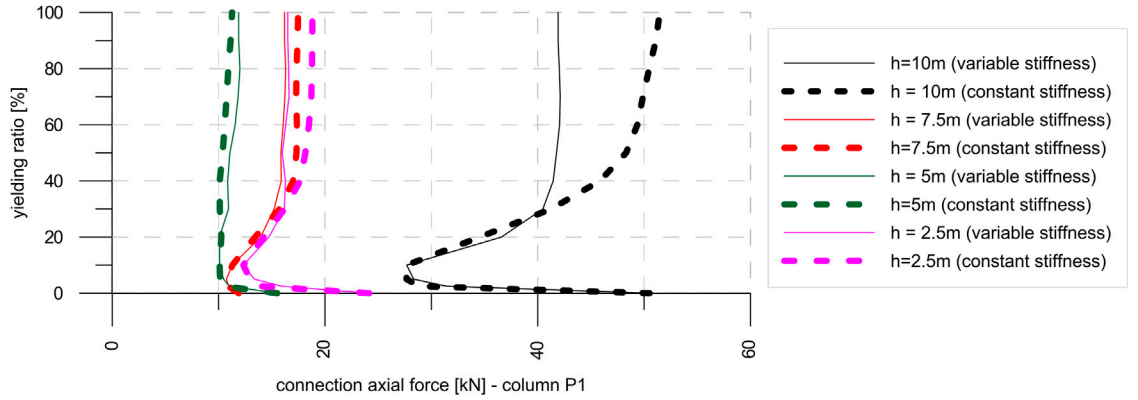

FIGURE 7 | CP/column P1 connections axial force – earthquake in X direction.

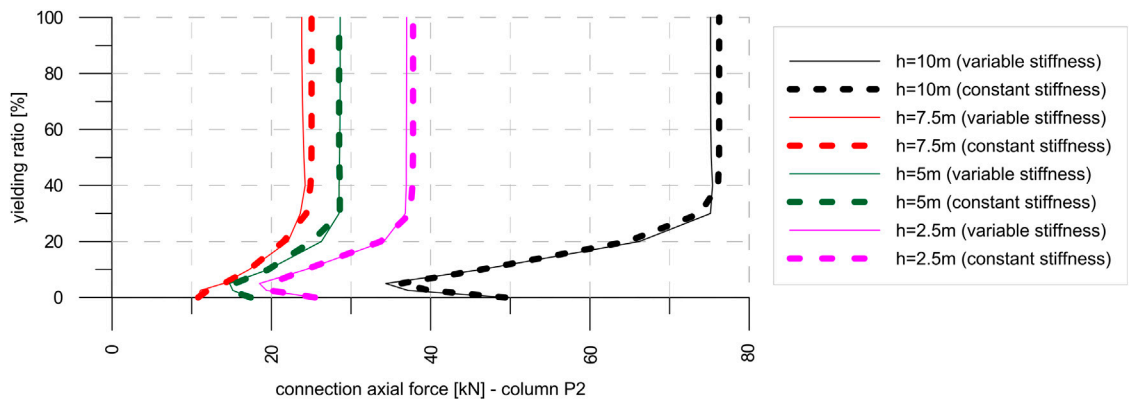

FIGURE 8 | CP/column P2 connections – earthquake in Y direction: axial force.

Table 2 summarizes all the variables adopted in the three sensitivity analyses.

In the following sections, the results of the simulations are summarized and discussed.

4 MODAL IDENTIFICATION ON REFERENCE ELASTIC MODEL WITHOUT CP/FRAME CONNECTIONS

The natural frequency analysis of the elastic FE model without CP/frame connections was used to define the structural frequencies and modal shapes of the case-study building. The results are listed in **Table 3** together with the corresponding mass participation. **Figure 4** shows the first four modal shapes characterized by modal participation greater than 3% and involving about 80% of the total mass. Local out-of-plane modes of CPs activate the remaining mass. The modal shapes clearly reveal the absence of a rigid roof.

The absence of a rigid roof causes asynchronous oscillation modes of the roof columns, and it produces opposite displacements perpendicular to the façade. This behavior induces the so-called skew effect forces on CP connections defined by Scotta et al. (2015) and subsequently analyzed by Belleri et al. (2018).

5 FIRST SENSITIVITY ANALYSIS VARYING CP/FRAME CONNECTION PARAMETERS WITH LINEAR ELASTIC COLUMNS.

Several parametric analyses were performed to evaluate the sensitivity of the seismic response of the building to the variations of yielding forces and stiffness of CP/frame connections.

In this first sensitivity analysis, the non-linearity is concentrated on the CP-frame connections only, and the columns are considered elastic. This assumption is used to evaluate only the energy dissipation effect given by the connections.

336 NLDAs were carried out with the above-described FE models (7 earthquake signals x two earthquake directions x 12 CP/frame connection yielding forces x two CP/frame connection

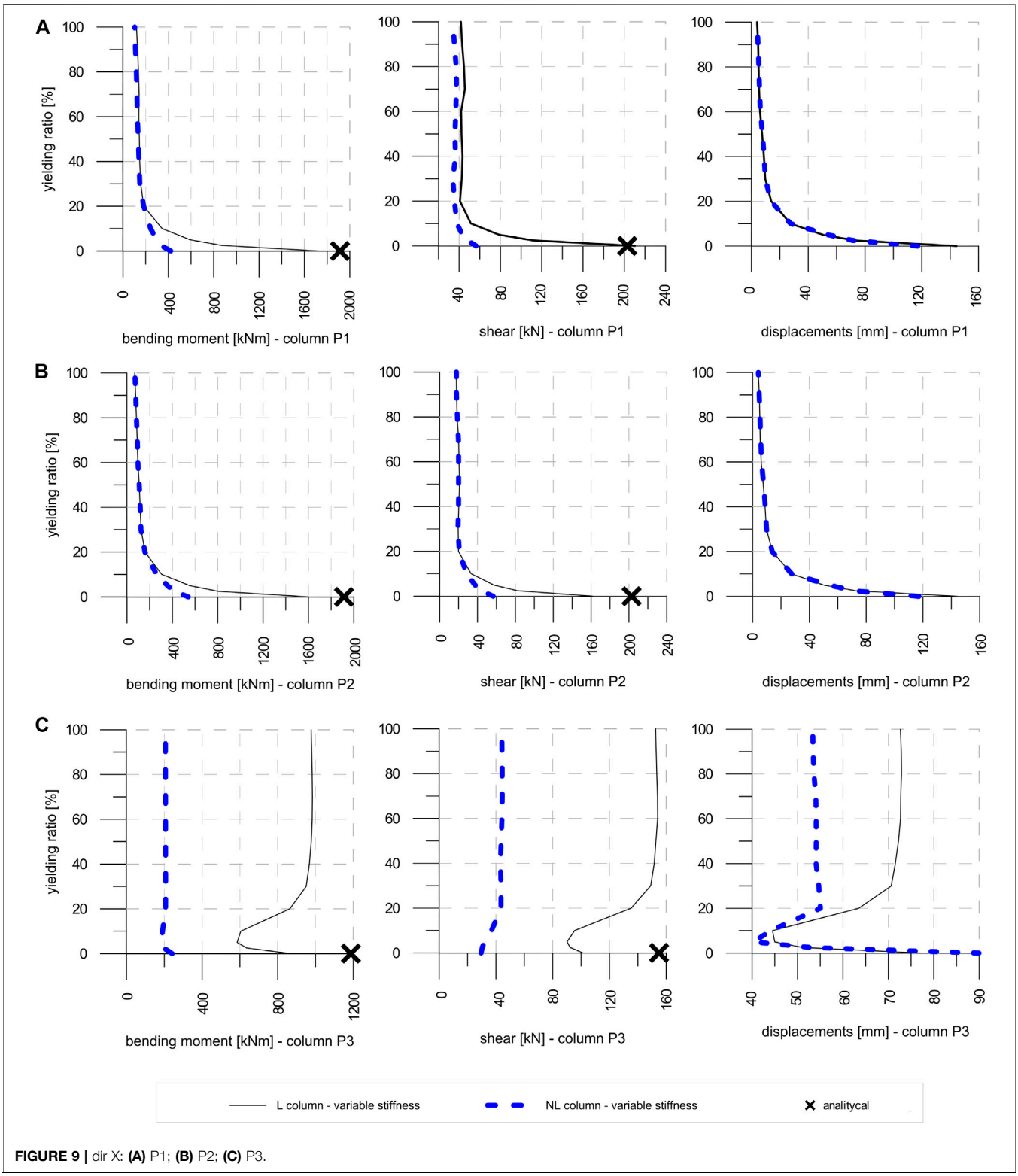

FIGURE 9 | dir X: **(A)** P1; **(B)** P2; **(C)** P3.

elastic stiffness). The average of the maximum absolute displacements and generalized stresses obtained from the seven input seismic signals are reported in **Figures 5–8**.

In the following sections, the results of the analyses are commented separately for each of the structural components.

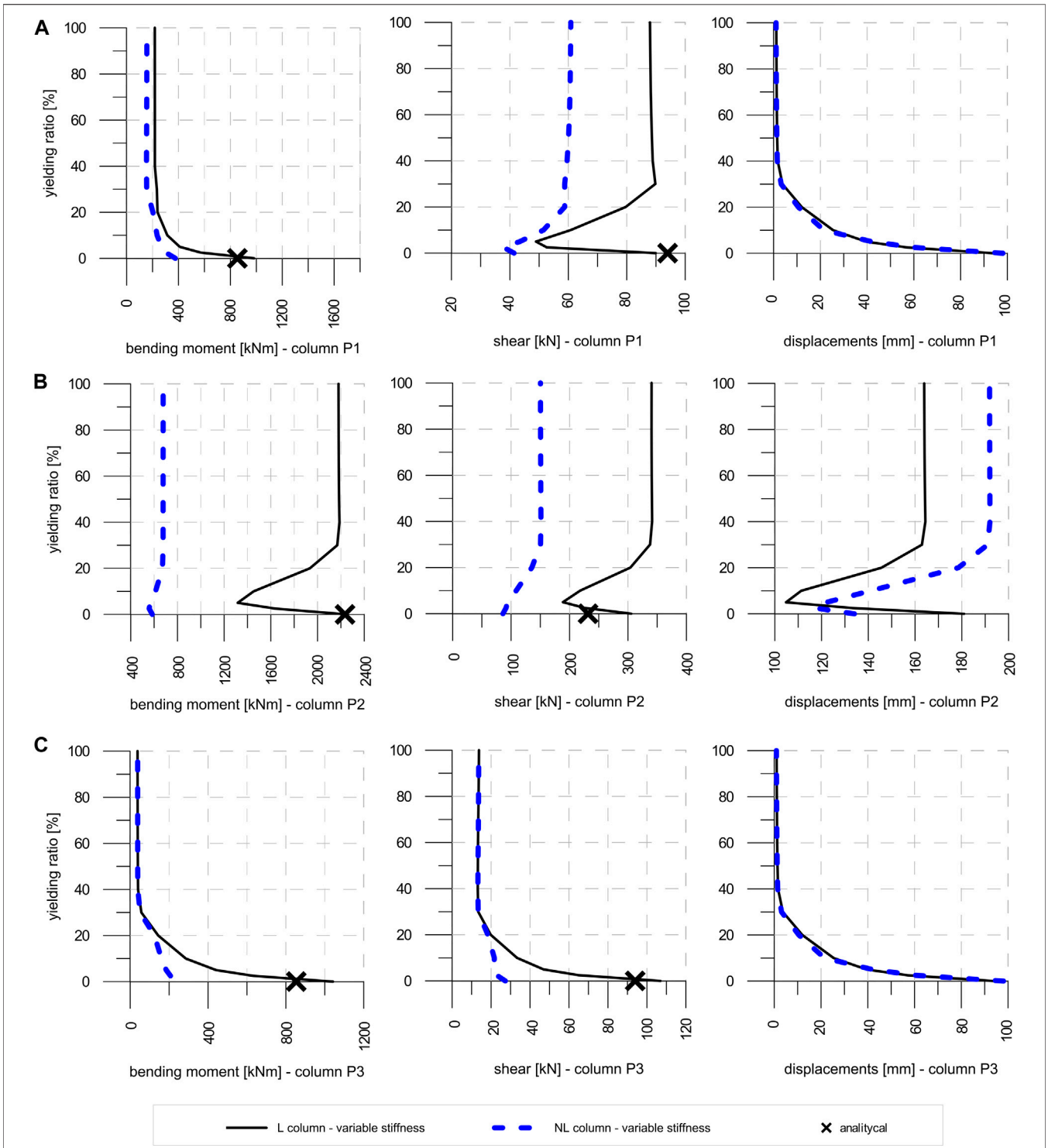

FIGURE 10 | dir Y: **(A)** P1, **(B)** P2, **(C)** P3.

5.1 Column Forces and Displacements

5.1.1 Results for Seismic Action Along the *X* Direction

For each column type P1, P2, and P3, **Figure 5** shows the envelopes of the maximum absolute values of bending moment and shear at the base and top displacements of columns when earthquake acts in the *X* direction.

The crosses in **Figure 5** indicate the values of bending moment and shear at the base of the columns obtained by the analytical

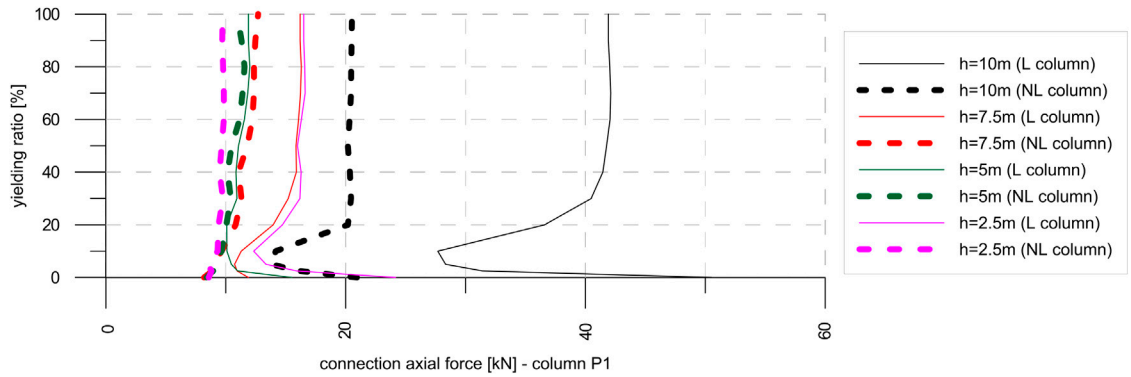

FIGURE 11 | CP/column P1 - axial force on connections– earthquake along X direction.

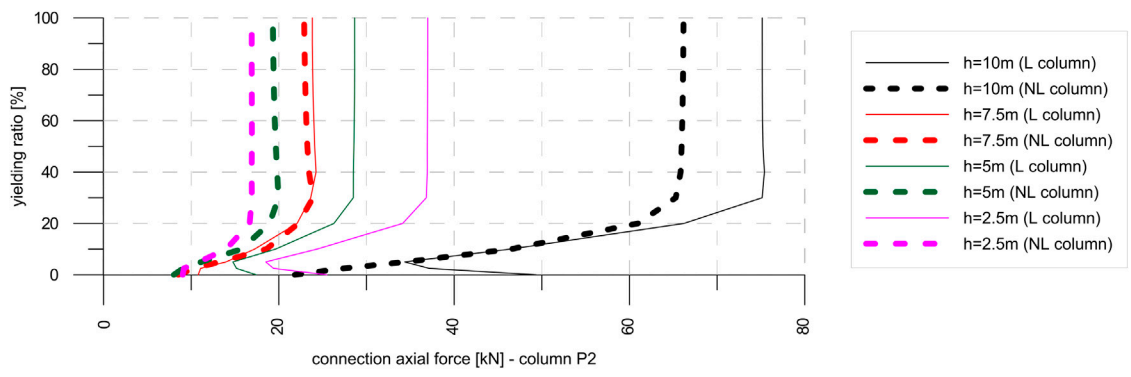

FIGURE 12 | CP/column P2 connections – Y direction - axial force.

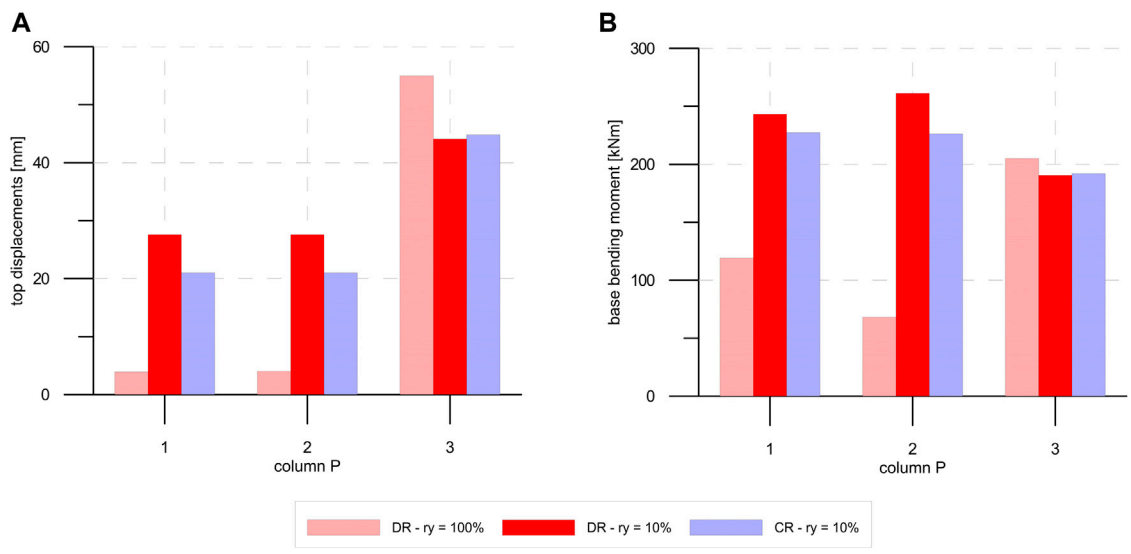

FIGURE 13 | seismic action along X direction: **(A)** column top displacements, **(B)** column base bending moment.

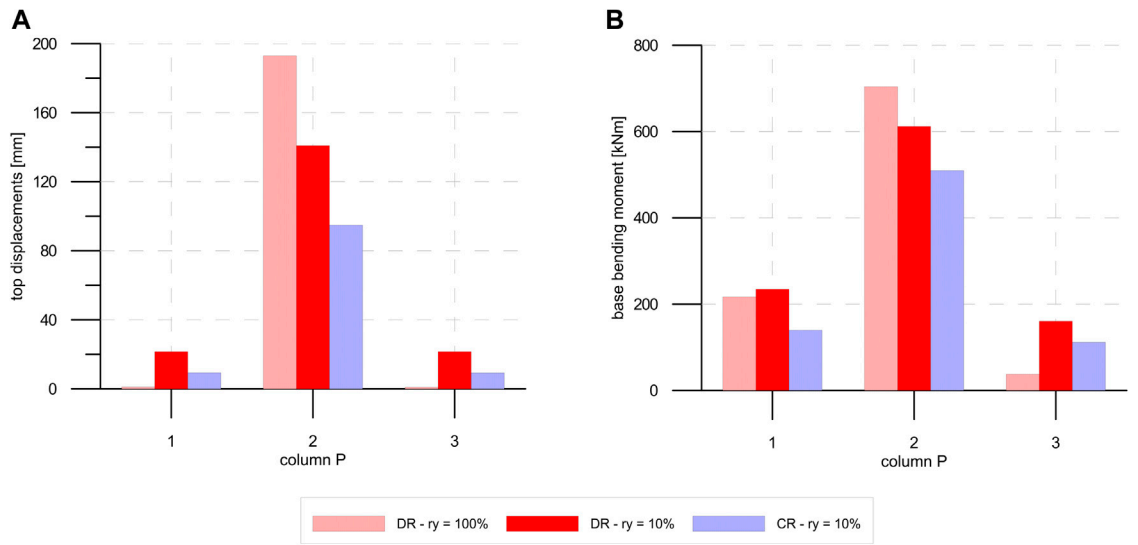

FIGURE 14 | Seismic action along Y direction: **(A)** column top displacements, **(B)** column base bending moment.

calculations; these highlight a good correspondence with numerical values derived by the models with $F_y = 0$.

Base forces and top displacements of P1 and P2 columns greatly reduce when yielding force of CP/frame connections increases. Moreover, it is worth noting that the numerical results highlight irrelevant variations for ratios r_y higher than 20%.

A different behavior occurs at intermediate column P3. These support the out-of-plane loaded CPs and are placed far from the in-plane loaded CPs. Base forces and top displacement reduce for yielding ratios r_y lower than 10% due to both the energy dissipation introduced by weak CP/frame connections and the "skew effect" which allows the migrations of the actions from out-of-plane loaded facades to the perpendicular ones, whereas base forces and top displacement increase for r_y>20%, especially for constant stiffness values of the connections.

The percentage increment of the base shear is greater than those of the base bending and top displacement. This behavior underlines that an excessive in-plane stiffness of the facades parallel to the seismic action amplifies local effects on P3 column (the amplification of skew effects in not balanced by the energy dissipation).

5.1.2 Results for Seismic Action Along the *Y* Direction

Figure 6 shows base forces and top displacements on columns obtained for seismic action along the *Y* direction. Numerical results highlight a similar pattern compared to the outcomings discussed in the previous section, except for some details and the inversion of the role of P2 and P3 columns. Results are almost independent from the hypothesis of constant stiffness or constant yielding displacements for connections.

Moreover, the analytical evaluation of shear at the base of P2 column strongly underestimates the correspondent results from numerical analyses without connections ($r_y = 0$) since the analytical model disregards the amplifications due to skew effect.

5.2 CP/Frame Connection Forces and CP Displacement

5.2.1 Results for Seismic Action Along the *X* Direction

Supplementary Figure S4 shows the force values and drift of CP/frame dissipative connections, whereas **Figure 7** shows axial forces on column/CP connections. Both **Supplementary Figure S4** and **Figure 7** display the results obtained from NLDAs with seismic action along the *X* direction.

Forces on CP/frame connections are linearly proportional to the yielding ratio (**Supplementary Figure S4A**). Since the achieved values are always greater than F_y, the yield strength of the connection is always exceeded. Stiffness variation does not affect the maximum recorded force.

By contrast, the variation of stiffness affects the displacement (drift) of the connection, especially for the highest values of r_y. For r_y<10%, connections with variable stiffness show greater drift than those with a constant stiffness, whereas for r_y> 10%, the trend is inverted.

Figure 7 shows axial forces on column/CP connections installed on P1 column at different heights, z, equal to 2.5, 5.0, 7.5, and 10 m. Comparing the results with values obtained for $r_y = 0$, axial forces decrease for yielding ratio r_y in the 0%÷10% range; that is, the energy dissipation due to the yielding of the connection has an actual role when drift between frame and cladding panels is allowed.

In the same range, the displacement reduction and the consequent decrease in out-of-plane deformation (skew effect) are recorded together with a reduction of the axial forces on CP/column connections.

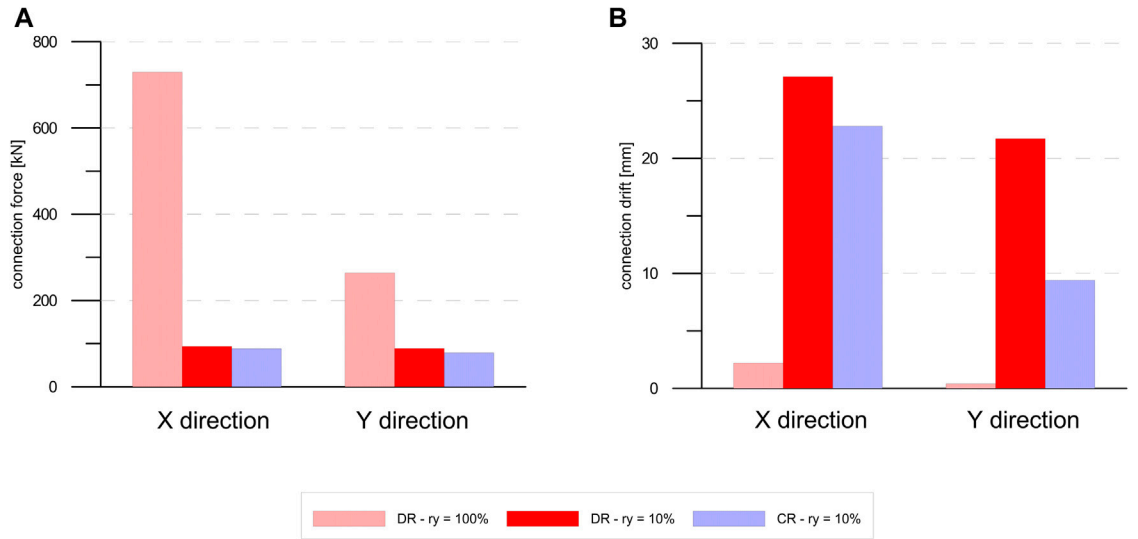

FIGURE 15 | CP/frame connections: **(A)** force; **(B)** drift.

For r_y>10%, the forces on the connections increase and reach higher values, especially for the connection at h = 10 m for which the plastic dissipation of the connections is no longer able to limit the skew effect.

5.2.2 Results for Seismic Action Along the *Y* Direction

Supplementary Figure S4 shows the forces and the drift of the CP/frame dissipative connections, and **Figure 8** presents the axial forces on the column/CP connections obtained from NLDAs with seismic action along the *Y* direction. The graphs highlight the same trend defined for the seismic actions in the *X* direction.

The forces on the CP/frame connections are linearly proportional to the yielding ratio (**Supplementary Figure S5A**) up to r_y<40%, which corresponds to the exceeding of the connection yielding strength. For r_y>40%, forces on CP/frame connections become constant and related to the seismic action intensity only.

For r_y>40%, the stiffness variation affects maximum force values: the connections with a constant stiffness underline a maximum force 15% higher than that in the variable stiffness case. The change in stiffness also affects the connection displacement (drift) (**Supplementary Figure S5B**), especially for the highest values of r_y. For r_y<10%, the connections with a variable stiffness show greater drifts than those with a constant stiffness, whereas for r_y>10%, the trend is inverted.

Figure 8 shows the axial forces on the column/CP connections for P2 column. Comparing the results with the values obtained assuming r_y = 0, the axial forces highlight a decrease for the yielding ratio r_y in the 0% ÷5% range, except for connections located at the height of h = 7.5 m.

For r_y> 5%, the axial forces on the connections increase, especially for connections at h = 10 m for which the damping due to the yielding of connections is not enough to limit the skew effect. The stiffness variability does not affect the maximum axial force significantly.

6 2ND SENSITIVITY ANALYSIS VARYING CP/FRAME CONNECTION YIELDING FORCE AND NON-LINEAR COLUMN

The effect of elastic–plastic with the hardening behavior of CP/frame connections was analyzed through 168 NLDAs with the FE model previously described (7 earthquakes x 12 connection yielding forces x two earthquake directions). Only the assumption of variable elastic stiffness was explored.

In the analyses discussed in **Section 5**, a linear elastic behavior of the columns was assumed. Generally, in precast buildings with cantilever columns, the energy dissipation develops at the base of the column by the formation of flexural plastic hinges. Their brittle shear collapse is avoided by placing an adequate quantity of confinement stirrups.

In this section, an improved numerical model has been adopted for the analyses: the actual hysteretic behavior of the columns (NLC) has been reproduced by introducing a lumped non-linear hinge at the base of the same.

This NLC model was used to perform the same analyses executed with the LC model for CP/frame connections with different elastic stiffness. The same geometry (B x H = 60 × 60 cm) and reinforcement bars (12Ø20 longitudinal rebars, four braces stirrups Ø10/150 mm) have been assumed for all the three column types, that is, P1–P2–P3. Since the columns are subjected to different values of the axial loads (710, 1,270, and 160 kN, respectively), three different "Takeda" hinges (Takeda et al., 1970) have been introduced in the NLC model for each column type.

Through incremental cyclic pushover analyses, the hysteretic behaviors of columns reported in **Supplementary Figure S6** have

been defined correlating the base bending moment and top displacement. The dashed black line in **Supplementary Figure S6** identifies the elastic stiffness assumed for columns in the LC model. More details about the definition of the Takeda model parameters can be found in the study by Scotta et al. (2015).

6.1 Column Forces and Displacements

6.1.1 Results for Seismic Action in the *X* Direction

Figure 9 shows that P1 and P2 columns highlight comparable base stresses values obtained from the LC and NLC models when r_y> 20%. Therefore, for r_y>20%, P1 and P2 columns remain in their linear elastic range. On the contrary, for r_y<20%, the base stresses of the NLC model are limited to their capacity values.

Top displacements of P1 and P2 columns defined with linear and non-linear analyses correspond regardless of the r_y value.

Conversely, with the LC model, P3 column (holder panel column) develops huge stresses compared to those obtained with the NLC model (blue dotted line inc **Figure 9C**).

For r_y>20%, the use of CP/frame connections is not very effective for P3 column. The large top displacement of the column highlights the need of suitable measures to avoid pounding between the top CP and the roof elements.

6.1.2 Results for Seismic Action in the *Y* Direction

Similar results have been obtained in this configuration (see **Figure 10A**). Different from the previous case, P2 column develops CPs when subjected to out-of-plane forces in the case of seismic action along the *Y* direction. P2 columns develop far higher stresses with the LC model than those obtained with the NLC model (see **Figure 10B**). Moreover, for r_y>20%, the introduction of CP/frame connections does not induce significant forces and stresses reductions on P2 column. To avoid out-of-plane deformation of this column, amplified by the skew effect, a rigid or semi-rigid roof diaphragm would be required.

6.2 Connection Forces and CP Displacement

6.2.1 Results for Seismic Action Along the *X* Direction

Supplementary Figure S7 shows the good correspondence of forces and drift of CP/frame dissipative connections evaluated with LC and NLC models. The comparison for the connections to column P1 in **Figure 11** evidences the reduction of the axial force due to the additional dissipation provided by the yielding at the base of the columns accounted for with the NLC model. The effectiveness of the energy dissipation is particularly pronounced for the connection at h = 10 m. A reduction of the differential displacement between columns induces an attenuation of the skew effect and makes the out-of-plane forces on connections increasing with their height from the ground.

6.2.2 Results for Seismic Action Along the *Y* Direction

For seismic action in the *Y* direction, **Supplementary Figure S8** shows forces and drift on CP/frame connections, while axial forces on column/CP connections are plotted in **Figure 12**.

Supplementary Figure S8A highlights the following:

- when r_y < 40%, the yield strength of the connection is always reached, with the forces being on CP/frame connections linearly proportional to the yielding ratio;
- when r_y > 40%, forces on CP/frame connections become constant; that is, their yield strength is not exceeded. Maximum force on the connection with the LC model is about 15% greater of that obtained with the NLC model.

The use of LC or the NLC model does not significantly affect the maximum drift of the connections in columns (**Supplementary Figure S8B**).

With the NLC model, a mitigation of the skew effect occurs due to the dissipation at the base of the columns. The attenuation of the skew effect leads to a distribution of forces on connections proportional to their height from the ground (**Figure 12**).

7 THIRD SENSITIVITY ANALYSES VARYING ROOF-FRAME CONNECTIONS

Results discussed in Section 5 and 6 refer to precast buildings with flexible diaphragms and show limited effectiveness of the proposed CP/frame dissipative connections for intermediate columns.

The realization of a rigid diaphragm on the roof would increase the effectiveness of the connection systems (Biondini et al., 2013b), but it is not always feasible as discussed previously. Therefore, in this section, a possible alternative solution is analyzed. Elastic–plastic translational connections are introduced between roof beams and main beams to create a semi-rigid and dissipative diaphragm.

The effectiveness of this solution is evaluated through the comparison of numerical results obtained with three different models having the following properties:

First model: deformable roof (DR), r_y = 100%

- elastic CP/frame connections (yielding ratio r_y = 100% and elastic stiffness K_{el} = 722.000 kN/m);
- non-linear columns (plastic Takeda hinges with the hysteretic law in **Supplementary Figure S6** are introduced at the base of the columns);
- deformable roof (pinned connections between roof beams and main beams).

2nd model: deformable roof (DR), r_y = 10%

It presents the same properties of the 1st model, except for the elastic–plastic hardening CP/frame connections characterized by r_y = 10% and elastic stiffness K_{el} = 80,000 kN/m;

Third model: flexible roof (CR), r_y = 10%

Equal to the 2nd model but with semi-rigid and dissipative roof diaphragm obtained by inserting translational elastic-perfect plastic connections between roof beams and main beams as depicted in **Supplementary Figure S1**, characterized by yielding force F_y = 10 kN and yielding displacement δ_y = 1 mm (K_{el} = 10.000 kN/m).

Results from NLDAs with the 1st and 2nd models (DR) have already been discussed and compared within the second sensitivity analysis reported in **Section 6**.

The effect of the flexible roof diaphragm (CR) was investigated through 14 NLDAs on the 3rd model (7 earthquakes x one set of connections characteristics x two earthquake directions). The comparison of the numerical results obtained with the three models is illustrated in the following sections.

7.1 Column Forces and Displacements

Figure 13 reports top displacements and bending moments at the base of P1, P2, and P3 columns for earthquakes in the *X* direction.

P1 and P2 columns show a top displacement and a bending moment reduction in the CR model compared to the DR 2nd model with the same yielding ratio r_y = 10%. By contrast, the creation of a semi-rigid floor does not significantly affect the results for P3 column. The worst conditions in terms of maximum top displacement and bending moment for P3 columns are represented by the case DR–r_y = 100% (1st model).

Therefore, when the earthquake is applied along the *X* direction, the CR solution does not relieve the solicitations on P3 column, which are not connected to the roof and therefore cannot take advantage of the semi-rigid roof diaphragm.

Only the insertion of horizontal connections placed between the top of P3 columns and the roof could reduce solicitations and displacement demand of P3 column.

Figure 14 reports the same results for seismic actions along the *Y* direction. In this case, the CR 3rd model - r_y = 10% allows a significant reduction of top displacements and base bending moments for all columns compared to the DR–r_y = 10% 2nd model. Moreover, P2 column shows a reduction of the top displacement and base moment, respectively, equal to 50 and 25%, which underlines that the seismic demand on columns can be significantly reduced using dissipative connections at the roof level.

7.2 Joint Forces

Figure 15 A, B show, respectively, forces and drifts of CP/frame connections from the three models and for both earthquake directions.

Force on connections obtained from the CR, r_y = 10% 3rd model is approximately equal to that obtained with the DR, r_y = 10% 2nd model since the yielding of the connection is achieved in both cases. Perhaps, connection drift is lowered with the CR, r_y = 10% 3rd model: the introduction of dissipative roof connections leads to a reduction of the deformation demand of CP/frame dissipative connections.

Force on connections with the DR, r_y = 100% 1st model is approximately equal to 720 kN along the *X* direction and to about 280 kN along the *Y* direction: such forces are hardly sustainable in practical installations. Therefore, the adoption of CP/frame deformable and/or elastic–plastic connections is mandatory to avoid fragile failure modes.

Supplementary Figure S9 and **Supplementary Figure S10** show axial forces arising on column/CP connections located at h = 2.5, 5.0, 7.5, and 10 m from the ground level, for earthquakes acting in *X* and *Y* directions, respectively.

Results in **Supplementary Figure S9** (*X* direction) are similar for the two r_y = 10% models (DR 2nd model and CR 3rd model); that is, the introduction of roof dissipative connections does not influence the connection forces. With the DR, ry = 100% 1st model higher forces develop especially at higher CP/frame connections due to their elastic behavior, which produces an amplification of local motion on P3 column and an amplification of the skew effect.

Supplementary Figure S10 shows that for earthquakes along the *Y* direction, the energy dissipation produced by introducing roof dissipative connections (CR model 3rd model) reduces the axial force value on CP/column connections of about 50 and 30% compared to the DR models with r_y = 100 (1st model) and r_y = 10% (2nd model), respectively.

CONCLUSION

In this article, a RC precast building with fully stacked horizontal cladding panels (CPs) has been considered as a case study. The CPs are placed horizontally, one on top of each other, and their weight loads to the foundation beam. Despite the simplicity and the small number of spans of the considered building, it allowed us to explore all the typical situations in R.C. precast buildings for varying direction of seismic excitation.

Generally, the analytical approach to the design of such buildings assumes the following constraint pattern for CPs: CP/frame in-plane sliding connections, CP/frame pinned out-of-plane connections, and panel-to-panel fixed connections. These assumptions lead to consider CPs as non-structural elements (NSEs) without any resistant function. Their connections are designed to resist statically determined wind or seismic actions.

The experience from past seismic events demonstrated that CPs interact with the frame producing unpredictable dynamic behavior and inadequate seismic performances. Moreover, unexpected relevant out-of-plane forces arise in CP/frame connections in precast buildings with a deformable roof (skew effect due to out-of-plane deformation of facades).

Therefore, the possibilities of using CPs as resistant shear walls have been explored in this work.

Dissipative elastic–plastic connections have been considered to connect CPs to the frame. Sensitivity analyses have been performed exploring the variation of the generalized stresses on columns, top displacements, and forces on connections obtained, modifying the yielding force and stiffness of connections and considering both elastic and inelastic behaviors of columns. A relevant reduction of stresses and top displacements on columns with limited forces on connections have been demonstrated in an optimal configuration with dissipative connections having yielding forces in the range of 5–10% of the elastic forces that would arise in the hypothesis of elastic connections.

However, with a flexible roof diaphragm condition, the introduction of proposed CP/frame connections has limited effectiveness in reducing seismic demand on intermediate columns, away from the facades parallel to seismic action. Moreover, the use of CP/frame connections with in-plane resistance exceeding 20–30% of the elastic demand results in a worse condition for such intermediate columns, but also for columns/CP connections, due to the high amplification of the skew effect.

The realization of the in-plane rigid roof would solve such limitations and drawbacks. However, it is not easy to create rigid

roof diaphragms in precast buildings due to large skylights between the roof elements or suspended plants in existing buildings.

An alternative solution consisting of a semi-rigid dissipative diaphragm's realization has been explored with a 3rd sensitivity analysis. Such conditions can be obtained by introducing easy-to-install translational elastic–plastic dissipative connections between roof beams and main beams. It has been demonstrated that the energy dissipation assured with such roof connections allows to considerably reduce stresses and top displacements also of intermediate columns (if connected to the roof, obviously) and forces in the columns/CP connections.

This work demonstrates that a combined intervention involving the introduction of low-strength elastic–plastic dissipative connections between frame and cladding panels, columns and cladding panels, and roof beams and main beams has a significant impact on reducing the seismic demand on precast RC buildings. The solution explored in this paper can be profitable if used not only in the design of new buildings but also for the seismic retrofitting of existing ones.

DATA AVAILABILITY STATEMENT

The raw data supporting the conclusions of this article will be made available by the authors, without undue reservation.

AUTHOR CONTRIBUTIONS

LD and RS contributed to the research reported in the paper in the same way.

ACKNOWLEDGMENTS

The authors acknowledge the contribution to the research given by Eng. Luca Grinzato with the development of his master thesis.

SUPPLEMENTARY MATERIAL

The Supplementary Material for this article can be found online at: https://www.frontiersin.org/articles/10.3389/fbuil.2021.639777/full#supplementary-material

SUPPLEMENTARY FIGURE 1 | Translational dissipative connections between roof beams and main beams.

SUPPLEMENTARY FIGURE 2 | Side views

SUPPLEMENTARY FIGURE 3 | Elastic-plastic laws for connections: (a) constant stiffness (b) variable stiffness.

SUPPLEMENTARY FIGURE 4 | CP/frame connections – earthquake in X direction: (a) force; (b) drift.

SUPPLEMENTARY FIGURE 5 | CP/frame connections – earthquake in Y direction: (a) force; (b) drift.

SUPPLEMENTARY FIGURE 6 | Hysteretic behaviour of Takeda hinges for columns P1–P2–P3.

SUPPLEMENTARY FIGURE 7 | CP/frame connection – earthquake along X direction: (a) force; (b) drift.

SUPPLEMENTARY FIGURE 8 | CP/frame connections – Y direction: (a) force; (b) drift.

SUPPLEMENTARY FIGURE 9 | Axial forces on connection - X direction – column P1.

SUPPLEMENTARY FIGURE 10 | Axial forces on connection - Y direction – column P2.

REFERENCES

Arnold, C. (1989).Cladding Design: Architectural Trends and Their Influence on Seismic Design. In Proceedings: architectural precast concrete cladding—it's contribution to lateral resistance of buildings. PCI. Chicago, 8–9.

Belleri, A., Cornali, F., Passoni, C., Marini, A., and Riva, P. (2018). Evaluation of Out-Of-Plane Seismic Performance of Column-To-Column Precast concrete Cladding Panels in One-Storey Industrial Buildings. *Earthquake Engng Struct. Dyn.* 47 (2), 397–417. doi:10.1002/eqe.2956

Belleri, A., Torquati, M., Marini, A., and Riva, P. (2016). Horizontal Cladding Panels: In-Plane Seismic Performance in Precast concrete Buildings. *Bull. Earthquake Eng.* 14 (4), 1103–1129. doi:10.1007/s10518-015-9861-8

Biondini, F., Dal Lago, B., and Toniolo, G. (2013b).Azione diaframma in strutture prefabbricate con pannelli di parete. In Proceedings of XV convegno ANIDIS. L'ingegneria Sismica in Italia. Padova: digilab, 2013.

Biondini, F., Dal Lago, B., and Toniolo, G. (2013a). Role of wall Panel Connections on the Seismic Performance of Precast Structures. *Bull. Earthquake Eng.* 11, 1061–1081. doi:10.1007/s10518-012-9418-z

CEN-EN-1998-1 (2004). *Eurocode 8: Design of Structures for Earthquake Resistance—Part 1: General Rules, Seismic Actions and Rules for Buildings*. Brussels: European Committee for Standardization.

Colombo, A., and Toniolo, G. (2012a). Precast concrete Structures: the Lesson Learnt from L'Aquila Earthquake. *Struct. Concr J. FIB* 13 (2), 71–139.

Colombo, A., and Toniolo, G. (2012b).Problems of Seismic Design of the Cladding Panels of Precast Buildings. In New Zealand society for earthquake engineering (NZSEE) annual conference. Christchurch, New Zealand, 13–15.

Craig, J., Goodno, B. J., Pinelli, J., and Moor, C. (1992).*Modeling and Evaluation of Ductile Cladding Connection Systems for Seismic Response Attenuation in Buildings10th World Conference on Earthquake Engineering (10WCEE)*. Madrid, 4183–4188.

Dal Lago, B., Lamperti Tornaghi, M., and Dal Lago, A. (2012).Studio sul comportamento bidirezionale di connessioni meccaniche scorrevoli pannello-telaio. In Proceedings of XIX convegno CTE. Bologna.

Ferrara, L., Felicetti, R., Toniolo, G., and Zenti, C. (2011). Friction Dissipative Devices for Cladding Panels in Precast Buildings. An Experimental Investigation. *Ejece* 15 (9), 1319–1338. doi:10.3166/ejece.15.1319-1338

Gasparini, D., and Vanmarcke, E. H. (1976). *SIMQKE: A Program for Artificial Motion Generation*. Cambridge: Department of Civil Engineering, Massachusetts Institute of Technology.

Gen, M. (2015). *MIDAS Information Technology Co., Ltd.*

Magliulo, G., Ercolino, M., and Manfredi, G. (2014). Influence of Cladding Panels on the First Period of One-story Precast Buildings. *Bull. Earthquake Eng.* 13, 1531–1555. doi:10.1007/s10518-014-9657-2

Menegotto, M. (2009). Observations on Precast concrete Structures of Industrial Buildings and Warehouses. *Progettazione sismica* 3, 149–153. Special issue on the 2009 L'Aquila earthquake.

National Institute of Standards and Technology (1998). Ductile Cladding Connection Systems for Seismic Design. 98–758.

Pinelli, J.-P., Craig, J. I., and Goodno, B. J. (1995). Energy-based Seismic Design of Ductile Cladding Systems. *J. Struct. Eng.* 121 (3), 567–578. doi:10.1061/(asce)0733-9445(1995)121:3(567)

Pinelli, J.-P., Moor, C., Craig, J. I., and Goodno, B. J. (1996). Testing of Energy Dissipating Cladding Connections. *Earthquake Engng. Struct. Dyn.* 25, 129–147. doi:10.1002/(sici)1096-9845(199602)25:2<129:aid-eqe542>3.0.co;2-0

Scotta, R., De Stefani, L., and Vitaliani, R. (2015). Passive Control of Precast Building Response Using Cladding Panels as Dissipative Shear walls.

Bull. Earthquake Eng. 13 (11), 3527–3552. doi:10.1007/s10518-015-9763-9

Shultz, A. E., Magana, R. A., Trados, M. K., and Huo, X. (1994). Experimental Study of Joint Connections in Precast concrete walls. In 5th US National conference on earthquake engineering, Chicago, IL, July 10–14, 1994.

Takeda, T., Sozen, M. A., and Nielsen, N. N. (1970). Reinforced Concrete Response to Simulated Earthquakes. *J. Struct. Div.* 96 (12), 2557–2573. doi:10.1061/jsdeag.0002765

Conflict of Interest: The authors declare that the research was conducted in the absence of any commercial or financial relationships that could be construed as a potential conflict of interest.

Publisher's Note: All claims expressed in this article are solely those of the authors and do not necessarily represent those of their affiliated organizations, or those of the publisher, the editors, and the reviewers. Any product that may be evaluated in this article, or claim that may be made by its manufacturer, is not guaranteed or endorsed by the publisher.

Advantages of publishing in Frontiers

OPEN ACCESS
Articles are free to read for greatest visibility and readership

FAST PUBLICATION
Around 90 days from submission to decision

HIGH QUALITY PEER-REVIEW
Rigorous, collaborative, and constructive peer-review

TRANSPARENT PEER-REVIEW
Editors and reviewers acknowledged by name on published articles

Frontiers
Avenue du Tribunal-Fédéral 34
1005 Lausanne | Switzerland

Visit us: www.frontiersin.org
Contact us: frontiersin.org/about/contact

REPRODUCIBILITY OF RESEARCH
Support open data and methods to enhance research reproducibility

DIGITAL PUBLISHING
Articles designed for optimal readership across devices

FOLLOW US
@frontiersin

IMPACT METRICS
Advanced article metrics track visibility across digital media

EXTENSIVE PROMOTION
Marketing and promotion of impactful research

LOOP RESEARCH NETWORK
Our network increases your article's readership